Supporting Information

Elucidating the Mechanism of Excited State Bond Homolysis in Nickel–Bipyridine Photoredox Catalysts

David A. Cagan[a], Daniel Bím[a], Breno Silva[a,b], Nathanael P. Kazmierczak[a], Brendon J. McNicholas[a], and Ryan G. Hadt[a,*]

[a]Division of Chemistry and Chemical Engineering, Arthur Amos Noyes Laboratory of Chemical Physics, California Institute of Technology, Pasadena, California 91125, United States

[b]Department of Chemistry and Biochemistry, Suffolk University, Boston, Massachusetts 02108, United States

*Corresponding Author: rghadt@caltech.edu

Table of Contents

S1. Experimental Section.

S1.1. General Considerations.

All purchased compounds were used as received unless otherwise noted. Bis-(1,5-cyclooctadiene) nickel(0) and bis(triphenylphosphino)(2-methylphenyl)chloronickel(II) were purchased from Strem Chemicals. Ligands 4,4′-dimethoxy-2,2′-bipyridine (^{MeO}bpy), 4,4′-di-*tert*-butyl-2,2′-bipyridine (^{tBu}bpy), 2,2′-bipyridine (bpy), and dimethyl-2,2′-bipyridine-4,4′-dicarboxylate (^{MeOOC}bpy), and *N,N,N′,N′*-tetramethyl ethylenediamine (TMEDA) were purchased from Sigma-Aldrich. Aryl halide compounds, 2-chlorotoluene, chlorobenzene, 2-chloroanisole, 1-chloro-2-fluorobenzene, 2-chlorobenzotrifluoride, and 2-bromotoluene were also obtained from Sigma-Aldrich. Solids were dried under vacuum and brought into a nitrogen-atmosphere glove box; liquids were sparged (N_2) and degassed via freeze-pump-thaw techniques, brought into the glove box, and stored over 3 Å molecular sieves. All solvents were air-free and collected from the solvent purification system (SPS), then stored in the glove box over 3 Å molecular sieves. Tetrahydrofuran (THF) was inhibitor-free. All synthesized compounds were made using air-free Schlenk techniques or made in the glove box. Compounds **1A**–**1C**, **2B**, **1B–Br**, and precatalyst, Ni(TMEDA)(CH_3Ph)Cl, were prepared following a modified literature procedure[1,2] (details below). All synthesized complexes are considered air and moisture sensitive. Light sensitivity was also seen even in the solid state if left exposed for extended time.

UV-vis spectra of the complexes were obtained on a Varian Cary 500 spectrophotometer using Starna Cells air free 9-SOG or 6-Q 10 mm path length cuvettes. Deuterated solvents were dried and stored over activated 3 Å molecular sieves in a nitrogen-filled glove box. Proton nuclear magnetic resonance (^{1}H NMR) and fluorine nuclear magnetic resonance (^{19}F NMR) spectra were recorded on a 400 MHz Varian Spectrometer with broadband auto-tune OneProbe. All ^{13}C NMR spectra were collected on a Bruker AV-III HD 400 MHz spectrometer. ^{13}C NMR spectra were ^{1}H decoupled. Chemical shifts are reported in parts per million (δ in ppm, s: singlet, d: doublet, t: triplet, m: multiplet) and are referenced to residual solvent signal (CD_2Cl_2 = δ 5.32 ppm, THF-d_8 = 3.58 ppm). Fluorine NMR were externally referenced to neat fluorobenzene (δ = -113.15 ppm). Fourier transform infrared (FTIR) spectra were collected using a Thermo Scientific Nicolet iS5 FTIR spectrometer with an iD5 diamond ATR accessory in an inert-atmosphere glove box.

S1.2. Photochemical Setup.

Photochemical stocks were prepared in a nitrogen-filled glove box and distributed into separate spectroscopic cuvettes (Starna Cells, 10 mm path length) with air-tight seals. Each cuvette cell had volume of 2.5 mL as determined by syringe and were placed 5 cm away from a Kessil PR160L LED (λ_{max} = 390 nm unless otherwise specified) on highest setting (Figure S1). Reactions were run in triplicate. A cooling fan was used to maintain room temperature irradiation during the experiment. Sample positions were rotated periodically to ensure even irradiation throughout the entire duration of the experiment.

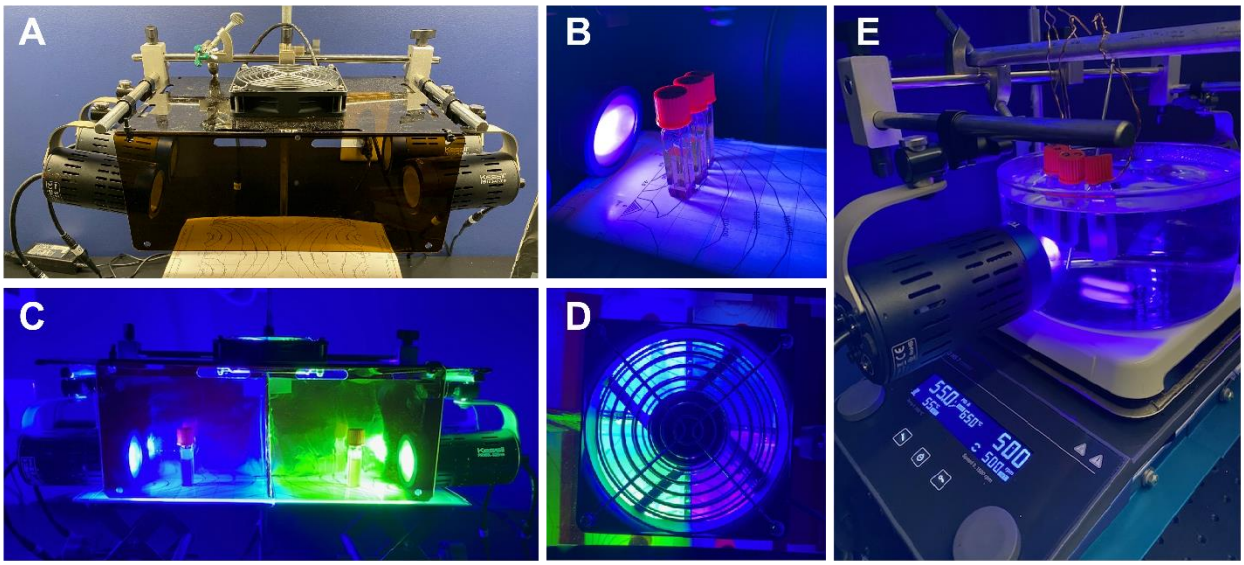

Figure S1. Photochemical setup. (A) Side view of Kessil LEDs with cooling fan on top. (B) Typical irradiation setup with cuvettes places on isopower curves 5 cm away from the light source. (C) Wavelength dependence experiment. (D) Top-down view of wavelength dependent experiment (LEDs 390 nm, 427 nm, 456 nm, and 525 nm). (D) Thermal dependence experiment using suspended cuvettes in a water bath.

S1.3. Synthetic Details.

Two primary approaches were utilized when undertaking the synthesis of the nickel complexes, the method of oxidative addition and the method of ligand substitution.[1–3] In the former, bis-(1,5-cyclooctadiene) nickel(0) was pre-stirred with a bipyridine ligand, then reacted with aryl halide resulting in the desired complex. The latter method called for either bis(triphenylphosphino)(2-methylphenyl)chloronickel(II) or the independent preparation of a pre-catalyst complex, Ni(TMEDA)(R′-Ph)Cl, R′ = CH_3 or CF_3.[3,4] These compounds afforded more labile ligands which could be substituted by bipyridine. The pre-catalyst complexes themselves were prepared by the method of oxidative addition. The method of ligand substitution was used in cases where oxidative addition proved slow, yielded inconsistent results, or would not produce the desired product.

The Method of Oxidative Addition:

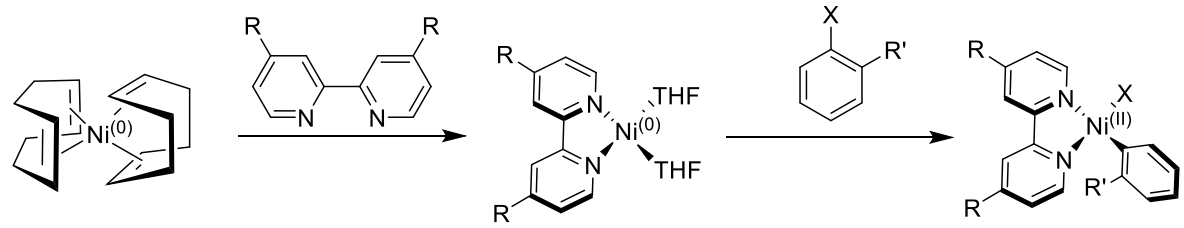

The Method of Ligand Substitution:

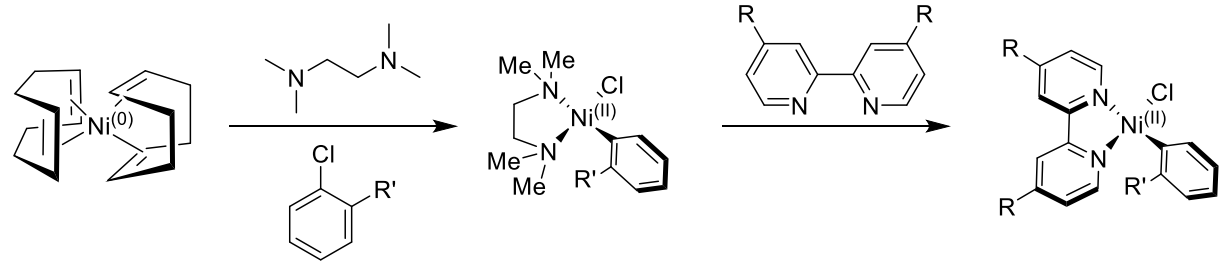

Scheme S1. The two general synthetic strategies employed in this study are shown.

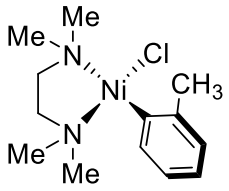

Ni(TMEDA)(CH₃Ph)Cl. Method of oxidative addition. In a nitrogen filled glove box, a 20 mL scintillation vial was charged with a Teflon coated stir bar and 1.0 g (1 eq., 3.6 mmol) of bis-(1,5-cyclooctadiene) nickel(0). Via micro syringe, 0.48 mL (1.3 eq., 1.95 mmol) of *N,N,N′,N′*-tetramethyl ethylenediamine was added along with 7.2 mL of 2-chlorotoluene (excess). After 6 hours stirring at room temperature, an orange solid could be seen in the vial. Hexanes was added (10 mL) to precipitate the solid and the mixture was left overnight. The solid was collected by vacuum filtration where it was rinsed with copious hexanes and dried, affording a yellow/orange solid (650 mg, 60% yield). Diffraction quality crystals were attempted from a concentrated solution of the complex in methylene chloride via vapor diffusion with hexanes,

however, green cubic-like crystals were yielded instead. These were identified as paramagnetic μ3-chloro-μ3-hydroxo-tris(μ-chloro)tris(tetramethylethylenediamine-nickel(II)) chloride, which has been reported to develop upon recrystallization of Ni(TMEDA)(CH_3Ph)Cl in chlorinated solvents. UV-vis (THF): λ = 470 nm, ε_{470nm} = 180 M^{-1} cm^{-1}. ^{1}H NMR (400 MHz, CD_2Cl_2): δ 7.38 (dd, *J* = 7.4, 1.4 Hz, 1H), 6.72 – 6.56 (m, 3H), 3.43 (s, 3H), 2.66 – 2.35 (m, 12H), 2.17 (s, 2H), 1.83 (s, 2H). ^{13}C{^{1}H} NMR (100 MHz, CD_2Cl_2) δ 146.1, 143.6, 135.5, 126.5, 122.4, 122.07, 61.5, 57.2, 50.4, 48.2, 48.0, 46.4, 25.9. FT-IR (ATR, cm^{-1}): 3355, 3038, 2975, 2893, 2872, 2841, 2787, 1559, 1458, 1403, 1370, 1277, 1194, 1122, 1019, 955, 806, 736, 650, 601.

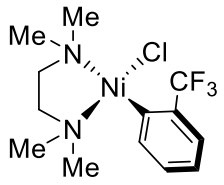

Ni(TMEDA)(CF$_3$Ph)Cl. Method of oxidative addition. In a nitrogen filled glove box, a 20 mL scintillation vial was charged with a Teflon coated stir bar and 0.41 g (1 eq., 1.5 mmol) of bis-(1,5-cyclooctadiene) nickel(0). Via micro syringe, 0.30 mL (1.3 eq., 1.95 mmol) of *N,N,N′,N′*-tetramethyl ethylenediamine was added along with 3.75 mL of 2-chlorobenzotrifluoride (excess). After 5 hours stirring at room temperature, a light red solid could be seen in the vial. Hexanes was added (10 mL) to precipitate the solid and the mixture was left overnight. The red/pink solid was collected by vacuum filtration where it was rinsed with copious hexanes and dried (464 mg, 87% yield). Diffraction quality crystals (red/orange and needle-like) were grown by vapor diffusion from a concentrated solution of the complex in methylene chloride with hexanes. UV-vis (THF): λ = 481 nm, ε_{481nm} = 180 M^{-1} cm^{-1}. ^{1}H NMR (400 MHz, CD_2Cl_2): δ 7.88 (d, *J* = 7.7 Hz, 1H), 7.13 (d, *J* = 8.1 Hz, 1H), 7.00 (t, *J* = 7.4 Hz, 1H), 6.82 (t, *J* = 7.5 Hz, 1H), 3.27–1.39 (m, *J* = 114.6 Hz, 16H). ^{13}C{^{1}H} NMR (100 MHz, CD_2Cl_2) δ 145.9 (q, J_{CF} = 4 Hz), 137.1, 136.8 (q, J_{CF} = 28 Hz), 127.0, 126.0 (q, J_{CF} = 273 Hz), 125.2 (q, J_{CF} = 4 Hz), 122.2, 61.1, 57.6, 50.9, 48.2. ^{19}F NMR (400 MHz, CD_2Cl_2): δ -56.58 (s). FT-IR (ATR, cm^{-1}): 3355, 3034, 2980, 2899, 2841, 2792, 1578, 1522, 1470, 1423, 1308, 1275, 1234, 1155, 1092, 1024, 951, 808, 777, 739, 674, 642, 604.

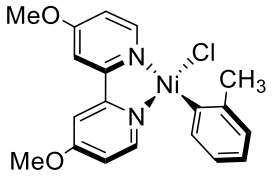

Ni(^{MeO}bpy)(CH$_3$Ph)Cl, ***1A****. Method of ligand substitution*. In a nitrogen filled glove box, a 20 mL scintillation vial was charged with a Teflon coated stir bar and bis(triphenylphosphino)(2-methylphenyl)chloronickel(II) (0.200 g, 0.281 mmol, 1 eq.). To this vial, 4,4′-dimethoxy-2-2′-bipyridine (0.061 g, 0.281 mmol, 1 eq.) and diethyl ether (6 mL) were added. The red/orange mixture was stirred for 6 hours affording an orange solid. This solid was washed with diethyl ether (2x1 mL) and hexanes (3x3 mL), then collected and dried under vacuum (0.081 g, 71% yield). UV-vis (THF): λ = 462 nm, ε_{462nm} = 3640 M^{-1} cm^{-1}. UV-vis (Toluene): λ = 479 nm, ε_{479nm} = 2000 M^{-1} cm^{-1}. ^{1}H NMR (400 MHz, CD_2Cl_2): δ 8.91 (d, *J* = 6.5 Hz, 1H), 7.53 (d,

J = 6.9 Hz, 1H), 7.32 (d, *J* = 13.7 Hz, 2H), 7.01 (s, 2H), 6.77 (d, *J* = 6.8 Hz, 3H), 6.59 (s, 1H), 3.98 (s, 3H), 3.88 (s, 3H), 3.07 (s, 3H). $^{13}C\{^{1}H\}$ NMR (100 MHz, CD_2Cl_2) δ 168.1, 167.3, 157.5, 154.2, 153.1, 151.1, 150.5, 142.8, 135.6, 127.4, 123.2, 122.7, 111.5, 111.1, 108.1, 107.5, 56.7, 25.2. FT-IR (ATR, cm^{-1}): 3115, 3068, 3032, 3012, 2975, 2953, 2929, 2843, 1608, 1557, 1493, 1473, 1455, 1436, 1419, 1338, 1312, 1277, 1245, 1226, 1105, 1038, 1026, 1007, 870, 837, 743, 695, 649, 596, 573.

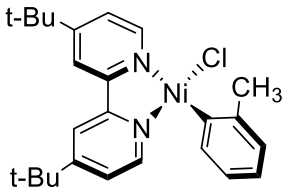

Ni(^{tBu}*bpy)(CH3Ph)Cl,* ***1B****. Method of oxidative addition.* In a nitrogen filled glove box, a 20 mL scintillation vial was charged with a Teflon coated stir bar, bis-(1,5-cyclooctadiene) nickel(0) (0.225 g, 1.0 mmol, 1 eq.), and 4,4′-*tert*-butyl-2-2′-bipyridine (0.268 g, 1.0 mmol, 1.0 eq.). To this vial, 3.0 mL THF was added, and the mixture was stirred for one hour affording a deep purple solution. Subsequently, 6.0 mL of 2-chlorotoluene (excess) was added, affording a red solution after 30 minutes of stirring at room temperature. Hexanes (10 mL) was used to precipitate the red solid. The vial was placed in the freezer (-35 °C) for ten minutes to complete precipitation. The red solid was collected by filtration, washed with hexanes (3x3 mL), diethyl ether (2x1 mL), and hexanes again (3x3 mL), then dried under vacuum (0.375 g, 83% yield). Diffraction quality crystals (deep red and needle-like) were grown by slow evaporation from THF.[5] UV-vis (THF): λ = 475 nm, ε_{475nm} = 4970 M^{-1} cm^{-1}. UV-vis (Toluene): λ = 493 nm, ε_{493nm} = 3790 M^{-1} cm^{-1}. ^{1}H NMR (400 MHz, CD_2Cl_2): δ 9.03 (d, *J* = 5.8 Hz, 1H), 7.85 (s, 1H), 7.80 (d, *J* = 2.1 Hz, 1H), 7.56 – 7.49 (m, 2H), 7.15 (d, *J* = 6.2 Hz, 1H), 7.10 (dd, *J* = 6.2, 2.1 Hz, 1H), 6.79 (dd, *J* = 7.6, 3.1 Hz, 3H), 3.04 (s, 3H), 1.42 (s, 9H), 1.34 (s, 9H). $^{13}C\{^{1}H\}$ NMR (100 MHz, CD_2Cl_2) δ 164.0, 162.9, 156.3, 152.9, 151.3, 149.3, 142.6, 135.7, 127.5, 123.9, 123.6, 123.2, 122.7, 117.8, 117.0, 35.7, 30.4, 30.2, 25.1. FT-IR (ATR, cm^{-1}): 3037, 2961, 2903, 2869, 1616, 1543, 1480, 1456, 1435, 1410, 1364, 1253, 1201, 1094, 1017, 863, 839, 736, 691, 601.

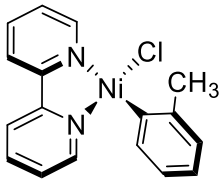

Ni(^{H}*bpy)(CH3Ph)Cl,* ***1C****. Method of ligand substitution*. In a nitrogen filled glove box, a 20 mL scintillation vial was charged with a Teflon coated stir bar and bis(triphenylphosphino)(2-methylphenyl)chloronickel(II) (0.450 g, 0.634 mmol, 1 eq.). To this vial, 2-2′-bipyridine (0.100 g, 0.641 mmol, 1 eq.) and diethyl ether (13 mL) was added. The red/orange mixture was stirred for 4 hours affording a bright red solid. This solid was washed with diethyl ether (2x5 mL) and hexanes (2x10 mL), then collected and dried under vacuum (0.193 g, 89% yield). UV-vis (THF): λ = 483 nm, ε_{483nm} = 4070 M^{-1} cm^{-1}. UV-vis (Toluene): λ = 502 nm, ε_{502nm} = 1600 M^{-1} cm^{-1}. ^{1}H NMR (400 MHz, CD_2Cl_2): δ 9.21 (s, 1H), 8.01 (s, 1H), 7.96 – 7.86 (m,

5H), 7.54 (d, *J* = 21.2 Hz, 2H), 7.32 (s, 1H), 7.13 (s, 1H), 6.81 (s, 3H), 3.04 (s, 3H). $^{13}C\{^{1}H\}$ NMR (100 MHz, CD_2Cl_2) δ 156.3, 152.9, 151.9, 150.2, 149.8, 142.6, 139.2, 138.1, 135.77, 127.7, 126.9, 126.4, 123.4, 123.0, 121.2, 120.5, 25.1. FT-IR (ATR, cm^{-1}): 3103, 3041, 2973, 1600, 1568, 1468, 1422, 1311, 1241, 1155, 1059, 1024, 899, 756, 727, 649, 637, 605.

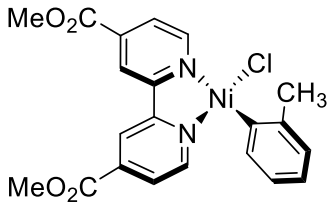

Ni(^{CH_3OOC}bpy)(CH_3Ph)Cl, ***1D***. *Method of ligand substitution.* In a nitrogen filled glove box, a 25 mL Schlenk flask was charged with a Teflon coated stir bar and Ni(TMEDA)(CH_3Ph)Cl (0.051 g, 0.168 mmol, 1 eq.). To this vial, dimethyl-2,2′-bipyridine-4,4′-dicarboxylate (0.053 g, 0.176 mmol, 1 eq.) was added along with 4.81 mL of heptane and 0.81 mL toluene (6:1 heptane/toluene). The flask was attached to the nitrogen Schlenk line, and the brown/orange mixture was stirred at 60 °C. After two hours the mixture became a deep purple solution. After 10 hours the Schlenk flask was brought back into the glove box where it was cooled in the freezer (-35 °C) for ten minutes precipitating a purple solid. This solid was collected by vacuum filtration, washed with pentanes (2x5 mL), ether (2x5 mL), and hexanes (2x5 mL), then was dried under vacuum (0.063 g, 84% yield). UV-vis (THF): λ = 532 nm, ε_{532nm} = 5259 M^{-1} cm^{-1}. UV-vis (Toluene): λ = 551 nm, ε_{551nm} = 1637 M^{-1} cm^{-1}. ^{1}H NMR (400 MHz, CD_2Cl_2): δ 9.50 (dd, *J* = 5.7, 1.1 Hz, 1H), 8.59 (d, *J* = 1.8 Hz, 1H), 8.53 – 8.48 (m, 1H), 8.17 – 8.11 (m, 1H), 7.72 – 7.65 (m, 1H), 7.57 (dd, *J* = 6.0, 1.1 Hz, 1H), 7.49 – 7.43 (m, 1H), 6.87 – 6.81 (m, 3H), 4.04 (s, 3H), 3.97 (s, 3H), 2.98 (s, 3H). $^{13}C\{^{1}H\}$ NMR (100 MHz, CD_2Cl_2) δ 164.5, 164.3, 156.3, 153.1, 152.6, 151.0, 149.3, 142.3, 140.3, 138.7, 135.3, 128.1, 126.7, 126.1, 123.8, 123.5, 121.2, 120.4, 25.0. FT-IR (ATR, cm^{-1}): 2981, 2961, 2852, 1730, 1618, 1557, 1434, 1398, 1358, 1295, 1252, 1233, 1190, 1124, 1012, 958, 764, 722, 698.

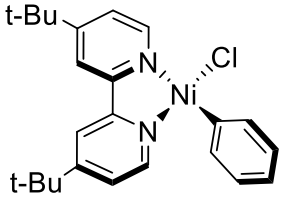

Ni(^{tBu}bpy)(Ph)Cl, ***2B***. *Method of oxidative addition*. The general procedure for the synthesis of **1B** was followed, except 0.4 mL of chlorobenzene was used as aryl halide. After 30 minutes of stirring at room temperature, the mixture became a red solution. Hexanes (10 mL) was used to precipitate the orange solid. The vial was placed in the freezer (-35 °C) for ten minutes to complete precipitation. The solid was collected by filtration, washed with hexanes (3x3 mL) and pentanes (3x3 mL), then dried under vacuum (0.290 g, 91% yield). UV-vis (THF): λ = 471 nm, ε_{471nm} = 3530 M^{-1} cm^{-1}. UV-vis (Toluene): λ = 489 nm, ε_{489nm} = 3905 M^{-1} cm^{-1}. ^{1}H NMR (400 MHz, CD_2Cl_2): δ 9.01 (d, *J* = 5.9 Hz, 1H), 7.85 (s, 1H), 7.80 (s, 1H), 7.53 – 7.47 (m, 3H), 7.30 (d, *J* = 6.3 Hz, 1H), 7.12 (d, *J* = 6.2 Hz, 1H), 6.94 (t, *J* = 7.4 Hz, 2H), 6.85 – 6.79 (m, 1H), 1.41 (s, 9H), 1.34 (s, 9H). $^{13}C\{^{1}H\}$ NMR (100 MHz, CD_2Cl_2) δ 163.7, 162.7, 151.9, 150.3, 149.2, 141.4, 136.3,

128.8, 128.5, 127.3, 127.1, 126.1, 125.8, 122.3, 117.5, 116.8, 35.4, 30.1, 29.9. FT-IR (ATR, cm^{-1}): 3048, 2961, 2904, 2868, 1611, 1562, 1458, 1407, 1366, 1249, 1202, 1060, 1018, 897, 856, 731, 694, 602, 555.

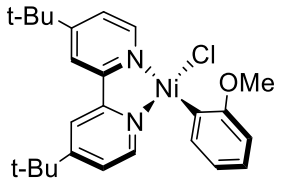

*Ni(^{tBu}bpy)(CH_3OPh)Cl, **3B**. Method of oxidative addition*. The general procedure for the synthesis of **1B** was followed, except 0.5 mL of 2-choloroanisole was added as aryl halide Upon stirring for 30 minutes at room temperature, a red solution was seen. Hexanes (10 mL) was added to precipitate the airy red solid (which clung to the sides of the glass). The vial was left in the freezer (-35 °C) for ten minutes to complete precipitation. The solid was collected by filtration, washed with hexanes (2x2 mL), diethyl ether (2x2 mL), and hexanes again (2x2 mL), then dried under vacuum (0.298 g, 88% yield). UV-vis (THF): λ = 464 nm, ε_{464nm} = 2660 M^{-1} cm^{-1}. UV-vis (Toluene): λ = 479 nm, ε_{479nm} = 2000 M^{-1} cm^{-1}. ^{1}H NMR (400 MHz, CD_2Cl_2): δ 9.01 (s, 1H), 7.83 (s, 1H), 7.80 (s, 1H), 7.51 (s, 1H), 7.42 (dd, *J* = 7.2, 1.7 Hz, 1H), 7.23 (s, 1H), 7.09 (s, 1H), 6.90 (td, *J* = 7.6, 1.8 Hz, 1H), 6.69 (td, *J* = 7.2, 1.4 Hz, 1H), 6.46 (dd, *J* = 8.0, 1.3 Hz, 1H), 3.94 (s, 3H), 1.41 (s, 9H), 1.34 (s, 9H). ^{13}C{^{1}H} NMR (100 MHz, CD_2Cl_2) δ 163.3, 151.9, 137.8, 134.5, 128.3, 124.1, 123.5, 119.8, 117.8, 117.0, 109.8, 56.2, 35.7, 30.4, 30.2. FT-IR (ATR, cm^{-1}): 3113, 3067, 3042, 2956, 2904, 2869, 1610, 1558, 1493, 1473, 1454, 1442, 1419, 1408, 1367, 1337, 1278, 1247, 1226, 1175, 1038, 1020, 898, 869, 854, 838, 783, 744, 720, 603, 571.

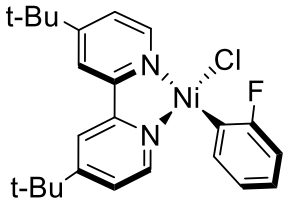

*Ni(^{tBu}bpy)(FPh)Cl, **4B**. Method of oxidative addition*. The general procedure for the synthesis of **1B** was followed, save 0.6 mL of 1-chloro-2-fluorobenzene was added as aryl halide A red solution was afforded upon stirring for 30 minutes at room temperature. The solid was precipitated with pentanes (10 mL), washed with copious hexanes and pentane (3x5 mL), then dried (0.279 g, 84% yield). UV-vis (THF): λ = 447 nm, ε_{447nm} = 1699 M^{-1} cm^{-1}. UV-vis (Toluene): λ = 463 nm, ε_{463nm} = 857 M^{-1} cm^{-1}. ^{1}H NMR (400 MHz, CD_2Cl_2): δ 8.98 (s, 1H), 7.85 – 7.81 (m, 2H), 7.55 – 7.45 (m, 2H), 7.28 – 7.22 (m, 1H), 7.15 (dd, *J* = 17.0, 7.8 Hz, 1H), 6.93 – 6.85 (m, 2H), 6.63 – 6.58 (m, 1H), 1.42 – 1.33 (m, 18H). ^{13}C{^{1}H} NMR (100 MHz, CD_2Cl_2) δ 165.7 (d, J_{CF} = 227 Hz), 163.4, 162.8, 155.4, 151.21, 148.6, 138.1 (d, J_{CF} = 17 Hz), 128.0 (d, J_{CF} = 80 Hz), 123.8 (d, J_{CF} = 7 Hz), 122.9, 121.8, 117.3, 116.6, 112.6 (d, J_{CF} = 28 Hz), 34.8, 29.4. ^{19}F NMR (400 MHz, CD_2Cl_2): δ -95.60 (s). FT-IR (ATR, cm^{-1}): 3351, 3052, 2959, 2871, 1618, 1579, 1545, 1462, 1411, 1312, 1239, 1154, 1111, 1091, 1075, 1018, 901, 860, 838, 763, 735, 677, 639, 602.

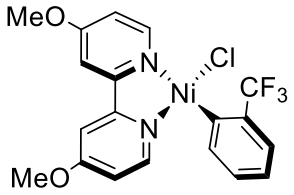

Ni(^{MeO}*bpy)(CF*$_3$*Ph)Cl,* ***5A****. Method of ligand substitution.* In a nitrogen filled glove box, a 20 mL scintillation vial was charged with a Teflon coated stir bar and Ni(TMEDA)(CF_3Ph)Cl (0.150 g, 0.42 mmol, 1 eq.). To this vial, 4,4′-dimethoxy-2-2′-bipyridine (0.091 g, 0.42 mmol, 1 eq.) and diethyl ether (6 mL) was added. The red/orange mixture was stirred overnight (~12 hrs.) affording a bright yellow solid. The solid was washed with hexanes (2x10 mL) and pentane (2x3 mL), then collected under vacuum (0.150 g, 78% yield). UV-vis (THF): λ = 432 nm, ε_{432nm} = 1090 M^{-1} cm^{-1}. UV-vis (Toluene): λ = 445 nm, ε_{445nm} = 2400 M^{-1} cm^{-1}. ^{1}H NMR (400 MHz, CD_2Cl_2): δ 8.87 (s, 1H), 8.07 (dd, *J* = 7.5, 1.4 Hz, 1H), 7.33 – 7.28 (m, 3H), 7.14 – 7.08 (m, 1H), 7.04 – 6.93 (m, 2H), 6.84 (s, 1H), 6.57 (s, 1H), 3.97 (s, 3H), 3.90 (s, 3H). ^{13}C{^{1}H} NMR (100 MHz, CD_2Cl_2) δ 168.3, 167.6, 157.5, 154.5, 153.5, 151.4, 149.5, 138.0, 135.8 (q, J_{CF} = 29 Hz), 128.0, 125.7 (q, J_{CF} = 273 Hz), 125.4, 125.3, 122.8, 111.2, 111.2, 108.1, 107.7. ^{19}F NMR (400 MHz, CD_2Cl_2): δ -58.13 (s). FT-IR (ATR, cm^{-1}): 3074, 3031, 2980, 2944, 2842, 1611, 1557, 1494, 1471, 1427, 1337, 1309, 1257, 1228, 1157, 1102. 1044, 1023, 923, 854, 768, 735, 677, 639, 576.

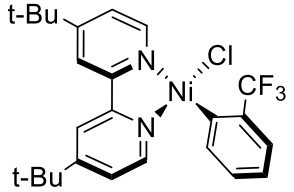

Ni(^{tBu}*bpy)(CF*$_3$*Ph)Cl,* ***5B****. Method of ligand substitution*. In a nitrogen filled glove box, a 20 mL scintillation vial was charged with a Teflon coated stir bar and Ni(TMEDA)(CF_3Ph)Cl (0.150 g, 0.42 mmol, 1 eq.). To this vial, 4,4′-*tert*-butyl-2-2′-bipyridine (0.113 g, 0.42 mmol, 1 eq.) and diethyl ether (6 mL) was added. The red/orange mixture was stirred overnight (~12 hrs.) affording a yellow/orange solid. This solid was washed with hexanes (2x10 mL) and pentane (2x3 mL), then collected under vacuum (0.153 g, 72% yield). UV-vis (THF): λ = 443 nm, ε_{443nm} = 1220 M^{-1} cm^{-1}. UV-vis (Toluene): λ = 461 nm, ε_{461nm} = 1890 M^{-1} cm^{-1}. ^{1}H NMR (400 MHz, CD_2Cl_2): δ 8.99 (s, 1H), 8.05 (d, *J* = 7.6 Hz, 1H), 7.82 (s, 2H), 7.52 (s, 1H), 7.31 (d, *J* = 7.8 Hz, 1H), 7.11 (q, *J* = 11.0, 9.2 Hz, 2H), 6.98 (t, *J* = 7.5 Hz, 2H), 1.41 (s, 9H), 1.34 (s, 9H). ^{13}C{^{1}H} NMR (100 MHz, CD_2Cl_2) δ 164.3, 163.6, 156.1, 153.1, 151.7, 149.8, 149.5, 137.8, 135.6 (q, J_{CF} = 29 Hz), 128.0, 125.6 (q, J_{CF} = 273 Hz) 125.4, 123.6, 122.8, 117.9, 117.3, 35.7, 30.3. ^{19}F NMR (400 MHz, CD_2Cl_2): δ -58.08 (s). FT-IR (ATR, cm^{-1}): 2961, 2906, 2869, 1618, 1579, 1545, 1411, 1365, 1312, 1239, 1154, 1111, 1091, 1075, 1018, 901, 860, 838, 763, 735, 677, 640, 602.

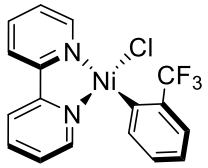

Ni(^{H}bpy)(CF_3Ph)Cl, ***5C***. *Method of ligand substitution.* In a nitrogen filled glove box, a 20 mL scintillation vial was charged with a Teflon coated stir bar and Ni(TMEDA)(CF_3Ph)Cl (0.130 g, 0.37 mmol, 1 eq.). To this vial, 2-2′-bipyridine (0.060 g, 0.38 mmol, 1 eq.) and diethyl ether (6 mL) was added. The red/orange mixture was stirred overnight (~12 hrs.) affording an orange solid. This solid was washed with hexanes (2x10 mL) and pentane (2x3 mL), then collected under vacuum (0.110 g, 75% yield). UV-vis (THF): λ = 453 nm, ε_{453nm} = 1110 M^{-1} cm^{-1}. UV-vis (Toluene): λ = 470 nm, ε_{470nm} = 930 M^{-1} cm^{-1}. ^{1}H NMR (400 MHz, CD_2Cl_2): δ 9.17 (s, 1H), 8.04 (d, J = 7.5 Hz, 2H), 7.91 (s, 3H), 7.56 (s, 1H), 7.37 – 7.27 (m, 1H), 7.13 (d, J = 7.0 Hz, 3H), 7.00 (t, J = 7.6 Hz, 1H). ^{19}F NMR (400 MHz, CD_2Cl_2): δ -58.11 (s). ^{13}C{^{1}H} NMR (100 MHz, CD_2Cl_2) δ 156.2, 153.1, 152.4, 150.3, 148.9, 139.6, 138.8, 137.8, 135.6 (q, J_{CF} = 29 Hz), 128.3, 126.6, 125.6 (q, J_{CF} = 4 Hz), 125.6 (q, J_{CF} = 273 Hz), 123.1, 121.2, 120.6. FT-IR (ATR, cm^{-1}): 3113, 3054, 3033, 1607, 1578, 1553, 1473, 1446, 1425, 1308, 1237, 1163, 1150, 1098, 1074, 1021, 759, 735, 727, 675, 638.

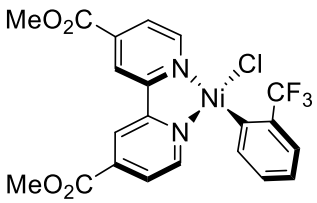

Ni(^{CH_3OOC}bpy)(CF_3Ph)Cl, ***5D***. *Method of ligand substitution.* In a nitrogen filled glove box, a 25 mL Schlenk flask was charged with a Teflon coated stir bar and Ni(TMEDA)(CF_3Ph)Cl (0.110 g, 0.309 mmol, 1 eq.). To this vial, dimethyl-2,2′-bipyridine-4,4′-dicarboxylate (0.108 g, 0.396 mmol, 1.3 eq.) was added along with 10 mL of 6:1 heptane/toluene solution. The flask was attached to the nitrogen Schlenk line, and the brown/orange mixture was stirred at 65 °C. After 10 hours, the Schlenk flask was brought back into the glove box where it was cooled in the freezer (-35 °C) for ten minutes precipitating a pale red/purple solid. This solid was collected by vacuum filtration, washed with pentanes (3x5 mL), ether (2x3 mL), and hexanes (3x5 mL). The solid was dried under vacuum (0.110 g, 72% yield). UV-vis (THF): λ = 497 nm, ε_{497nm} = 1830 M^{-1} cm^{-1}. UV-vis (Toluene): λ = 513 nm, ε_{513nm} = 2370 M^{-1} cm^{-1}. ^{1}H NMR (400 MHz, CD_2Cl_2): δ 9.44 (s, 1H), 8.58 (s, 1H), 8.53 (s, 1H), 8.13 (s, 1H), 8.05 – 7.94 (m, 1H), 7.67 (s, 1H), 7.36 (d, J = 8.5 Hz, 2H), 7.18 (d, J = 8.9 Hz, 1H), 7.04 (s, 1H), 4.03 (s, 3H), 3.98 (s, 3H). ^{13}C{^{1}H} NMR (100 MHz, CD_2Cl_2) δ 164.3, 164.1, 156.3, 153.3, 153.1, 151.4, 147.5, 140.7, 139.5, 137.4, 135.4 (q, J_{CF} = 29 Hz) 129.5, 128.7, 126.4, 126.1, 125.9 (q, J_{CF} = 4 Hz), 125.5 (q, J_{CF} = 273 Hz), 123.5, 121.4, 121.2, 120.6. ^{19}F NMR (400 MHz, CD_2Cl_2): δ -58.21 (s). FT-IR (ATR, cm^{-1}): 3088, 3063, 3044, 2981, 2961, 2860, 1725, 1578, 1558, 1435, 1401, 1326, 1309, 1254, 1232, 1150, 1092, 1022, 952, 902, 842, 765, 715, 677, 639.

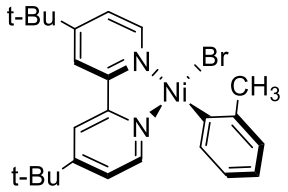

Ni(^{tBu}*bpy)(CH*$_3$*Ph)Br,* ***1B–Br****. Method of oxidative addition.* The general procedure for the synthesis of **1B** was followed, except 0.6 mL of 2-bromotoluene was used as aryl halide. After 30 minutes of stirring at room temperature, the mixture became a red solution. Pentanes (10 mL) was used to precipitate the orange solid. The vial was placed in the freezer (-35 ^{o}C) for ten minutes to complete precipitation. The solid was collected by filtration, washed with hexanes (3x3 mL) and pentanes (3x3 mL), then dried under vacuum (0.348 g, 96% yield). UV-vis (THF): λ = 479 nm. ^{1}H NMR (400 MHz, CD_2Cl_2): δ 9.25 (d, *J* = 5.9 Hz, 1H), 7.85 (d, *J* = 2.0 Hz, 1H), 7.81 (d, *J* = 2.1 Hz, 1H), 7.52 (dd, *J* = 8.3, 6.5, 1.8 Hz, 2H), 7.12 (dd, *J* = 6.2, 2.1 Hz, 1H), 7.03 (d, *J* = 6.2 Hz, 1H), 6.84 – 6.70 (m, 3H), 3.02 (s, 3H), 1.41 (s, 9H), 1.34 (s, 9H). ^{13}C{^{1}H}NMR (100 MHz, CD_2Cl_2) δ 162.7, 162.4, 162.4, 156.5, 154.5, 152.1, 152.0, 139.1, 138.9, 124.7, 123.8, 122.7, 113.6, 113.3, 35.7, 30.3, 25.6. FT-IR (ATR, cm^{-1}): 3038, 2961, 2903, 2868, 1615, 1543, 1455, 1408, 1363, 1251, 1201, 1016, 899, 862, 839, 735, 650, 601.

S1.4. X-ray Crystallography.

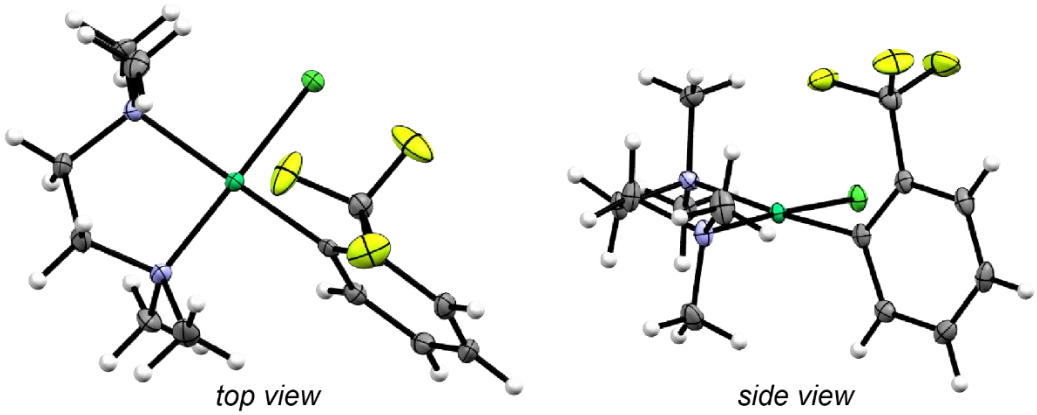

Figure S2. Top down and side views of the refined crystal structure of Ni(TMEDA)(CF_3Ph)Cl. Structure resembled refinement from a previous report.[4]

Collection and refinement details for Ni(TMEDA)(CF_3Ph)Cl.
Low-temperature diffraction data (ϕ-and ω-scans) were collected on a Bruker AXS D8 VENTURE KAPPA diffractometer coupled to a PHOTON II CPAD detector with Mo K_α radiation (λ = 0.71073 Å) from an IμS micro-source. The structure was solved by direct methods using SHELXS and refined against F^2 on all data by full-matrix least squares with SHELXL-2017 using established refinement techniques. All non-hydrogen atoms were refined anisotropically. All hydrogen atoms were included into the model at geometrically calculated positions and refined using a riding model. The isotropic displacement parameters of all hydrogen atoms were fixed to 1.2 times the U value of the atoms they are linked to (1.5 times for methyl groups). The compound crystallizes in the monoclinic space group $P2_1/n$ with one molecule in the asymmetric unit. These data are provided free of charge from The Cambridge Crystallographic Data Centre by The Cambridge Crystallographic Data Centre.

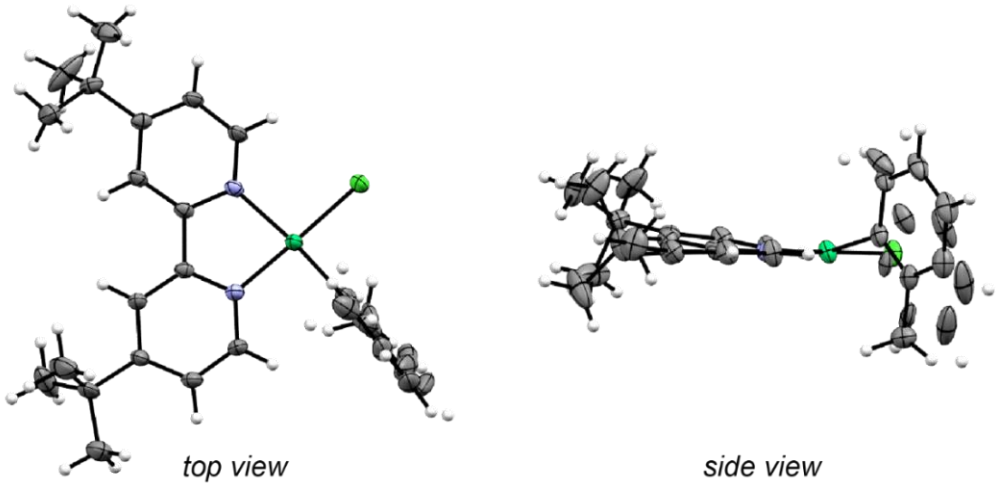

Figure S3. Top down and side views of the refined crystal structure of **1B**. Structure resembles previous refinement.[5]

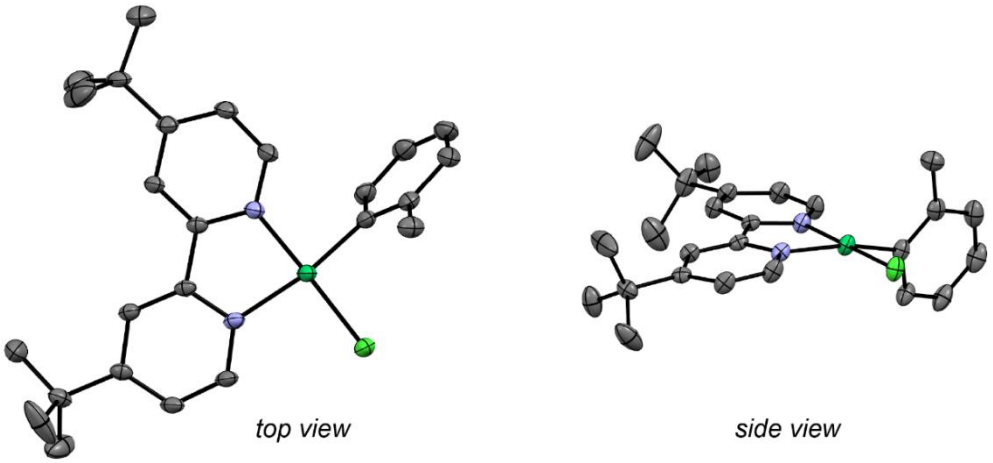

Figure S4. Top down and side views of the refined crystal structure of **1B**, showing only one aryl ligand conformer with hydrogens hidden for clarity.

Collection and refinement details for Ni(^{tBu}bpy)(CH_3Ph)Cl, 1B.
Low-temperature diffraction data (ϕ-and ω-scans) were collected on a Bruker AXS KAPPA APEX II diffractometer coupled to a PHOTON 100 CMOS detector with graphite monochromated Mo K_α radiation (λ = 0.71073 Å). The structure was solved by direct methods using SHELXS and refined against F^2 on all data by full-matrix least squares with SHELXL-2017 using established refinement techniques. All non-hydrogen atoms were refined anisotropically. All hydrogen atoms were included into the model at geometrically calculated positions and refined using a riding model. The isotropic displacement parameters of all hydrogen atoms were fixed to 1.2 times the *U* value of the atoms they are linked to (1.5 times for methyl groups). All disordered atoms were refined with the help of similarity restraints on the 1,2- and 1,3-distances and displacement parameters as well as enhanced rigid bond restraints for anisotropic displacement parameters. Compound **1B** crystallizes in the monoclinic space group $P2_1/c$ with one molecule in the asymmetric unit. One of the ligands is disordered over two positions. The highest residual electron density is located in a position that indicates additional disorder in one of the *tert*-butyl groups. Refinement of additional disorder did not lead to a stable refinement. These data are provided free of charge from The Cambridge Crystallographic Data Centre by The Cambridge Crystallographic Data Centre.

S1.5. Steady-State UV-vis Spectroscopy.

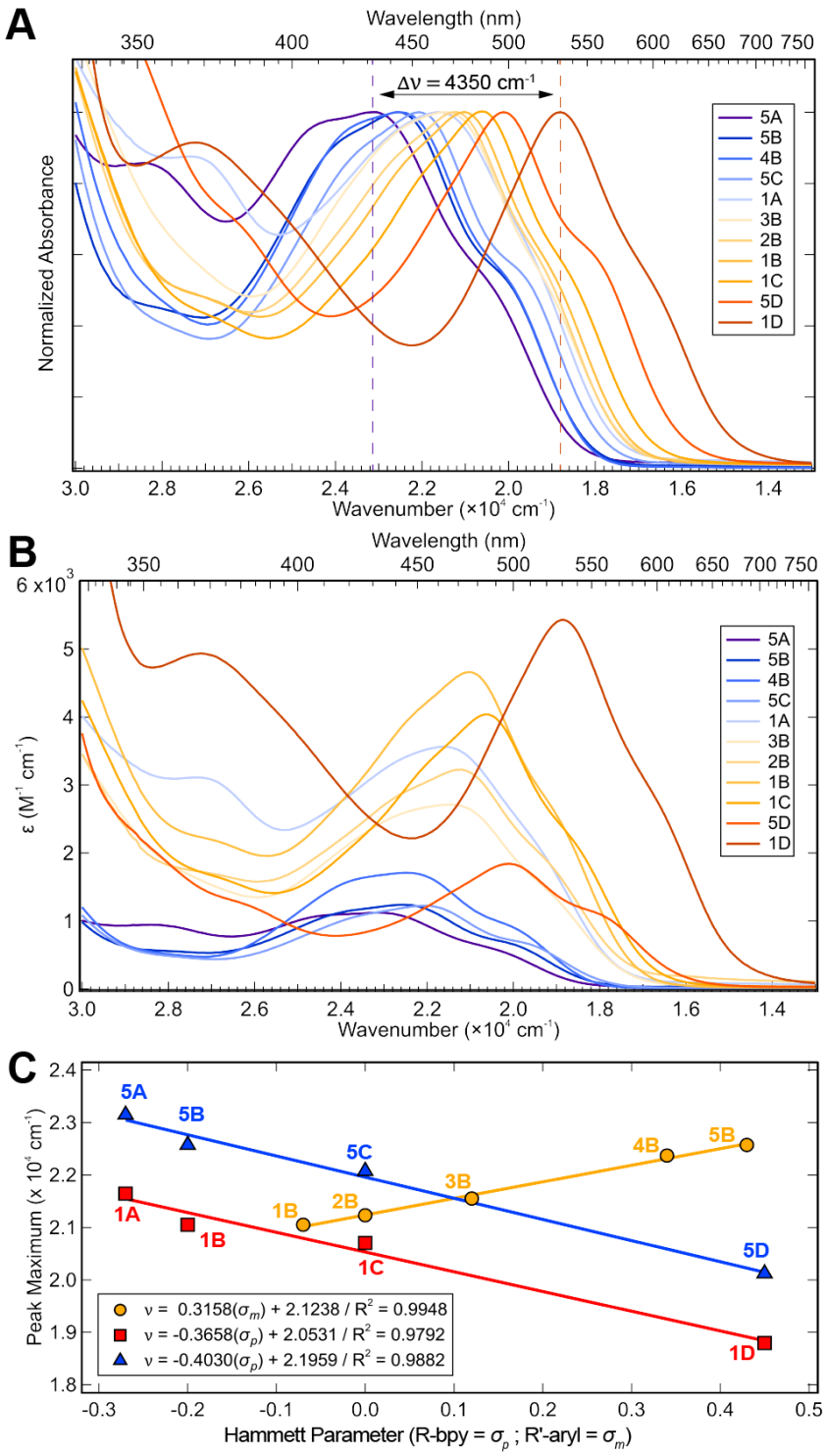

Figure S5. (A) Normalized and (B) extinction coefficient scaled UV-vis spectra in tetrahydrofuran (THF) of complexes synthesized here. (C) Correlation between the absorption peak maxima (dashed lines) in THF and the Hammett parameter (σ_p) for each bpy substituent or (σ_m) for each aryl substituent.[6] In part duplicated from main text Figure 3 for ease of comparison.

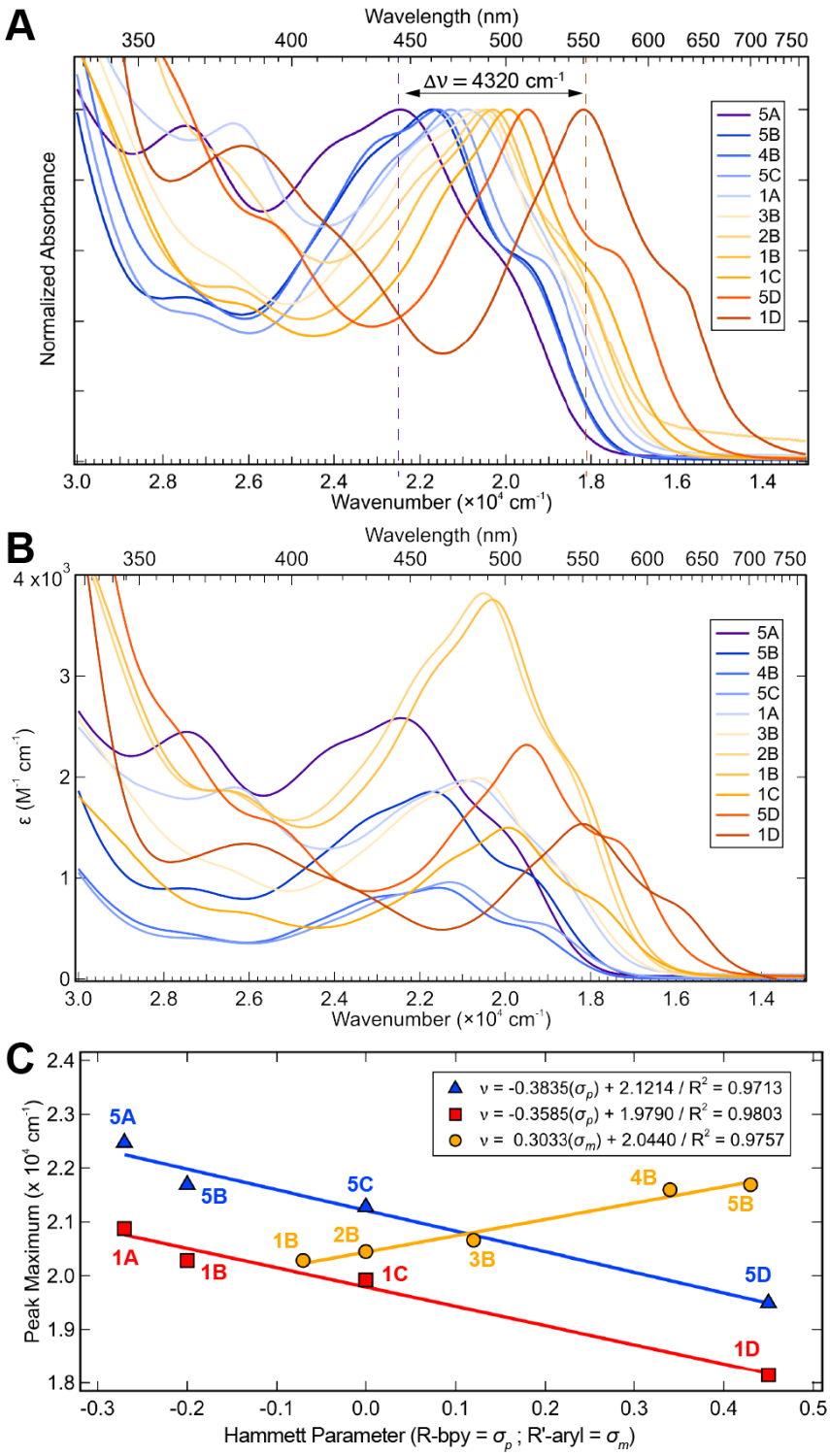

Figure S6. (A) Normalized and (B) extinction coefficient scaled UV-vis spectra in toluene of complexes synthesized here. (C) Correlation between the absorption peak maxima (dashed lines) in THF and the Hammett parameter (σ_p) for each bpy substituent or (σ_m) for each aryl substituent.[6]

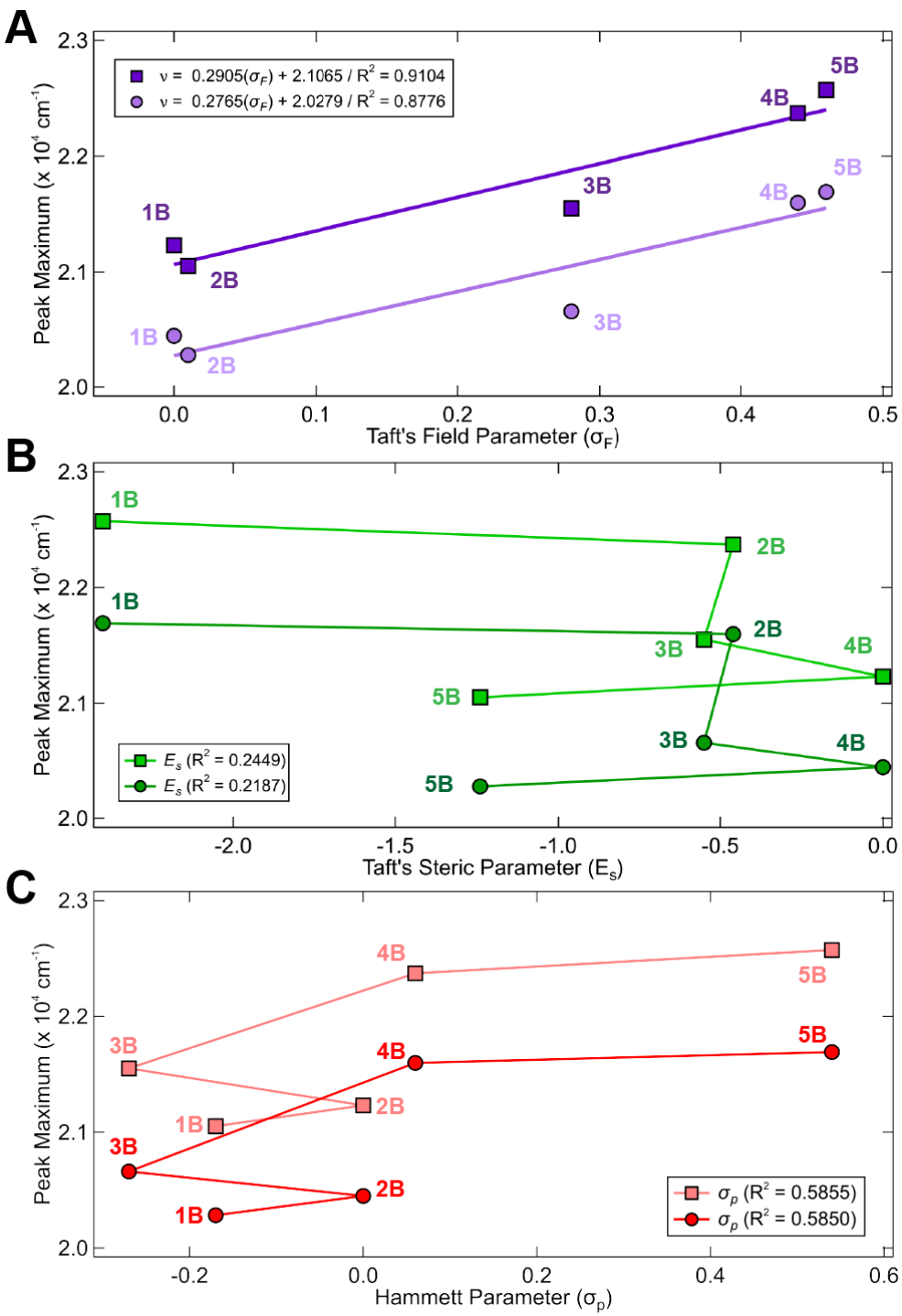

Figure S7. (A) Correlation between the absorption peak maxima in THF (dark purple, squares) and toluene (light purple, circles) and Taft's Field parameter (σ_F) for each aryl substituent. (B) Correlation between the absorption peak maxima in THF (light green, squares) and toluene (dark green, circles) and Taft's steric parameter (E_s) for each aryl substituent. (C) Correlation between the absorption peak maxima in THF (pink, squares) and toluene (red, circles) and Hammett's para-parameter (σ_p) for each aryl substituent.[6] Correlation coefficients (R^2) are given for linear fits.

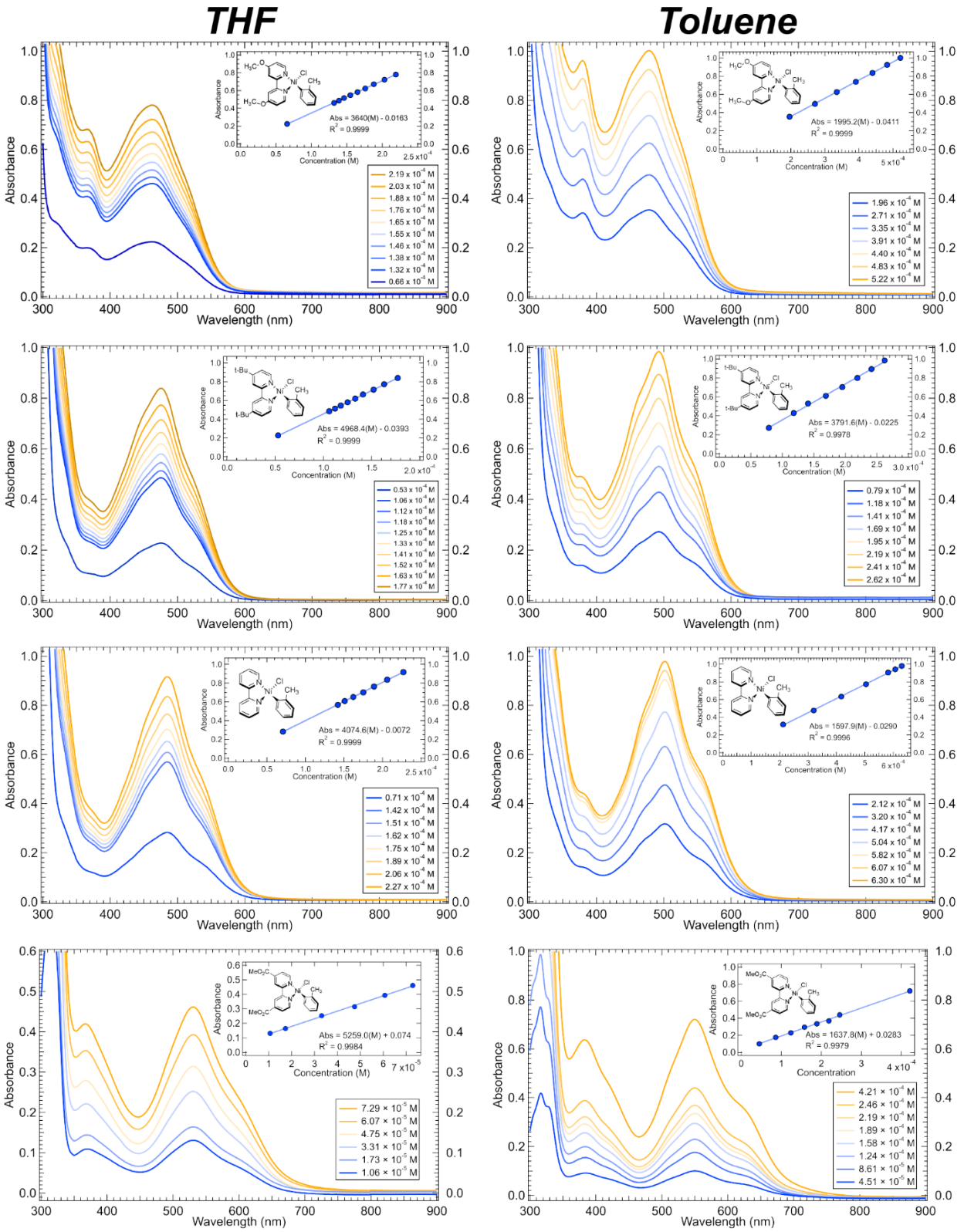

Figure S8. Concentration dependent UV-vis spectra in THF (left) and toluene (right) for **1A**–**1D**. Single wavelength molar absorptivity calibration curves are given as insets on each plot.

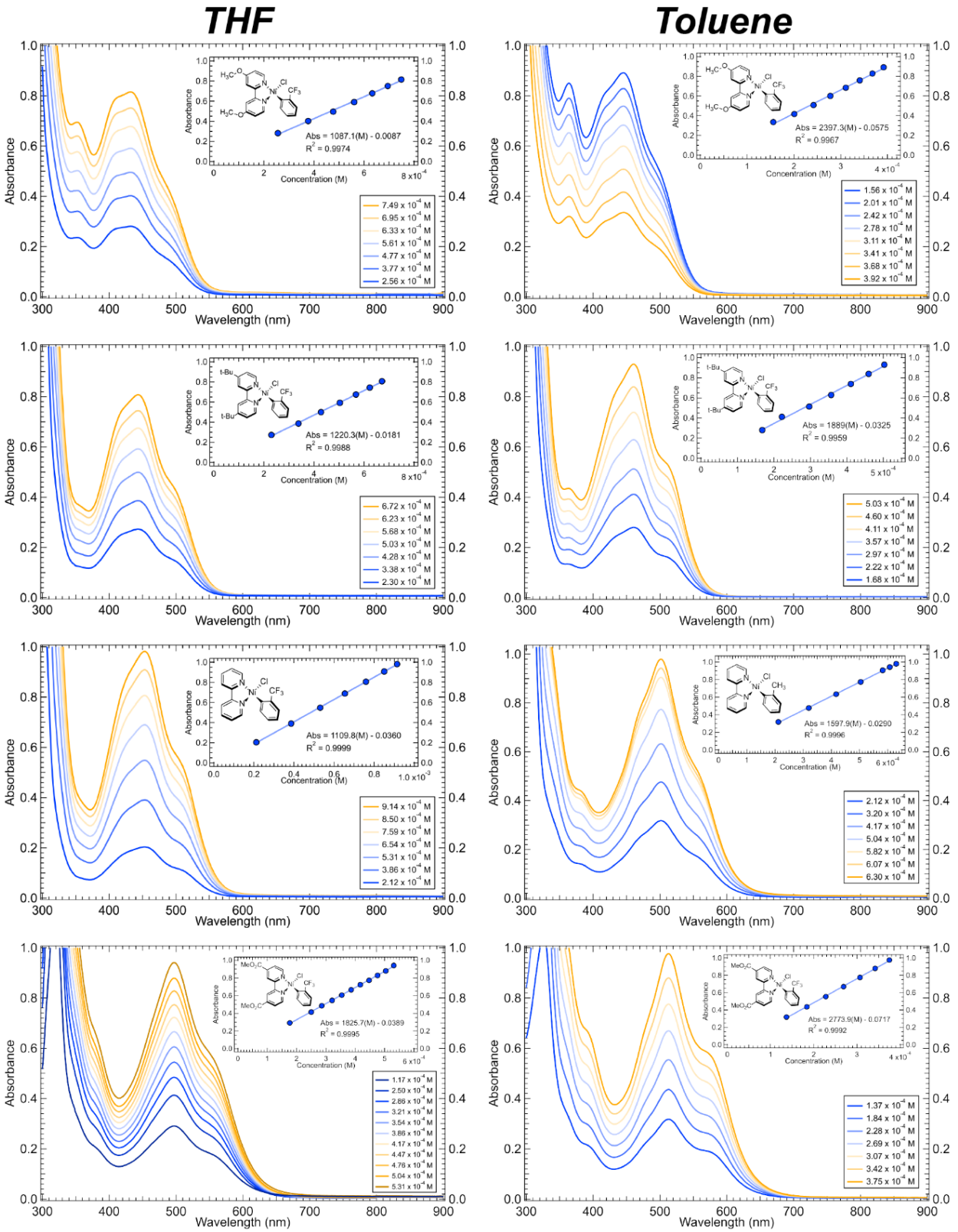

Figure S9. Concentration dependent UV-vis spectra in THF (left) and toluene (right) for **5A**–**5D**. Single wavelength molar absorptivity calibration curves are given as insets on each plot.

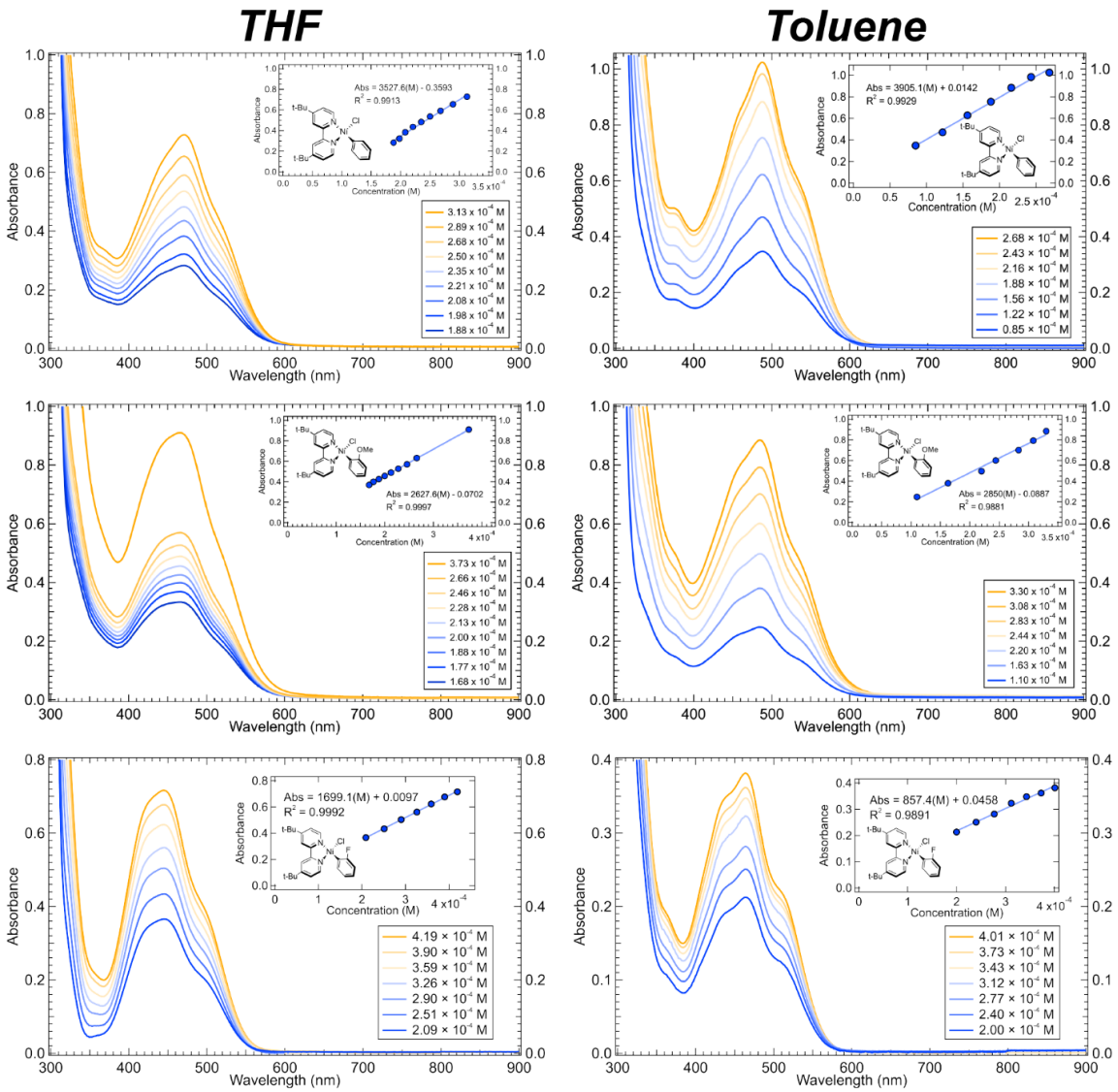

Figure S10. Concentration dependent UV-vis spectra in THF (left) and toluene (right) for **2B**–**4B**. Single wavelength molar absorptivity calibration curves are given as insets on each plot.

Table S1. Summary of molar extinction coefficients for **1A-5D** in THF and Toluene.

	Solvent = Tetrahydrofuran		Solvent = Toluene	
Compound	**MLCT λ_{max} (nm)**	**ε (M^{-1} cm^{-1})**	**MLCT λ_{max} (nm)**	**ε (M^{-1} cm^{-1})**
1A	462	3640	479	2000
1B	475	4970	493	3790
1C	483	4070	502	1600
1D	532	5259	551	1637
2B	471	3530	489	3905
3B	464	2660	479	2000
4B	447	1699	463	857
5A	432	1090	445	2400
5B	443	1220	461	1890
5C	453	1110	470	930
5D	497	1830	513	2370

S1.6. Photolysis Experiments.

We sought to confirm the formation of aryl radicals upon irradiation of our complexes. To do this, we selected the well characterized compound, **1B**,[2,5,7] as well as the novel compound, **5B**. These span a wide range of photolysis rates and are representative of the entire matrix of complexes, **1A-5D**. Solutions of **1B** and **5B** were prepared in the glovebox (solvent = THF-d_8) and transferred to J-Young tubes. Samples were placed 5 cm away from the Kessil PR160L 390 nm light source, as was typical for a photolysis experiment. Irradiation of **1B** in afforded the previously identified radical products, toluene, 2-(o-tolyl)tetrahydrofuran, and 2,2'-dimethyl-1,1'biphenyl (see Figure S11).[5] A concomitant loss of the diagnostic methyl singlet of the *o*-tolyl group at 3.0 ppm was observed. Similarly, the characteristic bipyridine peaks also decrease in intensity, illustrating the loss of the diamagnetic starting material (Figure S12). In the absence of light, however, no degradation of the starting material is observed. At elevated temperatures (55 ^{o}C), only minimal degradation is seen. However, thermal degradation does not result in the new product formation, evidenced by the lack of peak formation at 660 nm (Figure S13).

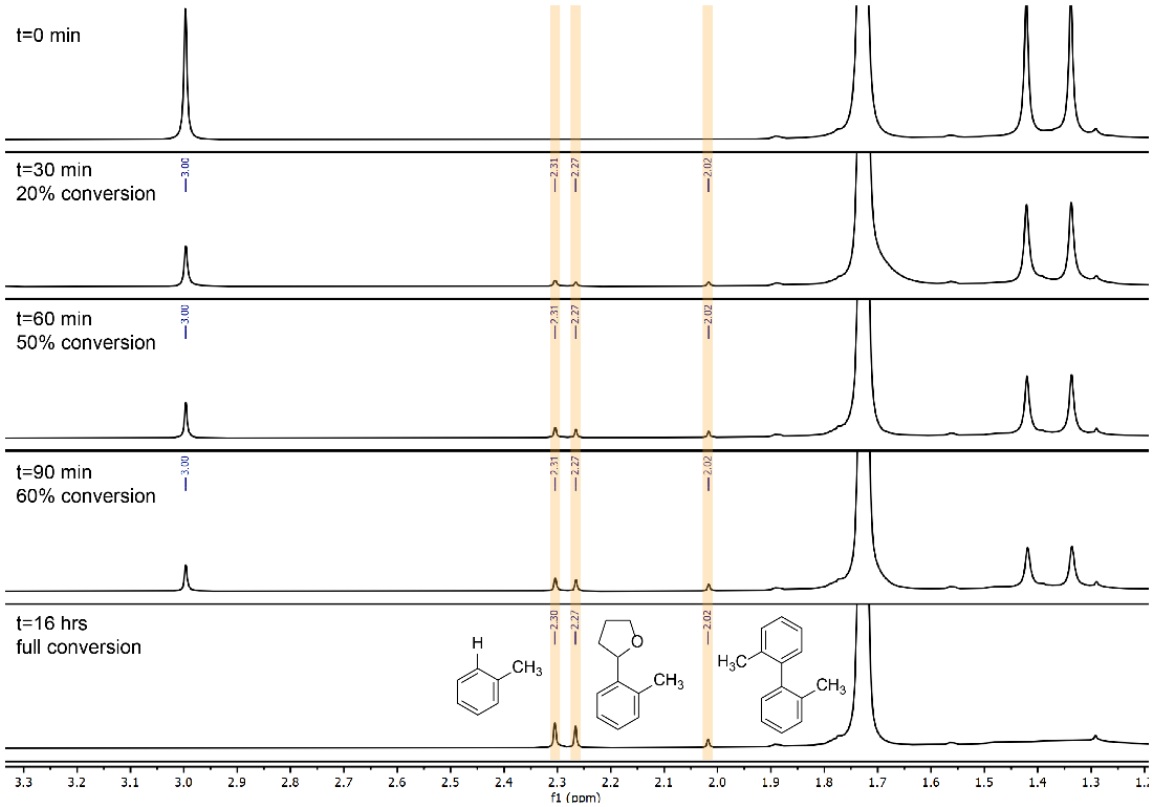

Figure S11. Aliphatic region ^{1}H NMR spectra of the irradiation of **1B** in THF-d_8 over time. Aryl radical products are observed at 2.3, 2.27, and 2.02 ppm.

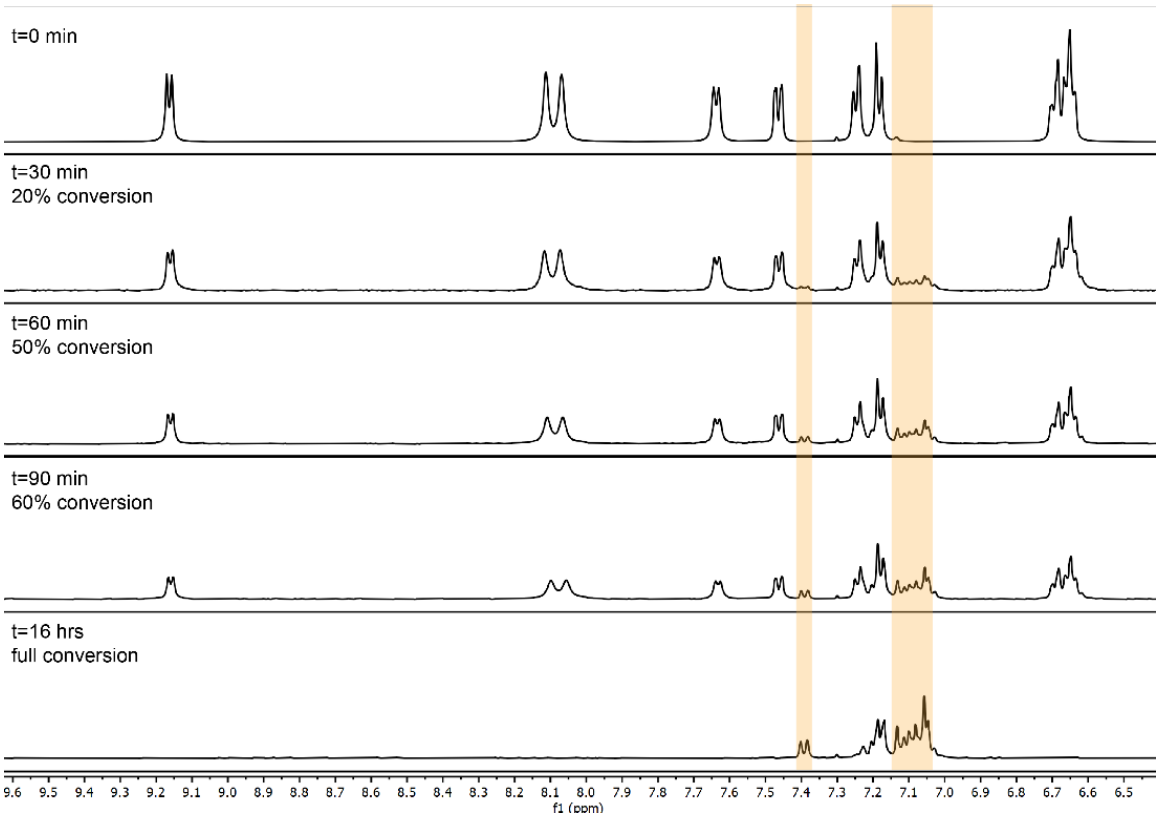

Figure S12. Aromatic region ^{1}H NMR spectra of the irradiation of **1B** in THF-d_8 over time. Starting material peaks give way to aryl radical products (highlighted in yellow).

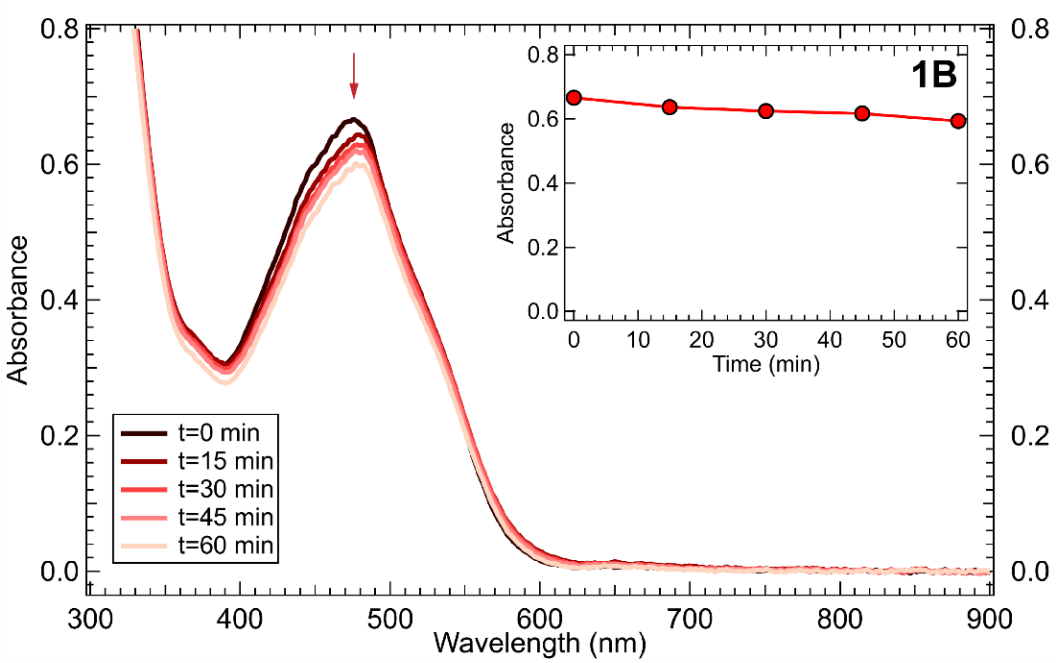

Figure S13. Thermal degradation of **1B** in THF at 55 °C monitored over an hour. Approximately 10% of the starting material is lost, but no new feature at 660 nm (or elsewhere) is seen.

We also tracked the photolysis of **5B** by ^{19}F NMR, identifying the aryl radical products, α,α,α-trifluorotoluene and 2-(2-(trifluoromethyl)phenyl)tetrahydrofuran upon irradiation (Figure S14). The homo-coupled bis-aryl product was not seen, likely the result of the slower photolysis rate for **5B**. Lower production of radicals more significantly impacts the rate of formation of the bis-aryl as it is a second-order kinetic product.

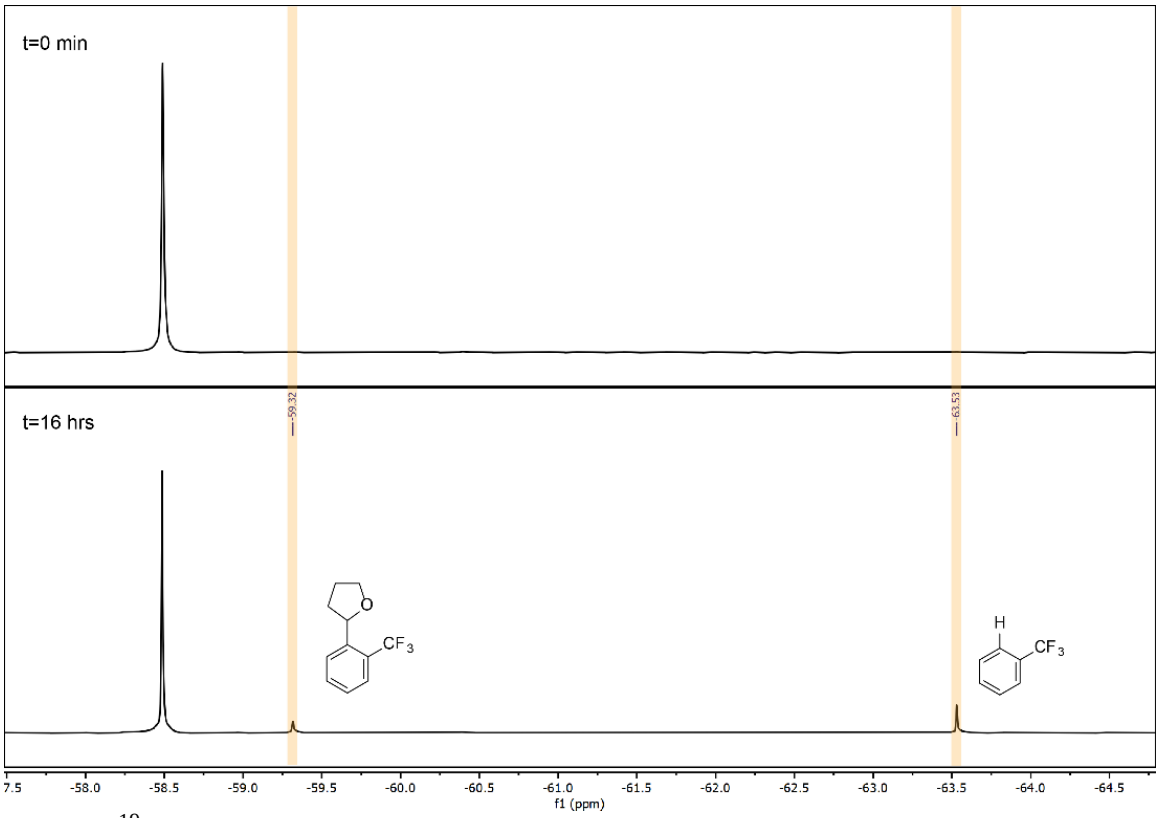

Figure S14. ^{19}F NMR spectra of the irradiation of **5B** in THF-d_8 over time. Starting material peaks give way to aryl radical products (highlighted in yellow).

Finally, we investigated the photolysis of the pre-catalyst compounds, Ni(TMEDA)($^{R'}$Ph)Cl, (R′ = CH_3, CF_3). Although these compounds do not contain π* acceptor orbitals to facilitate a metal-to-ligand charge transfer, we noted a spin-allowed ligand field band at 470 and 483 nm, for CH_3 and CF_3 respectively (Figure S15). We conceptualized a possible ligand field [Ni d → d(x^2-y^2)] transition, followed by a ligand-to-metal electron transfer step [bonding d(x^2-y^2)/C(sp^2) → Ni d], which would result a reduction of the Ni(II)–C bond order and subsequent bond cleavage. Irradiation of the complexes with 390 nm incident light produces an insoluble precipitate which coats the cuvette walls with an opaque film. Accordingly, we observe an increase in the peak maxima upon irradiation due to light scattering effects (Figure S16). Note that similar behavior is seen when irradiating nearer to the peak maxima (using incident light of 456 nm).

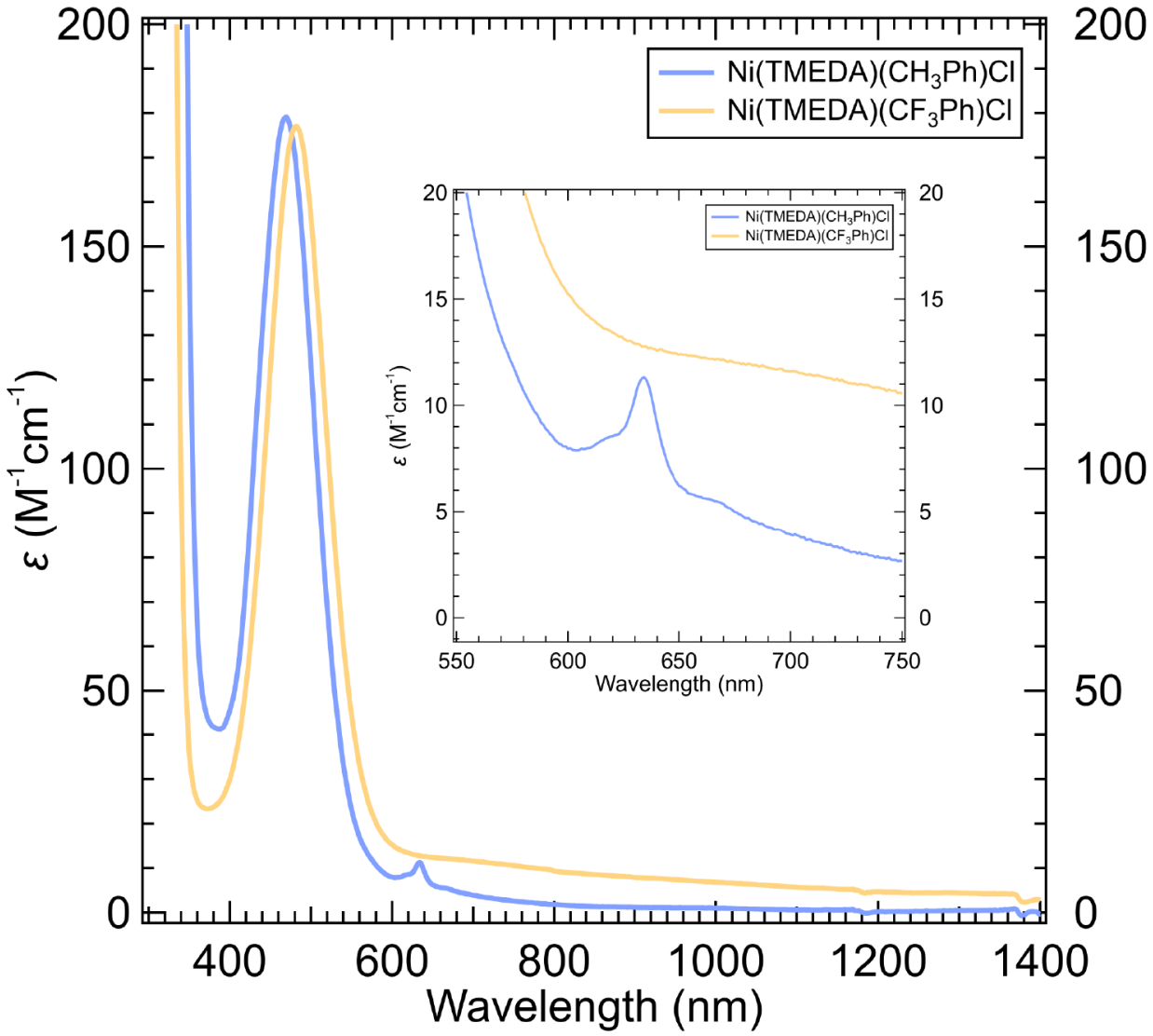

Figure S15. UV-vis absorption spectra of Ni(TMEDA)(CH_3Ph)Cl (blue line) and Ni(TMEDA)(CF_3Ph)Cl (orange line) on a molar absorptivity scale. There is a small peak at 635 nm in the *o*-tolyl complex, likely owing to a spin-forbidden ^{3}(d-d) transition (ε = 5-10 M^{-1} cm^{-1} when accounting for the shift in the baseline). TD-DFT assigns the singlet transition as $^1[d(z^2) \rightarrow d(x^2\text{-}y^2)]$; the triplet transition is assigned as $^3[d(xz) \rightarrow d(x^2\text{-}y^2)]$. Computational details are given in Table S10.

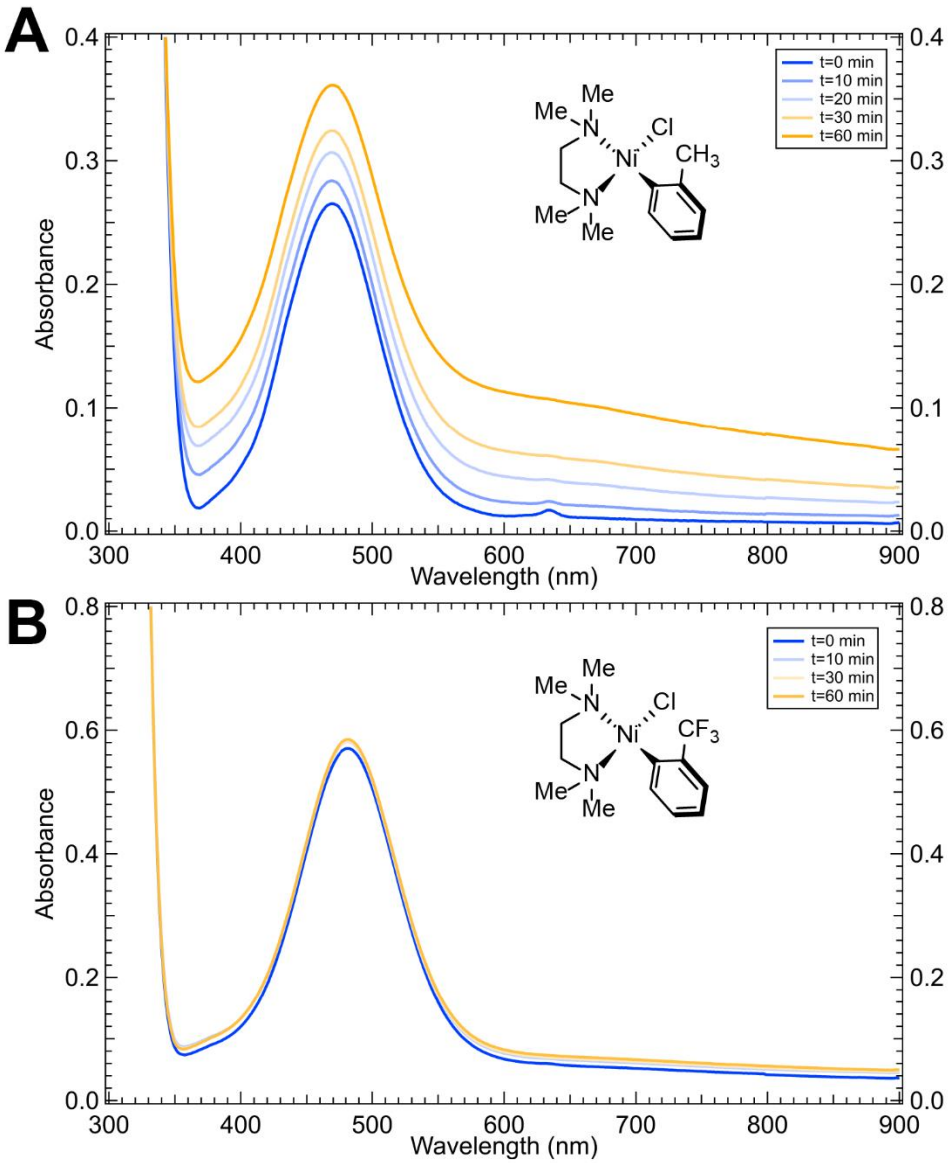

Figure S16. Irradiation of Ni(TMEDA)(CH_3Ph)Cl (panel A) and Ni(TMEDA)(CH_3Ph)Cl (panel B) using 390 nm light. Note the peak increase in both cases is likely the result of scattering upon precipitation of an insoluble species.

In the same fashion as for **1B** and **5B**, we dissolved these TMEDA complexes in THF-d_8, transferred them to air-tight J-Young tubes, and subjected them to irradiation with 390 nm light. Herein we observed the formation of the same radical products identified previously by NMR, albeit at slower rates (Figure S17-S18). Therefore, these pre-catalyst complexes can undergo light-induced homolysis of the Ni–C bond, likely utilizing the ^{1}(d-d) state described previously. Indeed, Park et al. found repulsive ^{1}(d-d) → ^{3}LMCT photolysis pathways in related Ni(II) complexes.[8]

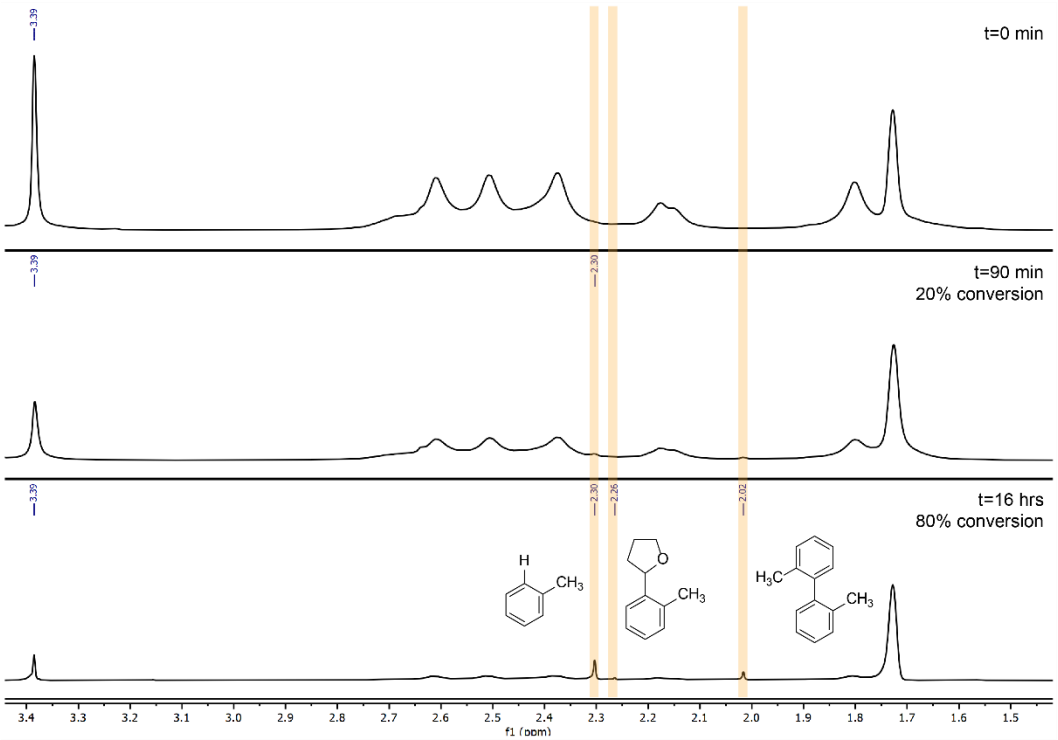

Figure S17. Aliphatic region ^{1}H NMR spectra of the irradiation of Ni(TMEDA)(CH_3Ph)Cl in THF-d_8 over time. Aryl radical products are observed at 2.3, 2.26, and 2.02 ppm.

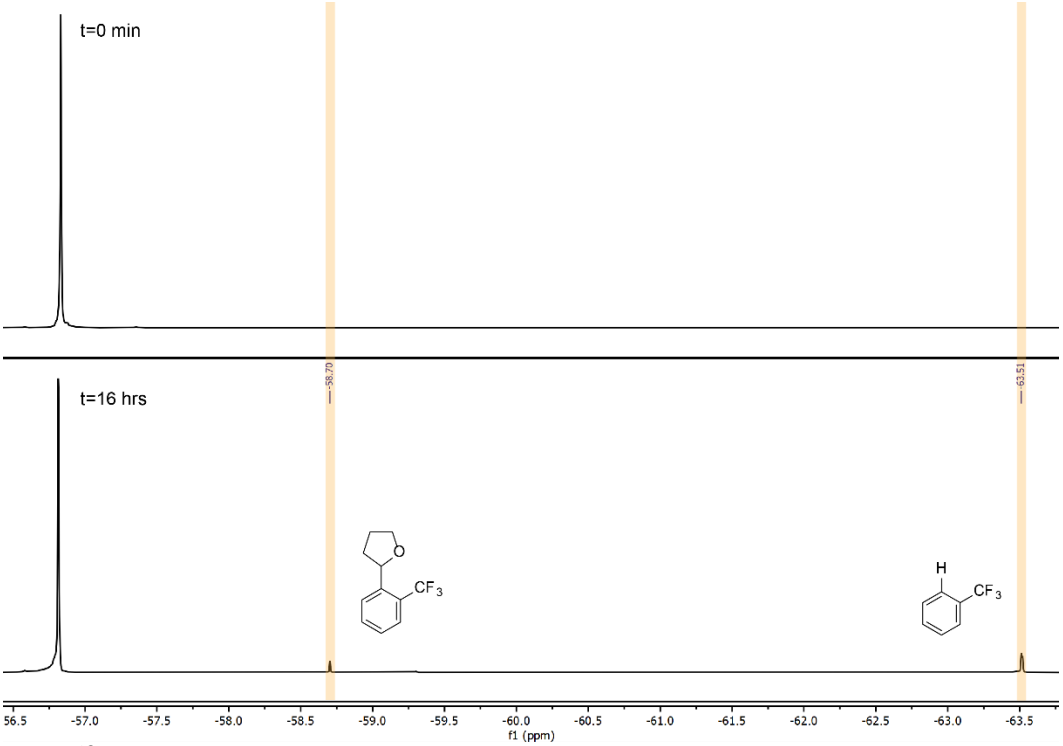

Figure S18. ^{19}F NMR spectra of the irradiation of Ni(TMEDA)(CF_3Ph)Cl in THF-d_8 over time. Starting material peaks give way to aryl radical products (highlighted in yellow).

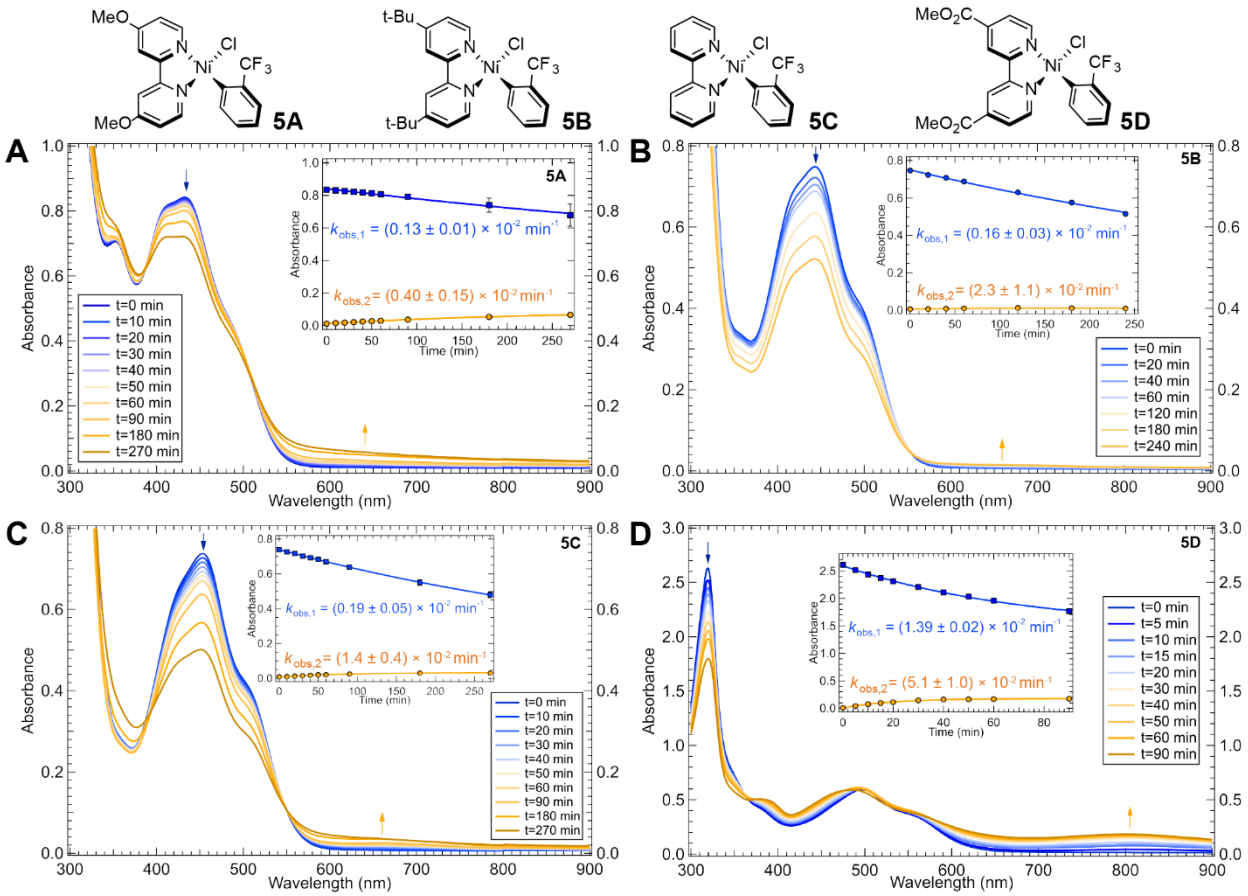

Figure S19. Photolysis profiles of **5A**–**5D** in THF for 390 nm excitation. Photolysis kinetics were monitored at two wavelengths indicated by the blue and orange arrows in each panel. Insets correspond to the fitted kinetic data (blue curve for the decay of the starting material, orange curve for the formation of the new species). Data were fit using a single exponential; error bars are one standard deviation.

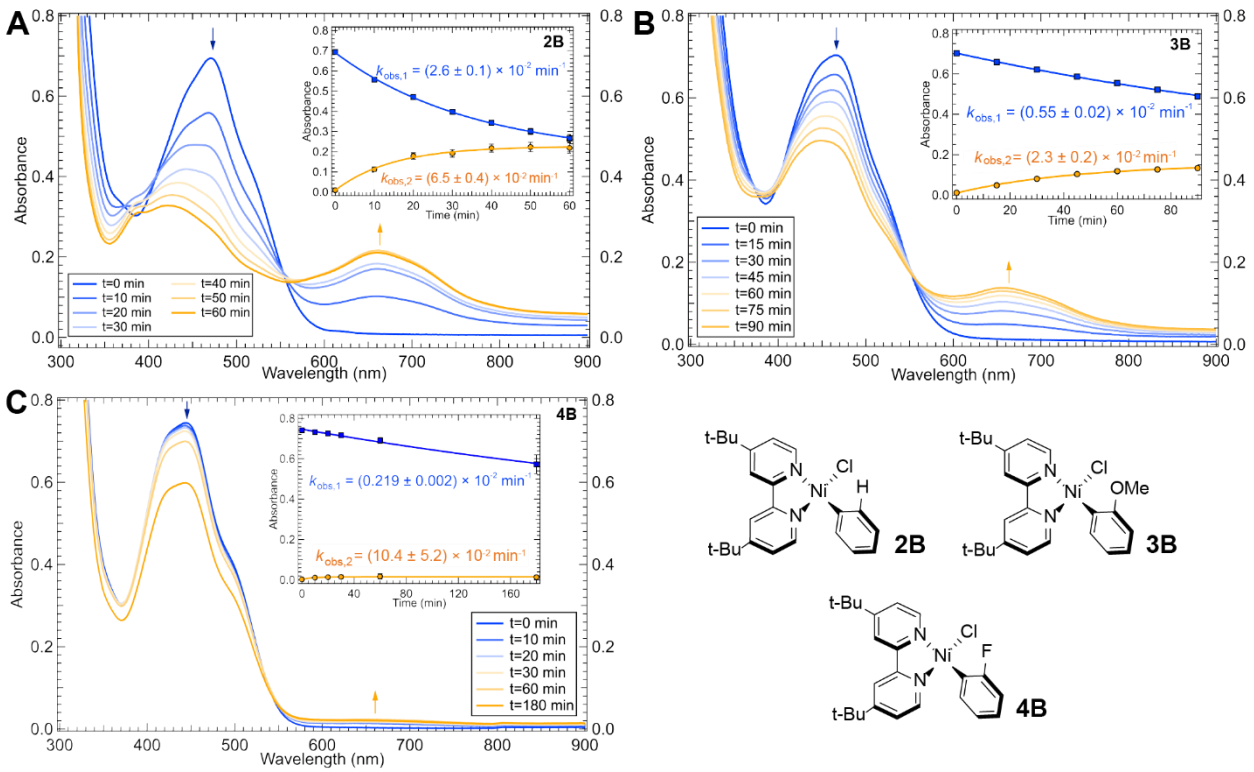

Figure S20. Photolysis profiles of **2B**–**4B** in THF using 390 nm excitation. Photolysis kinetics were monitored at two wavelengths indicated by the blue and orange arrows in each panel. Insets correspond to the fitted kinetic data (blue curve for the decay of the starting material, orange curve for the formation of the new species). Data were fit using a single exponential; error bars are one standard deviation.

S1.7. Wavelength Dependence Studies.

We undertook wavelength dependence studies on **1B**, **1D**, and **5D**. Samples were prepared following standard protocol: solutions were prepared in the glovebox in THF, distributed into cuvettes with an air-tight seal, then placed 5 cm away from the Kessil PR160L LED light source (incident light λ_{max} = 390 nm, 427 nm, 456 nm, and 525 nm) on maximum intensity. Measured power using a Thorlabs S425C thermal detector power meter at 5 cm distance from the LED are as follows: 390 nm (0.49 W), 427 nm (0.54 W), 456 (0.54 W), and 525 nm (0.25 W). The emission spectra of these LEDs are given in Figure S21; sample photochemical setup is given in Figure S1. In all cases, there is a clear wavelength dependence observed on the photolysis step; with lowest energy incident light unable to initiate the Ni–C bond cleavage.

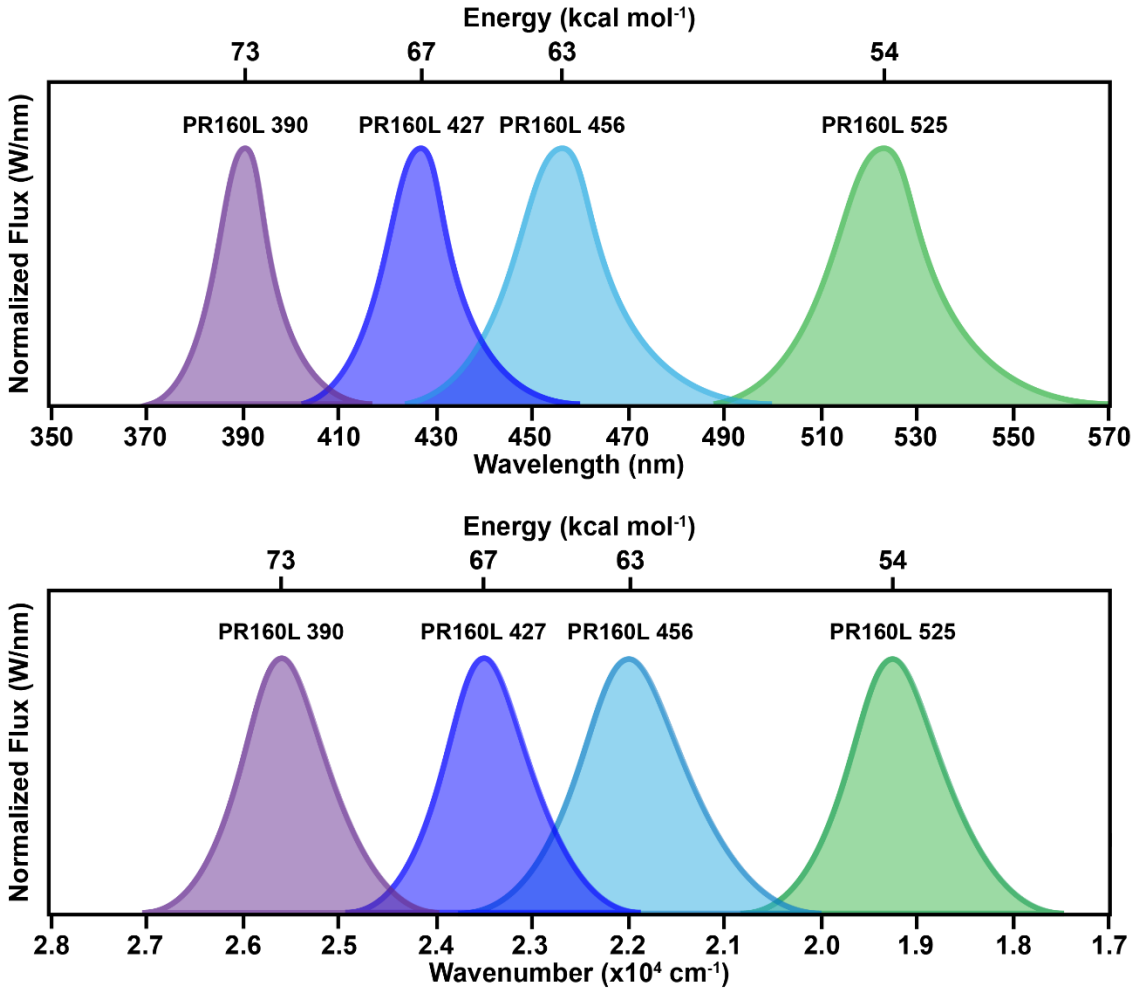

Figure S21. Kessil PR160L emission spectra with peak width as given by the manufacturer. Energy markers (kcal mol^{-1}) are given at the peak maxima.

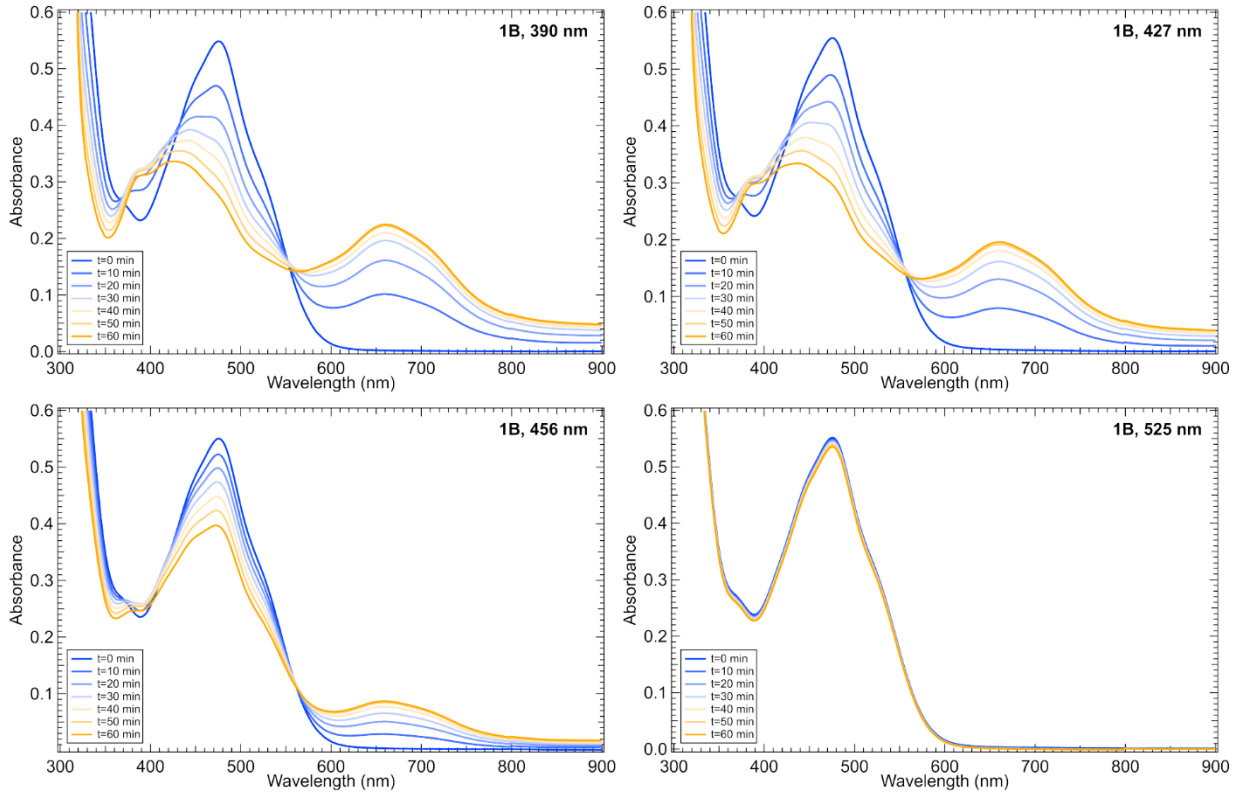

Figure S22. Wavelength dependent photolysis of **1B** in THF.

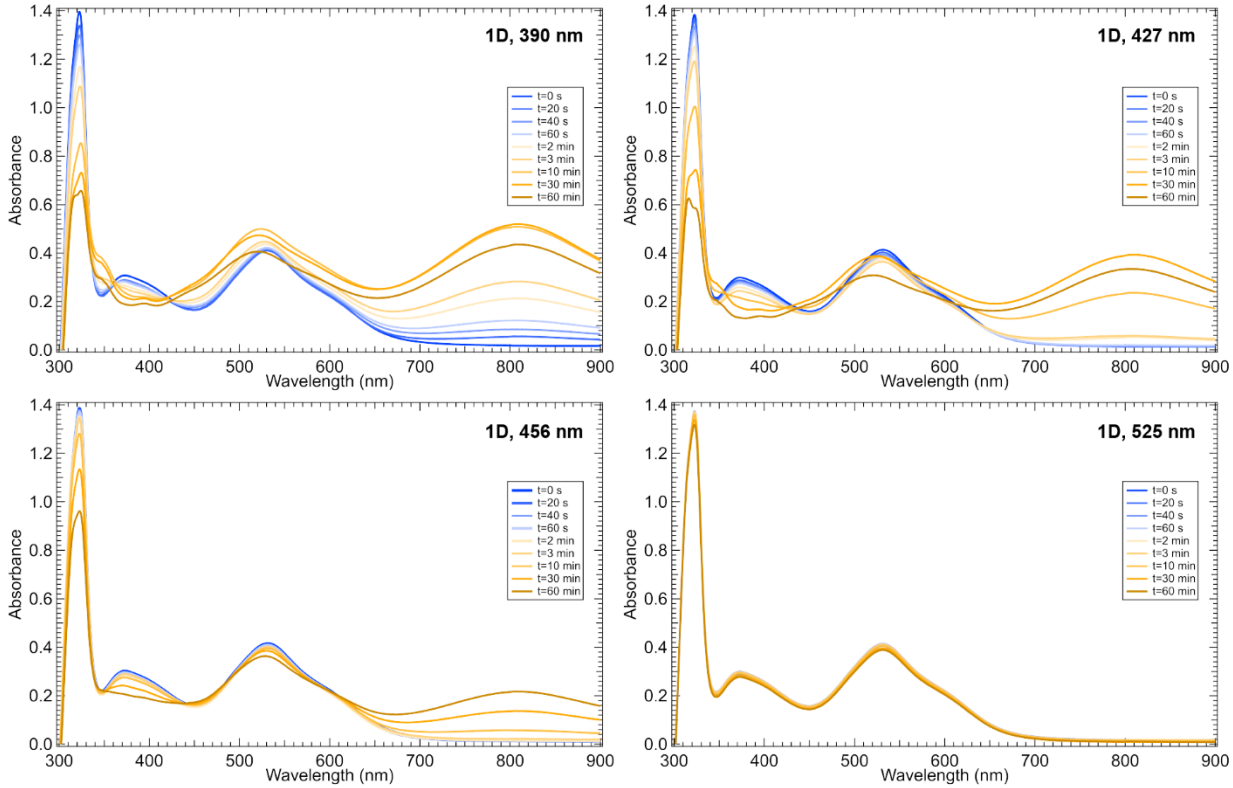

Figure S23. Wavelength dependent photolysis of **1D** in THF.

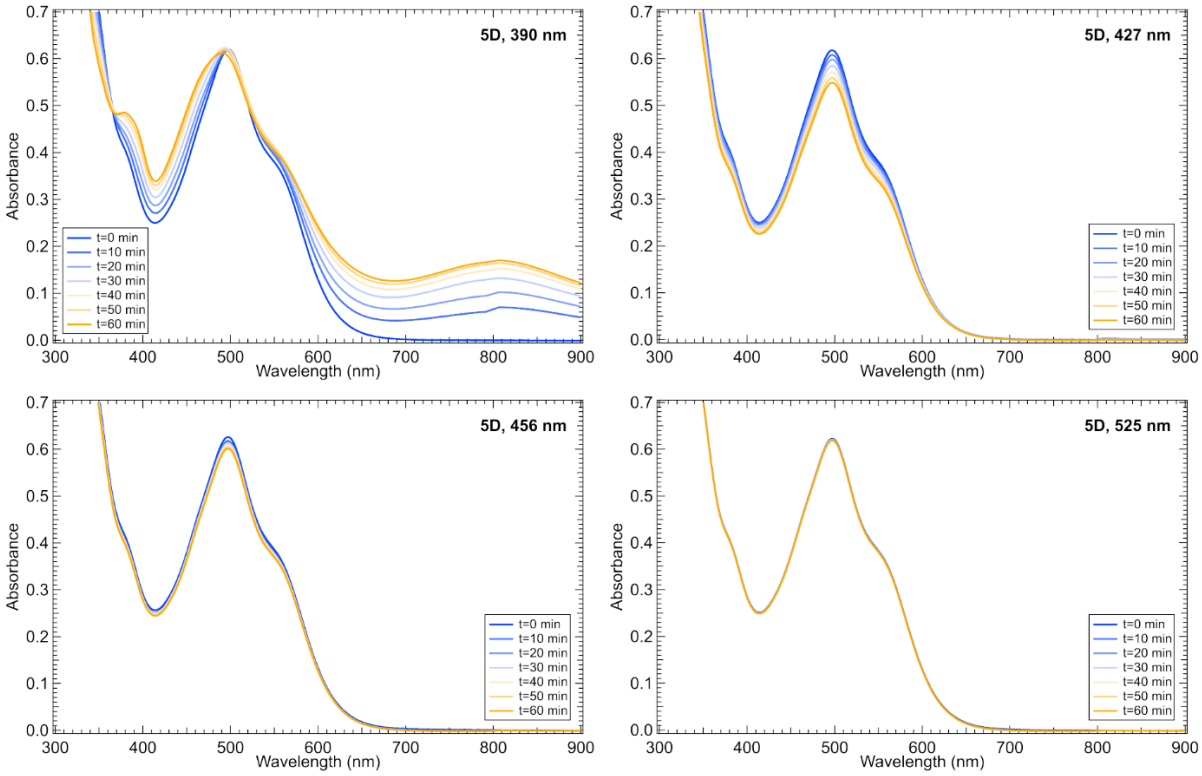

Figure S24. Wavelength dependent photolysis of **5D** in THF.

To more fully account for the wavelength-dependent behavior, wavelength-dependent quantum yields can be considered. Quantum yields account for power variance among the four LEDs used and the differential absorbance at each wavelength irradiated. For a more complete description of the quantum yield determination, refer to Supporting Information Section S1.11. Importantly, the wavelength-dependent quantum yields suggest the same conclusion as the kinetic fits (main text Figure 8 and Figure S25).

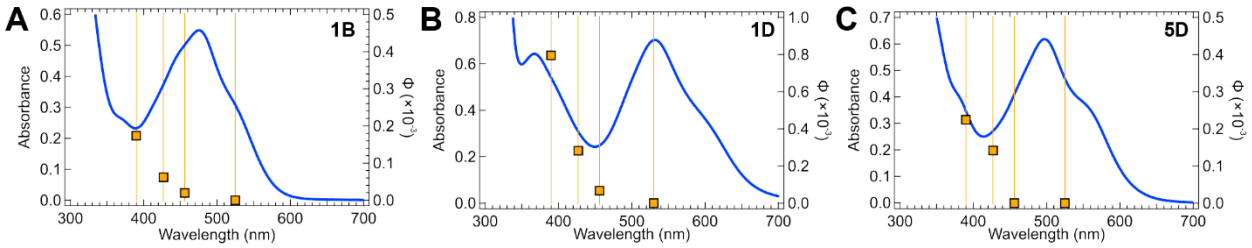

Figure S25. Wavelength-dependent photolysis for **1B**, **1D**, and **5D**. The absorption spectra are shown in blue; the observed photolysis quantum yields (squares) and incident wavelengths are given in orange. Quantum yields were calculated at each wavelength using equation S7.

S1.8. Thermal Dependence Studies – Eyring Analysis.

Temperature dependent photolyses allowed for the experimental determination of the barrier for light-induced Ni–C bond homolysis. The rate of the initial excitation step (MLCT) is negligible given the time scales of these experiments, so the bond-breaking step is rate determining. A plot of $\ln(k_{1,obs})/T$ versus 1/T gives a line. We examined the well-characterized complexes, **1B** and **1B–Br**. Samples were prepared as is typical for our photolysis experiments. Cuvettes were suspended in a large water bath kept at specific temperatures. Samples were allowed to equilibrate with the water bath before irradiation was begun. Example setup is given in Figure S1.

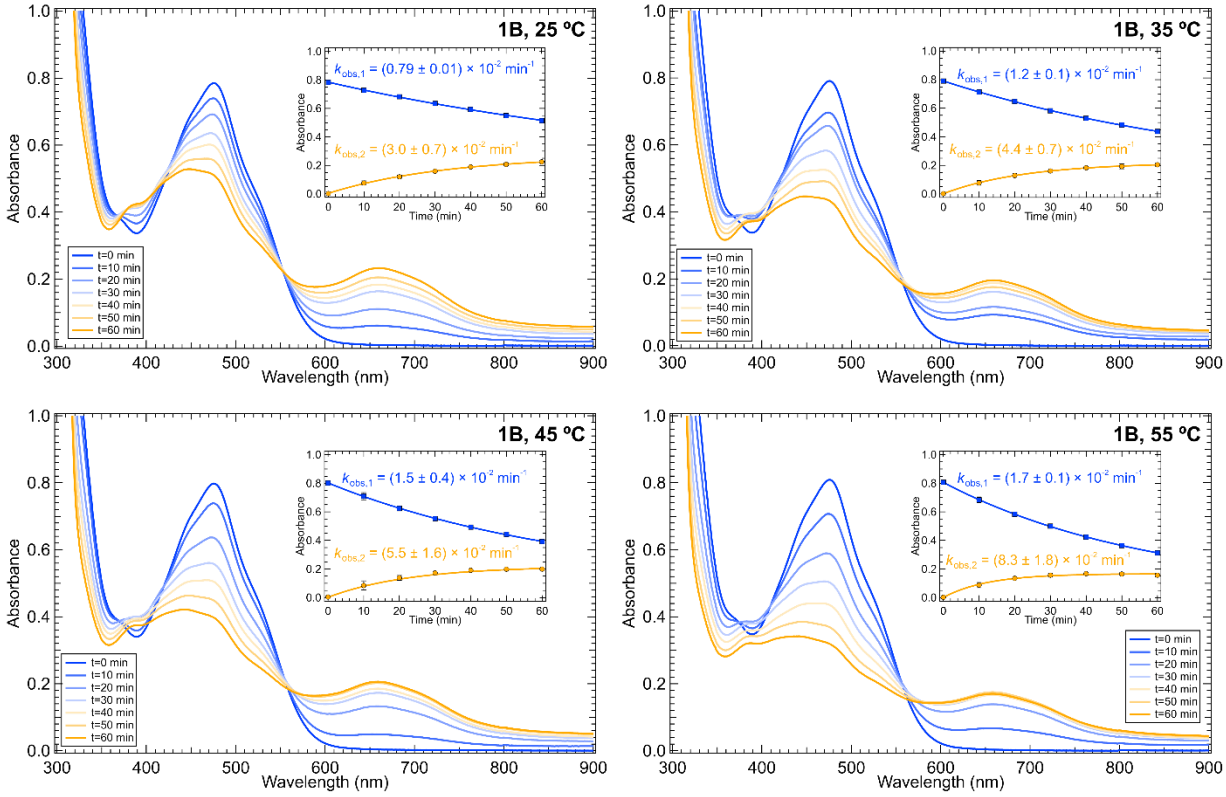

Figure S26. Thermal dependence on photolysis rate for **1B** in THF monitored at the λ_{max} of the starting compound, 475 nm, and the new peak, 660 nm.

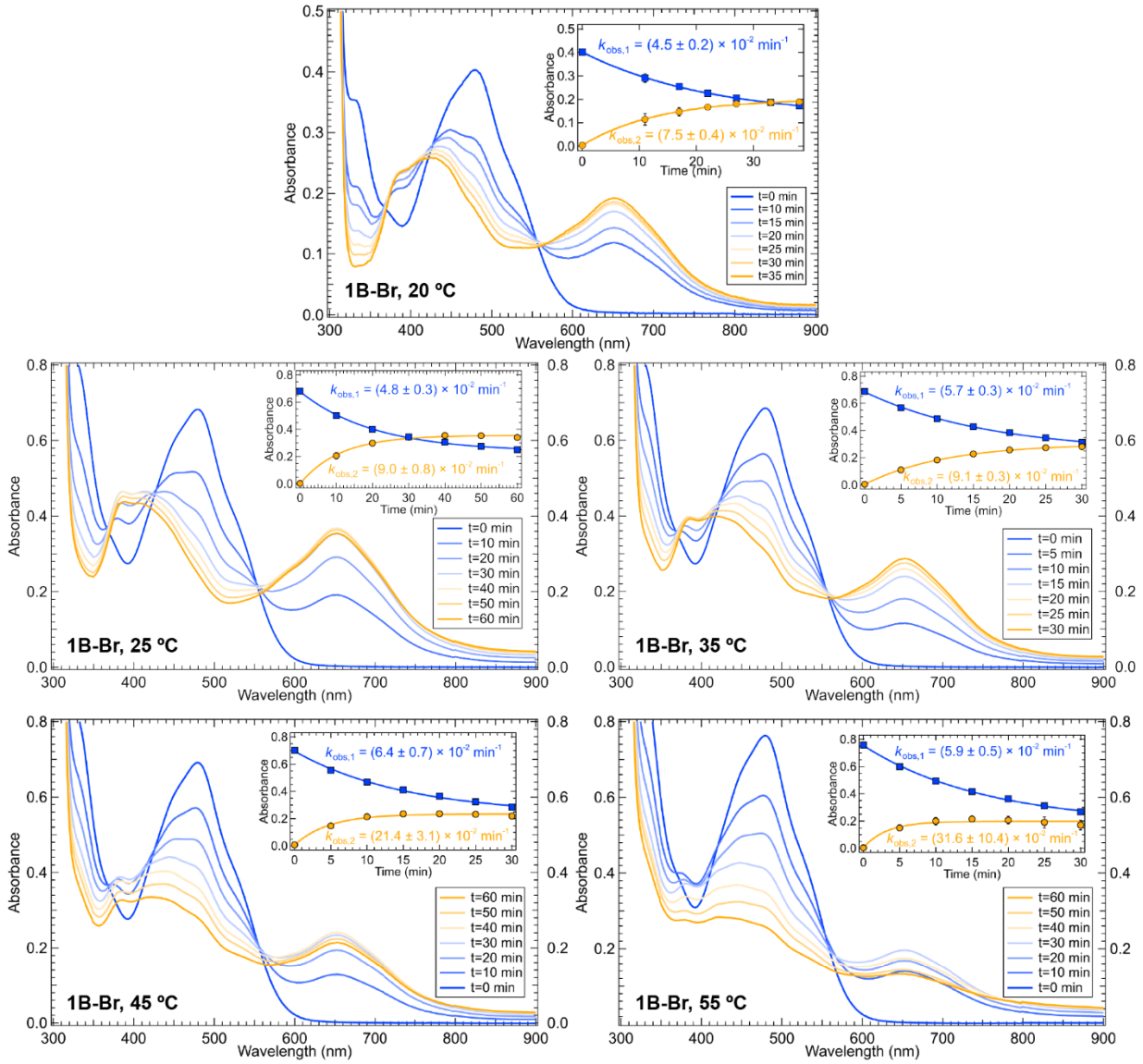

Figure S27. Thermal dependence on photolysis rate for **1B–Br** in THF monitored at the λ_{max} of the starting compound, 479 nm, and the new peak, 653 nm. Note that the thermal decomposition contributions are much more pronounced at 55 °C, causing a lack of linearity in the final Eyring analysis.

We observed linear behavior for **1B** at all temperatures studied, but a loss of linearity for **1B–Br** at the highest temperature utilized. This change in behavior is likely due to thermal degradation of the sample and was omitted from the final Eyring analysis (note that loss of linearity at high temperatures has also been seen by Bird et. al for the same complex).[9] Interestingly, a thermal dependence on the decomposition of the product species was also observed. Current work is underway to further investigate this new species, including the decay rate, barrier of formation, reactivity, and further characterization of the resulting compound.

S1.9. Global Analysis Modeling of Kinetics.

The single wavelength exponential fits used in the main text may contain spectral overlap of the starting material and the photolysis product. Additionally, they cannot explain the systematic difference between $k_{1,obs}$ and $k_{2,obs}$. To account for these additional complexities, time-resolved photolysis absorbance data were fit to global kinetic models using in-house Matlab scripts patterned after established programs.[10,11] Global kinetics modeling enables calculation of a unique molar absorptivity curve for each absorbing species in the reaction, thereby addressing potential spectral overlap. Global kinetics also calculates rate constants for elementary reaction steps (k_p and k_d in Scheme S2), whereas $k_{2,obs}$ depends on multiple elementary reaction steps (*vide infra*). The global kinetics modeling supports all the conclusions of the single-wavelength fits, but displays moderately increased uncertainty due to the larger number of parameters to be fit. Therefore, we elected to employ $k_{1,obs}$ in the main text.

Initial screening of the data by singular value decomposition (SVD) suggests that at least two absorbing species are required in a general kinetic model, in agreement with the two isosbestic points visible in many of the datasets. Both two- and three-absorber kinetic models were tested, but the molar absorptivity curves of the third component tended to duplicate the profiles from the first two species. We therefore employed two absorbing species in our kinetic models. Spectral non-negativity was enforced by truncation, and all rate constant fits were started from multiple initial guesses to ensure robust convergence of the nonlinear optimizer. Numerical integration was performed with the *ode15s* stiff solver to eliminate numerical noise. Initial concentration conditions were obtained using the experimental molar absorptivity coefficients from S1.5.

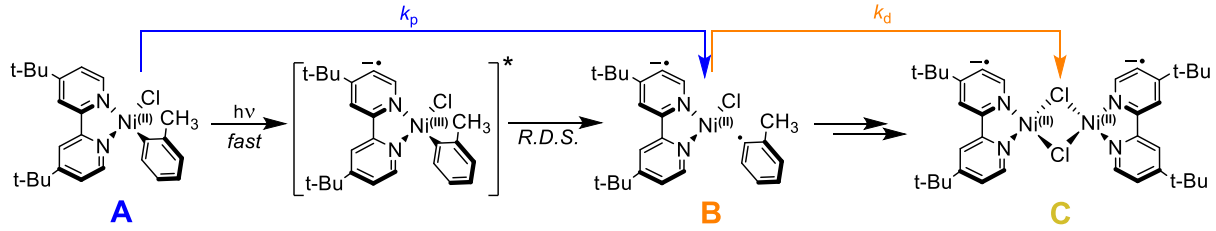

Scheme S2. Reaction pathway modeled using global analysis showing the photolysis of **1B** as an example. We use k_p for the photolysis step and k_d for the decay step in this model. The decomposition product, ***C***, is shown as the formal Ni(I)bpy halide-bridged dimer,[12] but its exact identity has not yet been confirmed; investigations are ongoing.

Though two absorbing species can account for the observed data, a simple [$\boldsymbol{A} \rightarrow \boldsymbol{B}$] model provides a poor fit to the kinetics. This is manifest in the disparate values of $k_{1,obs}$ and $k_{2,obs}$ obtained by exponential fitting to single wavelength traces (Table 1, main text Figure 4, Figure S19-S20). We therefore tested a variety of kinetic models involving a third species, (***C***), which does not absorb in the visible region, forming from either the starting material or the photolysis product. The absorptivity of ***C*** was constrained to be zero over the wavelength range investigated (300-900 nm). Table S2 quantifies the goodness of fit of each model via the root-mean-square of the residual absorbance matrix (RMSR). As the RMSR values for the [$\boldsymbol{A} \rightarrow \boldsymbol{B}$, $\boldsymbol{B} \rightarrow \boldsymbol{C}$] and [$\boldsymbol{A} \rightarrow \boldsymbol{B}$, $2\boldsymbol{B} \rightarrow \boldsymbol{C}$] models are very similar in all cases, these two models are analyzed as a pair; similarly for the models [$\boldsymbol{A} \rightarrow \boldsymbol{C}$, $\boldsymbol{C} \rightarrow \boldsymbol{B}$] and [$\boldsymbol{A} \rightarrow \boldsymbol{C}$, $2\boldsymbol{C} \rightarrow \boldsymbol{B}$].

Table S2. Root-mean-square of the residuals (RMSR) for seven kinetic models (Abs). ***A*** represents the starting material, ***B*** represents an absorbing product, and ***C*** represent a non-absorbing product. The best pair of overall models is surrounded by a dark black border; the best pair of models for each particular dataset highlighted in green.

Dataset	$A \rightarrow B$	$2A \rightarrow B$	$A \rightarrow B$ $A \rightarrow C$	$A \rightarrow B$ $B \rightarrow C$	$A \rightarrow B$ $2B \rightarrow C$	$A \rightarrow C$ $C \rightarrow B$	$A \rightarrow C$ $2C \rightarrow B$
1A	1.75×10^{-2}	1.78×10^{-2}	1.75×10^{-2}	1.42×10^{-2}	1.35×10^{-2}	1.75×10^{-2}	1.77×10^{-2}
1B	9.24×10^{-3}	9.15×10^{-3}	9.24×10^{-3}	2.40×10^{-3}	2.39×10^{-3}	9.20×10^{-3}	8.31×10^{-3}
1C	6.61×10^{-3}	7.13×10^{-3}	6.61×10^{-3}	6.61×10^{-3}	6.61×10^{-3}	3.56×10^{-3}	3.37×10^{-3}
1D	8.91×10^{-3}	1.18×10^{-2}	8.91×10^{-3}	8.81×10^{-3}	8.17×10^{-3}	7.76×10^{-3}	8.17×10^{-3}
2B	9.93×10^{-3}	9.79×10^{-3}	9.93×10^{-3}	3.71×10^{-3}	3.84×10^{-3}	9.85×10^{-3}	9.97×10^{-3}
3B	4.79×10^{-3}	4.78×10^{-3}	4.79×10^{-3}	1.50×10^{-3}	1.40×10^{-3}	4.79×10^{-3}	4.65×10^{-3}
4B	3.20×10^{-3}	3.58×10^{-3}	3.20×10^{-3}	2.02×10^{-3}	1.96×10^{-3}	3.20×10^{-3}	3.25×10^{-3}
5A	2.55×10^{-3}	2.75×10^{-3}	2.55×10^{-3}	2.54×10^{-3}	2.54×10^{-3}	2.55×10^{-3}	2.54×10^{-3}
5C	7.58×10^{-3}	7.78×10^{-3}	7.58×10^{-3}	7.58×10^{-3}	7.58×10^{-3}	3.41×10^{-3}	3.43×10^{-3}
5D	8.10×10^{-3}	8.49×10^{-3}	8.10×10^{-3}	5.25×10^{-3}	5.21×10^{-3}	8.12×10^{-3}	8.09×10^{-3}
1B–Br	4.46×10^{-3}	4.61×10^{-3}	4.46×10^{-3}	2.72×10^{-3}	2.65×10^{-3}	4.36×10^{-3}	4.11×10^{-3}

Table S2 shows evidence that the non-absorbing third species (***C***) forms in sequence after the monomeric photolysis product. When the non-absorbing species is included along either a branching pathway (e.g. [$\boldsymbol{A \rightarrow B}$, $\boldsymbol{A \rightarrow C}$]) or included prior to the formation of monomer, ***B*** (e.g. [$\boldsymbol{A \rightarrow C}$, $\boldsymbol{C \rightarrow B}$]), the RMSR is worsened in most cases. Datasets **1C**, **1D**, and **5C** provide exceptions to the general trend, in which the [$\boldsymbol{A \rightarrow C}$, $\boldsymbol{C \rightarrow B}$] model provides an improved mathematical fit. The nearly equivalent RMSR values for the [$\boldsymbol{A \rightarrow B}$, $\boldsymbol{B \rightarrow C}$] and [$\boldsymbol{A \rightarrow B}$, $\boldsymbol{2B \rightarrow C}$] reaction models preclude conclusive identification of the chemical identity of ***C***. Although we speculate that ***C*** is the non-absorbing halide bridged dimeric species[12] shown in Scheme S2, this study is agnostic as to the identity of the decomposition product ***C***. Therefore, we elected to continue with the simplest possible kinetic model, namely the first-order decay [$\boldsymbol{A \rightarrow B}$, $\boldsymbol{B \rightarrow C}$]. Further studies to identify monomer decomposition products, dimer or otherwise, are ongoing.

Owing to the sequential mechanism, [$\boldsymbol{A \rightarrow B}$, $\boldsymbol{B \rightarrow C}$], the consumption of ***A*** can be described as a pure monoexponential decay, but the formation of the monomer product ***B*** is actually described by a sum of two exponentials expressing competing formation and decomposition processes.[13] That is, as a result of the competing supply and removal, ***B*** approaches steady state at a condition determined by the ratio of the elementary rate constants for photolysis, k_p [$\boldsymbol{A \rightarrow B}$] and decomposition, k_d [$\boldsymbol{B \rightarrow C}$]. The decomposition process truncates the rise of the monomer species and gives its concentration profile a sharper bend than would otherwise be obtained. The concentration of the monomer will begin to decrease if the reaction is run for a

sufficient amount of time. These effects can be seen in the modeled concentration profiles below in Figures S28–S39 (refer to the bottom left panels).

In the main text, $k_{obs,1}$ and $k_{obs,2}$ are monoexponential fits to the characteristic starting material and monomer absorbance features, respectively. If decomposition of the monomeric species is negligible, $k_{obs,1}$ and $k_{obs,2}$ should be nearly equal, and additionally the isosbestic points will show high fidelity. This is the case for the compound **1C**, for example (main text Figure 4C), which has $k_{obs,1}$ = 3.6 ± 0.6, and $k_{obs,2}$ = 2.9 ± 0.3, and comparatively clean isosbestic points. However, if the photoproduct's decomposition is significant, then the fitted value $k_{obs,2}$ will be elavated due to the increased curvature of the monomer's concentration profile. For example, compound **1B** (main text Figure 4B) exhbits this feature, and has $k_{obs,1}$ = 2.5 ± 0.2, and $k_{obs,2}$ = 7.6 ± 0.7, and a 400 nm isosbestic point showing substantial drift. Since the $k_{obs,2}$ constitutes a mono-exponential fit to a concentration profile that is not a true mono-exponential process, it is additionally likely that the $k_{obs,2}$ fits will display a higher variance than when fitting a mono-exponential function to a true mono-exponential concentration profile ($k_{obs,1}$).

This analysis indicates that $k_{obs,1}$ represents the truer rate of the bond homolysis process, while $k_{obs,2}$ is a convolution of the elementary rate constants k_p (photolysis) and k_d (decomposition) included in our global fitting kinetic model. We have therefore used $k_{obs,1}$ in our correlations of rate constants and electronic effects. We further note that k_p gives the same qualitative trends as $k_{1,obs}$ (Figure S40). Table S3 gives the optimized rate constants for the [$\boldsymbol{A} \rightarrow \boldsymbol{B}$, $\boldsymbol{B} \rightarrow \boldsymbol{C}$] reaction model.

Table S3. Optimized rate constants for the [$\boldsymbol{A} \rightarrow \boldsymbol{B}$, $\boldsymbol{B} \rightarrow \boldsymbol{C}$] reaction model compared to experimental data with first-order fits.

Dataset	$k_{obs,1}$ (x 10^{-2} min^{-1})	k_p [$A \rightarrow B$] (x 10^{-2} min^{-1})	k_d [$B \rightarrow C$] (x 10^{-2} min^{-1})
1A	*n.d.*[a]	0.9 ± 0.1	0.84 ± 0.2
1B	2.5 ± 0.2	4.1 ± 0.4	0.70 ± 0.03
1C	3.6 ± 0.6	3.3 ± 0.5	0
1D	17.0 ± 0.7	15.0 ± 0.8	0.27 ± 0.06
2B	2.6 ± 0.1	4.4 ± 0.1	0.64 ± 0.1
3B	0.55 ± 0.02	1.6 ± 0.1	0.32 ± 0.05
4B	0.219 ± 0.002	0.14 ± 0.18	4.9 ± 2.5
5A	0.13 ± 0.01	0.08 ± 0.03	0.003 ± 0.04
5B	0.16 ± 0.03	*n.d.*[b]	*n.d.*[b]
5C	0.19 ± 0.05	0.16 ± 0.01	0
5D	1.39 ± 0.02	3.0 ± 0.5	0.22 ± 0.05
1B–Br	6.9 ± 0.4	8.1 ± 0.8	0.26 ± 0.09

[a]Because the new species formed upon Ni(II)–C bond homolysis has absorption underneath that of the starting material, we were unable to obtain $k_{1,obs}$ for this compound. [b]Complex **5B** was omitted owing to poor convergence of the global kinetics model.

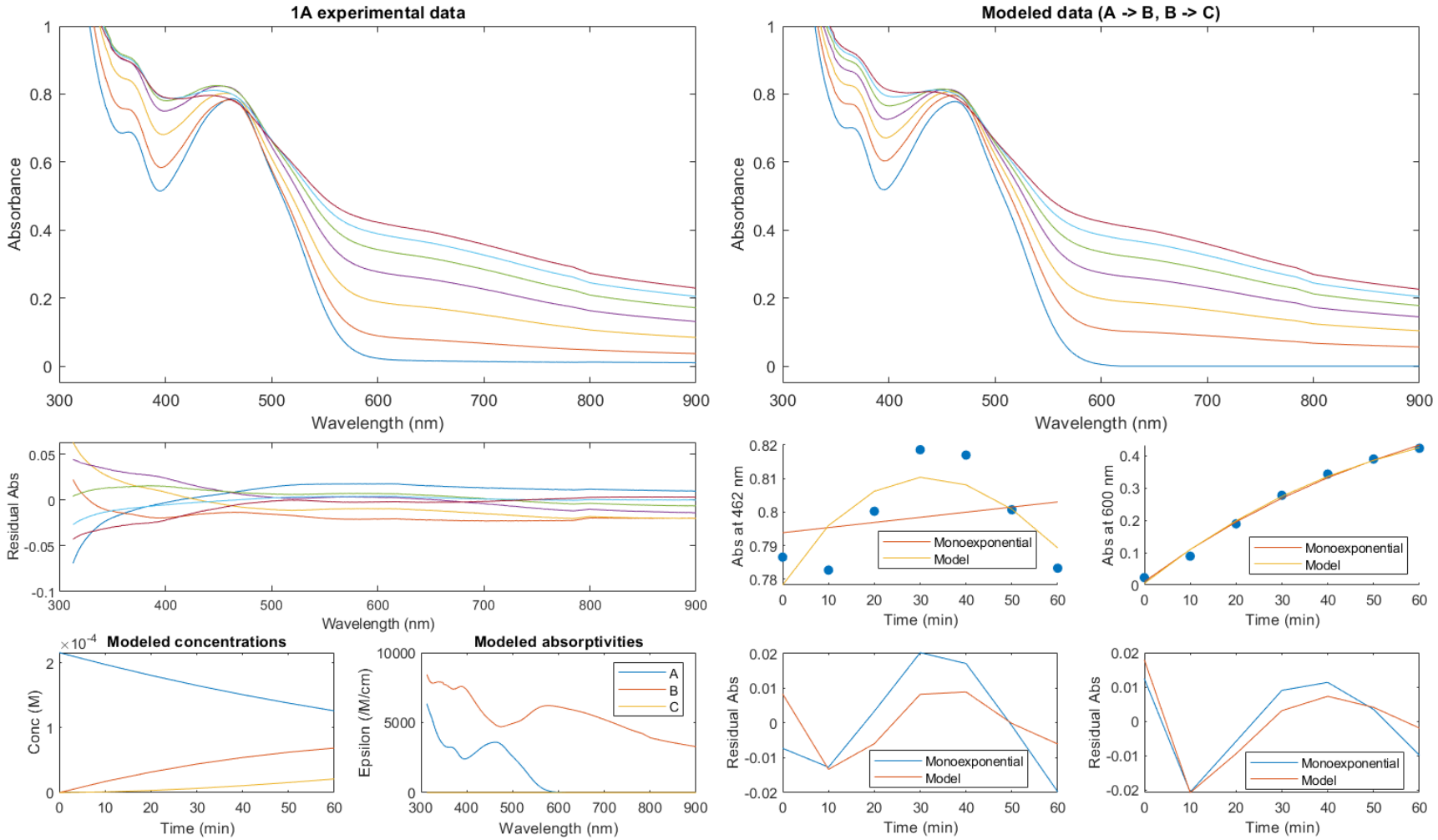

Figure S28. Kinetic modeling fit to **1A**. Top left: raw experimental absorbance data. Top right: absorbance data reproduced by the [$\boldsymbol{A \rightarrow B}$, $\boldsymbol{B \rightarrow C}$] kinetic model. Center left: model residuals as a function of wavelength. Bottom left: concentration profiles and molar absorptivity curves reconstructed by the kinetic model. Center right: single-wavelength absorbance traces at 462 nm and 600 nm as a function of time, with monoexponential ($k_{1,obs}$, $k_{2,obs}$) and kinetic model (k_p, k_d) fits superimposed. Bottom right: single-wavelength residuals as a function of time.

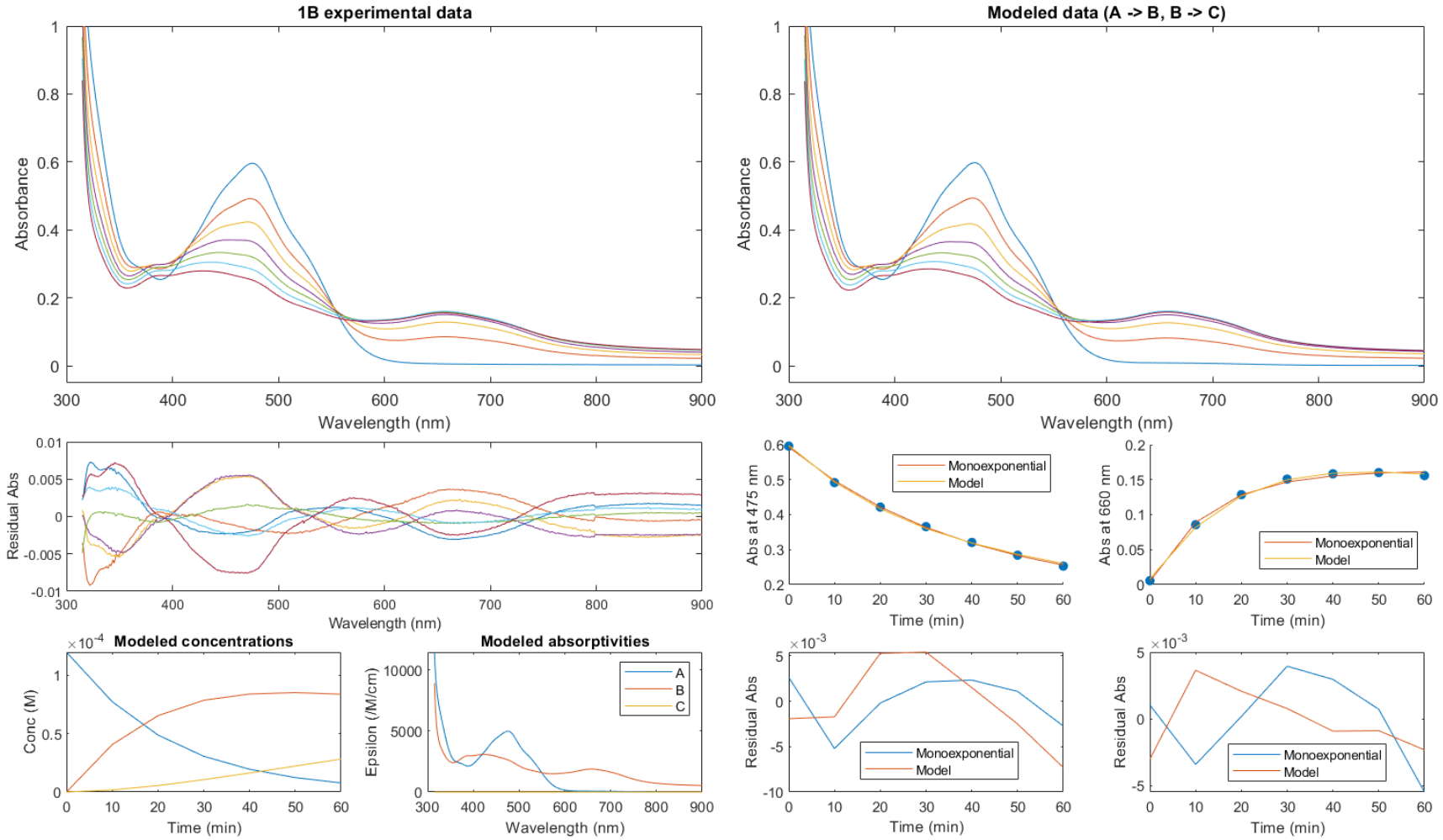

Figure S29. Kinetic modeling fit to **1B**. Top left: raw experimental absorbance data. Top right: absorbance data reproduced by the [$\boldsymbol{A \rightarrow B}$, $\boldsymbol{B \rightarrow C}$] kinetic model. Center left: model residuals as a function of wavelength. Bottom left: concentration profiles and molar absorptivity curves reconstructed by the kinetic model. Center right: single-wavelength absorbance traces at 475 nm and 660 nm as a function of time, with monoexponential ($k_{1,obs}$, $k_{2,obs}$) and kinetic model (k_p, k_d) fits superimposed. Bottom right: single-wavelength residuals as a function of time.

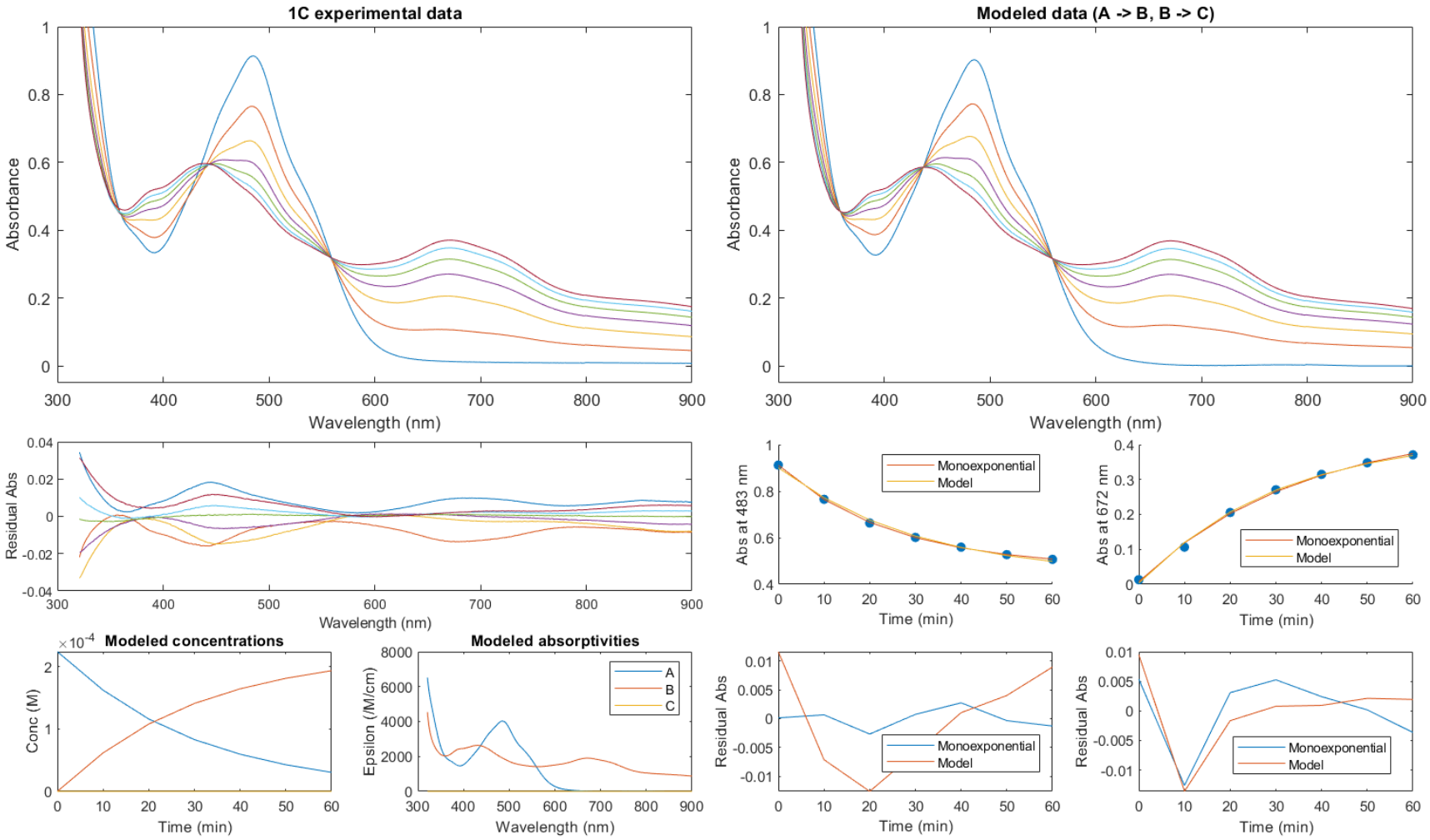

Figure S30. Kinetic modeling fit to **1C**. Top left: raw experimental absorbance data. Top right: absorbance data reproduced by the [$\boldsymbol{A \rightarrow B}$, $\boldsymbol{B \rightarrow C}$] kinetic model. Center left: model residuals as a function of wavelength. Bottom left: concentration profiles and molar absorptivity curves reconstructed by the kinetic model. Center right: single-wavelength absorbance traces at 483 nm and 672 nm as a function of time, with monoexponential ($k_{1,obs}$, $k_{2,obs}$) and kinetic model (k_p, k_d) fits superimposed. Bottom right: single-wavelength residuals as a function of time.

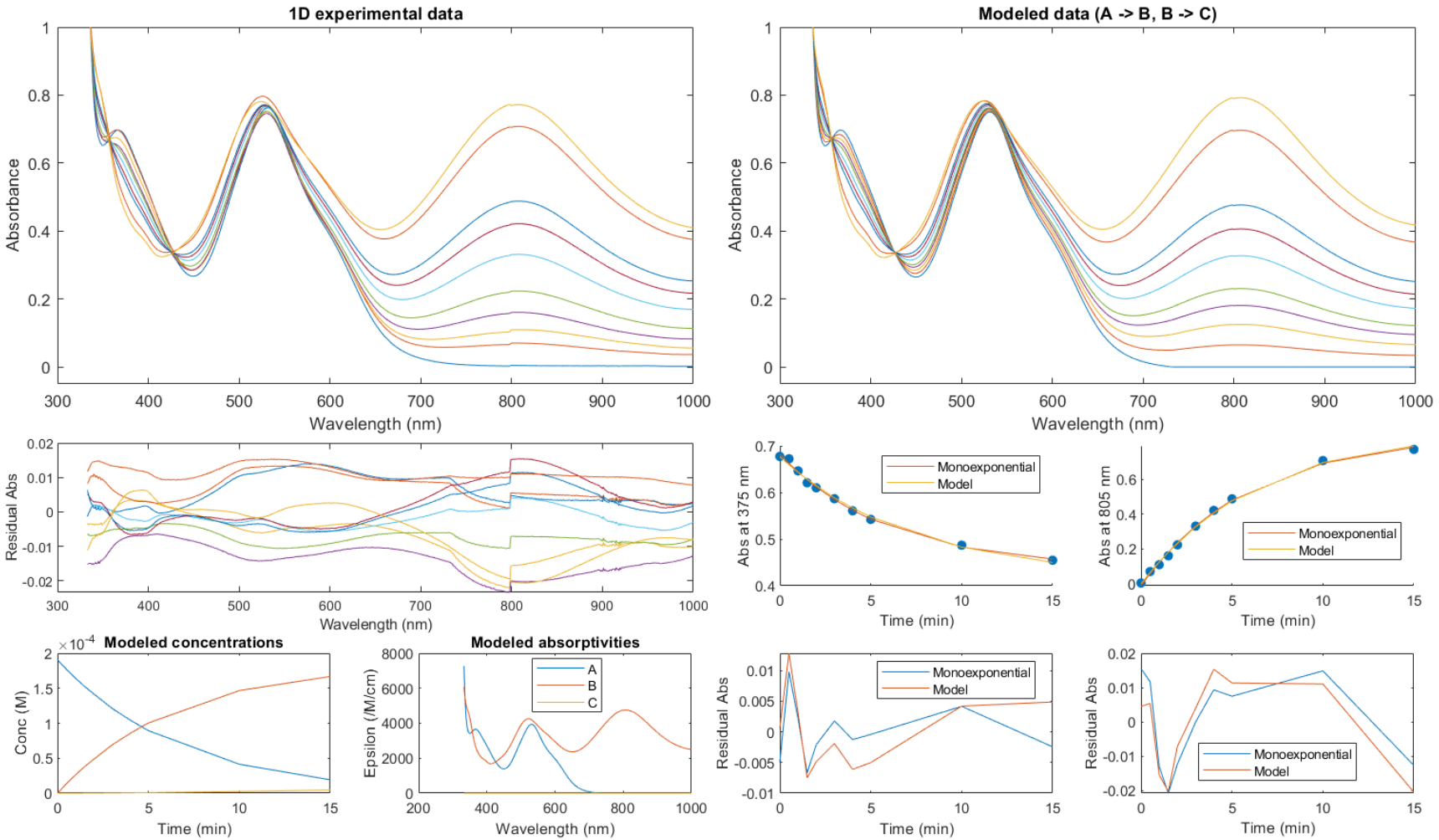

Figure S31. Kinetic modeling fit to **1D**. Top left: raw experimental absorbance data. Top right: absorbance data reproduced by the [$\boldsymbol{A \rightarrow B}$, $\boldsymbol{B \rightarrow C}$] kinetic model. Center left: model residuals as a function of wavelength. Bottom left: concentration profiles and molar absorptivity curves reconstructed by the kinetic model. Center right: single-wavelength absorbance traces at 375 nm and 805 nm as a function of time, with monoexponential ($k_{1,obs}$, $k_{2,obs}$) and kinetic model (k_p, k_d) fits superimposed. Bottom right: single-wavelength residuals as a function of time.

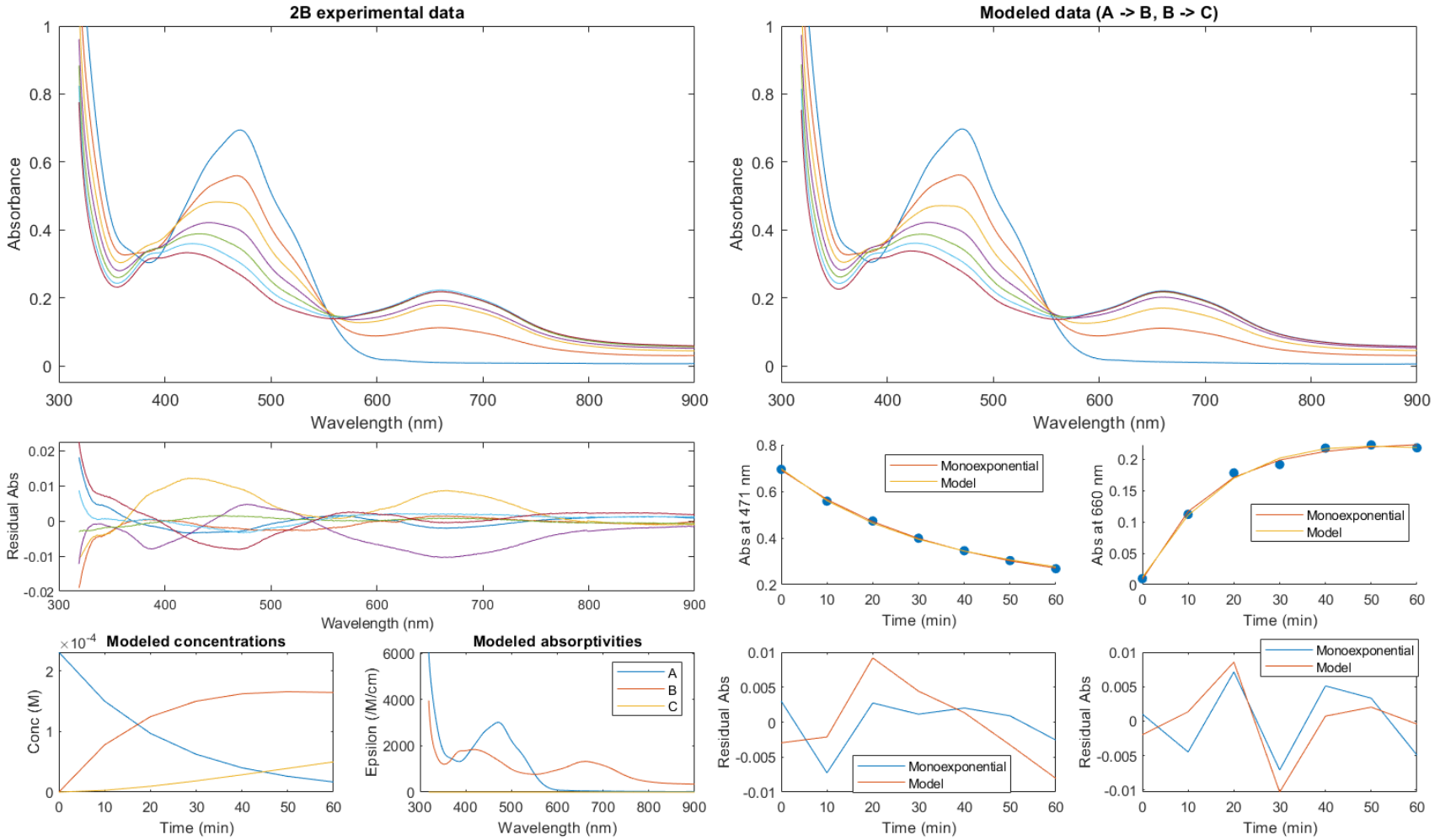

Figure S32. Kinetic modeling fit to **2B**. Top left: raw experimental absorbance data. Top right: absorbance data reproduced by the [$\boldsymbol{A \rightarrow B}$, $\boldsymbol{B \rightarrow C}$] kinetic model. Center left: model residuals as a function of wavelength. Bottom left: concentration profiles and molar absorptivity curves reconstructed by the kinetic model. Center right: single-wavelength absorbance traces at 471 nm and 660 nm as a function of time, with monoexponential ($k_{1,obs}$, $k_{2,obs}$) and kinetic model (k_p, k_d) fits superimposed. Bottom right: single-wavelength residuals as a function of time.

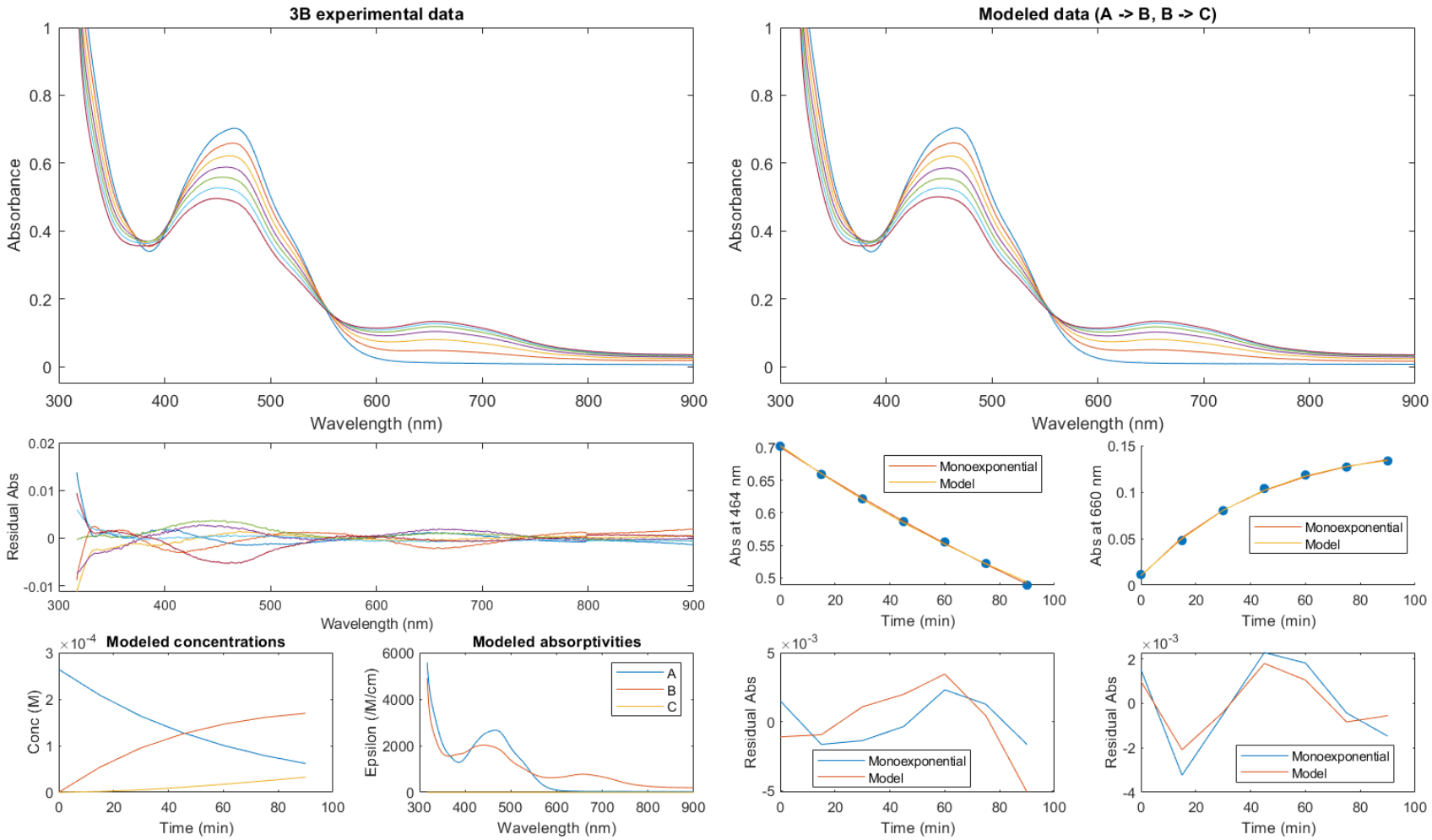

Figure S33. Kinetic modeling fit to **3B**. Top left: raw experimental absorbance data. Top right: absorbance data reproduced by the [$\boldsymbol{A \rightarrow B}$, $\boldsymbol{B \rightarrow C}$] kinetic model. Center left: model residuals as a function of wavelength. Bottom left: concentration profiles and molar absorptivity curves reconstructed by the kinetic model. Center right: single-wavelength absorbance traces at 464 nm and 660 nm as a function of time, with monoexponential ($k_{1,obs}$, $k_{2,obs}$) and kinetic model (k_p, k_d) fits superimposed. Bottom right: single-wavelength residuals as a function of time.

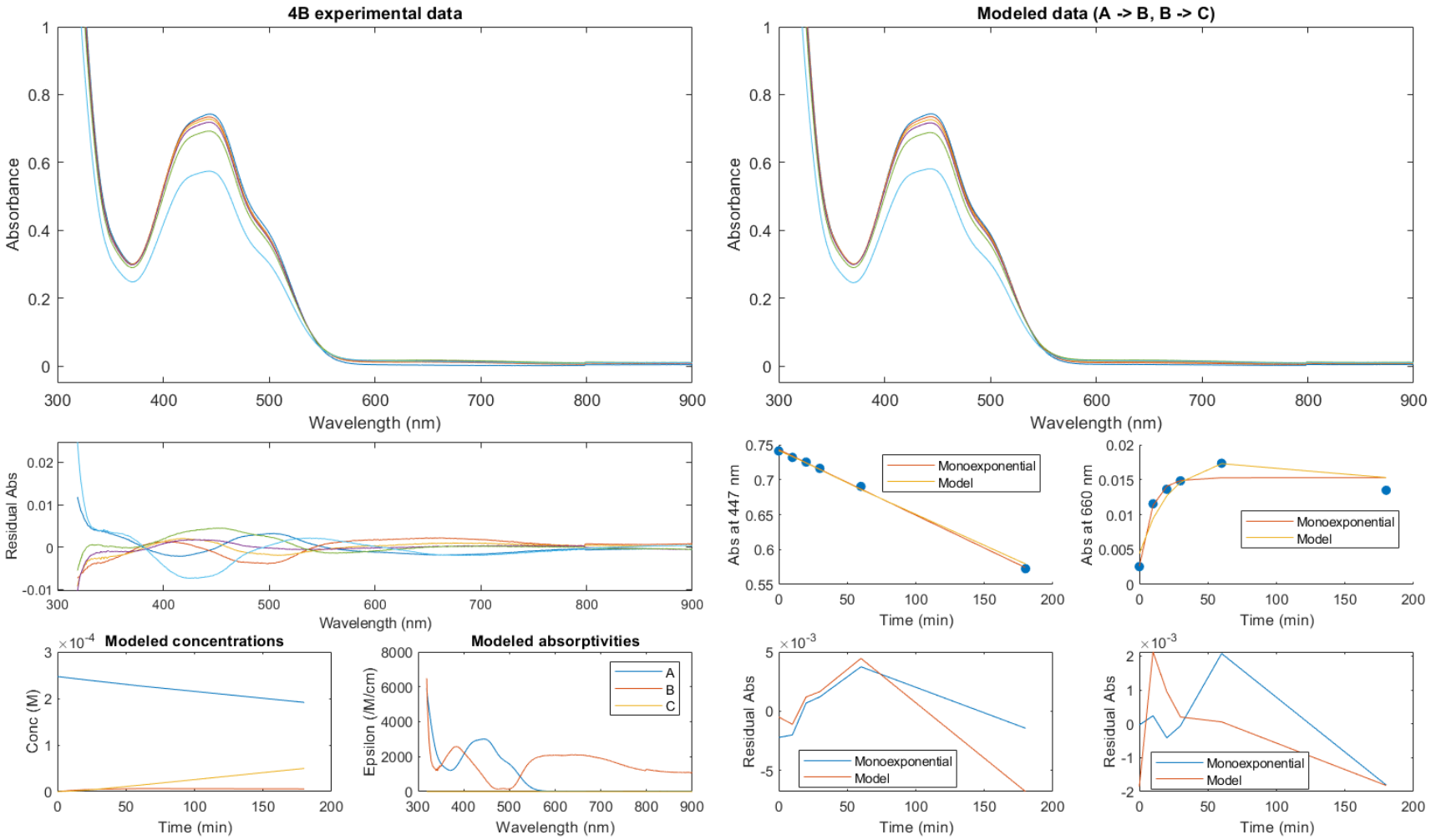

Figure S34. Kinetic modeling fit to **4B**. Top left: raw experimental absorbance data. Top right: absorbance data reproduced by the [$\boldsymbol{A \rightarrow B}$, $\boldsymbol{B \rightarrow C}$] kinetic model. Center left: model residuals as a function of wavelength. Bottom left: concentration profiles and molar absorptivity curves reconstructed by the kinetic model. Center right: single-wavelength absorbance traces at 447 nm and 660 nm as a function of time, with monoexponential ($k_{1,obs}$, $k_{2,obs}$) and kinetic model (k_p, k_d) fits superimposed. Bottom right: single-wavelength residuals as a function of time.

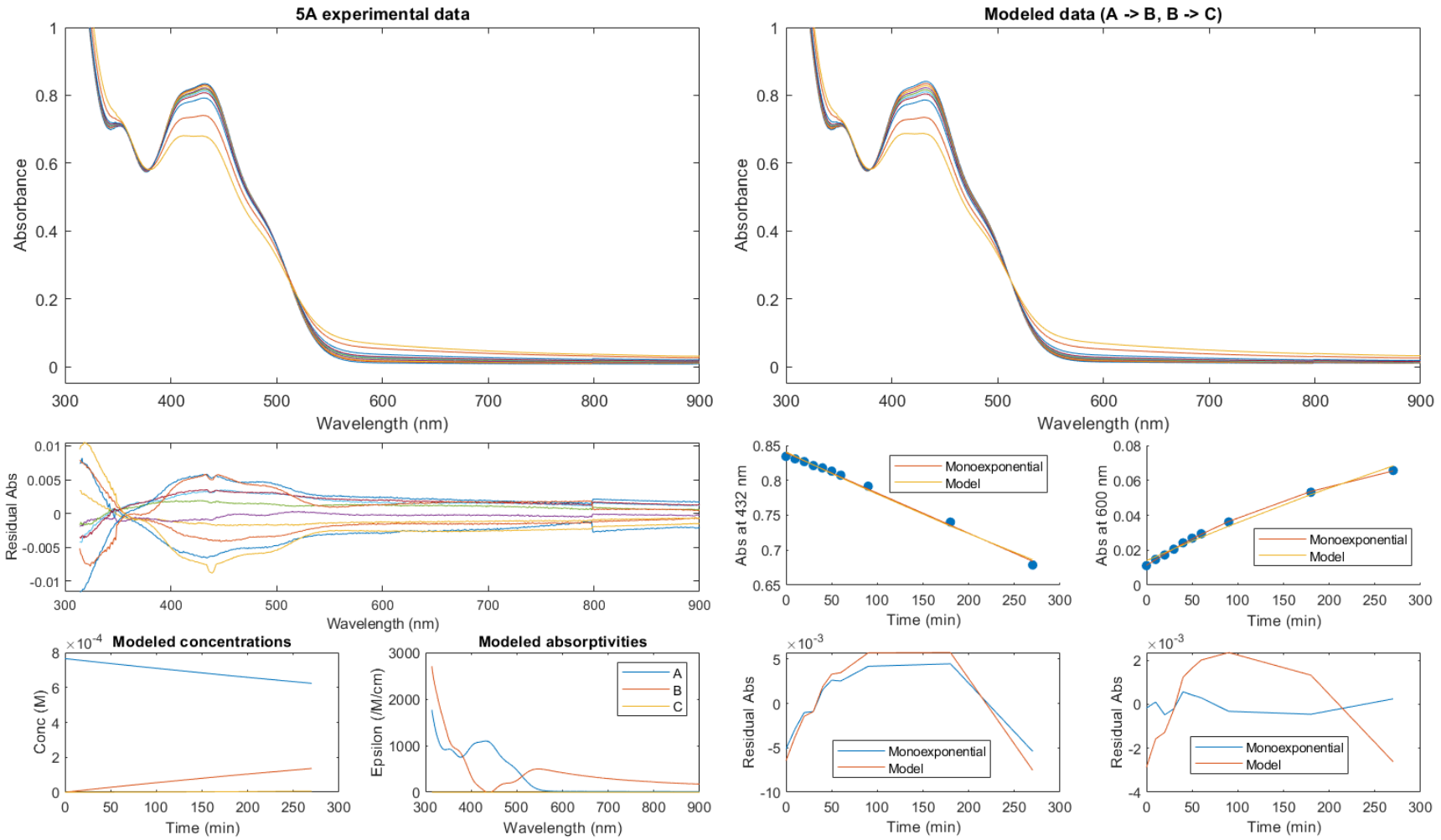

Figure S35. Kinetic modeling fit to **5A**. Top left: raw experimental absorbance data. Top right: absorbance data reproduced by the [$\boldsymbol{A \rightarrow B}$, $\boldsymbol{B \rightarrow C}$] kinetic model. Center left: model residuals as a function of wavelength. Bottom left: concentration profiles and molar absorptivity curves reconstructed by the kinetic model. Center right: single-wavelength absorbance traces at 432 nm and 600 nm as a function of time, with monoexponential ($k_{1,obs}$, $k_{2,obs}$) and kinetic model (k_p, k_d) fits superimposed. Bottom right: single-wavelength residuals as a function of time.

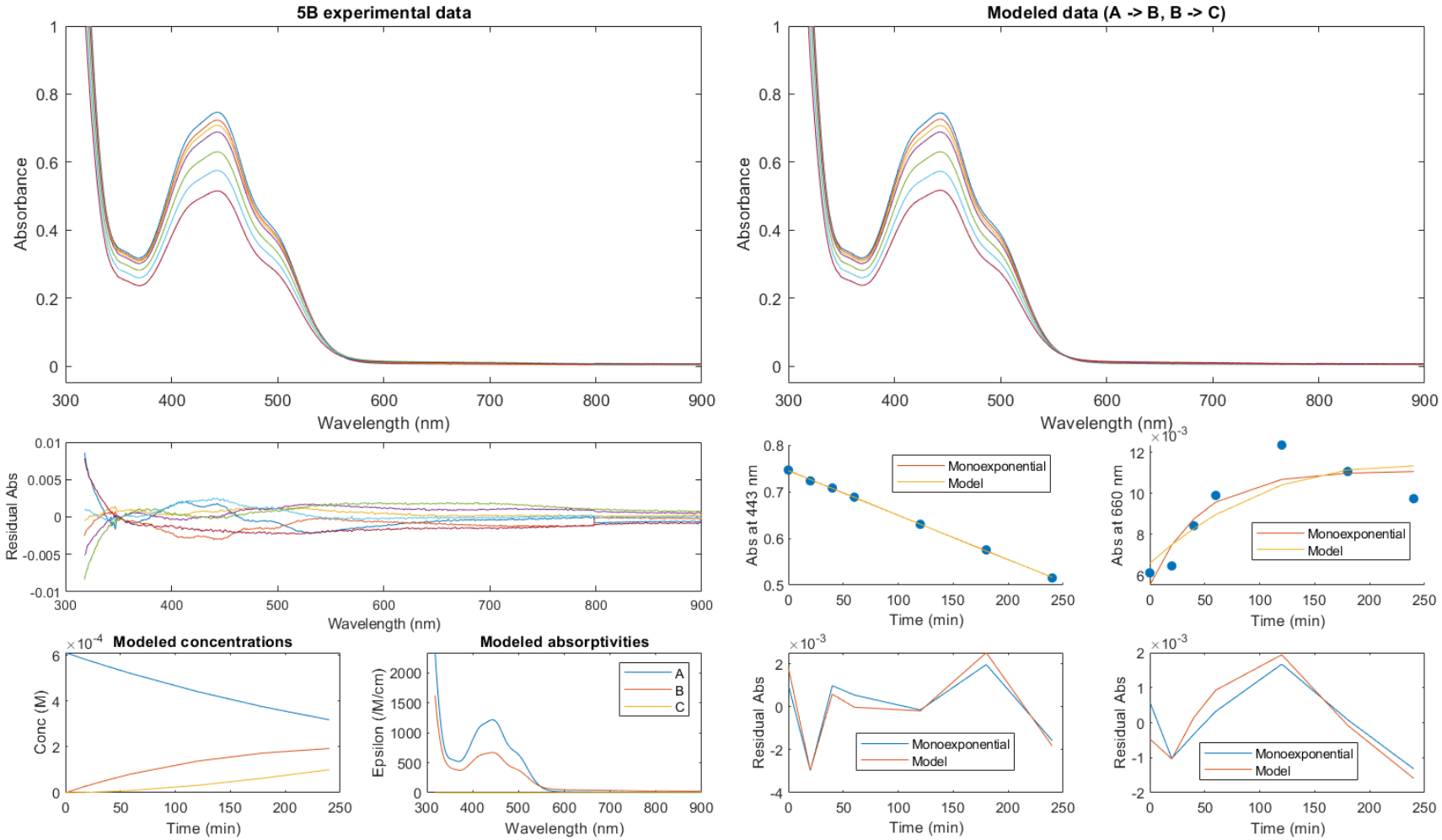

Figure S36. Kinetic modeling fit to **5B**. Top left: raw experimental absorbance data. Top right: absorbance data reproduced by the [$\boldsymbol{A \rightarrow B}$, $\boldsymbol{B \rightarrow C}$] kinetic model. Center left: model residuals as a function of wavelength. Bottom left: concentration profiles and molar absorptivity curves reconstructed by the kinetic model. Center right: single-wavelength absorbance traces at 443 nm and 660 nm as a function of time, with monoexponential ($k_{1,obs}$, $k_{2,obs}$) and kinetic model (k_p, k_d) fits superimposed. Bottom right: single-wavelength residuals as a function of time.

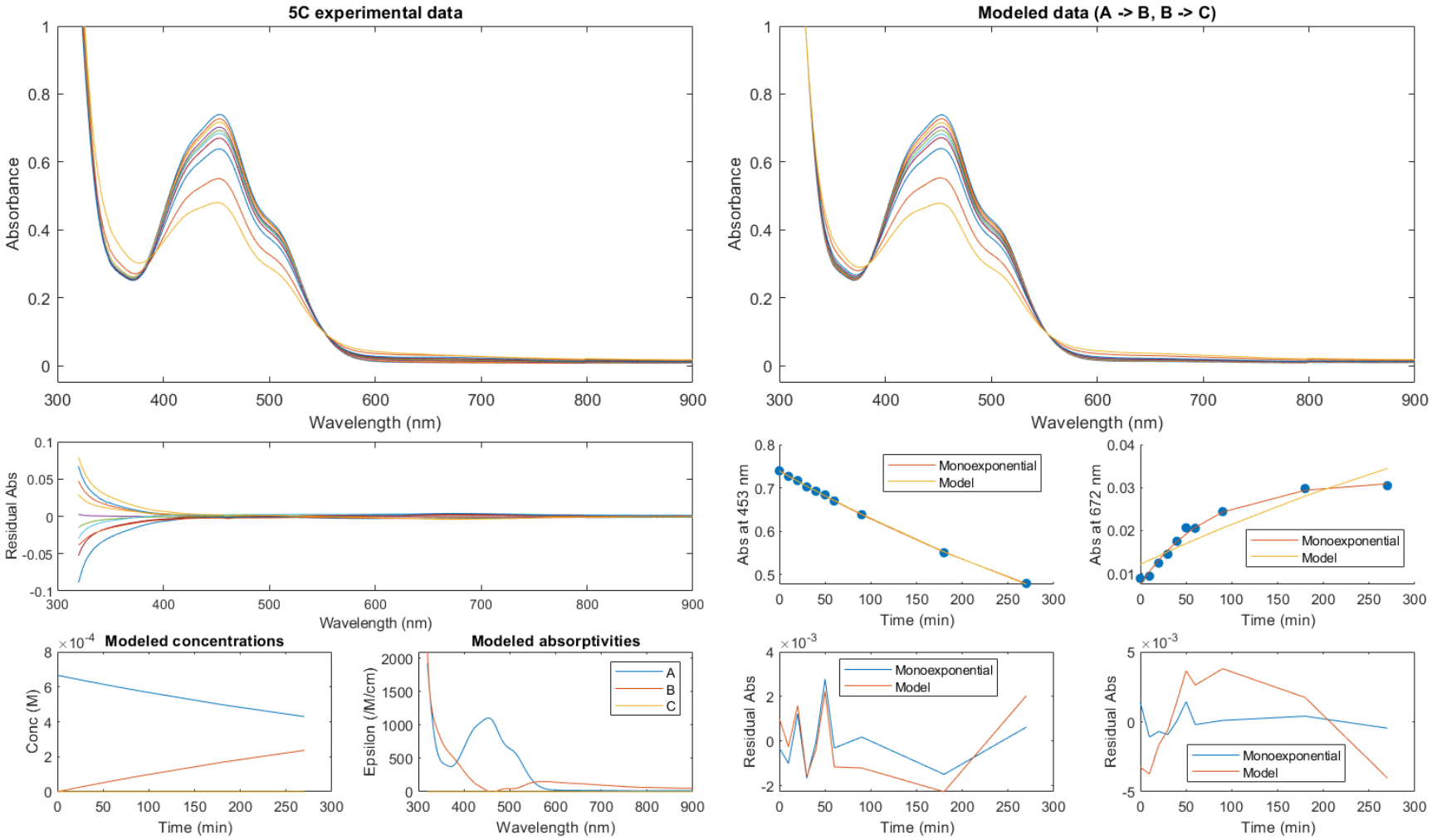

Figure S37. Kinetic modeling fit to **5C**. Top left: raw experimental absorbance data. Top right: absorbance data reproduced by the [$\boldsymbol{A \rightarrow B}$, $\boldsymbol{B \rightarrow C}$] kinetic model. Center left: model residuals as a function of wavelength. Bottom left: concentration profiles and molar absorptivity curves reconstructed by the kinetic model. Center right: single-wavelength absorbance traces at 453 nm and 672 nm as a function of time, with monoexponential ($k_{1,obs}$, $k_{2,obs}$) and kinetic model (k_p, k_d) fits superimposed. Bottom right: single-wavelength residuals as a function of time.

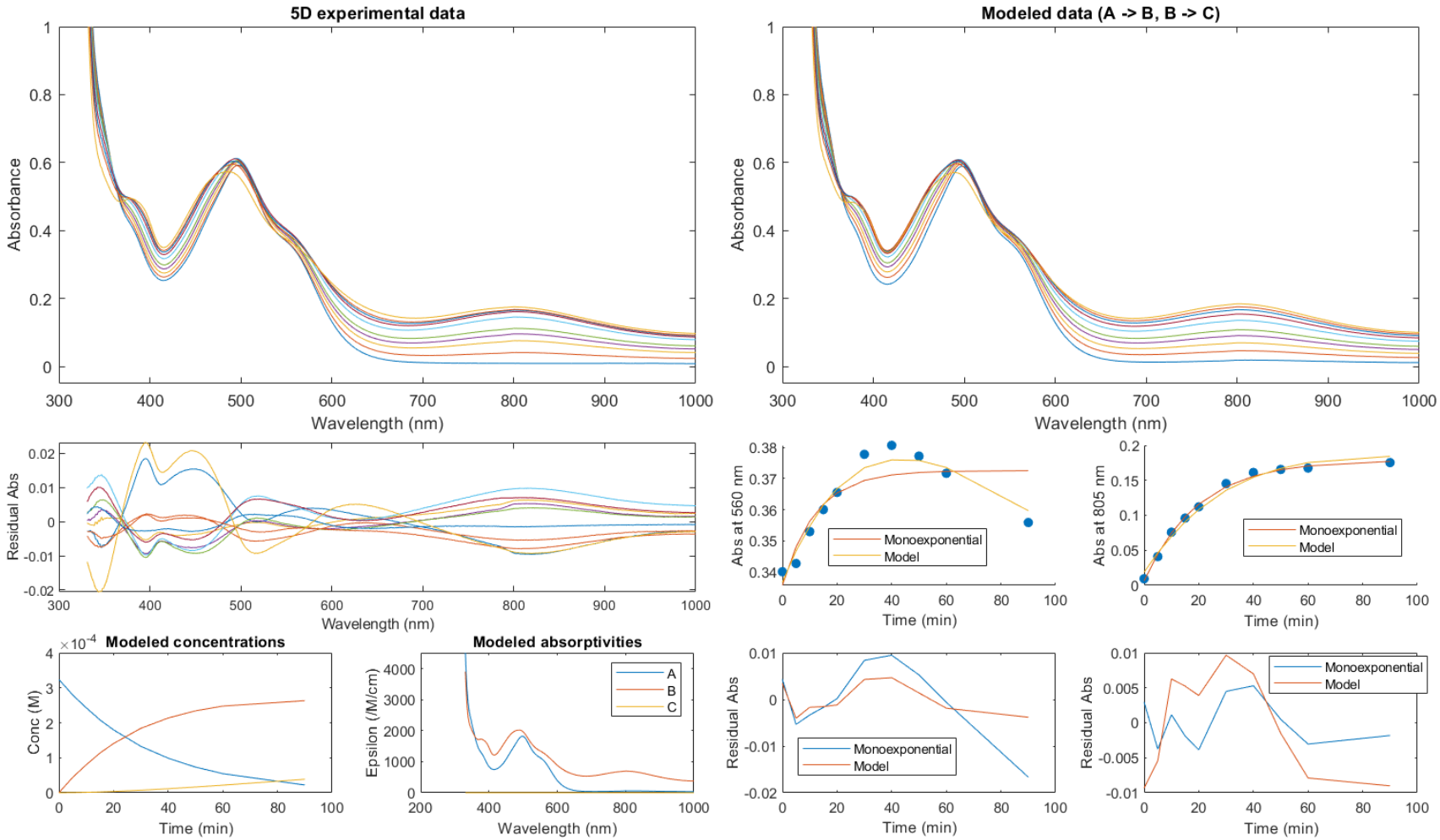

Figure S38. Kinetic modeling fit to **5D**. Top left: raw experimental absorbance data. Top right: absorbance data reproduced by the [$\boldsymbol{A \rightarrow B}$, $\boldsymbol{B \rightarrow C}$] kinetic model. Center left: model residuals as a function of wavelength. Bottom left: concentration profiles and molar absorptivity curves reconstructed by the kinetic model. Center right: single-wavelength absorbance traces at 560 nm and 805 nm as a function of time, with monoexponential ($k_{1,obs}$, $k_{2,obs}$) and kinetic model (k_p, k_d) fits superimposed. Bottom right: single-wavelength residuals as a function of time.

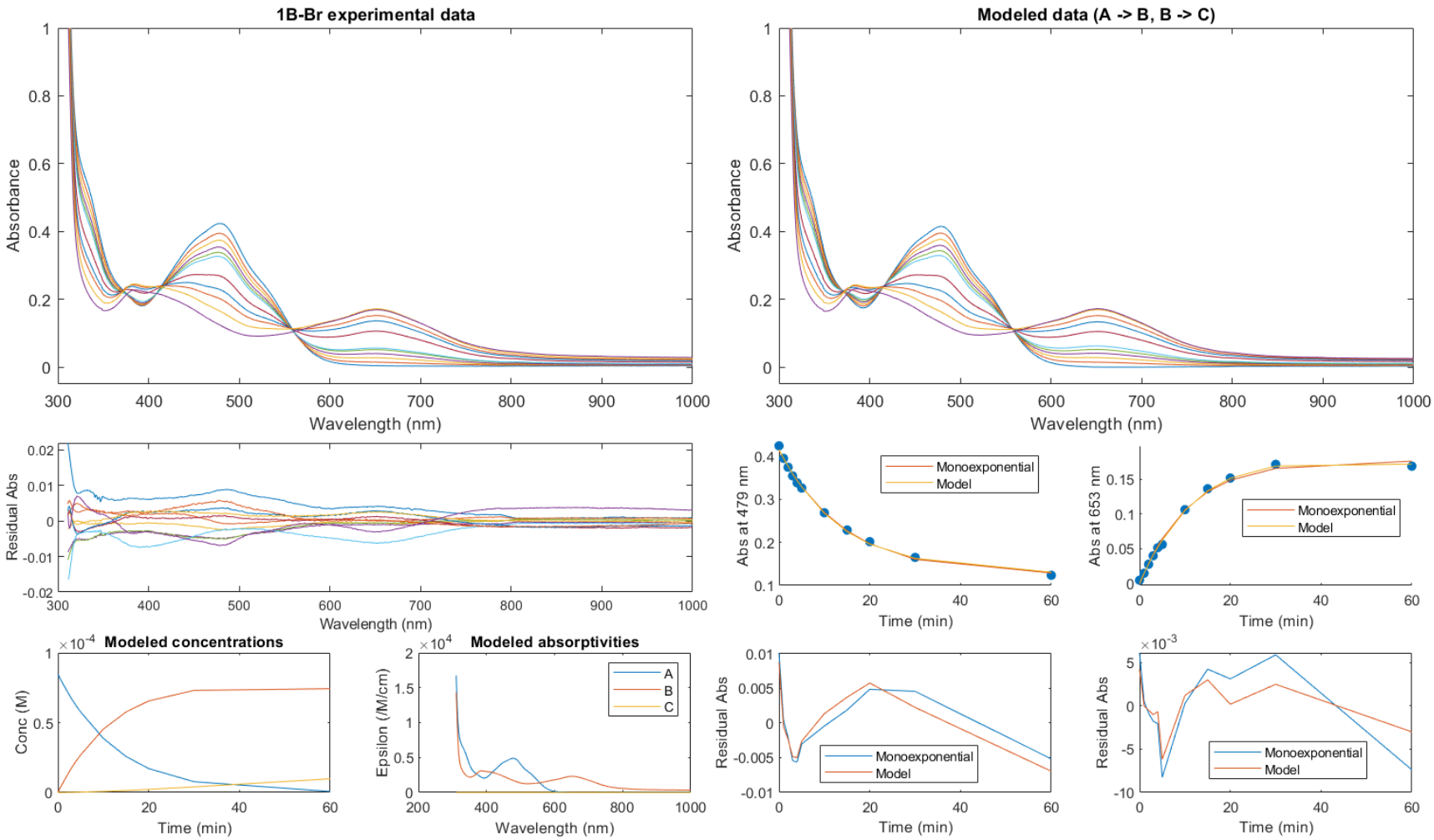

Figure S39. Kinetic modeling fit to **1B–Br**. Top left: raw experimental absorbance data. Top right: absorbance data reproduced by the [$\boldsymbol{A \rightarrow B}$, $\boldsymbol{B \rightarrow C}$] kinetic model. Center left: model residuals as a function of wavelength. Bottom left: concentration profiles and molar absorptivity curves reconstructed by the kinetic model. Center right: single-wavelength absorbance traces at 479 nm and 653 nm as a function of time, with monoexponential ($k_{1,obs}$, $k_{2,obs}$) and kinetic model (k_p, k_d) fits superimposed. Bottom right: single-wavelength residuals as a function of time.

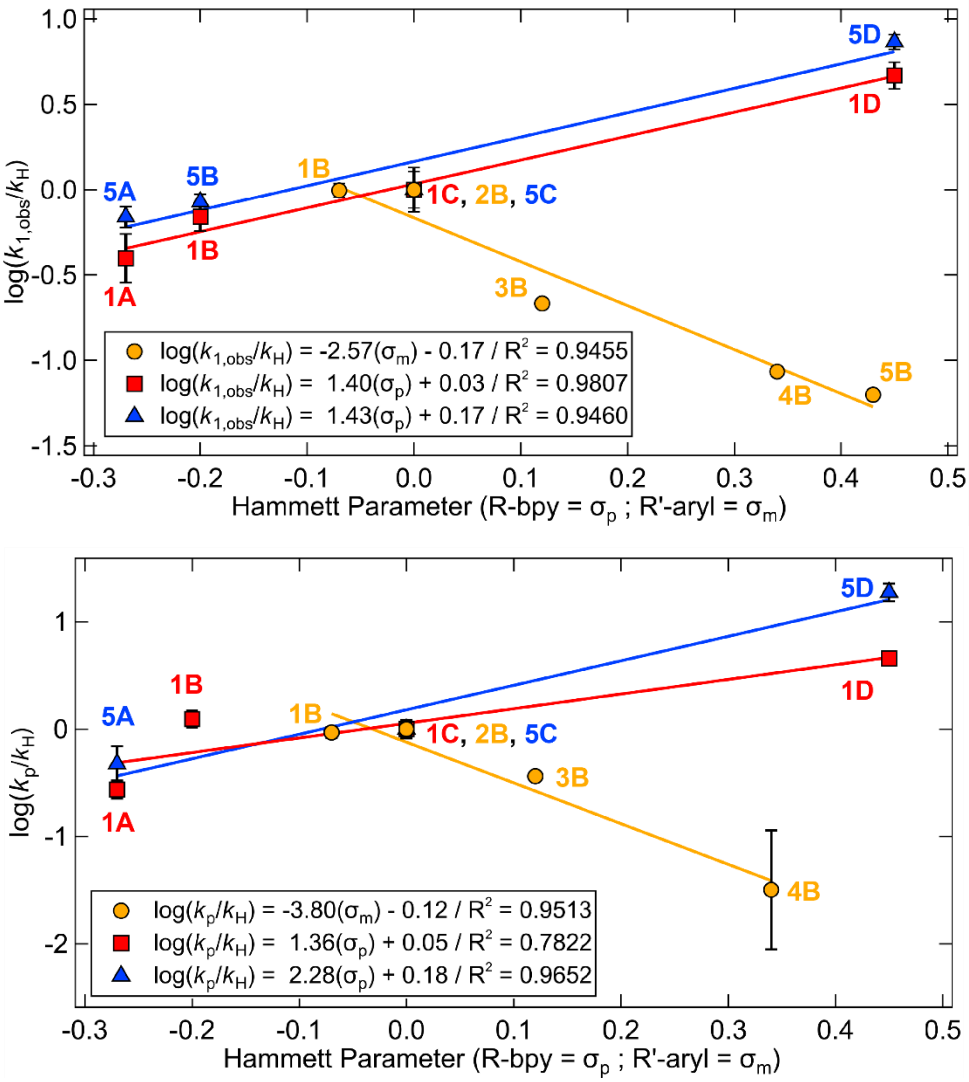

Figure S40. Comparison between Hammett plots made using experimentally obtained rate constants, $\log(k_{1,obs}/k_H)$ (top, from main text Figure 5), and rate constants obtained via the global kinetics model, $\log(k_p/k_H)$ (bottom). For $k_{1,obs}$, compound **1A** is approximated by $k_{2,obs}$; for k_p, compound **5B** was omitted owing to poor convergence of the global kinetics model.

Molar absorptivity curves for the monomer ***B*** can also be extracted from the global analysis model. The extracted curves have the correct magnitude and a characteristic two-peaked shape. The normalized ***B*** absorptivity curves obtained from the model for the long-wavelength feature (~660 nm) are nearly identical to those obtained from the final time point of the kinetics absorbance data as expected (Figure S41), as only ***B*** absorbs in this spectral window. However, the global analysis also resolves the short-wavelength feature (~400 nm) in the spectral window where starting material and photolysis product overlap. By obtaining the peak maxima for both features (Table S4) and plotting against the appropriate Hammett parameters (see Figure 3B in the text), we can then further support the three-coordinate monomeric identity of the photolysis product.

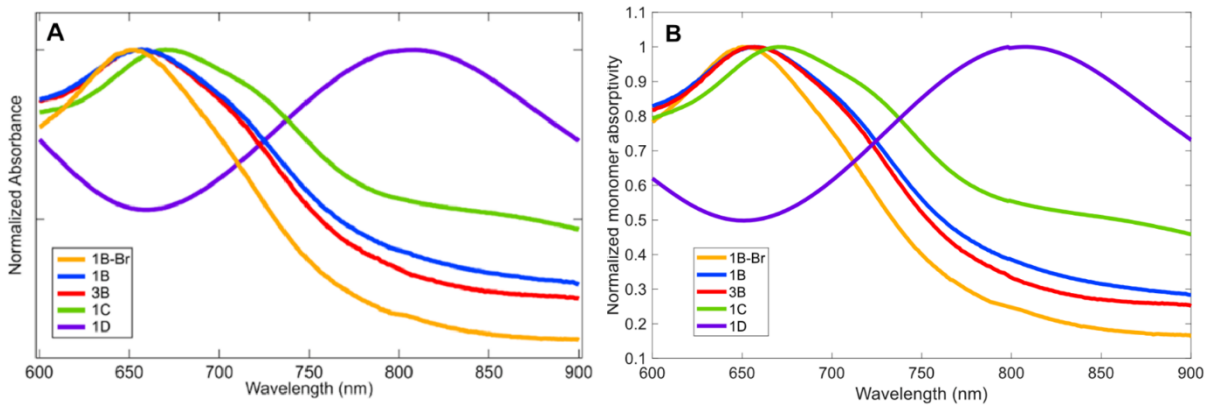

Figure S41. Comparison of normalized absorptivity curves obtained from (A) the normalized final absorbance traces from each experimental dataset and (B) the normalized absorptivity curve for species ***B*** in the [***A*** → ***B***, ***B*** → ***C***] global kinetics model.

Table S4. Peak maxima for photolysis product ***B*** absorption features obtained from global kinetic fitting. Molar absorptivity curves extracted from the [***A*** → ***B***, ***B*** → ***C***] reaction model with nonabsorbing ***C***.

Dataset	Peak 1 (cm^{-1})	Peak 2 (cm^{-1})
1A	25840	17330
1B	23700	15220
1C	23200	14930
1D	19120	12390
2B	23920	15110
3B	22620	15220
4B	26400	15337
5A	27170	18280
5C	26730	17610
5D	20530	12500
1B–Br	25906	15380

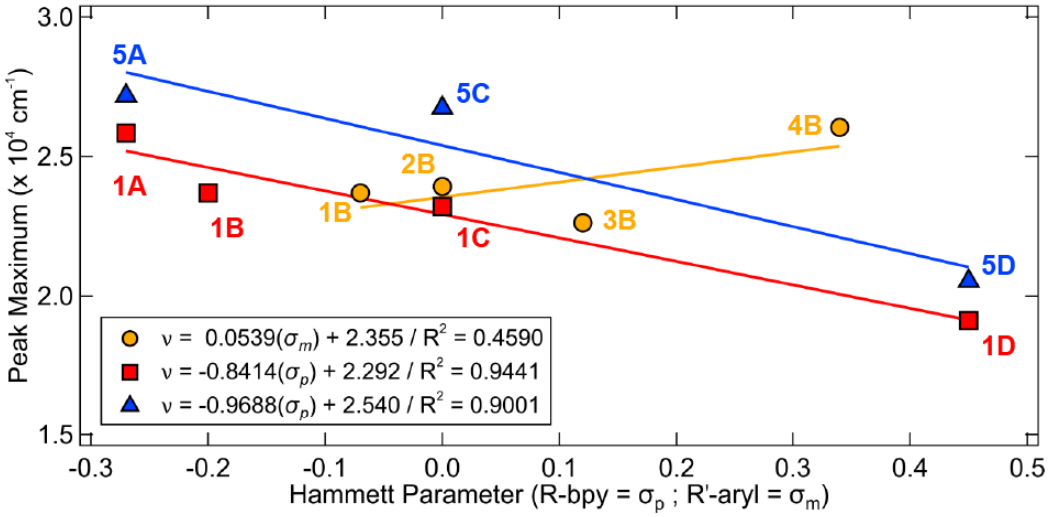

Figure S42. Hammett plot of monomer absorption peak 1 (higher energy). Complex **5B** was omitted owing to poor convergence of the global kinetics model.

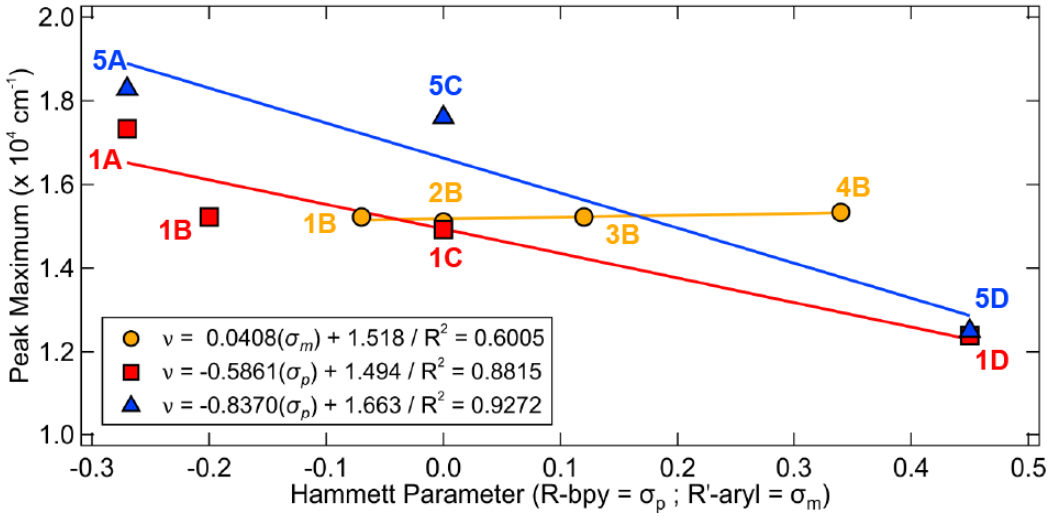

Figure S43. Hammett plot of monomer absorption peak 2 (lower energy). Complex **5B** was omitted owing to poor convergence of the global kinetics model.

Figures S42–S43 show that both absorbance features of ***B*** shift linearly with a similar slope against the Hammett parameter when varying the bpy ligand (**1A**–**1D** and **5A**–**5D**). This observation is consistent with the inclusion of the bpy ligand in the photolysis product ***B***. However, the absorbance features of ***B*** show no systematic shift when varying the aryl substituent in the starting material (**1B**–**5B**). This result is consistent with the loss of the aryl in the photolysis step prior to the formation of ***B***, supporting its identity as three-coordinate monomeric Ni(^{R}bpy)X, X = Cl, Br.[9]

S1.10. Kinetic Trends and Miscellaneous Photolysis Data.

Concentration dependence studies were conducted on a range of starting absorbances (Figure S44). Again, **1B** was selected as a representative compound. The slight decrease in rate constant at the highest concentration is attributed to the inner filter effect. Overall, no appreciable change in the rate constant was detected across the range of concentrations tested (5.1×10^{-5} M – 2.1×10^{-4} M). Kinetic analysis yields a unimolecular, first order decay for the reaction.

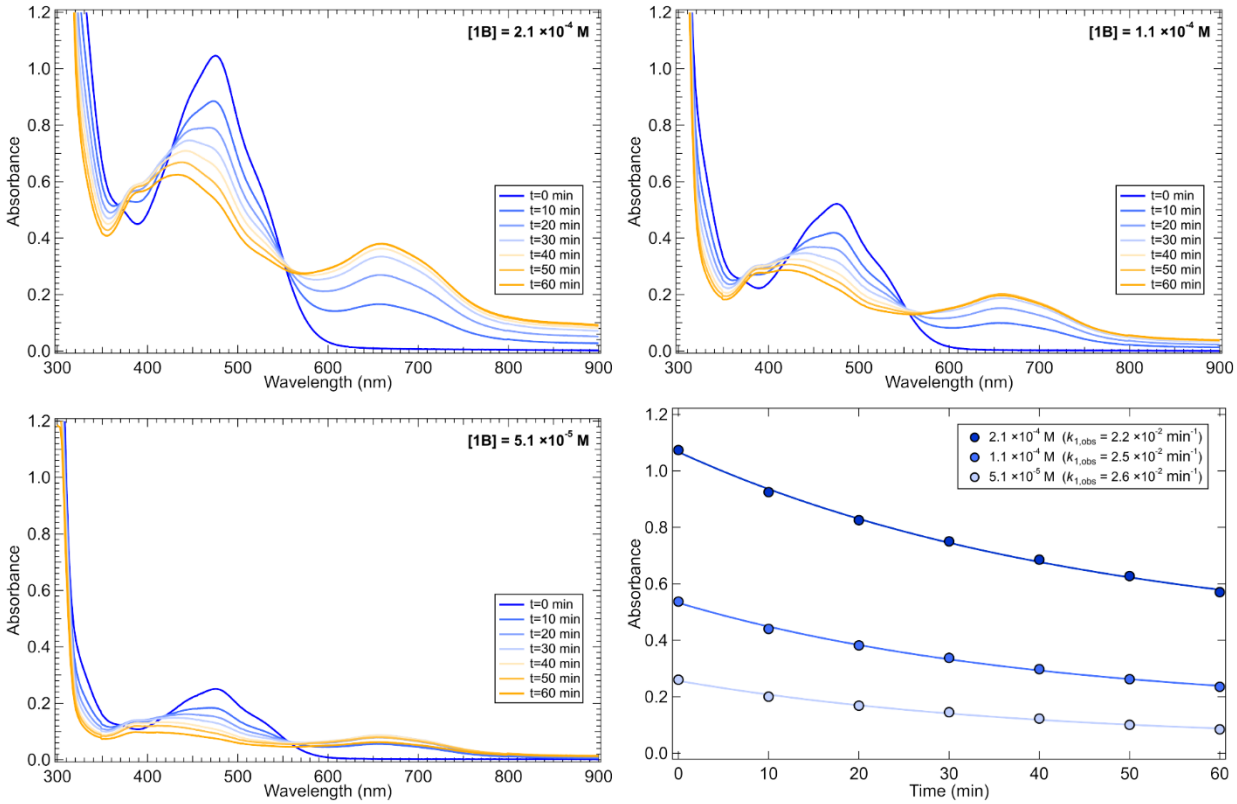

Figure S44. Concentration dependence studies on **1B** in THF. Decay of the complex was measured at 475 nm.

Table S5. Concentration dependence kinetic data for **1B** in THF.

Experiment	$[1B]_0$ ($\times 10^{-4}$ M)	Initial Rate ($\times 10^{-6}$ M min^{-1})
1	2.11	4.64
2	1.05	2.63
3	0.51	1.33

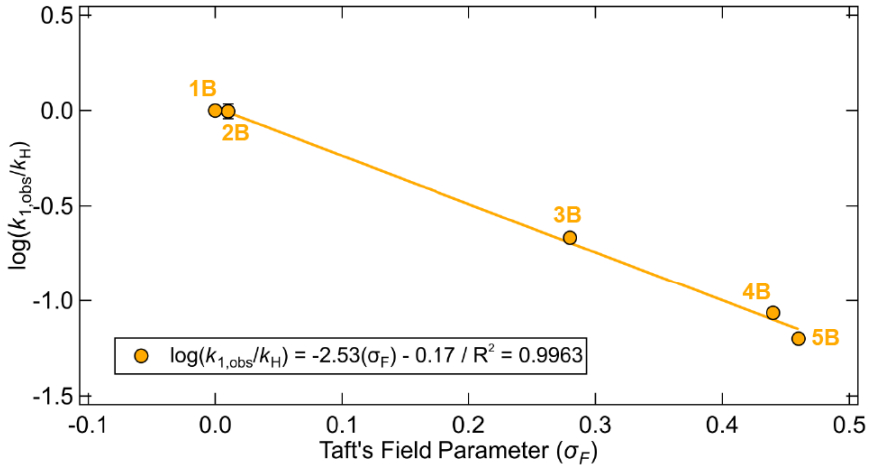

Figure S45. Correlation between normalized rates of homolysis of the aryl series (**1B**–**5B**) and Taft's field parameter, σ_F.[6]

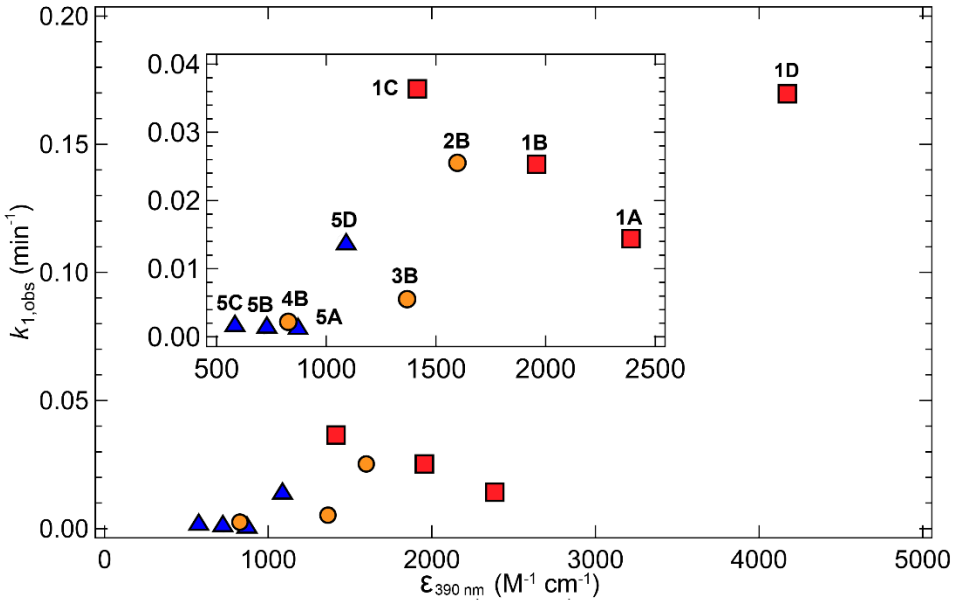

Figure S46. Plot of the observed photolysis rate constant versus the molar absorptivity at the incident light wavelength (390 nm). A linear trend (likely with positive slope) is expected if there is a rate dependence on the molar absorptivity. However, complexes **1A**-**1D** and **5A**-**5D** do not see this trend. Compounds **1B**-**5B** may see a trend weakly (R^2 = 0.80).

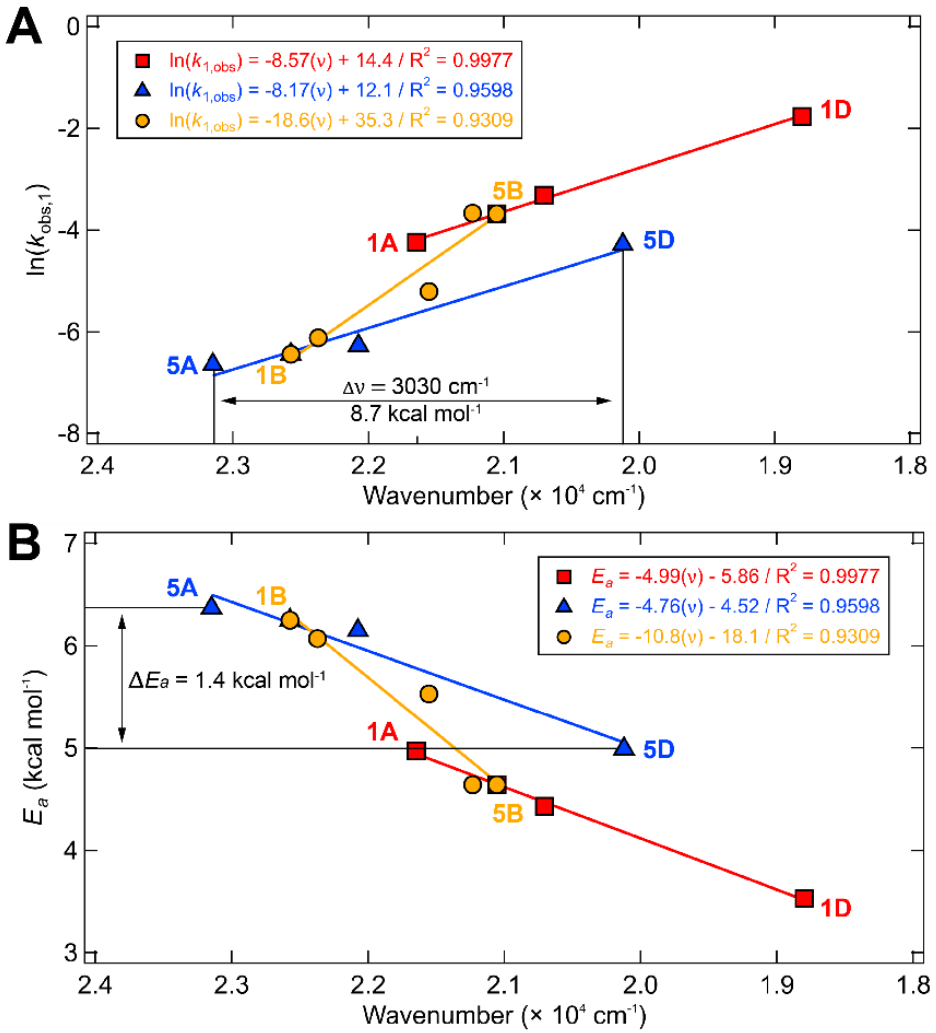

Figure S47. (A) Comparison between the change in energy of the MLCT peak maxima and (B) the change in energy for the energetic barrier for photolysis between **5A** and **5D**. Barriers are calculated using the Arrhenius equation assuming a uniform preexponential factor and are normalized to the experimental value obtained for **1B**.

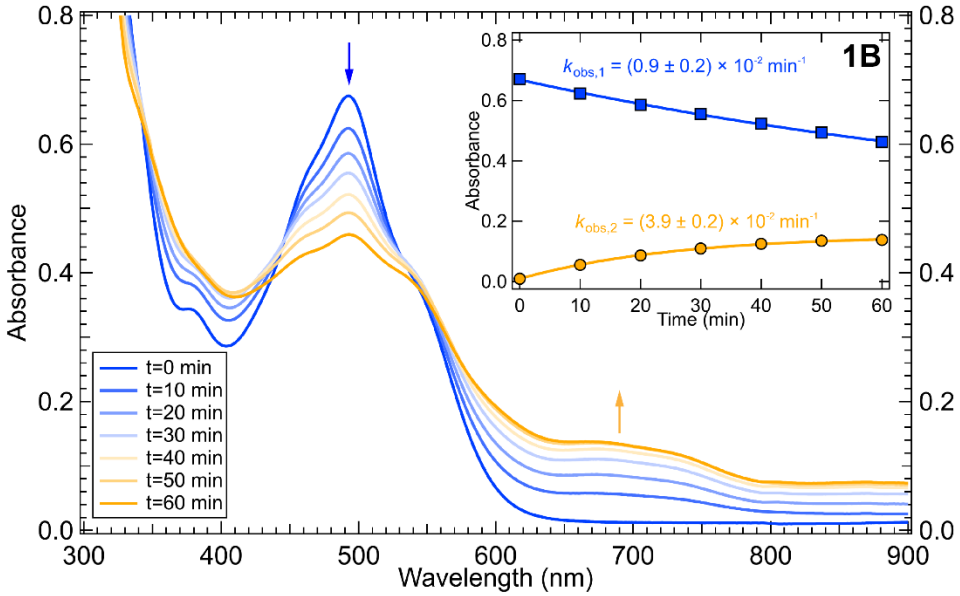

Figure S48. Photolysis profile of **1B** in toluene (λ_{max} is red shifted from 475 nm THF to 493 nm in toluene: $\Delta\nu_{max}$ = 770 cm^{-1}). Photolysis kinetics were monitored at two wavelengths indicated by the blue and orange arrows in each panel. Insets correspond to the fitted kinetic data (blue curve for the decay of the starting material, orange curve for the formation of the new species). Data were fit using first-order kinetics; error bars are one standard deviation.

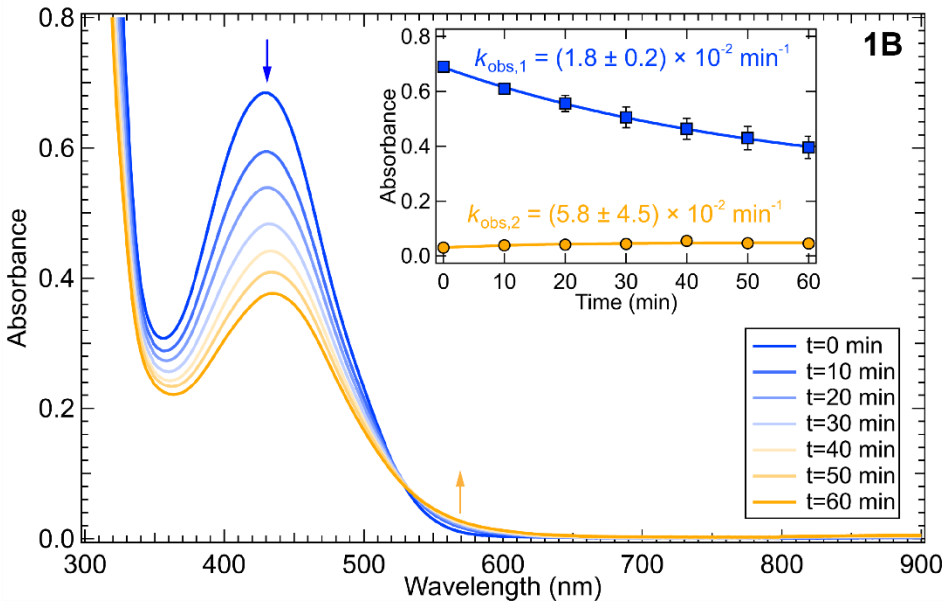

Figure S49. Photolysis profile of **1B** in DMF (λ_{max} is blue shifted from 475 nm THF to 429 nm in DMF: $\Delta\nu_{max}$ = 2260 cm^{-1}). Photolysis kinetics were monitored at two wavelengths indicated by the blue and orange arrows in each panel. Insets correspond to the fitted kinetic data (blue curve for the decay of the starting material, orange curve for the formation of the new species). Data were fit using first-order kinetics; error bars are one standard deviation. Note that the absorption of the new species is seen only in small amounts, possibly the result of a competing supply and removal via a decomposition pathway (see kinetics model, k_d [$\boldsymbol{B} \rightarrow \boldsymbol{C}$]) or other solvent effect.

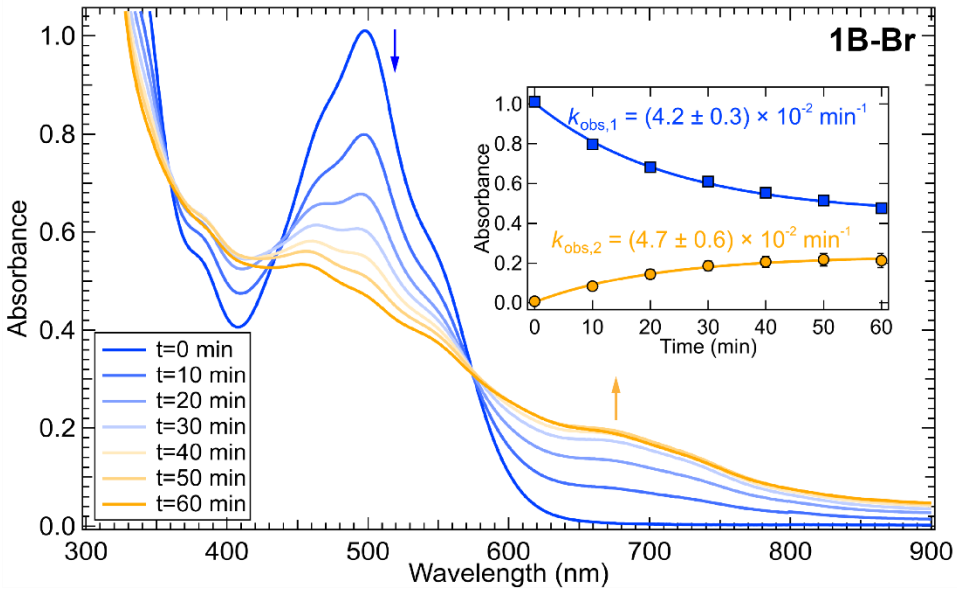

Figure S50. Photolysis profile of **1B**–**Br** in toluene (λ_{max} is red shifted from 479 nm in THF to 499 nm in toluene: $\Delta\nu_{max}$ = 840 cm^{-1}). Photolysis kinetics were monitored at two wavelengths indicated by the blue and orange arrows in each panel. Insets correspond to the fitted kinetic data (blue curve for the decay of the starting material, orange curve for the formation of the new species). Data were fit using first-order kinetics; error bars are one standard deviation.

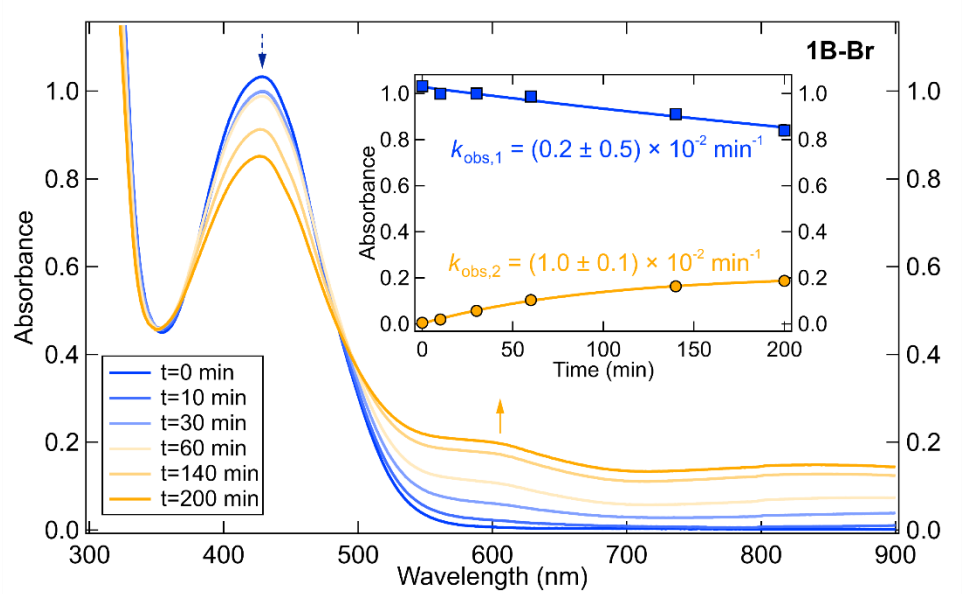

Figure S51. Photolysis profile of **1B**–**Br** in dimethylformamide, DMF (λ_{max} is blue shifted from 479 nm in THF to 428 nm in DMF: $\Delta\nu_{max}$ = 2490 cm^{-1}) Photolysis kinetics were monitored at two wavelengths indicated by the blue and orange arrows in each panel. Inset corresponds to the first-order kinetics fitted data (blue curve for the decay of the starting material, orange curve for the formation of the new species). Error bars are one standard deviation. Note that the absorption of the new species precludes definitive assignment of $k_{1,obs}$ for this compound from λ_{max} of the starting material. Nevertheless, a slower photolysis rate is observed for this complex in DMF than in THF (main text, Figure 6).

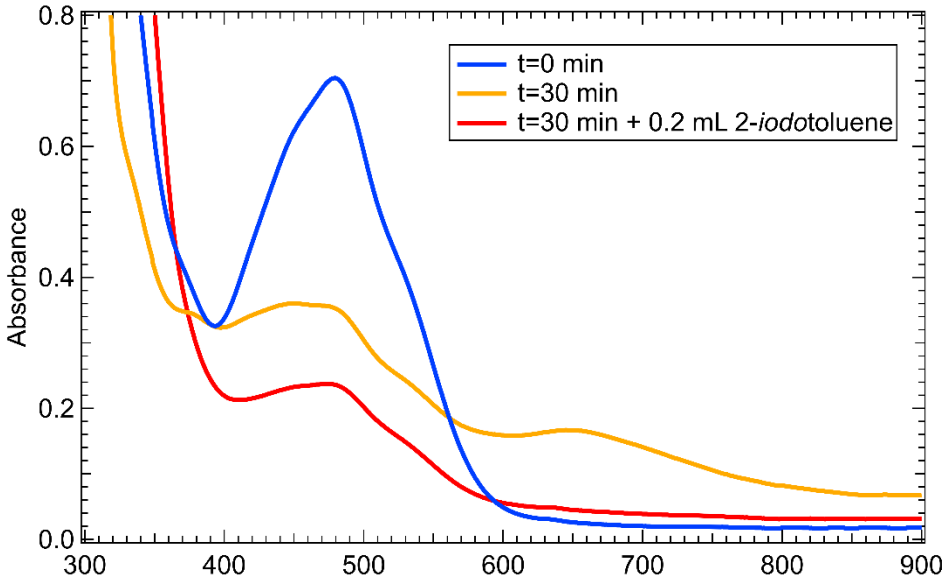

Figure S52. Photolysis experiment of **1B-Br** in THF showing the formation of the photoproduct (orange line, primary peak at 653 nm) which is subsequently quenched by the addition of 0.2 mL of 2-*iodo*toluene (red line). The resultant spectrum shows broadened absorbance features tailing to long wavelengths.

S1.11. Quantum Yield Determination.

Quantum yields were calculated using the method developed by Gescheidt et al.[13] For the unimolecular, first order photolysis reaction given in equation S1, the following rate expression may be written (eq. S2):

$$\mathrm{NiC} \xrightarrow{k_1} \mathrm{Ni} + \mathrm{C} \qquad \textbf{(eq. S1)}$$

$$rate = -\frac{d[\mathrm{NiC}]}{dt} = k_1[\mathrm{NiC}] \qquad \textbf{(eq. S2)}$$

The rate of the reaction is proportional to the intensity of photons absorbed by the starting material, I_{Abs}^{NiC} (in mol L^{-1} s^{-1}), and the quantum yield for the photochemical conversion process, Φ. Therefore, the rate can also be written as equation S3.

$$-\frac{d[\mathrm{NiC}]}{dt} = I_{Abs}^{\mathrm{NiC}}\Phi \qquad \textbf{(eq. S3)}$$

Combining equations S2 and S3 and rearranging gives equation S4.

$$\Phi = \frac{k_1[\mathrm{NiC}]}{I_{Abs}^{\mathrm{NiC}}} \qquad \textbf{(eq. S4)}$$

Application of the Beer-Lambert law gives equation S5, where $I_{\mathrm{o}}^{\mathrm{NiC}}$ is the initial intensity of photons received by the reactant solution from the light source (i.e., the photon flux in mol L^{-1} s^{-1}). Combining eq. S4 and eq. S5 and considering initial starting conditions (t = 0, more details are provided in reference 11) gives equation S6, where λ is the primary wavelength of the light source (in meters), P_{LED} is the power of the light source (in J s^{-1}), h is Planck's constant, c is the speed of light in a vacuum, N_A is Avogadro's constant, and V is the volume of the reactant solution irradiated (in liters). Note that the value, Abs_{NiC}^{390}, is the measured absorbance of the reactant solution at the primary light source wavelength (most commonly 390 x10^{-9} m in our study).

$$I_{Abs}^{\mathrm{NiC}} = I_{\mathrm{o}}^{\mathrm{NiC}}\left(1 - 10^{-Abs_{\mathrm{NiC}}^{390}}\right) \qquad \textbf{(eq. S5)}$$

$$\Phi = \frac{k_1[\mathrm{NiC}]}{I_{\mathrm{o}}^{\mathrm{NiC}}\left(1 - 10^{-Abs_{\mathrm{NiC}}^{390}}\right)};\ I_{\mathrm{o}}^{\mathrm{NiC}} = \frac{\lambda P_{LED}}{hcN_aV} \qquad \textbf{(eq. S6)}$$

Rearranging and bringing the constants to the front yields equation S7. Note that in our case, all standard photolysis experiments were conducted with a constant volume (0.0025 L) and at a constant distance from the same light source (i.e., constant P_{LED}). Therefore, these are also brought to the front of the equation.

$$\Phi = \frac{hcN_aV}{\lambda P_{LED}}\frac{k_1[\mathrm{NiC}]}{1 - 10^{-Abs_{\mathrm{NiC}}^{390}}} \qquad \textbf{(eq. S7)}$$

Absolute quantum yield determination by equation S7 necessitates the careful identification of the power of the light source through actinometry or calibrated instruments. Using a Thorlabs S425C thermal detector power meter 5 cm away from the light source, we determined the power of the PR160L 390 nm LED to be 198 W cm^{-2}. Given an irradiation surface area of 2.5 cm^2, we found P_{LED} = 0.494 W. We further note that eq. S7 assumes the absorption band monitored (Abs_{NiC}^{390}) is comprised of only one transition. A recent report by Park et al.[8] proposes possible low intensity ligand field transitions which overlap with the dominant MLCT bands in the absorption spectra of related Ni–bipyridine complexes. While we cannot rule out the presence of an obscured ligand field transition at 390 nm, computational analysis suggests that the observed absorption band is a charge transfer transition (d(yz)→ π*(2), for more details see Tables S10-S11). Therefore, we tentatively calculate the quantum yields of our complexes (Figure S53).

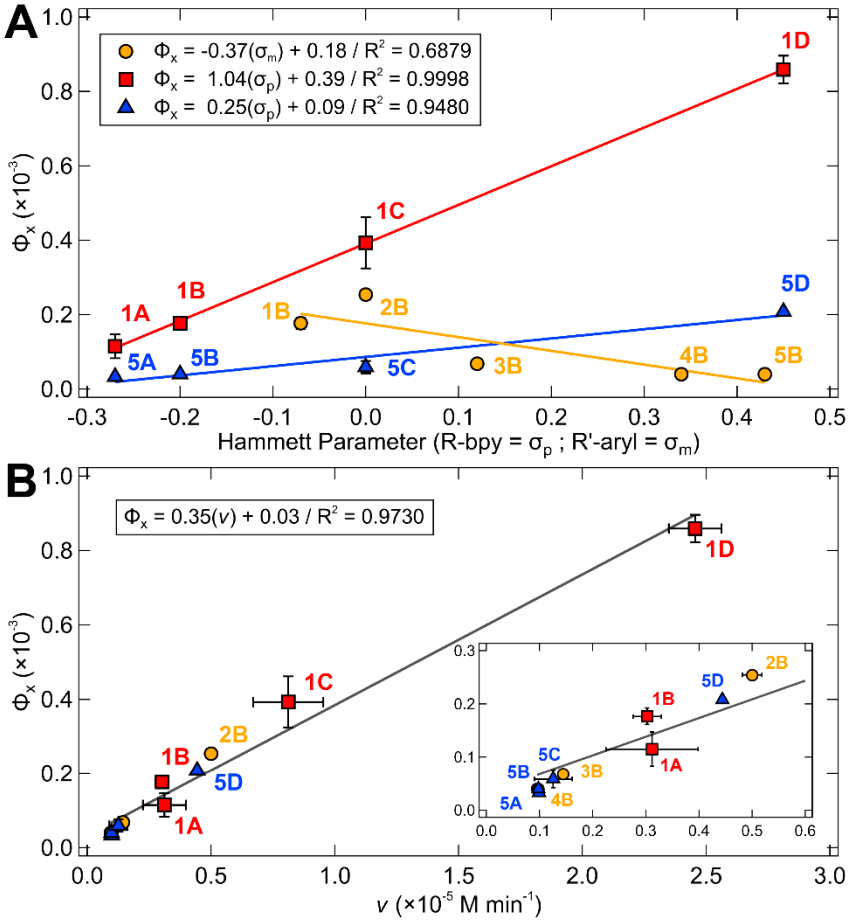

Figure S53. (A) Plot of the quantum yield in THF obtained by equation S7 using P_{LED} = 0.494 W and the experimentally measured absorbance at 390 nm for each complex versus the Hammett σ parameter for a given complex. The error in the aryl series (**1B**-**5B**, orange line) likely arises from an overestimation in rate for **2B**, which is also our most air/moisture sensitive compound. (B) The calculated quantum yields trend linearly with the observed rate of decay of the Ni(II)–bpy complexes (R^2 = 0.9730).

By normalizing the quantum yield of a given reactant, Φ_x, to that of its unsubstituted counterpart, Φ_H, (both defined in equation S8), we arrive at equation S9 in the same style as a Hammett kinetic analysis. These relative quantum yields allow for the examination of substituent effects and trends across our three series of complexes, **1A-1D**, **5A-5D**, and **1B-5B**.

$$\Phi_x = \frac{hcN_aV}{\lambda P_{LED}} \frac{k_{1,x}[\mathrm{NiC}]_x}{1-10^{-Abs^{390}_{\mathrm{NiC_x}}}};\ \Phi_H = \frac{hcN_aV}{\lambda P_{LED}} \frac{k_{1,H}[\mathrm{NiC}]_H}{1-10^{-Abs^{390}_{\mathrm{NiC_H}}}} \qquad \textbf{(eq. S8)}$$

$$\frac{\Phi_x}{\Phi_H} = \frac{k_{1,x}[\mathrm{NiC}]_x}{k_{1,H}[\mathrm{NiC}]_H}\left(\frac{1-10^{-Abs^{390}_{\mathrm{NiC_H}}}}{1-10^{-Abs^{390}_{\mathrm{NiC_x}}}}\right) \qquad \textbf{(eq. S9)}$$

Notably, the relative kinetic trends are mirrored by the relative quantum yield trends (Figure S54).

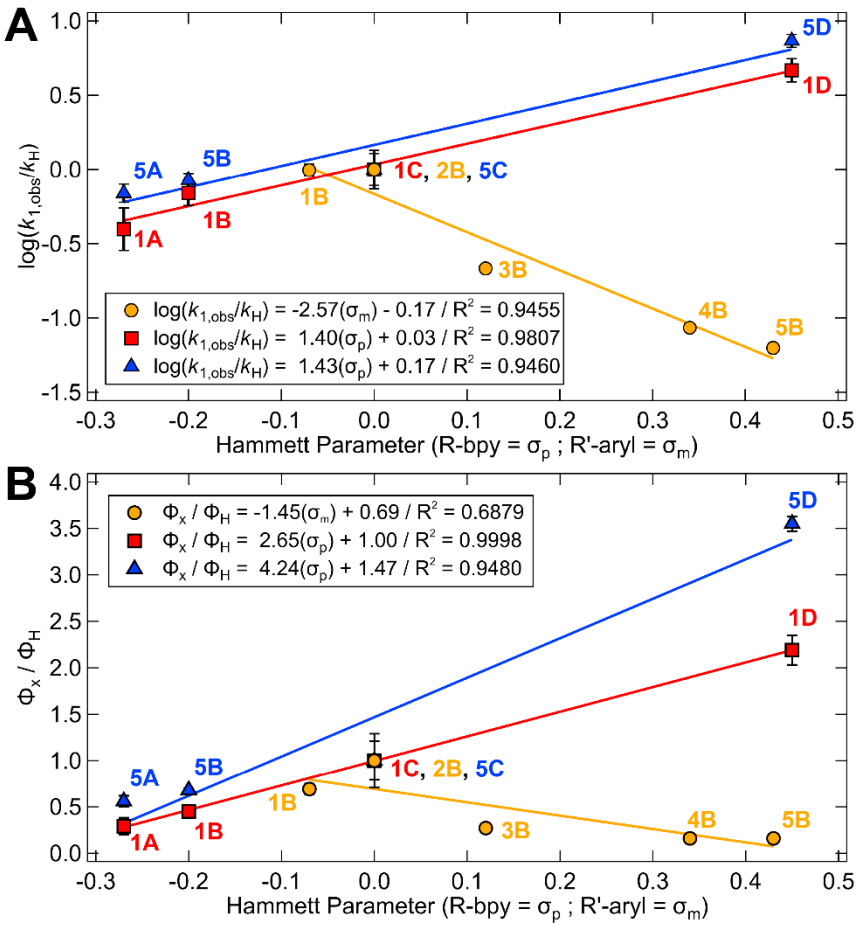

Figure S54. (A) Correlation between normalized rates of excited state bond homolysis and specific Hammett σ parameters of the bpy and aryl ligands. Note that in **1A**, the rate is approximated by $k_{2,\mathrm{obs}}$. Reproduced from main text Figure 5 for ease of comparison. (B) Relative quantum yields for each series plotted against the Hammett parameter for each complex. The error in the aryl series (**1B-5B**, orange line) likely arises from an overestimation in rate for **2B**, which is also our most air/moisture sensitive compound.

S2. Computational Section.

S2.1. General Computational Considerations.

All the computations were performed using ORCA 5.0 software.[14,15]

Density Functional Theory Calculations.
The molecular structures were optimized with DFT using the BP86[16,17] functional with def2-TZVPP(Ni)+def2-TZVP basis set,[18] D3BJ dispersion correction,[19,20] and the CPCM solvation model (THF).[21,22] The calculations were expedited by expanding the Coulomb integrals in an auxiliary basis set, the resolution-of-identity (RI-J) approximation.[23] The unrestricted Kohn-Sham formalism was used to approximate the lowest-energy broken-symmetry singlet (BSS) and triplet spin states, which were confirmed by performing the Löwdin spin population analysis.[24] The Ni–C bond homolysis reaction coordinate was obtained from the relaxed one-dimensional PES scans by incrementally increasing the Ni–C bond distance by 0.2 Å from 1.90 Å (equilibrium distance) to 3.50 Å. On top of the optimized geometries, the electronic energy terms and molecular properties were evaluated using the hybrid B3LYP[25,26] functional with the same def2-TZVPP(Ni)+def2-TZVP basis set, D3BJ dispersion correction, CPCM solvation model, and RIJCOSX approximation.[27]

Time-Dependent Density Functional Theory
To inspect the excited-state PESs and compare computations with the experimental UV/Vis spectra, we have performed TD-DFT calculations (total of 150 roots) on top of the BSS geometries. Additionally, the triplet excited-state surfaces were obtained from the TD-DFT calculations in the triplet spin state on top of the BSS geometries.

Multireference Calculations
As implemented in ORCA 5.0, multiconfigurational/multireference approximations to wave function theory such as CASSCF,[28,29] NEVPT2,[30–32] QD-NEVPT2[33,34] were applied in the combination with the def2-TZVPP(Ni)+def2-TZVP basis set and CPCM (THF) on top of the DFT-optimized BSS geometries. State-averaged calculations with 15 singlets and 25 triplets were used. Complete active spaces included 10 electrons in 9 orbitals (10e, 9o): Ni d(yz), d(z^2), d(xy), d(xz), a pair of bonding and antibonding Ni d(x^2-y^2)/aryl C(sp^2) orbitals, and three bpy π^* orbitals.

RI-SCS-MP2 and DLPNO-CCSD(T) Calculations
For **1B**, we have also computed the Ni–C bond dissociation coordinate using RI-SCS-MP2[35] and DLPNO-CCSD(T)[36,37] methods, which were performed on top of the reference UHF wave functions. For these calculations, we have used the larger def2-QZVPP(Ni)+def2-QZVP basis set.[15]

Optimized structures of all of the studied complexes are attached as the XYZ coordinates in a separate zip archive.

Sample Inputs

Example DFT Geometry Optimization

```
! UKS BP86 def2-TZVP def2/J
!RI D3BJ Opt CPCM(THF)
!SlowConv MORead
%moinp "orca.ges"
%basis
newgto Ni "def2-TZVPP" end
end
%maxcore 3000

*xyzfile 0 1 orca.xyz
```

Example TD-DFT Calculation

```
! UKS B3LYP def2-TZVP def2/J
!RIJCOSX TightSCF CPCM(THF)
!Normalprint MORead
%moinp "orca.ges"
%basis
newgto Ni "def2-TZVPP" end
end
%pal
nprocs 8
end
%maxcore 3000
%tddft
  maxdim 5
  nroots 150
  end

*xyzfile 0 1 orca.xyz
```

Example CASSCF/QD-NEVPT2 Calculation

```
! def2-TZVP AutoAUX RIJCOSX
!TightSCF CPCM(THF)
!MORead NormalPrint
%basis
newgto Ni "def2-TZVPP" end
end
%moinp "orca.ges"
%casscf
      nel     10
      norb    8
      nroots  25,15
      mult    3,1
      TrafoStep RI
      orbstep SuperCI
      switchstep DIIS
      MaxIter 500
      etol 3e-7
      printwf 1
      ptmethod sc_nevpt2
      ptsettings
      qdtype qd_vanvleck
      end
      rel
      printlevel 3
      dosoc true
      gtensor true
      dtensor true
      end
end
%pal
nprocs 8
end
%maxcore 16000

* xyzfile 0 1 orca.xyz
```

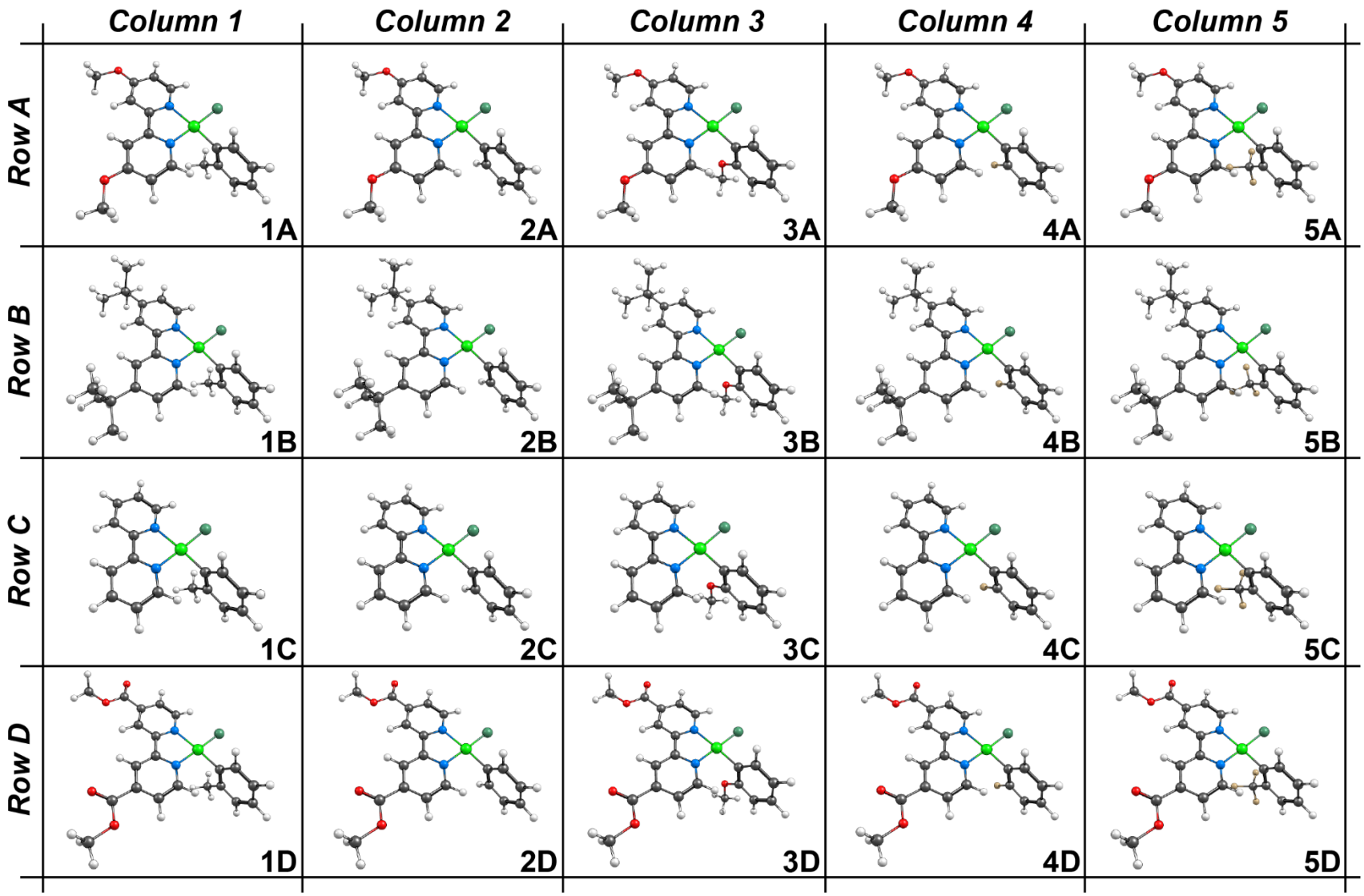

Figure S55. All DFT optimized structures (S = 0) for the matrix of Ni(^{R}bpy)($^{R'}$Ph)Cl (R = CH_3O, t-Bu, H, CH_3OOC; R′ = CH_3, H, OCH_3, F, CF_3) examined in this study.

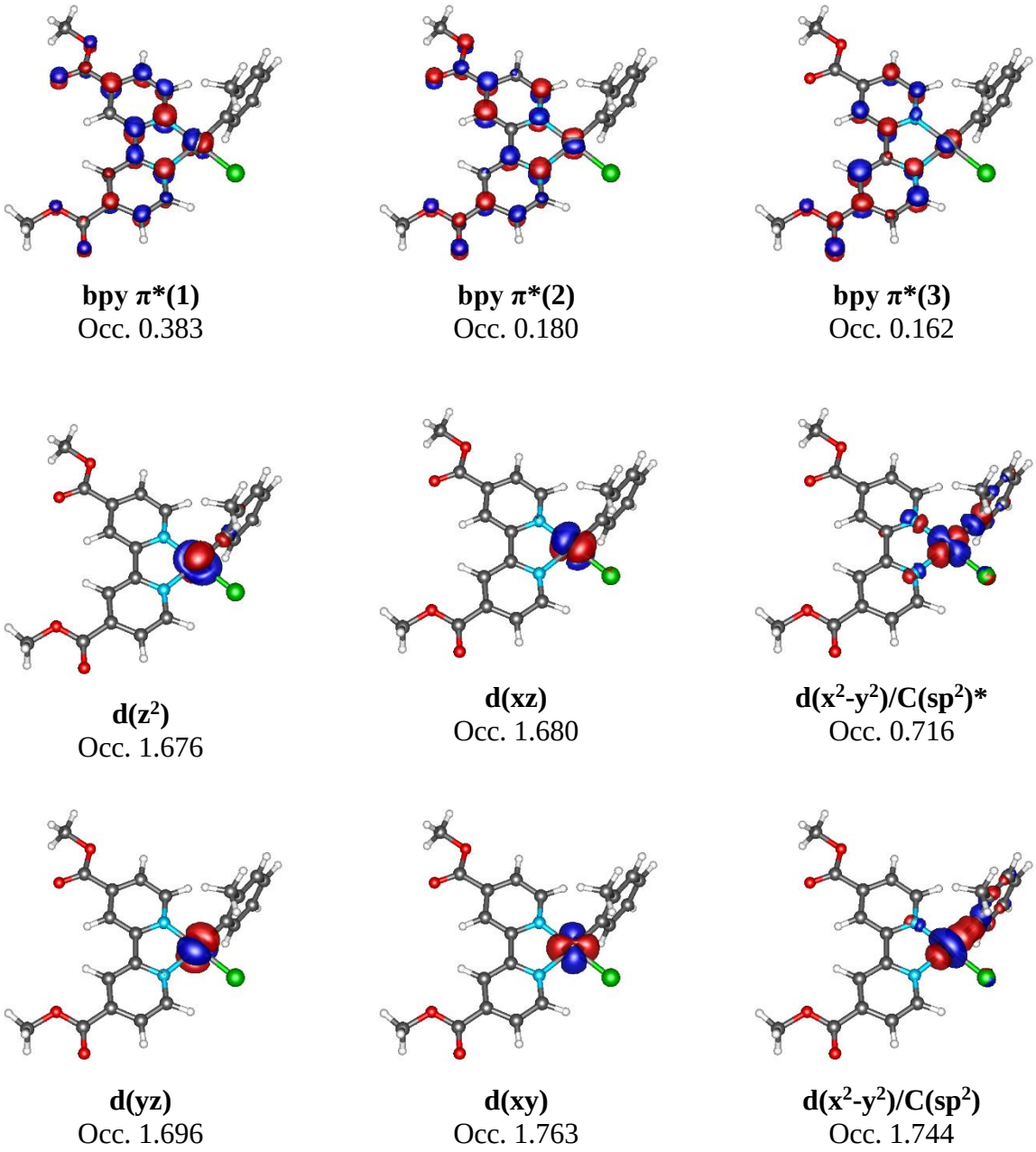

Figure S56. An example active space given for the **1D** complex, with x-axis along the Ni–halide bond and y-axis along the Ni–aryl bond. The CASSCF complete active space consists of 10 electrons in 9 orbitals (10e, 9o): Ni d(yz), d(z^2), d(xy), d(xz), a pair of bonding and antibonding Ni d(x^2-y^2)/aryl C(sp^2) orbitals, and three bpy π* orbitals.

S2.2 Limitations of the Computational Methods.

Multireference methods

The ground state wave functions of **1A**–**5D** exhibited a substantial multiconfigurational character. However, except for **1D**, the CASSCF/QD-NEVPT2 calculations predict only minor differences in the amount of closed-shell singlet (CSS) contribution in the configuration interaction (CI) vectors among the series of studied complexes, with the maximum CSS weight of ~60 % (Figure S57; *bottom*). This contrasts with the description at the CASSCF-only level, where the CSS contribution responds linearly to the Hammett parameters (Figure S57; *top*). Following the CASSCF trend, **1D** is predicted with the CSS weight of only 13 %, whereas the ^{1}MLCT [d(xz) → π*(1)] becomes the dominant configuration in the ground state wave function (with the weight of ~51 %). We believe that such a different description of the CASSCF reference wave function eventually renders an incomplete description of **1D** at the CASSCF/QD-NEVPT2 level; exhibited, e.g., by a deviation of **1D** from the CASSCF/QD-NEVPT2 composition trend in Figure S57; *bottom*.

As discussed in the main text, there is also a significant discrepancy in the activation energies obtained with TD-DFT and CASSCF/QD-NEVPT2 for the same photolysis mechanism, i.e., exploiting the ^{3}(MLCT+LMCT) pathway. This is likely due to the higher Ni(II)–C BDEs predicted with CASSCF/QD-NEVPT2 (Table S6), raising the energies of the repulsive one-photon, two-electron excited-state surfaces. In this respect, we note that the calculated BDEs vary significantly with the amount of the exact exchange (Table S7); the BDE from S = 0 ground state decreases with increasing exchange (e.g., in **1B**, the BDE is ~54 kcal mol^{-1} for pure BP86, ~48 kcal mol^{-1}for BP86+10% of exact exchange, ~39 kcal mol^{-1} for BP86+25%, and ~27 kcal mol^{-1}for BP86+50%). Notably, the Hartree-Fock and CASSCF methods severely underestimates the BDE at ~10 kcal mol^{-1} and ~5 kcal mol^{-1} for **1A–5D**, respectively.

Further exhibited by the excessive corrections of the second-order perturbation theory (UHF/RI-SCS-MP2, CASSCF/QD-NEVPT2) and domain based local pair natural orbital coupled-cluster theory (UHF/DLPNO-CCSD(T)) (Table S7), we believe that description of the **1A**–**5D** complexes is rather incomplete at the UHF and CASSCF level. In particular, we note the absence of the ^{3}[d(x^2-y^2)/C(sp^2) → d(x^2-y^2)/C(sp^2)*] state in the CASSCF calculation. This state is not observed even when increasing the number of triplet excited states present in the state-averaged CASSCF calculation to 100.

While this excited state is predicted at the TD-DFT level from the triplet state (*vide supra*) at ~80-90 kcal mol^{-1} for **1A–5D** in their singlet equilibrium geometries, the excited state was not observed in the lowest 25 triplets in our CASSCF reference wave functions (accounting for the excited states within ~100 kcal mol^{-1}). Note that the surface can be detected in CASSCF after excluding the bpy π* orbitals in the state-averaged calculations with 15 singlets/15 triplets and the 10e, 6o active spaces (Table S8). However, the corresponding excited states are raised up to the energies of ~170-190 kcal mol^{-1}, hence the absence in the calculations with 25 triplets/15 singlets and the 10e, 9o active spaces. In addition, the NEVPT2 and QD–NEVPT2 corrections predict an excited state energy for the ^{3}[d(x^2-y^2)/C(sp^2) → d(x^2-y^2)/C(sp^2)*] transition of ~0.5-8 kcal mol^{-1} and ~22-32 kcal mol^{-1}, respectively, indicative of a rather deficient description at the CASSCF level. Finally, we note that the ^{3}[d(x^2-y^2)/C(sp^2) → d(x^2-y^2)/C(sp^2)*] configuration decreases in the CI vectors of the lowest-lying singlet states along the Ni–C bond dissociation coordinates (Section S2.5), which is consistent with underestimated (CASSCF) or overestimated (CASSCF/NEVPT2 and CASSCF/QD-NEVPT2) BDEs as compared to the DFT methods.

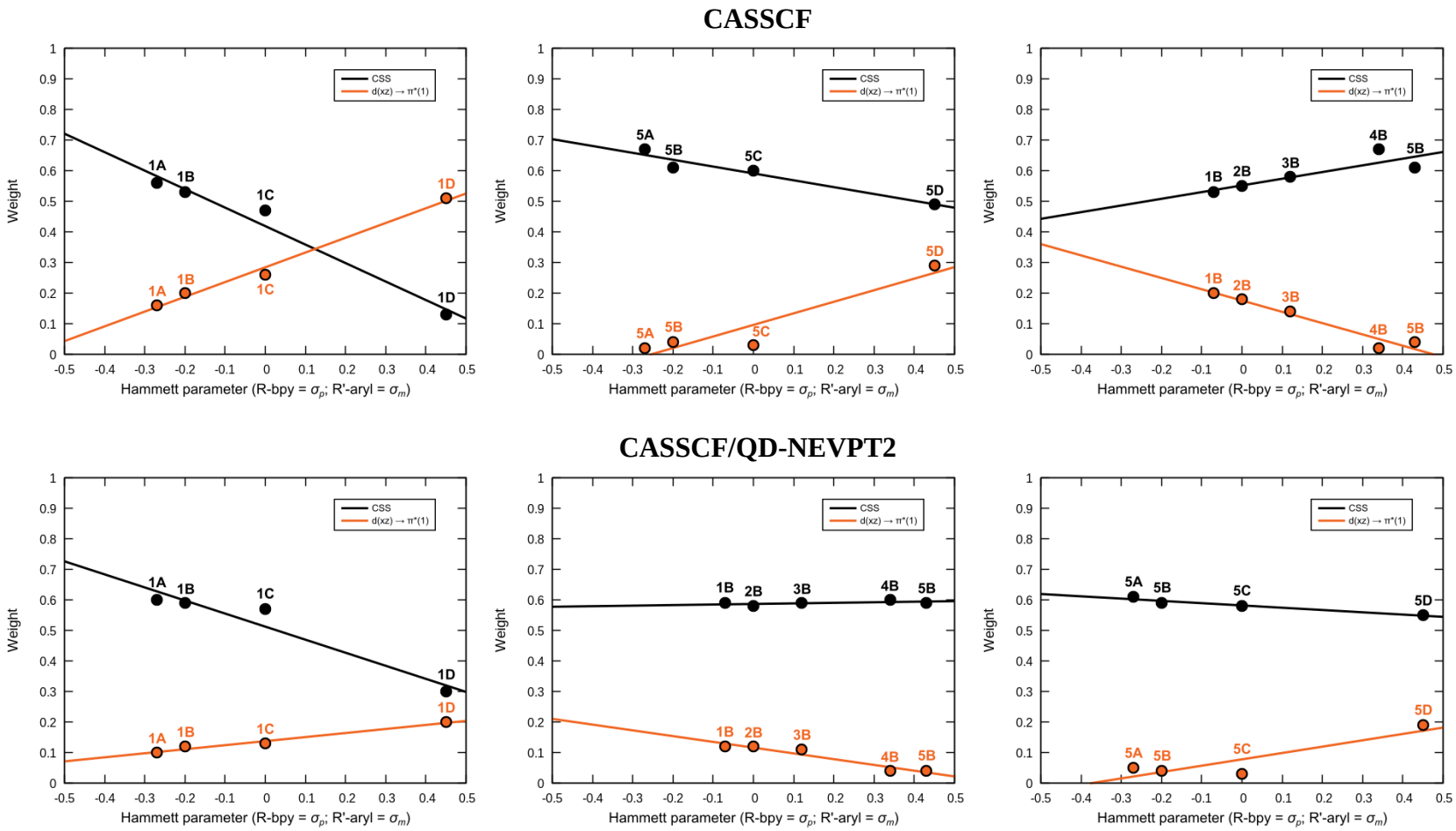

Figure S57. Hammett correlations for the weights of the closed-shell singlet (CSS) and Ni d(xz) → bpy π*(1) configurations in the lowest-energy singlet CI vectors of the equilibrium-geometry structures at the CASSCF (top) and CASSCF/QD-NEVPT2 (bottom) levels with the CPCM(THF) solvation model; 10e,9o Active Space – 25 triplet roots, 15 singlet roots.

Table S6. Difference in the BDEs for **1A**–**5D** and Ni(TMEDA)(CH_3Ph)Cl complexes obtained at the DFT (B3LYP) and CASSCF/QD-NEVPT2 level. The BDEs are significantly increased with CASSCF/QD-NEVPT2 method. The energies are referenced to the energies of the singlet ground states at their equilibrium geometries.

Compound	B3LYP	CASSCF/QD-NEVPT2
1A	41.3	90.1
1B	40.3	87.7
1C	38.9	84.6
1D	38.9	58.4
2A	42.0	---
2B	41.5	85.2
2C	41.6	---
2D	39.9	---
3A	42.2	---
3B	40.5	91.5
3C	41.9	---
3D	39.1	---
4A	44.4	---
4B	41.8	92.3
4C	44.5	---
4D	40.3	---
5A	43.6	91.6
5B	41.8	92.8
5C	42.2	90.3
5D	40.3	77.3
Ni(TMEDA)(CH_3Ph)Cl	43.8	62.7

Table S7. Comparison of the BDEs for **1B** obtained using different methods. The BDE is demonstrated to be related to the amount of HF exchange. The energies are given in kcal mol^{-1}

	BP86	BP86 +10%HF	BP86 +25%HF	BP86 +50%HF	UHF	CASSCF	SCS-MP2	DLPNO-CCSD(T)
1B (S=0)	53.7	48.0	39.2	27.2	12.3	3.1	52.3	52.8

Table S8. Energy of the $^3[d(x^2\text{-}y^2)/C(sp^2) \rightarrow d(x^2\text{-}y^2)/C(sp^2)^*]$ excited state (in kcal mol^{-1}) at different levels of theory.

Compound	CASSCF	CASSCF/NEVPT2	CASSCF/QD-NEVPT2
1A	175.5	3.5	28.7
1B	174.7	3.0	29.4
1C	173.2	2.7	30.3
1D	170.3	0.5	31.9
5A	189.2	5.7	22.0
5B	188.7	7.8	27.0
5C	186.5	6.8	27.1
5D	183.5	5.2	27.6

TD-DFT

A standard TD-DFT approach does not allow two-electron excitations. Therefore, it is not possible to inspect the 'one-photon, two-electron' triplet repulsive surfaces, denoted in the main text as ^{3}(MLCT+LMCT), from the singlet ground states. Additionally, the spin-forbidden one-electron

excitations to generate 'one-photon, one-electron' triplet excited-state surfaces (including, e.g., ^{3}LMCT proposed to be operative for Ni–TMEDA complexes) can be generated only via spin-flip transitions from the restricted Kohn-Sham orbitals. For that reason, we have also performed TD-DFT from the triplet excited states (at the singlet geometries) to complement the singlet TD-DFT computations of the conventional ^{1}MLCT bands.

Note that the lowest-energy triplet reference state has the electronic configuration described in Figure S58 with the singly-occupied d(z^2) and d(x^2-y^2)/C(sp^2)* orbitals. This represents limitations to our computational model, since only one single-electron (spin-allowed; β-to-β) excitation can produce the two-electron ^{3}(MLCT+LMCT) repulsive surface, d(x^2-y^2)/C(sp^2) → bpy π*(1) (blue panel in Figure S58). This contrasts with the CASSCF/QD-NEVPT2 method, for which all four ^{3}(MLCT+LMCT) surfaces with different MLCT donor-orbital components are in principle attainable.

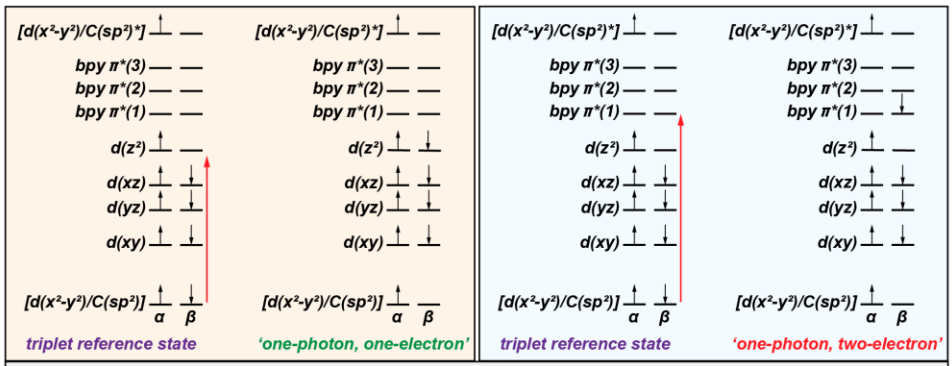

Triplet Repulsive Transitions	TDDFT	CASSCF/QD-NEVPT2
d(x^2-y^2)/C(sp^2) → d(x^2-y^2)/C(sp^2)*	✓	*not found*
d(x^2-y^2)/C(sp^2) + d(z^2) → d(x^2-y^2)/C(sp^2)* + bpy π*(1)	✓	✓
d(x^2-y^2)/C(sp^2) + d(xz) → d(x^2-y^2)/C(sp^2)* + bpy π*(1)	x	✓
d(x^2-y^2)/C(sp^2) + d(yz) → d(x^2-y^2)/C(sp^2)* + bpy π*(1)	x	✓
d(x^2-y^2)/C(sp^2) + d(xy) → d(x^2-y^2)/C(sp^2)* + bpy π*(1)	x	✓

Figure S58. The lowest-energy triplet reference state has the electronic configuration with the singly-occupied d(z^2) and d(x^2-y^2)/C(sp^2)* orbitals. Using the TD-DFT from the triplet reference, two energetically accessible triplet repulsive excited-state surfaces can be described: ^{3}LMCT surface (d(x^2-y^2)/C(sp^2) → d(x^2-y^2)/C(sp^2)*) and ^{3}(MLCT+LMCT) surface (d(x^2-y^2)/C(sp^2) + d(z^2) → d(x^2-y^2)/C(sp^2)* + bpy π*(1)). In contrast, four different ^{3}(MLCT+LMCT) triplet repulsive surfaces can be obtained using the CASSCF/QD-NEVPT2 method. However, due to deficiencies in the CASSCF reference wave function (as described above), the ^{3}LMCT surface cannot be identified.

Overall, the TD-DFT and CASSCF/QD-NEVPT2 trends are relatively consistent. However, both of the methods are assumed to be more reliable at the equilibrium geometries, which is exhibited by their good correlations with the experimental UV/Vis absorption spectra and Hammett parameters and calculated activation energies vs. the experimental rates of Ni–C homolysis. Since the multiconfigurational character of **1A**–**5D** complexes increases by moving from the equilibrium geometry, the deficient CASSCF reference wave functions appear to be less reliable. Similarly, the multiconfigurational nature and the large spin-population build-up at the near-dissociation limit present complications for the single-determinant TD-DFT method.

S2.3 Ground-State Calculated Properties

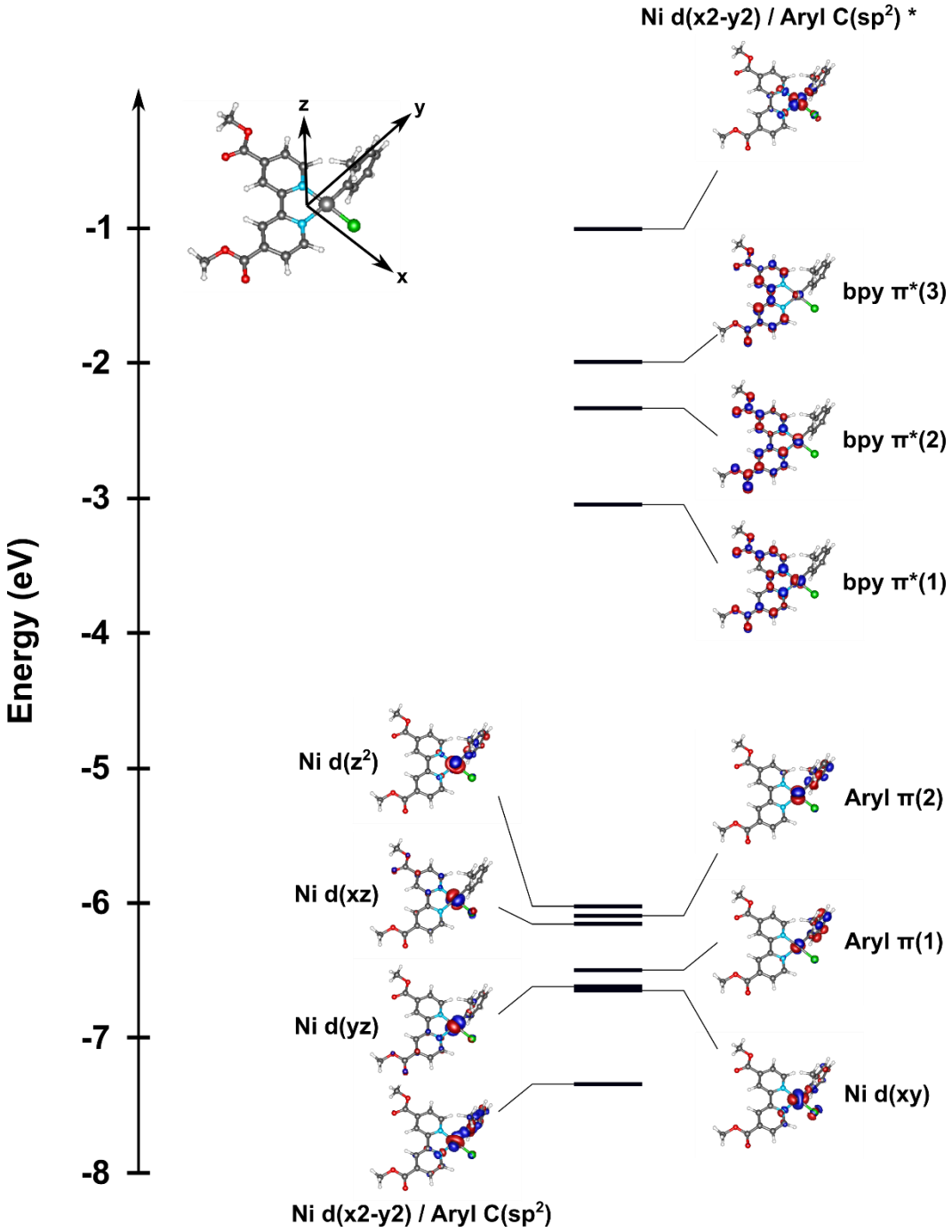

Figure S59. An example molecular orbital diagram given for the **1D** complex at the DFT level, with x-axis along the Ni–halide bond and y-axis along the Ni–aryl bond.

Columns:

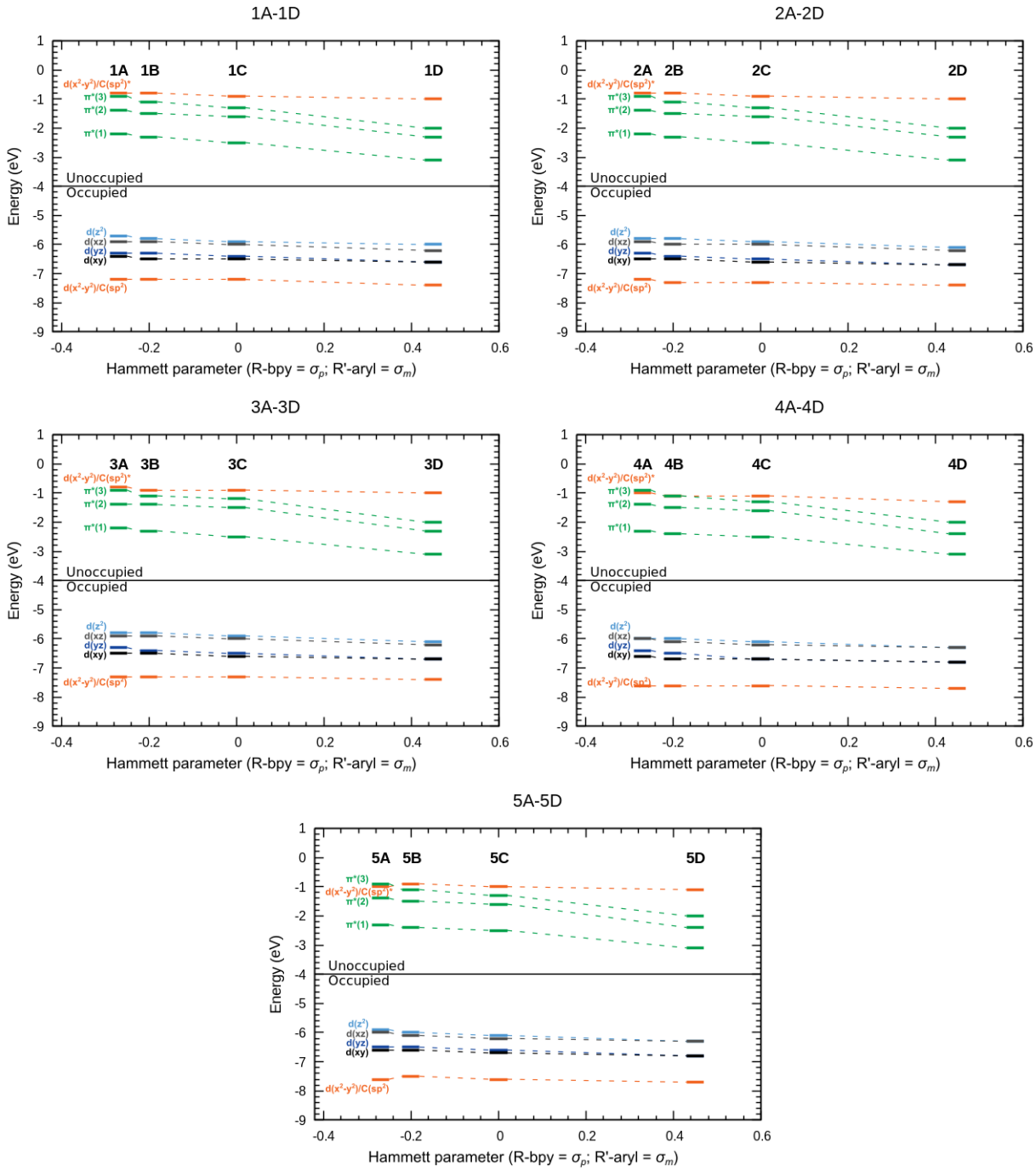

Figure S60. Comparison of the ground-state orbital energies for **1A-5D**, **1B–Br**, and Ni(TMEDA)(CH_3Ph)Cl complexes in their equilibrium geometries at the DFT (B3LYP) level with the CPCM(THF) solvation model.

Rows:

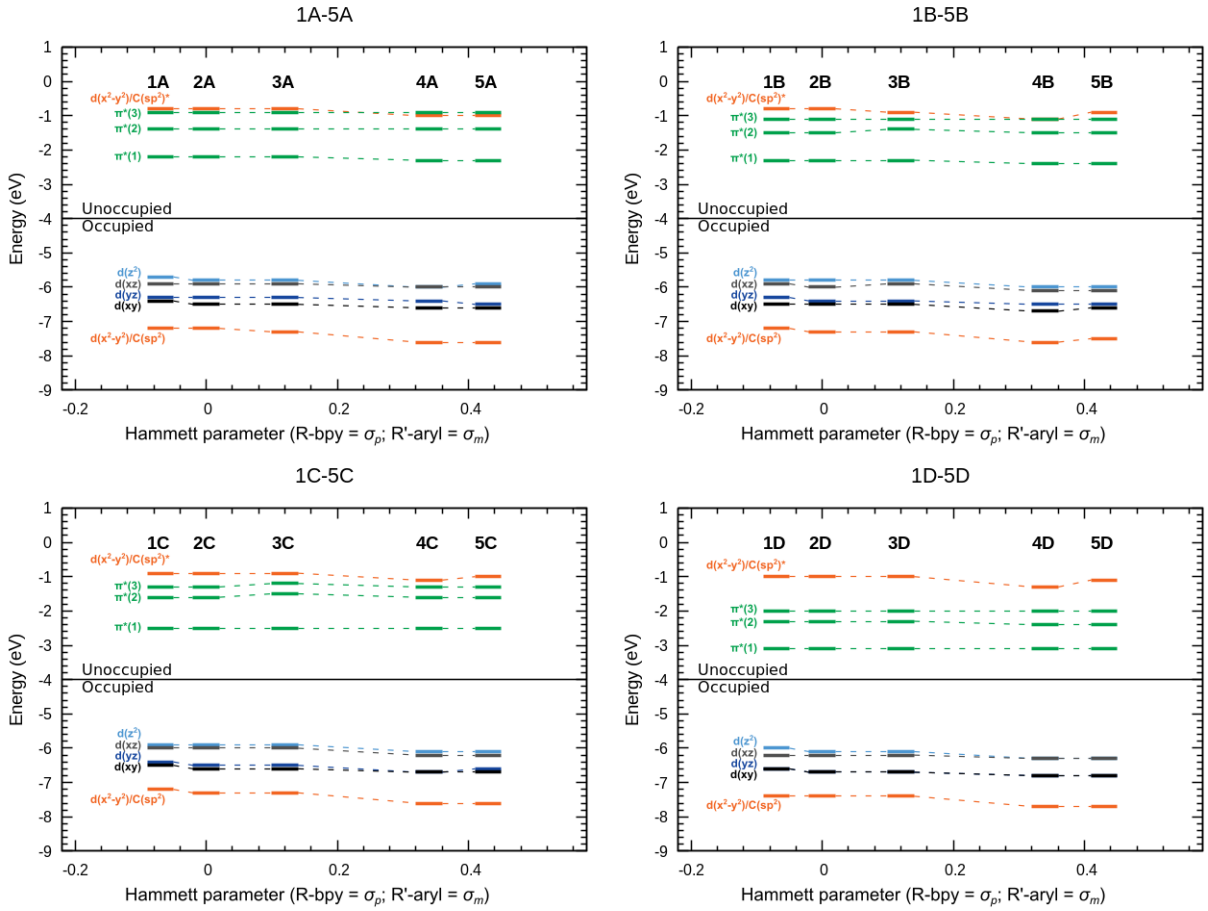

1B–Br and Ni(II)TMEDA:

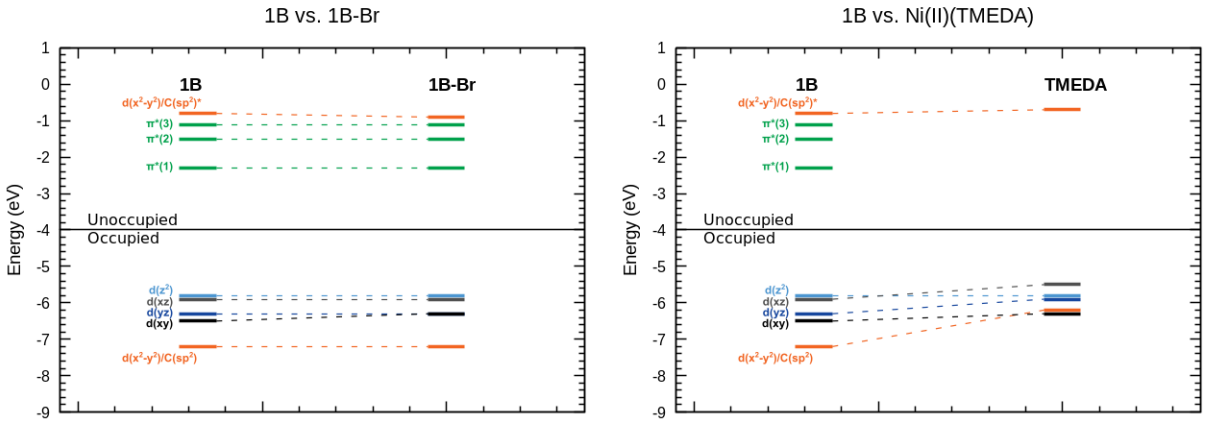

Figure S60, cont. Comparison of the ground-state orbital energies for **1A-5D**, **1B–Br**, and Ni(TMEDA)(CH_3Ph)Cl complexes in their equilibrium geometries at the DFT (B3LYP) level with the CPCM(THF) solvation model.

Table S9. Covalency of the low-spin d(x^2-y^2) ground states of **1A**–**5D** at the DFT (left) and CASSCF/QD-NEVPT2 (right) level. States with weights > 1% were included in the sum.

Compound	Ni character (%)	bpy character (%)	CSS (%)	Sum of all MLCT states (%)	Sum of all d-d states (%)	Sum of mixed MLCT + d-d states (%)
1A	53	12	60	16	17	1
1B	53	11	59	18	16	2
1C	52	11	57	20	15	2
1D	53	11	30	47	8	5
2A	53	12	---	---	---	---
2B	53	11	58	19	16	2
2C	53	11	---	---	---	---
2D	53	11	---	---	---	---
3A	47	20	---	---	---	---
3B	53	11	59	18	15	1
3C	53	12	---	---	---	---
3D	53	11	---	---	---	---
4A	54	12	---	---	---	---
4B	54	12	60	18	14	1
4C	54	12	---	---	---	---
4D	54	11	---	---	---	---
5A	53	13	61	15	18	0
5B	51	13	59	18	15	0
5C	53	12	58	20	13	1
5D	53	12	55	24	11	1

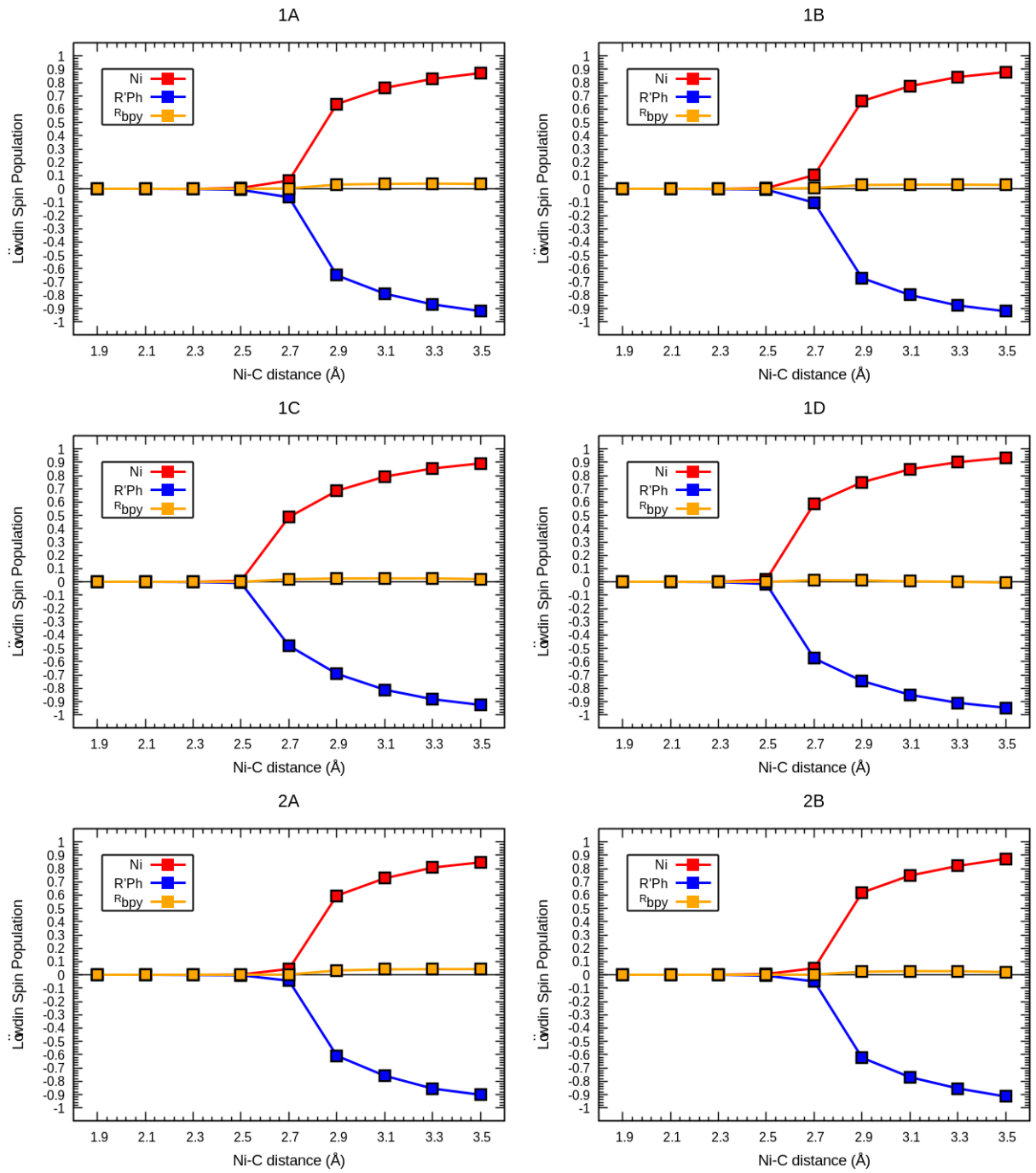

Figure S61. Evolution of the Löwdin spin populations for the BSS singlet state along the Ni–C bond dissociation coordinate at the DFT (B3LYP) level with the CPCM(THF) solvation model.

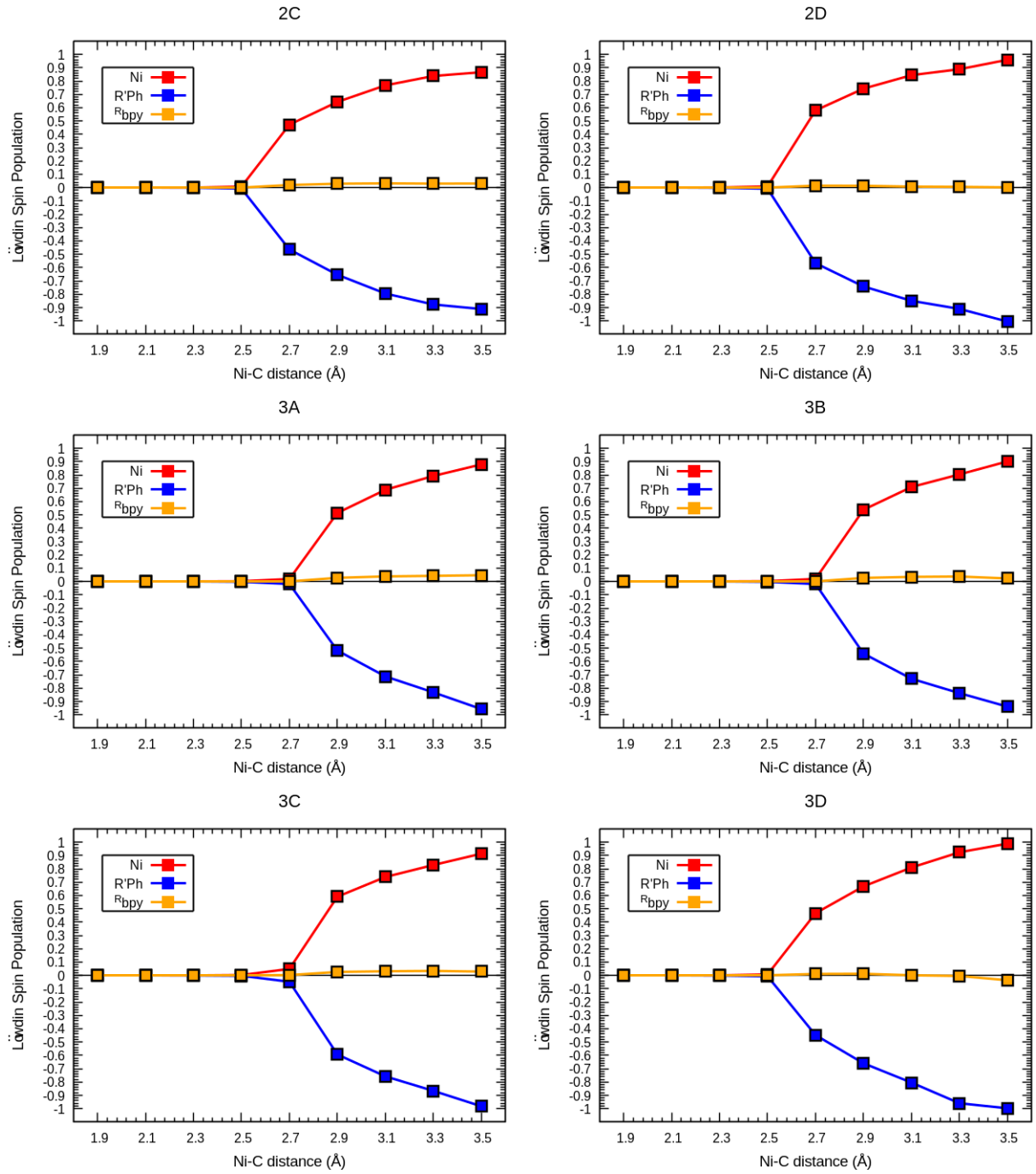

Figure S61, cont. Evolution of the Löwdin spin populations for the BSS singlet state along the Ni–C bond dissociation coordinate at the DFT (B3LYP) level with the CPCM(THF) solvation model.

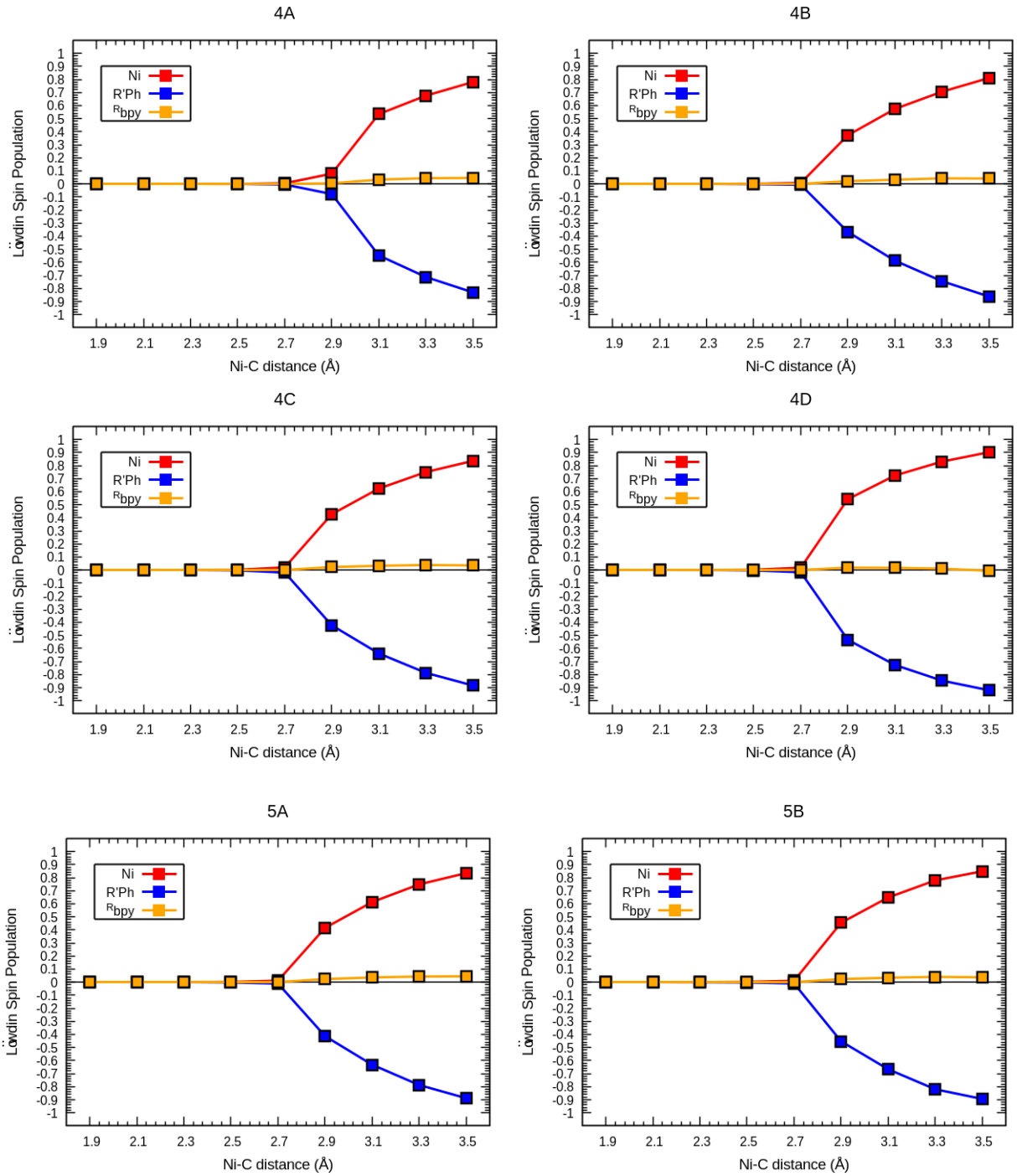

Figure S61, cont. Evolution of the Löwdin spin populations for the BSS singlet state along the Ni–C bond dissociation coordinate at the DFT (B3LYP) level with the CPCM(THF) solvation model.

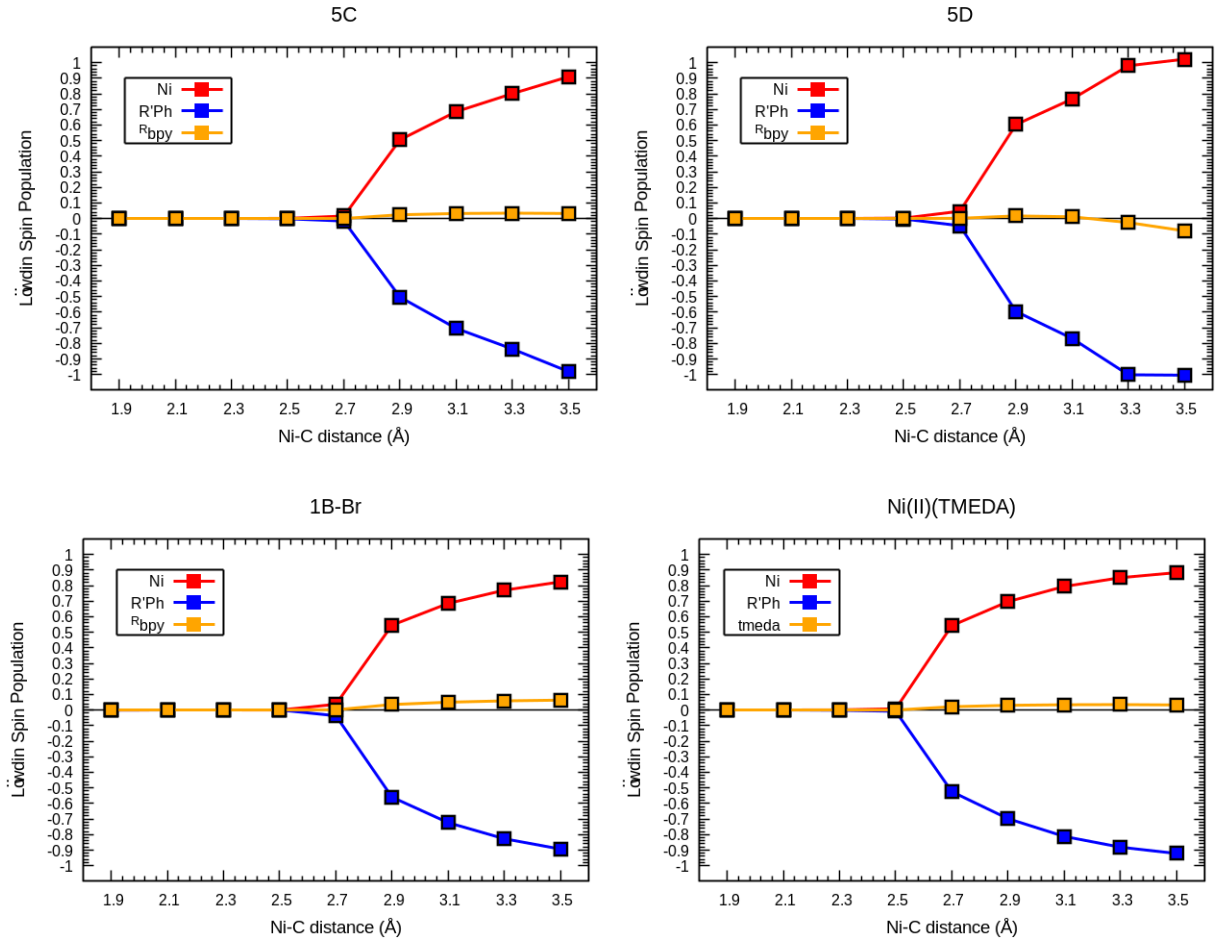

Figure S61, cont. Evolution of the Löwdin spin populations for the BSS singlet state along the Ni–C bond dissociation coordinate at the DFT (B3LYP) level with the CPCM(THF) solvation model.

S2.4 Excited-State Calculated Properties.

Table S10. Comparison of selected excited-states energies (kcal mol^{-1}) for **1A-5D**, **1B–Br**, and Ni(TMEDA)(CH_3Ph)Cl (abbreviated as Ni–TMEDA) complexes in their equilibrium geometries at the TD-DFT (UKS; B3LYP) level with the CPCM(THF) solvation model.

Transition	1A	1B	1C	1D	2B	3B	4B	5A	5B	5C	5D	1B–Br	Ni–TMEDA
							***S* = 0**						
$d(x^2\text{-}y^2)/C(sp^2) \rightarrow d(x^2\text{-}y^2)/C(sp^2)^*$	---	---	---	---	---	---	---	---	---	---	99.7	---	---
$d(x^2\text{-}y^2)/C(sp^2) \rightarrow \pi^*(1)$	85.5	84.9	82.0	71.2	84.8	88.0	95.4	97.1	92.4	89.1	79.4	85.0	---
$d(x^2\text{-}y^2)/C(sp^2) \rightarrow \pi^*(2)$	106.1	105.3	108.5	89.9	106.5	109.5	115.6	119.7	114.2	113.0	97.3	105.6	---
$d(yz) \rightarrow d(x^2\text{-}y^2)/C(sp^2)^*$	62.3	62.9	63.1	63.7	63.1	61.8	60.7	60.3	64.1	64.5	63.5	61.6	60.1
$d(yz) \rightarrow \pi^*(1)$	62.1	61.4	64.1	49.5	62.0	62.6	69.4	67.0	64.5	62.9	53.5	61.7	---
$d(yz) \rightarrow \pi^*(2)$	84.3	86.2	83.8	72.9	86.9	86.1	90.7	89.1	91.9	89.3	79.0	85.6	---
$d(xy) \rightarrow d(x^2\text{-}y^2)/C(sp^2)^*$	---	62.6	62.7	63.0	63.2	60.9	61.4	61.6	65.4	65.1	66.8	61.2	58.8
$d(xy) \rightarrow \pi^*(1)$	65.6	64.4	61.4	51.3	65.4	65.0	67.0	69.8	68.4	66.5	55.5	61.6	---
$d(xy) \rightarrow \pi^*(2)$	86.2	85.2	84.1	69.5	85.3	---	85.8	95.2	89.7	88.6	76.4	82.6	---
$d(z^2) \rightarrow d(x^2\text{-}y^2)/C(sp^2)^*$	56.0	56.2	55.9	60.5	56.7	54.7	54.7	54.3	57.2	56.3	62.1	54.9	53.7
$d(z^2) \rightarrow \pi^*(1)$	48.2	47.5	44.9	37.5	47.6	48.1	51.4	53.0	51.5	49.3	40.6	48.0	---
$d(z^2) \rightarrow \pi^*(2)$	69.3	69.0	68.6	55.0	69.0	69.7	72.8	74.1	73.8	73.5	61.1	69.5	---
$d(xz) \rightarrow d(x^2\text{-}y^2)/C(sp^2)^*$	57.2	58.2	58.9	60.4	57.7	56.2	56.2	55.5	58.8	59.3	60.8	55.9	55.9
$d(xz) \rightarrow \pi^*(1)$	52.6	51.7	48.8	38.9	51.9	52.5	55.3	56.6	54.9	52.3	42.7	51.5	---
$d(xz) \rightarrow \pi^*(2)$	78.8	77.9	72.3	64.1	73.3	78.8	81.4	82.3	82.2	80.1	62.9	77.0	---
							***S* = 1**						
$d(z^2) \rightarrow d(x^2\text{-}y^2)/C(sp^2)^*$	31.5	32.1	32.5	33.6	32.4	29.9	29.5	28.9	32.4	33.0	34.7	31.2	29.3
$d(x^2\text{-}y^2)/C(sp^2) \rightarrow d(x^2\text{-}y^2)/C(sp^2)^*$	83.7	83.5	83.4	83.0	85.9	77.7	84.3	89.3	91.8	90.5	91.7	82.2	69.3
$[d(x^2\text{-}y^2)/C(sp^2) + d(z^2)] \rightarrow [\pi^*(1) + d(x^2\text{-}y^2)/C(sp^2)^*]$	109.1	108.2	105.1	96.9	108.3	109.5	119.1	120.0	116.5	112.5	105.0	107.0	---
$d(z^2) \rightarrow \pi^*(1)$	41.4	40.6	37.7	27.8	40.9	41.7	45.4	47.1	45.6	43.1	34.6	40.2	---
$d(z^2) \rightarrow \pi^*(2)$	61.9	61.3	60.2	45.7	61.7	62.5	66.3	67.8	67.0	66.2	52.4	60.9	---

Table S10, cont. Comparison of selected excited-states energies (nm) for **1A-5D**, **1B–Br**, and Ni(TMEDA)(CH_3Ph)Cl (abbreviated as Ni–TMEDA) complexes in their equilibrium geometries at the TD-DFT (UKS; B3LYP) level with the CPCM(THF) solvation model.

Transition	1A	1B	1C	1D	2B	3B	4B	5A	5B	5C	5D	1B–Br	Ni–TMEDA
								***S* = 0**					
$d(x^2\text{-}y^2)/C(sp^2) \rightarrow d(x^2\text{-}y^2)/C(sp^2)^*$	---	---	---	---	---	---	---	---	---	---	287	---	---
$d(x^2\text{-}y^2)/C(sp^2) \rightarrow \pi^*(1)$	334	337	349	402	337	325	300	294	309	321	360	336	---
$d(x^2\text{-}y^2)/C(sp^2) \rightarrow \pi^*(2)$	269	272	264	318	268	261	247	239	250	253	294	271	---
$d(yz) \rightarrow d(x^2\text{-}y^2)/C(sp^2)^*$	459	455	453	449	453	463	471	474	446	443	450	464	476
$d(yz) \rightarrow \pi^*(1)$	460	466	446	578	461	457	412	427	443	455	534	463	---
$d(yz) \rightarrow \pi^*(2)$	339	332	341	392	329	332	315	321	311	320	362	334	---
$d(xy) \rightarrow d(x^2\text{-}y^2)/C(sp^2)^*$	---	457	456	454	452	469	466	464	437	439	428	467	486
$d(xy) \rightarrow \pi^*(1)$	436	444	466	557	437	440	427	410	418	430	515	464	---
$d(xy) \rightarrow \pi^*(2)$	332	336	340	411	335	---	333	300	319	323	374	346	---
$d(z^2) \rightarrow d(x^2\text{-}y^2)/C(sp^2)^*$	511	509	511	473	504	523	523	527	500	508	460	521	532
$d(z^2) \rightarrow \pi^*(1)$	593	602	637	762	601	594	556	539	555	580	704	596	---
$d(z^2) \rightarrow \pi^*(2)$	413	414	417	520	414	410	393	386	387	389	468	411	---
$d(xz) \rightarrow d(x^2\text{-}y^2)/C(sp^2)^*$	500	491	485	473	496	509	509	515	486	482	470	511	511
$d(xz) \rightarrow \pi^*(1)$	544	553	586	735	551	545	517	505	521	547	670	555	---
$d(xz) \rightarrow \pi^*(2)$	363	367	395	446	390	363	351	347	348	357	455	371	---
								***S* = 1**					
$d(z^2) \rightarrow d(x^2\text{-}y^2)/C(sp^2)^*$	908	891	880	851	882	956	969	989	882	866	824	916	976
$d(x^2\text{-}y^2)/C(sp^2) \rightarrow d(x^2\text{-}y^2)/C(sp^2)^*$	342	342	343	344	333	368	339	320	311	316	312	348	413
$[d(x^2\text{-}y^2)/C(sp^2) + d(z^2)] \rightarrow [\pi^*(1) + d(x^2\text{-}y^2)/C(sp^2)^*]$	262	264	272	295	264	261	240	238	245	254	272	267	---
$d(z^2) \rightarrow \pi^*(1)$	691	704	758	1028	699	686	630	607	627	663	826	711	---
$d(z^2) \rightarrow \pi^*(2)$	462	466	475	626	463	457	431	422	427	432	546	469	---

Table S11. Comparison of selected excited-states energies (kcal mol^{-1}) for **1A-5D**, **1B–Br**, and Ni(TMEDA)(CH_3Ph)Cl (abbreviated as Ni–TMEDA) complexes in their equilibrium geometries at the CASSCF/QD-NEVPT2 level with the CPCM(THF) solvation model; 10e,9o Active Space – 25 triplet roots, 15 singlet roots. For a complete list of excited state energies refer to Section 2.5, Additional Calculated Properties.

Transition	1A	1B	1C	1D	2B	3B	4B	5A	5B	5C	5D	1B–Br	Ni–TMEDA
							***S* = 0**						
d(yz) → d(x^2-y^2)/C(sp^2)*	68.0	67.5	65.2	---	69.2	70.7	66.1	65.0	75.0	67.3	70.9	67.6	63.3
d(yz) → π*(1)	52.8	52.1	48.7	40.3	52.2	54.2	50.3	52.9	55.3	53.8	41.4	51.1	---
d(yz) → π*(2)	76.9	76.4	75.9	57.5	76.0	77.4	73.8	74.3	77.9	---	69.7	75.1	---
d(xy) → d(x^2-y^2)/C(sp^2)*	62.5	65.1	65.9	---	66.0	64.2	69.1	67.6	68.2	68.0	---	63.7	62.1
d(xy) → π*(1)	62.8	63.4	62.0	48.0	62.0	60.3	58.4	71.6	60.1	59.4	59.0	61.1	---
d(xy) → π*(2)	90.9	90.3	---	71.5	90.5	91.9	---	---	93.5	---	---	89.5	---
d(z^2) → d(x^2-y^2)/C(sp^2)*	65.0	61.7	61.7	---	71.4	61.0	65.3	63.2	67.4	74.8	68.7	60.2	59.2
d(z^2) → π*(1)	43.5	42.6	39.9	23.0	42.0	43.2	39.7	38.8	---	47.1	35.4	41.3	---
d(z^2) → π*(2)	60.6	65.6	64.7	46.1	60.2	66.6	63.4	---	73.5	73.4	59.4	64.3	---
d(xz) → d(x^2-y^2)/C(sp^2)*	64.0	62.6	62.7	---	63.8	63.5	---	59.5	63.6	63.8	67.5	62.6	57.6
d(xz) → π*(1)	47.7	47.6	45.0	30.4	47.1	48.3	41.3	44.4	43.1	41.9	---	46.6	---
d(xz) → π*(2)	71.2	61.7	61.7	51.2	64.0	72.7	71.7	73.1	67.0	67.8	60.3	69.7	---
							***S* = 1**						
d(yz) → d(x^2-y^2)/C(sp^2)*	33.3	34.2	33.4	16.1	34.8	33.8	34.0	31.3	36.4	37.1	33.5	34.0	35.3
d(yz) → π*(1)	52.9	52.2	48.9	34.1	51.6	52.8	48.4	51.3	52.2	51.2	44.9	50.7	---
d(yz) → π*(2)	75.9	76.1	75.1	58.4	75.7	76.9	72.9	74.0	75.8	70.5	69.5	74.5	---
d(xy) → d(x^2-y^2)/C(sp^2)*	42.3	43.3	44.2	55.6	45.5	42.2	43.0	41.4	45.3	46.2	47.9	45.6	22.5
d(xy) → π*(1)	67.7	66.9	64.4	48.1	66.6	65.8	64.5	67.2	68.6	66.0	61.1	65.7	---
d(xy) → π*(2)	90.6	88.9	---	72.2	89.9	91.5	88.5	89.2	92.3	93.1	86.2	89.0	---
d(z^2) → d(x^2-y^2)/C(sp^2)*	26.6	27.4	26.4	10.6	27.9	26.5	27.2	25.1	32.9	33.4	29.3	27.2	19.8
d(z^2) → π*(1)	42.8	41.7	38.9	22.2	41.0	42.4	38.7	41.9	46.2	---	---	40.4	---
d(z^2) → π*(2)	62.8	65.3	---	46.6	62.7	66.3	63.1	64.2	69.8	76.8	59.3	63.8	---
d(xz) → d(x^2-y^2)/C(sp^2)*	30.5	31.4	30.8	7.1	31.9	30.7	30.5	28.1	28.9	29.5	34.1	31.4	15.6
d(xz) → π*(1)	46.0	44.9	42.4	25.9	42.2	45.9	42.2	45.0	42.3	41.1	---	40.8	---
d(xz) → π*(2)	67.7	68.0	67.7	50.0	67.6	69.3	66.1	66.7	66.7	67.2	62.7	67.1	---
[d(x^2-y^2)/C(sp^2) + d(yz)] → [π*(1) + d(x^2-y^2)/C(sp^2)*]	---	110.5	109.4	87.8	110.6	114.7	---	119.6	121.6	120.1	---	108.4	---
[d(x^2-y^2)/C(sp^2) + d(xy)] → [π*(1) + d(x^2-y^2)/C(sp^2)*]	---	---	---	82.6	---	---	---	---	---	---	---	---	---
[d(x^2-y^2)/C(sp^2) + d(z^2)] → [π*(1) + d(x^2-y^2)/C(sp^2)*]	120.0	120.7	115.9	95.0	120.3	123.1	---	---	---	---	119.4	116.7	---
[d(x^2-y^2)/C(sp^2) + d(xz)] → [π*(1) + d(x^2-y^2)/C(sp^2)*]	117.4	117.3	114.7	---	117.4	119.4	---	---	---	---	116.5	115.3	---

Table S11, cont. Comparison of selected excited-states energies (nm) for **1A-5D**, **1B–Br**, and Ni(TMEDA)(CH_3Ph)Cl (abbreviated as Ni–TMEDA) complexes in their equilibrium geometries at the CASSCF/QD-NEVPT2 level with the CPCM(THF) solvation model; 10e,9o Active Space – 25 triplet roots, 15 singlet roots. For a complete list of excited state energies refer to Section 2.5, Additional Calculated Properties.

Transition	1A	1B	1C	1D	2B	3B	4B	5A	5B	5C	5D	1B–Br	Ni–TMEDA
							***S* = 0**						
$d(yz) \rightarrow d(x^2\text{-}y^2)/C(sp^2)^*$	420	424	439	---	413	404	433	440	381	425	403	423	452
$d(yz) \rightarrow \pi^*(1)$	542	549	587	709	548	528	568	540	517	531	691	560	---
$d(yz) \rightarrow \pi^*(2)$	372	374	377	497	376	369	387	385	367	---	410	381	---
$d(xy) \rightarrow d(x^2\text{-}y^2)/C(sp^2)^*$	457	439	434	---	433	445	414	423	419	420	---	449	460
$d(xy) \rightarrow \pi^*(1)$	455	451	461	596	461	474	490	399	476	481	485	468	---
$d(xy) \rightarrow \pi^*(2)$	315	317	---	400	316	311	---	---	306	---	---	319	---
$d(z^2) \rightarrow d(x^2\text{-}y^2)/C(sp^2)^*$	440	463	463	---	400	469	438	452	424	382	416	475	483
$d(z^2) \rightarrow \pi^*(1)$	657	671	717	1243	681	662	720	737	---	607	808	692	---
$d(z^2) \rightarrow \pi^*(2)$	472	436	442	620	475	429	451	---	389	390	481	445	---
$d(xz) \rightarrow d(x^2\text{-}y^2)/C(sp^2)^*$	447	457	456	---	448	450	---	481	450	448	424	457	496
$d(xz) \rightarrow \pi^*(1)$	599	601	635	941	607	592	692	644	663	682	---	614	---
$d(xz) \rightarrow \pi^*(2)$	402	463	463	558	447	393	399	391	427	422	474	410	---
							***S* = 1**						
$d(yz) \rightarrow d(x^2\text{-}y^2)/C(sp^2)^*$	859	836	856	1776	822	846	841	913	785	771	853	841	810
$d(yz) \rightarrow \pi^*(1)$	540	548	585	838	554	542	591	557	548	558	637	564	---
$d(yz) \rightarrow \pi^*(2)$	377	376	381	490	378	372	392	386	377	406	411	384	---
$d(xy) \rightarrow d(x^2\text{-}y^2)/C(sp^2)^*$	676	660	647	514	628	678	665	691	631	619	597	627	1271
$d(xy) \rightarrow \pi^*(1)$	422	427	444	594	429	435	443	425	417	433	468	435	---
$d(xy) \rightarrow \pi^*(2)$	316	322	---	396	318	312	323	321	310	307	332	321	---
$d(z^2) \rightarrow d(x^2\text{-}y^2)/C(sp^2)^*$	1075	1043	1083	2697	1025	1079	1051	1139	869	856	976	1051	1444
$d(z^2) \rightarrow \pi^*(1)$	668	686	735	1288	697	674	739	682	619	---	---	708	---
$d(z^2) \rightarrow \pi^*(2)$	455	438	---	614	456	431	453	445	410	372	482	448	---
$d(xz) \rightarrow d(x^2\text{-}y^2)/C(sp^2)^*$	937	911	928	4027	896	931	937	1017	989	969	838	911	1833
$d(xz) \rightarrow \pi^*(1)$	622	637	674	1104	678	623	678	635	676	696	---	701	---
$d(xz) \rightarrow \pi^*(2)$	422	420	422	572	423	413	433	429	429	425	456	426	---
$[d(x^2\text{-}y^2)/C(sp^2) + d(yz)] \rightarrow [\pi^*(1) + d(x^2\text{-}y^2)/C(sp^2)^*]$	---	259	261	326	259	249	---	239	235	238	---	264	---
$[d(x^2\text{-}y^2)/C(sp^2) + d(xy)] \rightarrow [\pi^*(1) + d(x^2\text{-}y^2)/C(sp^2)^*]$	---	---	---	346	---	---	---	---	---	---	---	---	---
$[d(x^2\text{-}y^2)/C(sp^2) + d(z^2)] \rightarrow [\pi^*(1) + d(x^2\text{-}y^2)/C(sp^2)^*]$	238	237	247	301	238	232	---	---	---	---	239	245	---
$[d(x^2\text{-}y^2)/C(sp^2) + d(xz)] \rightarrow [\pi^*(1) + d(x^2\text{-}y^2)/C(sp^2)^*]$	244	244	249	---	244	239	---	---	---	---	245	248	---

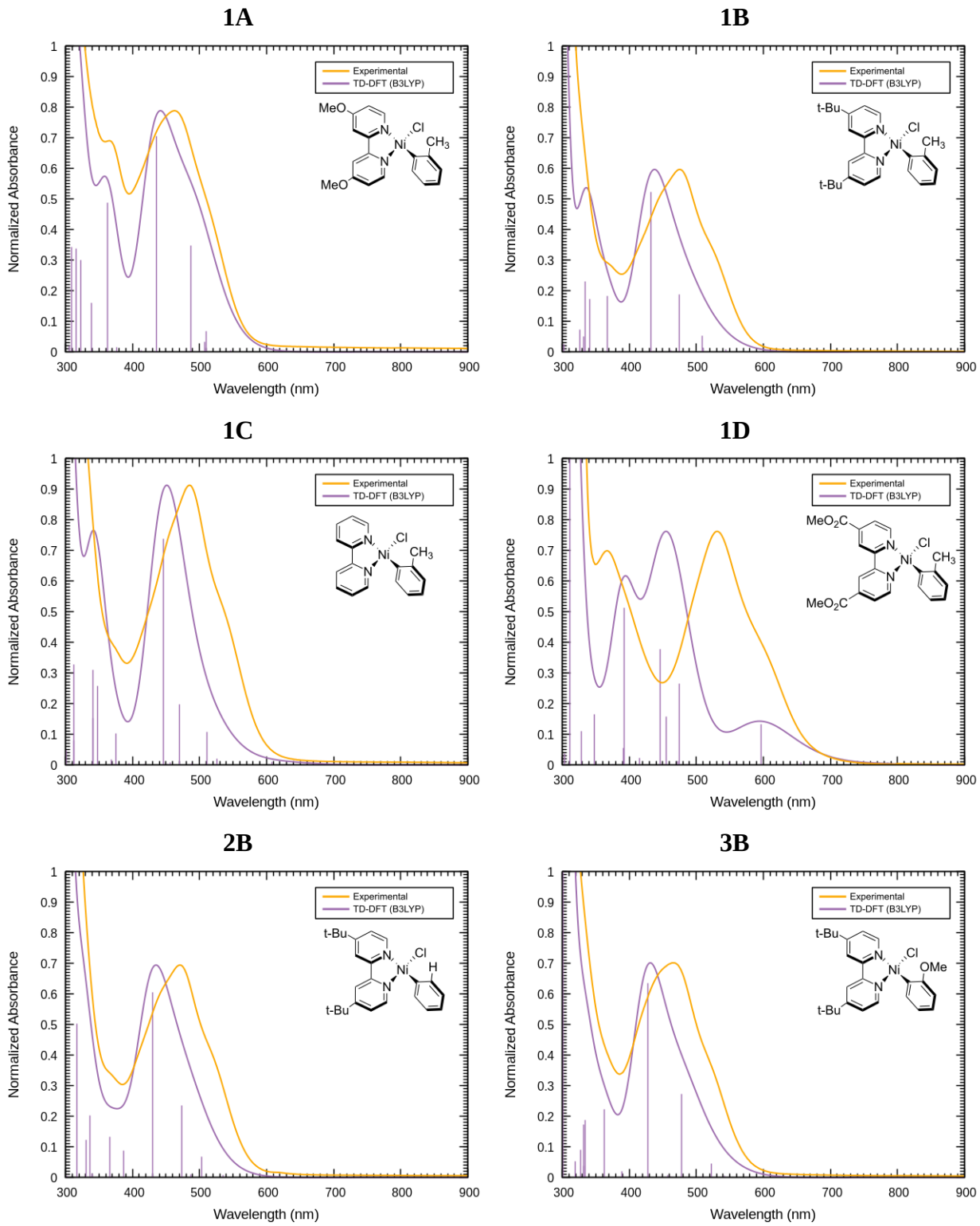

Figure S62. Overlay of the experimental (THF) (orange) and calculated (purple) UV-vis spectra for the equilibrium structures of **1A**–**5D** at the TD-DFT (B3LYP) level with the CPCM(THF) solvation model.

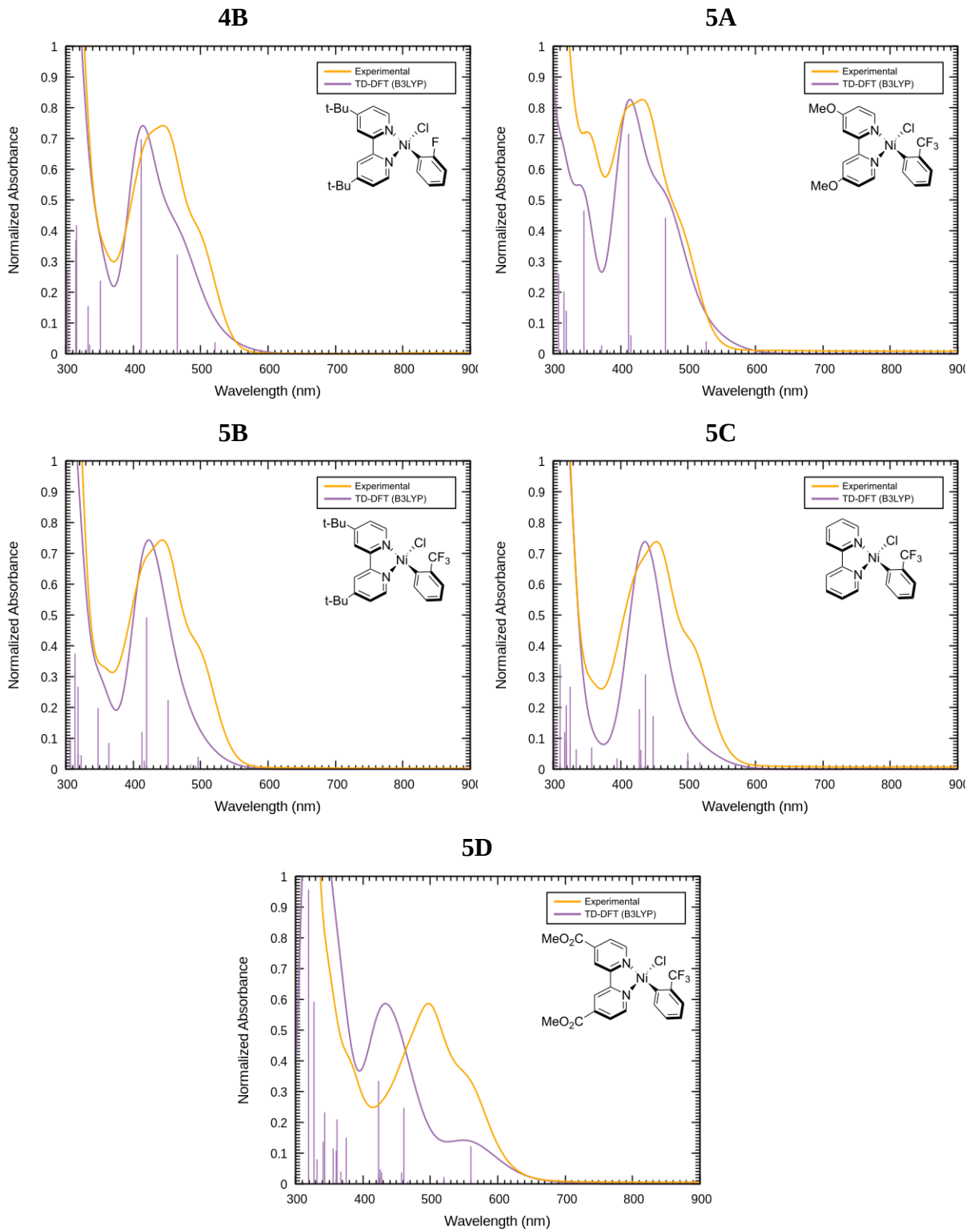

Figure S62, cont. Overlay of the experimental (THF) (orange) and calculated (purple) UV-vis spectra for the equilibrium structures of **1A**–**5D** at the TD-DFT (B3LYP) level with the CPCM(THF) solvation model.

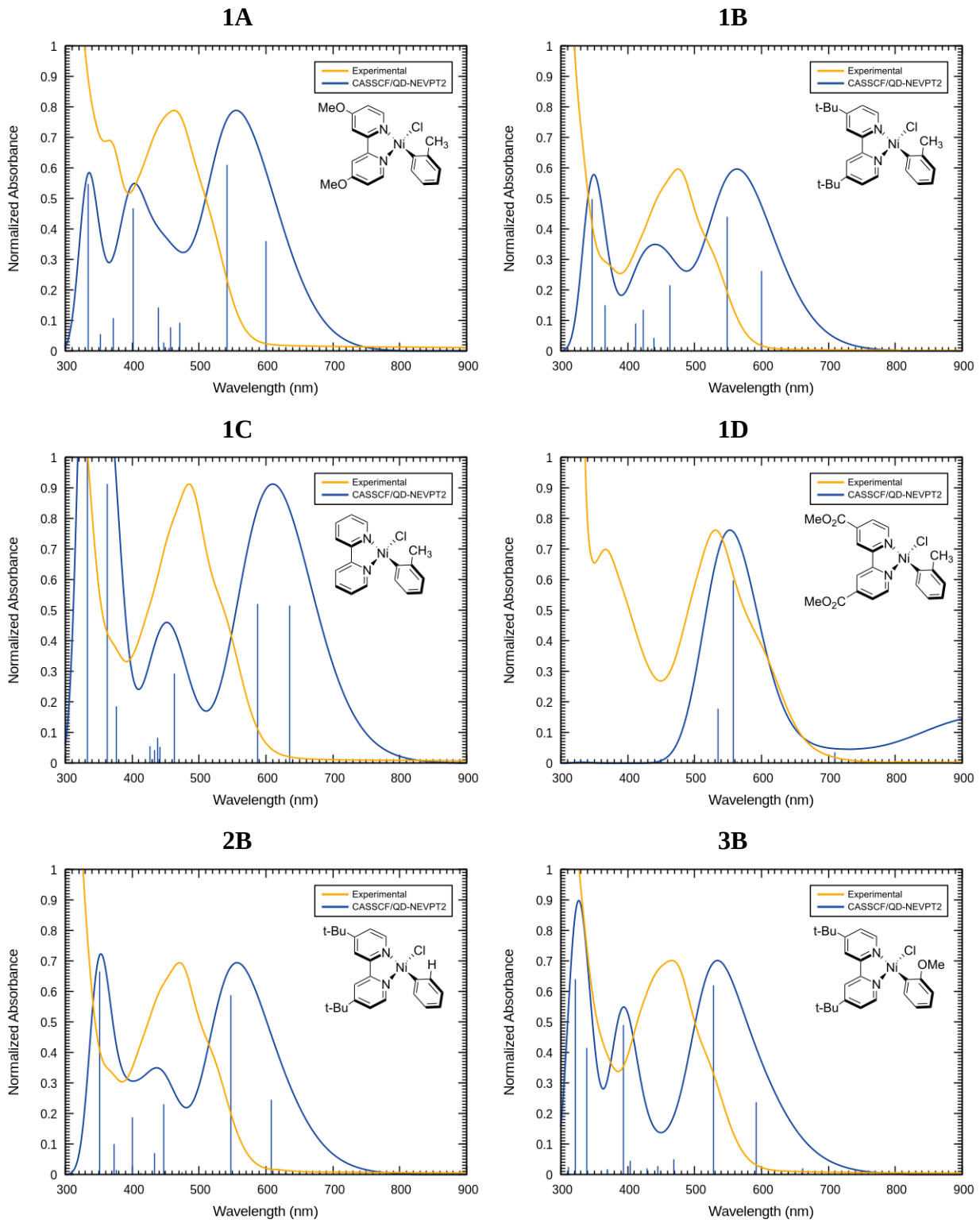

Figure S63. Overlay of the experimental (THF) (orange) and calculated (blue) UV-vis spectra for the equilibrium structures of **1A**–**5D** at the CASSCF/QD-NEVPT2 level with the CPCM(THF) solvation model; 10e,9o Active Space – 25 triplet roots, 15 singlet roots.

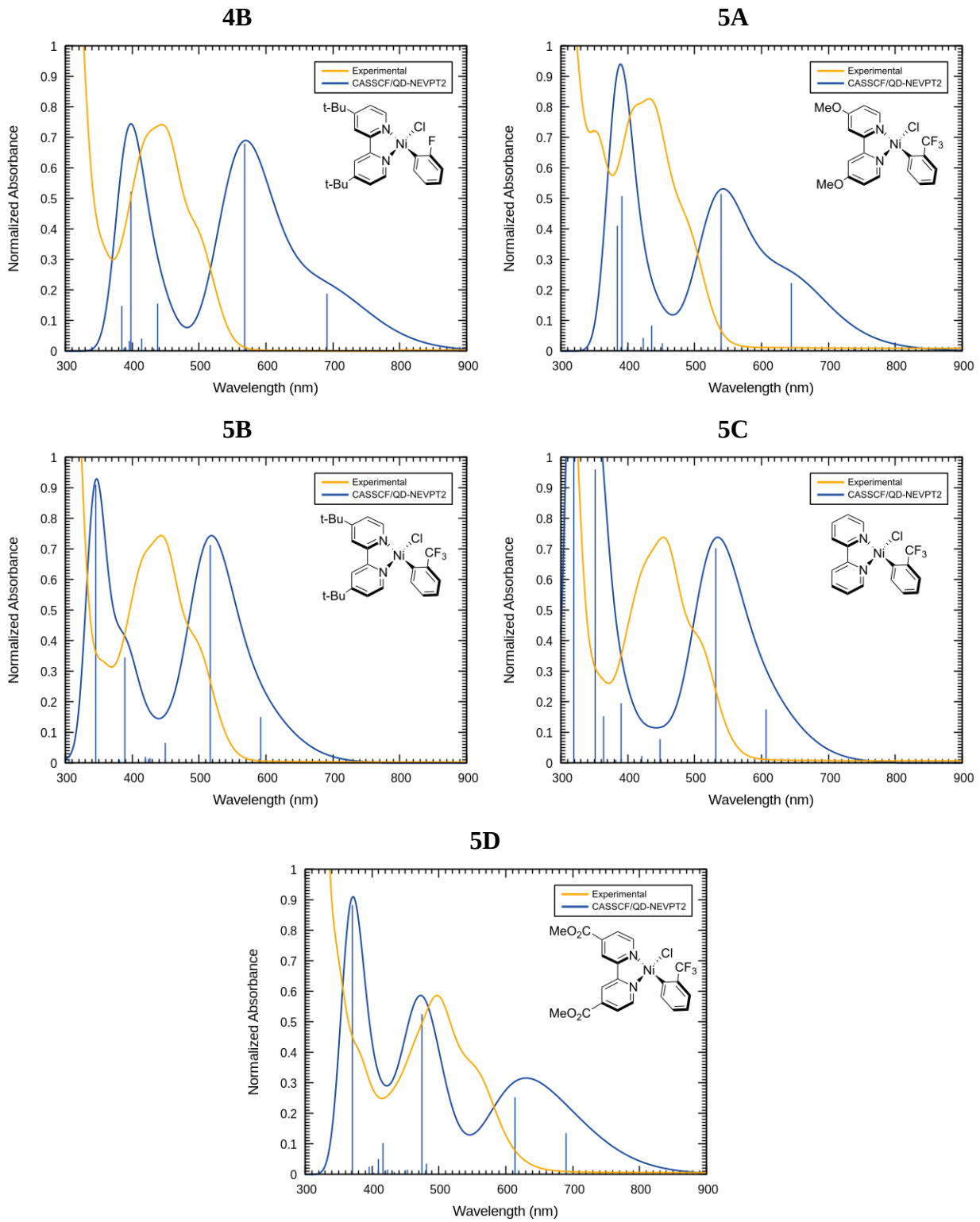

Figure S63, cont. Overlay of the experimental (THF) (orange) and calculated (blue) UV-vis spectra for the equilibrium structures of **1A**–**5D** at the CASSCF/QD-NEVPT2 level with the CPCM(THF) solvation model; 10e,9o Active Space – 25 triplet roots, 15 singlet roots.

1B–Br

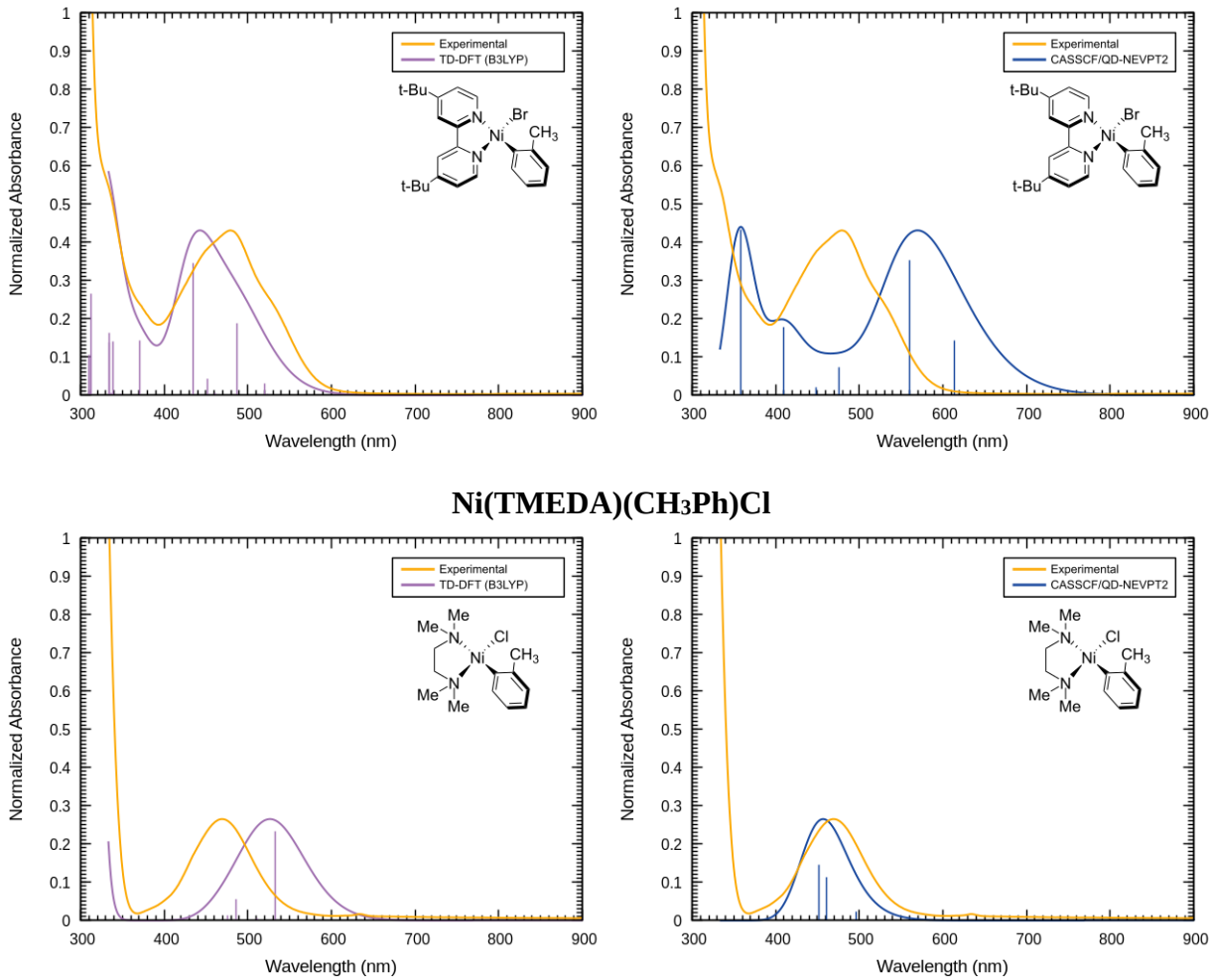

Ni(TMEDA)(CH_3Ph)Cl

Figure S64. Overlay of the experimental (THF) (orange) and calculated UV-vis spectra of the equilibrium structures for **1B–Br** and Ni(TMEDA)(CH_3Ph)Cl complexes at the TD-DFT (B3LYP) (purple) and CASSCF/QD-NEVPT2 (blue) levels with the CPCM(THF) solvation model.

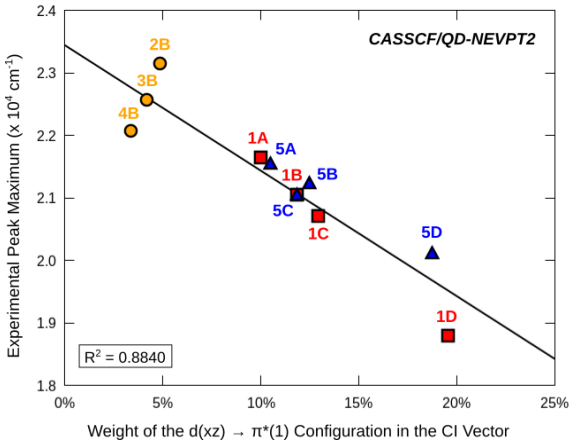

Figure S65. Correlation between the experimental peak maxima measured in THF solvent vs. the weight of the Ni d(xz) → bpy π*(1) configuration in the lowest-energy singlet CI vector of the equilibrium-geometry structures at the CASSCF/QD-NEVPT2 level; 10e, 9o Active Space – 25 triplet roots, 15 singlet roots.

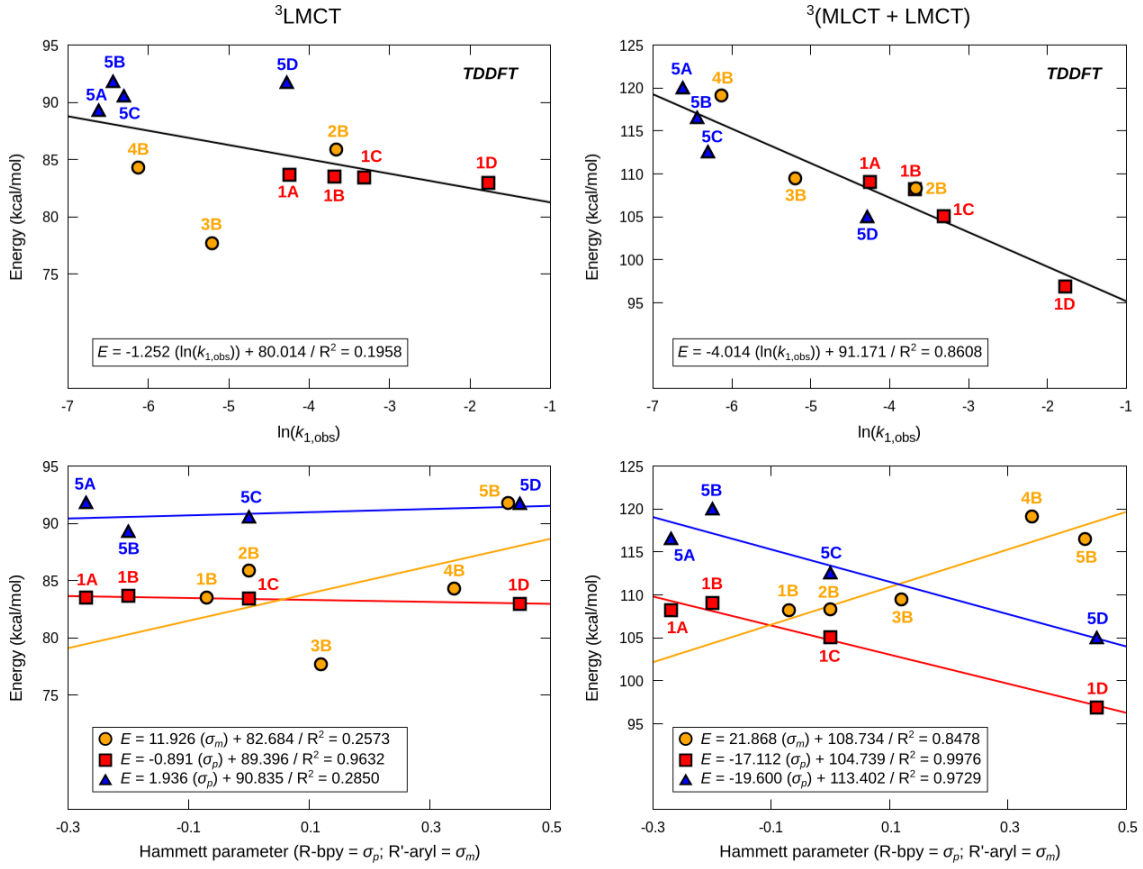

Figure S66. Correlation of the TD-DFT energies of the 'one-photon, one-electron' (left) and 'one-photon, two-electron' (right) triplet repulsive surfaces (*cf.* Figure 10 in the main text) at the singlet equilibrium geometry vs. the experimental rates of the Ni–C homolysis (top) and Hammett parameters (bottom) for **1A**–**5D** complexes.

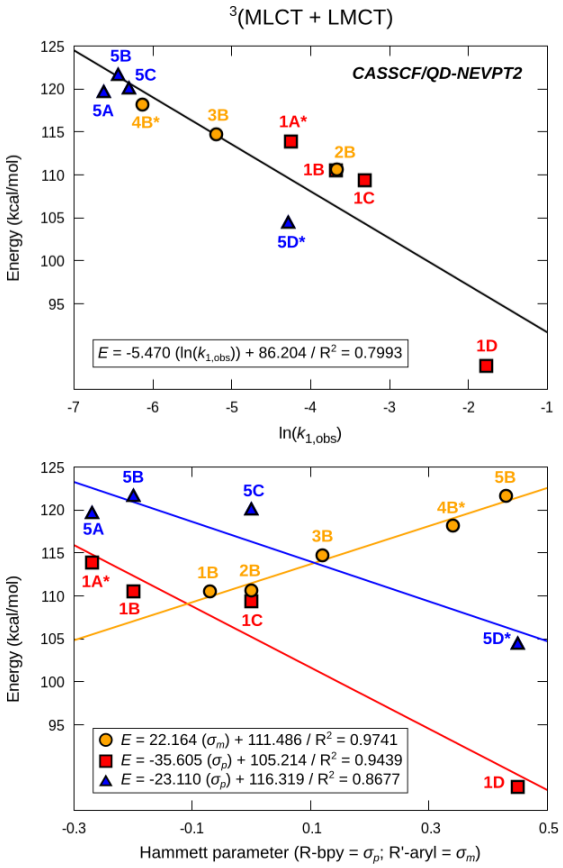

Figure S67. Correlation of the CASSCF/QD-NEVPT2 energies of the 'one-photon, two-electron' triplet repulsive surface ($d(x^2\text{-}y^2)/C(sp^2) + d(yz) \rightarrow d(x^2\text{-}y^2)/C(sp^2)^* + bpy\ \pi^*(1)$; *cf.* Figure 10 in the main text) at the singlet equilibrium geometry vs. the experimental rates of the Ni–C homolysis (top) and Hammett parameters (bottom) for **1A**–**5D** complexes. The asterisks indicate the ^{3}(MLCT+LMCT) energies obtained from computations with increased number of triplet states to 30 in the state-averaged CASSCF/QD-NEVPT2 references. For these cases, the ^{3}(MLCT+LMCT) surface was otherwise not observed in the original calculations with 25 triplets.

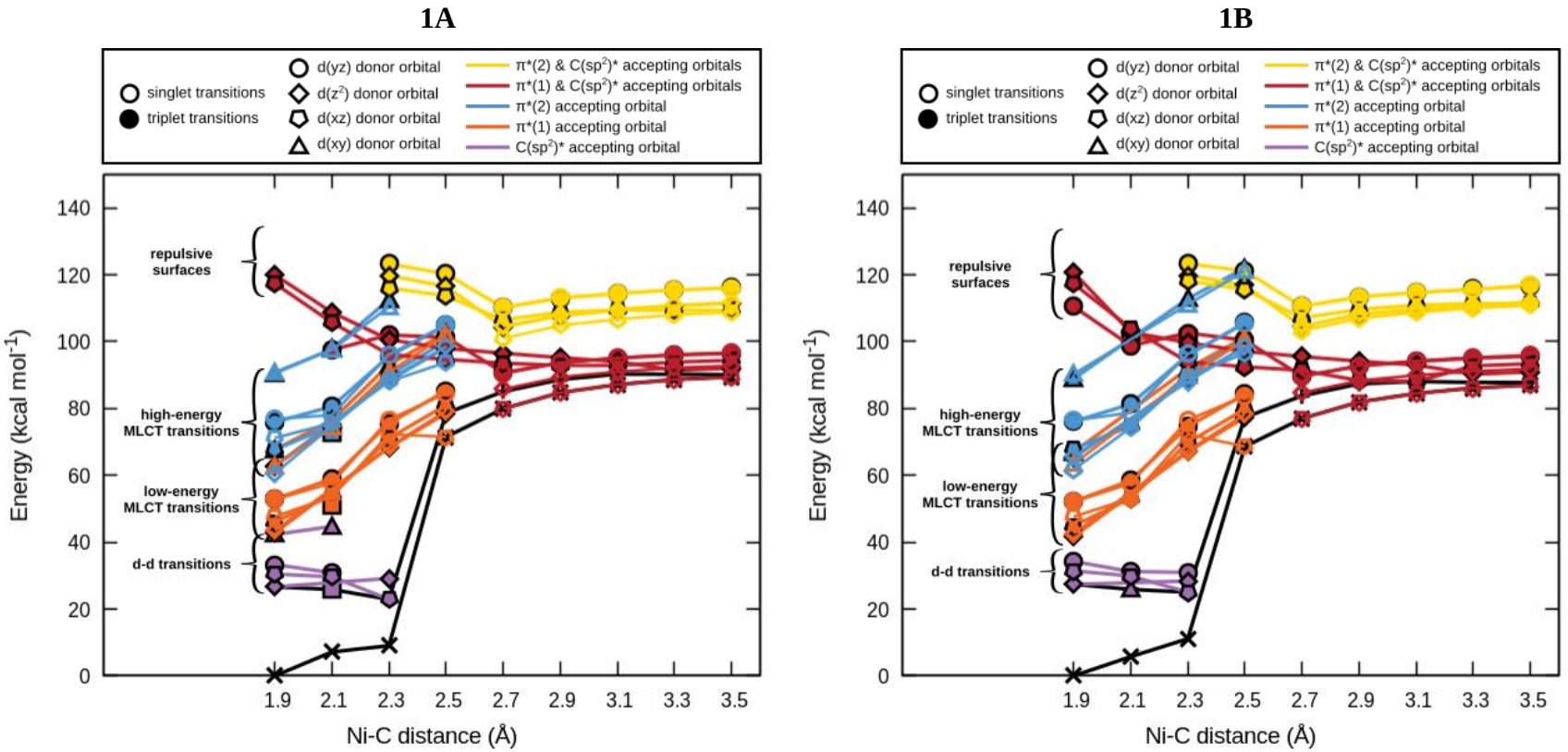

Figure S68. Relaxed ground and excited-state potential energy surfaces for **1A** (left) and **1B** (right) along the Ni−C coordinate at the CASSCF/QD-NEVPT2 level with the CPCM(THF) solvation model; 10e,9o Active Space – 25 triplet roots, 15 singlet roots. The structures were optimized at the DFT (BP86-D3) level with the CPCM(THF) solvation model as the BSS singlet ground states.

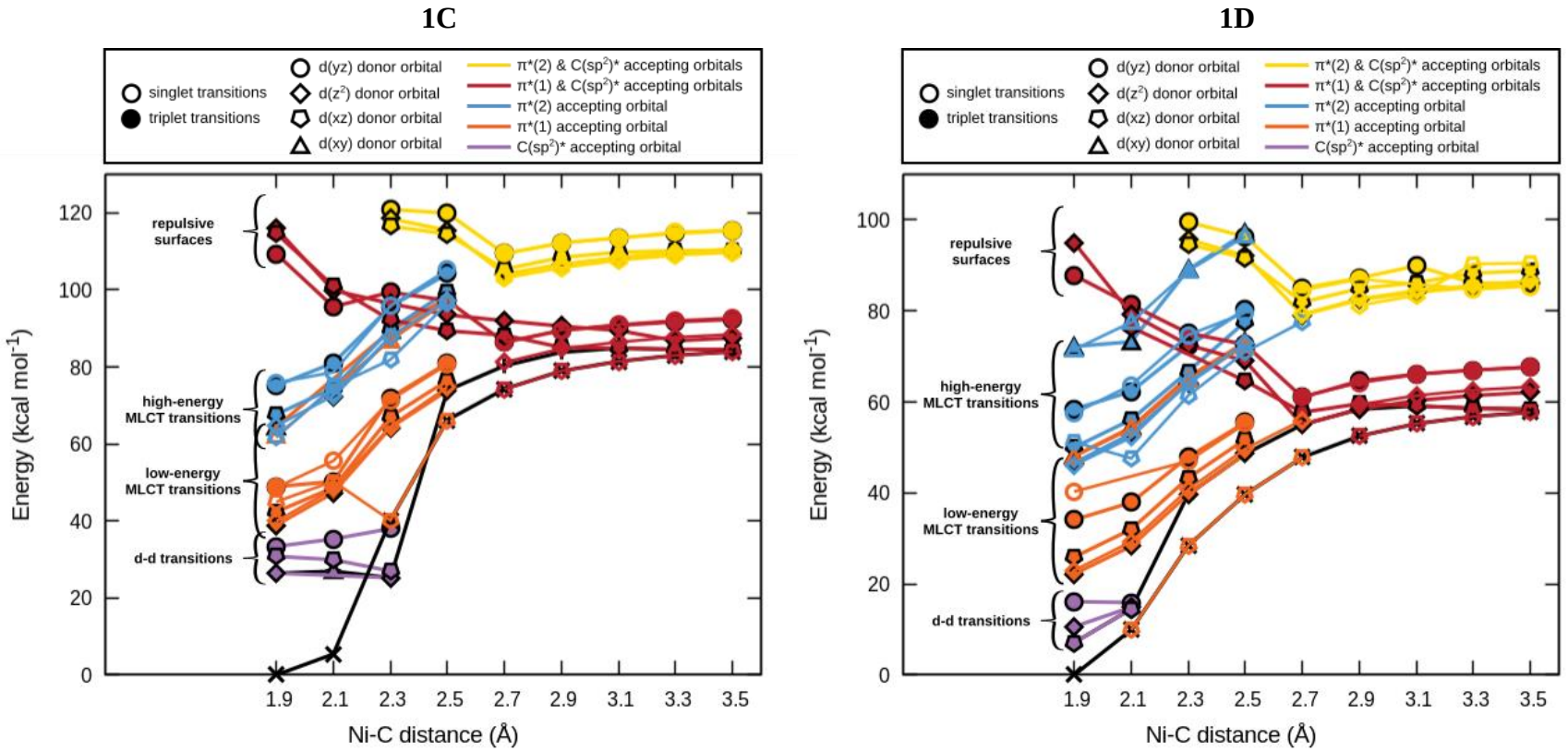

Figure S68, cont. Relaxed ground and excited-state potential energy surfaces for **1C** (left) and **1D** (right) along the Ni−C coordinate at the CASSCF/QD-NEVPT2 level with the CPCM(THF) solvation model; 10e,9o Active Space – 25 triplet roots, 15 singlet roots. The structures were optimized at the DFT (BP86-D3) level with the CPCM(THF) solvation model as the BSS singlet ground states.

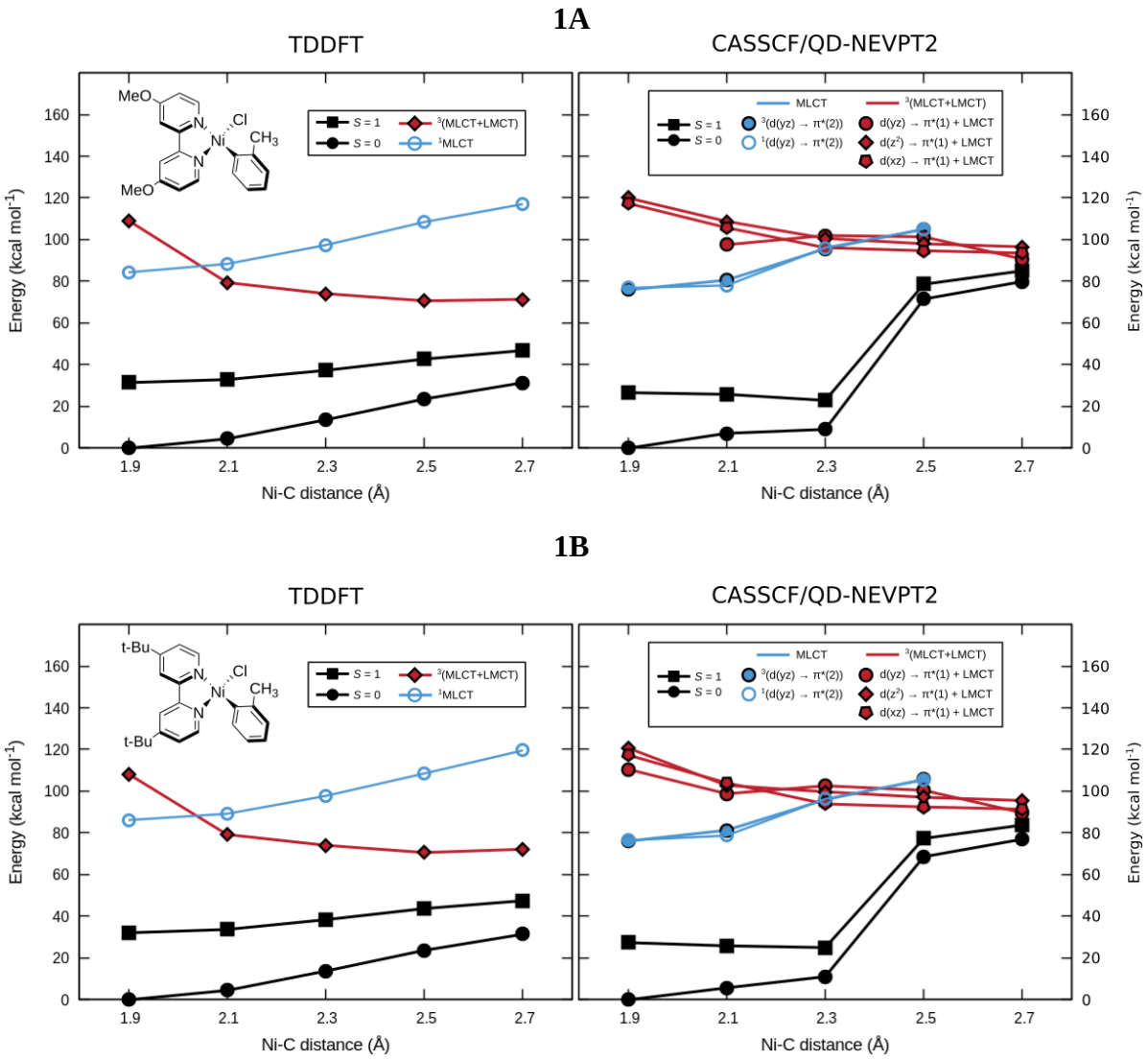

Figure S69. Relaxed ground and selected excited-state potential energy surfaces along the Ni−C coordinate at the TD-DFT (B3LYP) level (left) and CASSCF/QD-NEVPT2 level (right). The structures were optimized at the DFT (BP86-D3) level with CPCM(THF) solvation model as the BSS singlet ground states. The 10e, 9o active space with 25 triplet roots and 15 singlet roots was used for *ab initio* calculations at the equilibrium geometry, while the 10e, 8o active space was used for the structures with stretched (out-of-equilibrium) Ni−C bond distance where the bpy π*(3) orbital occupancy is close to zero.

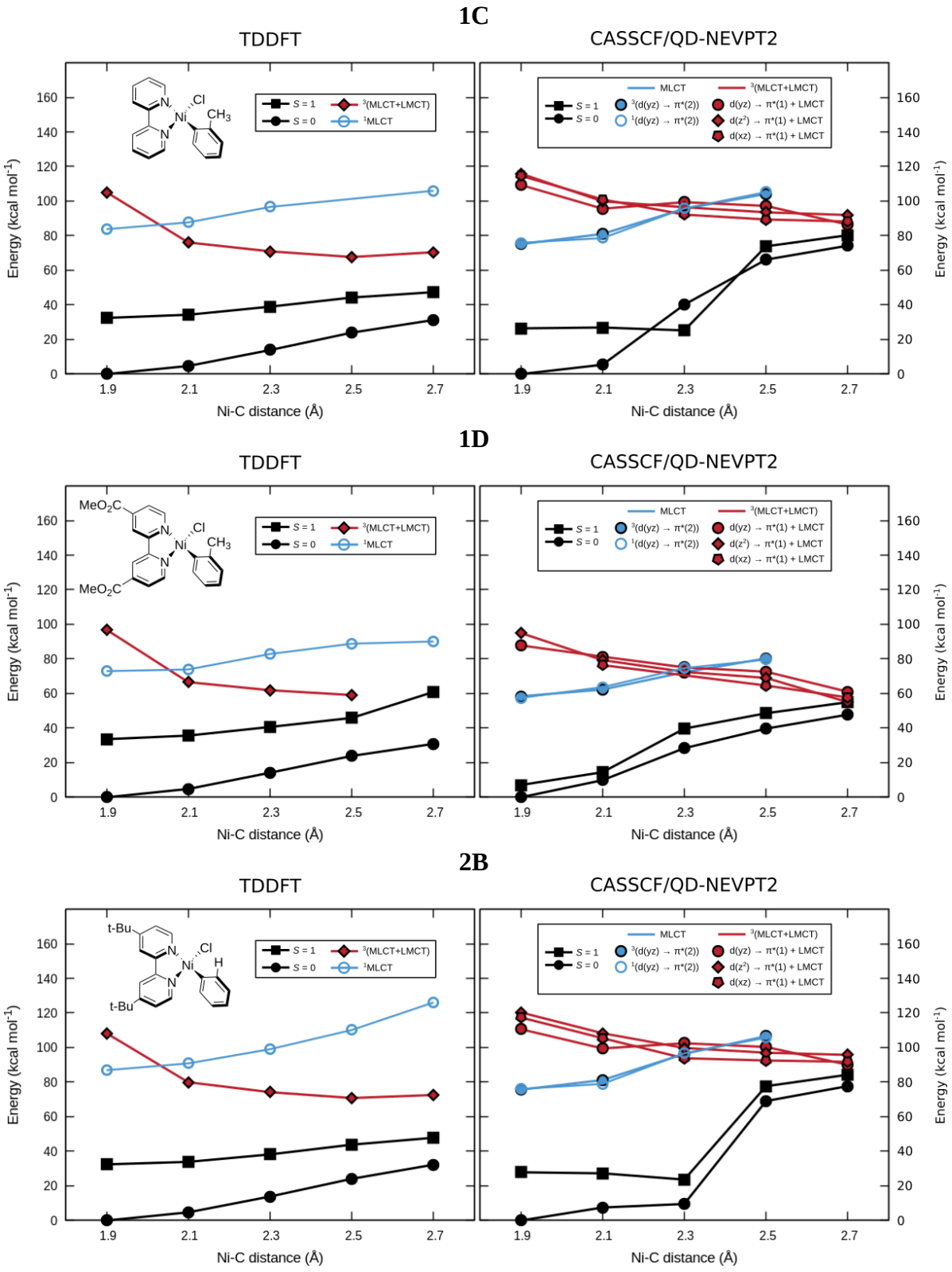

Figure S69, cont. Relaxed ground and selected excited-state potential energy surfaces along the Ni−C coordinate at the TD-DFT (B3LYP) level (left) and CASSCF/QD-NEVPT2 level (right).

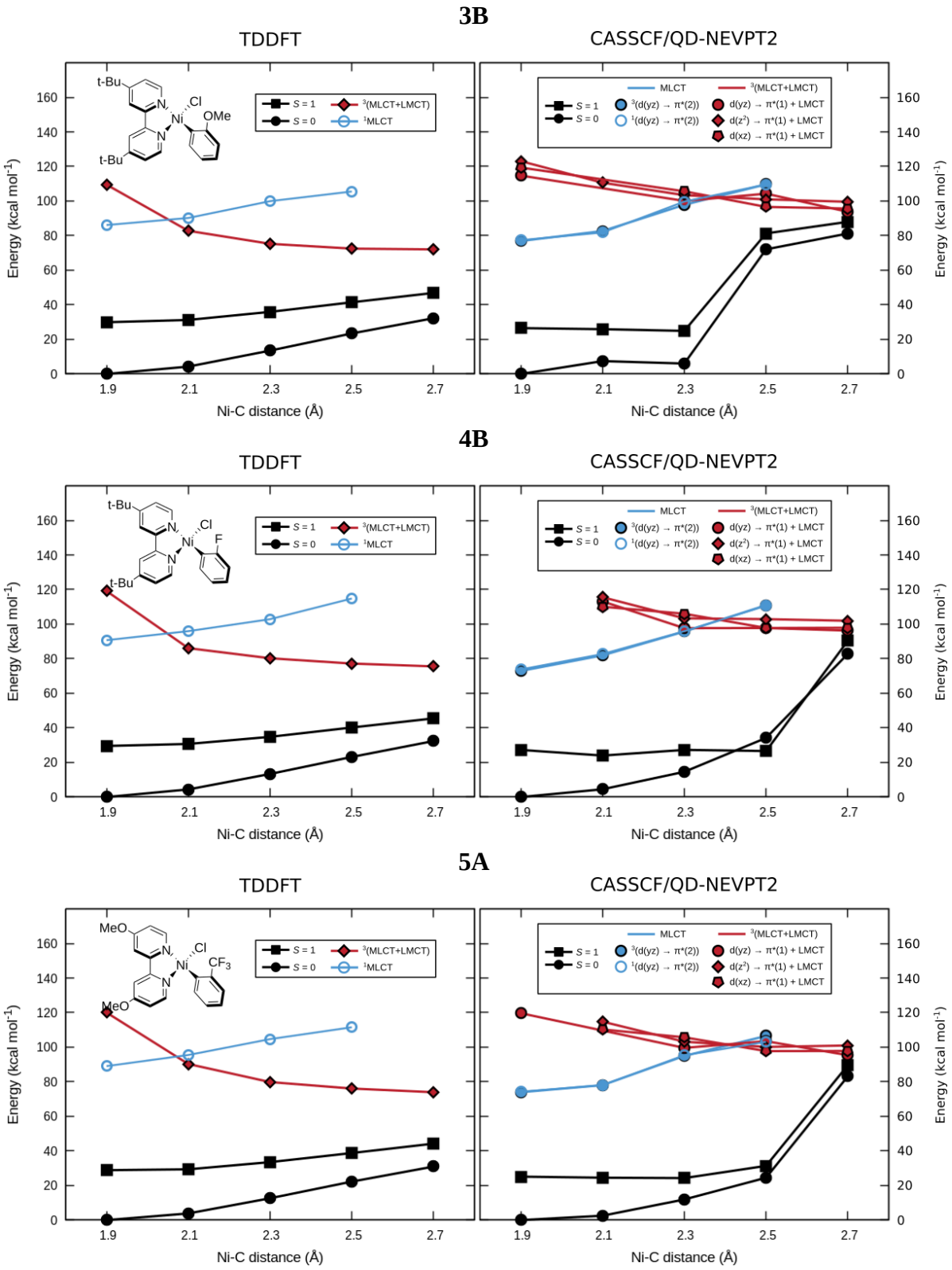

Figure S69, cont. Relaxed ground and selected excited-state potential energy surfaces along the Ni−C coordinate at the TD-DFT (B3LYP) level (left) and CASSCF/QD-NEVPT2 level (right).

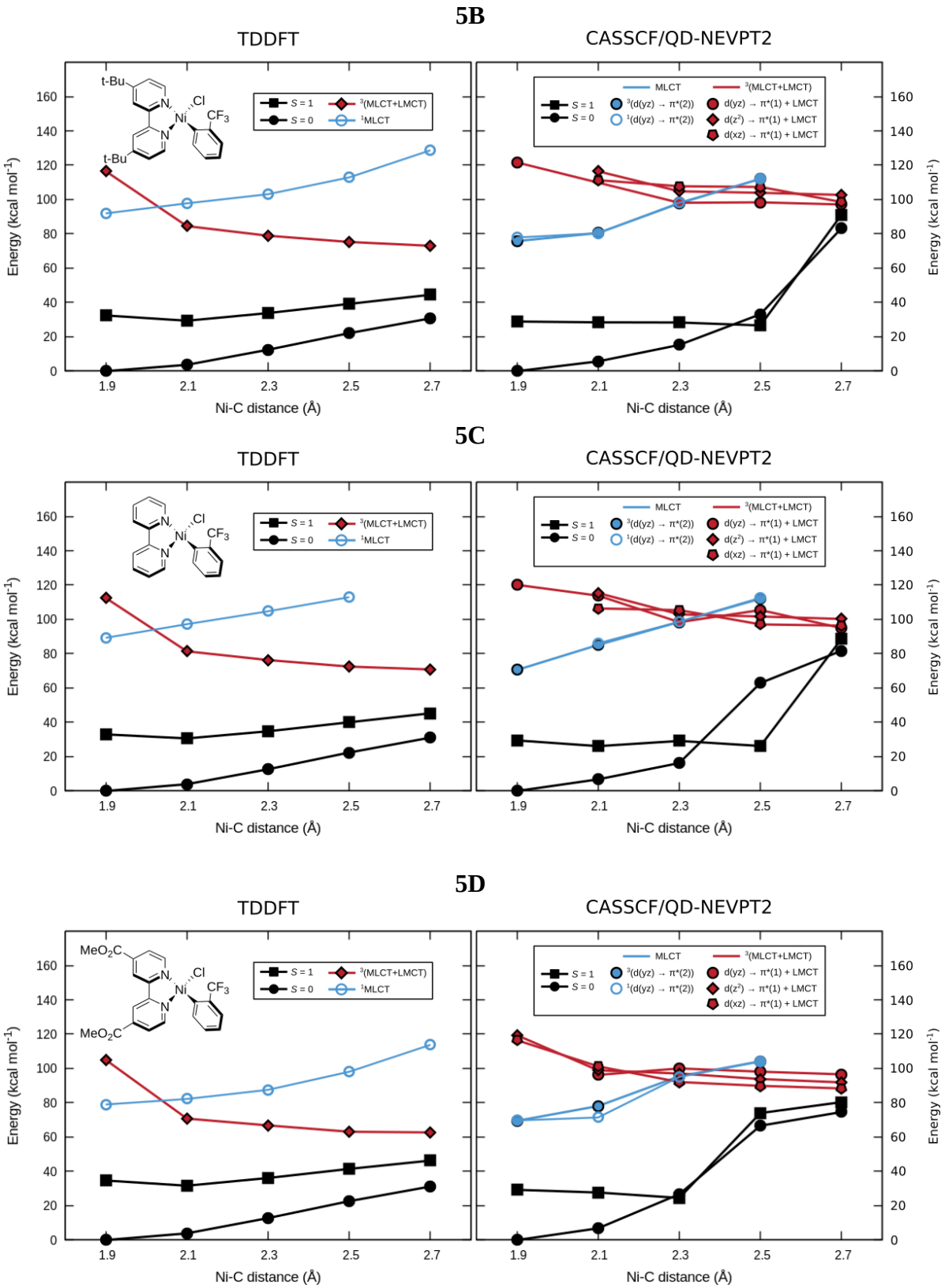

Figure S69, cont. Relaxed ground and selected excited-state potential energy surfaces along the Ni−C coordinate at the TD-DFT (B3LYP) level (left) and CASSCF/QD-NEVPT2 level (right).

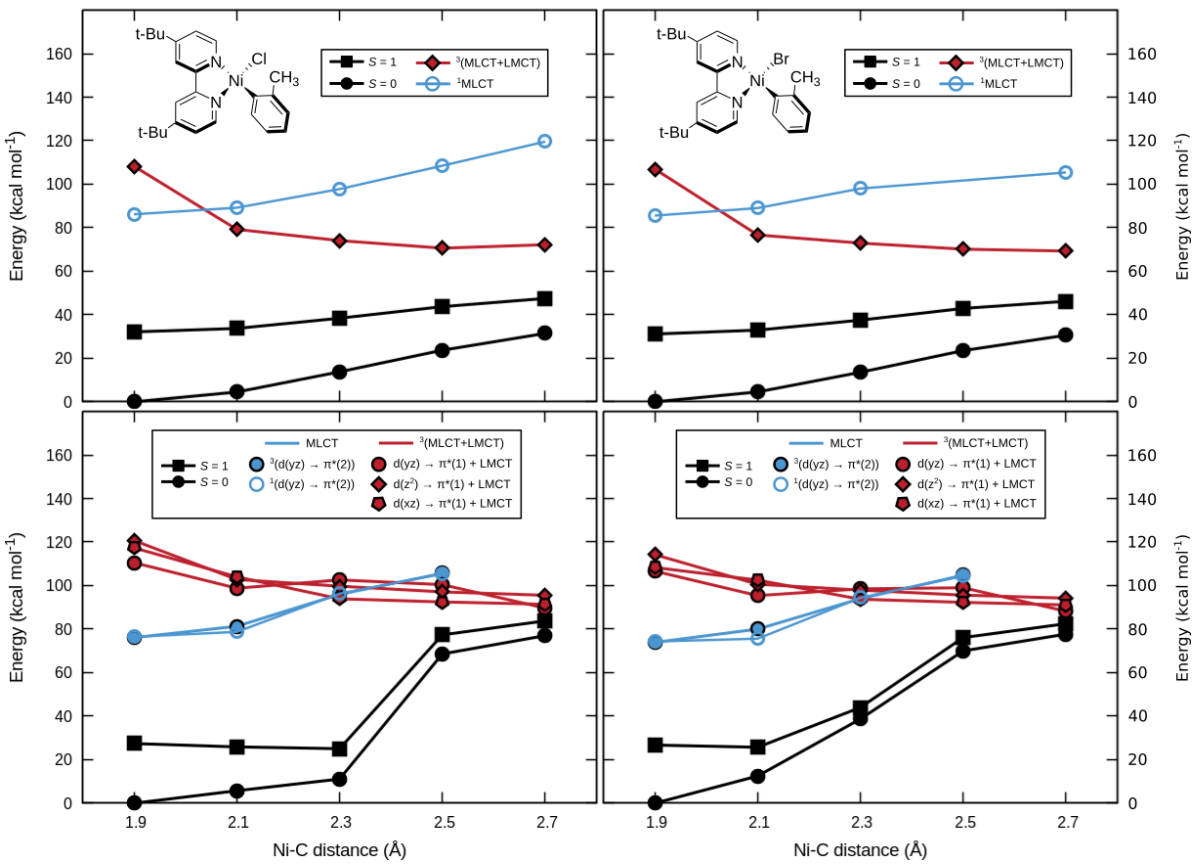

Figure S70. Comparison of the relaxed ground and selected excited-state potential energy surfaces for **1B** (left) and **1B**–**Br** (right) along the Ni−C coordinate at the TD-DFT (B3LYP) level (top) and CASSCF/QD-NEVPT2 level (bottom). The structures were optimized at the DFT (BP86-D3) level with CPCM(THF) solvation model as the BSS singlet ground states. The 10e, 9o active space with 25 triplet roots and 15 singlet roots was used for *ab initio* calculations at the equilibrium geometry, while the 10e, 8o active space was used for the structures with stretched (out-of-equilibrium) Ni−C bond distance where the bpy π*(3) orbital occupancy is close to zero.

S2.5 Additional Calculated Properties.

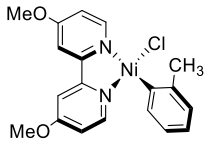

1A with Ni–C distance of 1.90 Å (near-equilibrium geometry) – CASSCF/NEVPT2 lowest transition energies with CPCM(THF) (10e,9o Active Space) – 25 triplet roots, 15 singlet roots. Active Space Orbitals (in order for CI vector notation below): d(x^2-y^2)/C(sp^2), d(xy), d(yz), d(z^2), d(xz), d(x^2-y^2)/C(sp^2)*, π*(1), π*(2), π*(3).

State	Root	Multiplicity	ΔE/nm	ΔE/kcal mol^{-1}	CI vector	Contribution
0	0	1	---	---	222220000	0.5585
					222210100	0.1562
					122221000	0.1275
1	0	3	1091.4	26.2	222121000	0.7735
					122122000	0.1652
2	1	3	946.7	30.2	222211000	0.5935
					221221000	0.1979
					122212000	0.1282
3	2	3	870.7	32.8	221221000	0.5710
					222211000	0.2047
4	3	3	676.4	42.3	222120100	0.8075
5	1	1	664.9	43.0	222120100	0.8057
6	4	3	643.6	44.4	212221000	0.6927
					221212000	0.1528
					112222000	0.1091
7	5	3	630.5	45.3	222210100	0.8161
8	2	1	606.6	47.1	222210100	0.4909
					221220100	0.2488
9	3	1	547.7	52.2	221220100	0.5070
					222210100	0.1522
10	6	3	546.4	52.3	221220100	0.7944
11	4	1	464.0	61.6	222121000	0.4639
					222120010	0.2353
12	5	1	457.9	62.4	222211000	0.5524
					212221000	0.1733
13	6	1	454.6	62.9	212220100	0.5178
					221221000	0.1544
14	7	1	451.0	63.4	212221000	0.5586
					222211000	0.1811
15	8	1	450.9	63.4	222120010	0.5624
					222121000	0.1910
16	9	1	428.9	66.7	221221000	0.5948
					212220100	0.1936
17	7	3	425.0	67.3	222210010	0.8153
18	8	3	423.8	67.5	212220100	0.7334
19	9	3	422.5	67.7	222120010	0.6999
20	10	1	408.1	70.1	222210010	0.5853

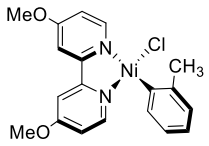

1A with Ni–C distance of 1.90 Å (near-equilibrium geometry) – CASSCF/QD-NEVPT2 lowest transition energies with CPCM(THF) (10e,9o Active Space) – 25 triplet roots, 15 singlet roots. Active Space Orbitals (in order for CI vector notation below): d(x^2-y^2)/C(sp^2), d(xy), d(yz), d(z^2), d(xz), d(x^2-y^2)/C(sp^2)*, π*(1), π*(2), π*(3).

State	Root	Multiplicity	ΔE/nm	ΔE/kcal mol^{-1}	CI vector	Contribution
0	0	1	---	---	222220000	0.5978
					122221000	0.1372
					222210100	0.1002
1	0	3	1073.2	26.6	222121000	0.7669
					122122000	0.1613
2	1	3	937.9	30.5	222211000	0.6345
					221221000	0.1537
					122212000	0.1367
3	2	3	859.0	33.3	221221000	0.6117
					222211000	0.1617
4	3	3	675.8	42.3	212221000	0.7049
5	4	3	668.0	42.8	222120100	0.8035
6	1	1	656.9	43.5	222120100	0.8005
7	5	3	621.3	46.0	222210100	0.7498
8	2	1	599.5	47.7	222210100	0.5744
					221220100	0.1661
9	3	1	541.7	52.8	221220100	0.5834
					222210100	0.1000
10	6	3	540.2	52.9	221220100	0.7875
11	4	1	471.7	60.6	222120010	0.5749
					222121000	0.1430
12	5	1	457.1	62.5	212221000	0.4106
					222211000	0.2097
13	7	3	455.6	62.8	222120010	0.7808
14	6	1	455.3	62.8	212220100	0.6890
15	7	1	446.7	64.0	222211000	0.5926
					212221000	0.1153
16	8	1	439.8	65.0	222121000	0.2981
					212221000	0.1886
					222120010	0.1628
					222210010	0.1243
17	8	3	422.5	67.7	222210010	0.7926
18	9	3	422.1	67.7	212220100	0.7247
19	9	1	420.6	68.0	221221000	0.7703
20	10	1	401.6	71.2	222210010	0.3262
					222121000	0.2591

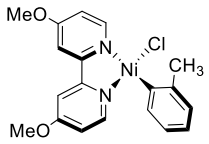

1A with Ni–C distance of 3.50 Å (dissociation limit) – CASSCF/NEVPT2 lowest transition energies with CPCM(THF) (10e,8o Active Space) – 25 triplet roots, 15 singlet roots. Active Space Orbitals (in order for CI vector notation below): d(xy), d(yz), d(z^2), d(xz), d(x^2-y^2)/C(sp^2), d(x^2-y^2)/C(sp^2)*, π*(1), π*(2).

State	Root	Multiplicity	ΔE/nm	ΔE/kcal mol^{-1}	CI vector	Contribution
0	0	1	---	---	22211110	0.7924
1	0	3	46636.0	0.6	22211110	0.8265
2	1	3	14702.6	1.9	22121110	0.9140
3	1	1	10708.2	2.7	22121110	0.9115
4	2	3	8819.9	3.2	22121110	0.9527
5	3	3	6645.8	4.3	22211110	0.8465
6	4	3	4511.7	6.3	21221110	0.8599
7	2	1	4317.6	6.6	21221110	0.8317
8	5	3	3990.1	7.2	21221110	0.8702
9	3	1	1551.5	18.4	22211101	0.6801
					22121101	0.1246
10	6	3	1503.7	19.0	22211101	0.7281
					22121101	0.1109
11	4	1	1474.2	19.4	21212110	0.4625
					12221110	0.4583
12	7	3	1451.2	19.7	12221110	0.4718
					21212110	0.4667
13	8	3	1363.0	21.0	12221110	0.4860
					21212110	0.4484
14	5	1	1344.6	21.3	22121101	0.7815
					22211101	0.1173
15	9	3	1343.1	21.3	22121101	0.8996
16	10	3	1301.6	22.0	22121101	0.8457
17	11	3	1242.0	23.0	22211101	0.8249
18	12	3	1225.9	23.3	22220110	0.8298
19	6	1	1225.3	23.3	22220110	0.8305
20	13	3	1100.3	26.0	21221101	0.8411

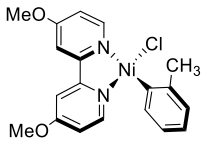

1A with Ni–C distance of 3.50 Å (dissociation limit) – CASSCF/QD-NEVPT2 lowest transition energies with CPCM(THF) (10e,8o Active Space) – 25 triplet roots, 15 singlet roots. Active Space Orbitals (in order for CI vector notation below): d(xy), d(yz), d(z^2), d(xz), d(x^2-y^2)/C(sp^2), d(x^2-y^2)/C(sp^2)*, π*(1), π*(2).

State	Root	Multiplicity	ΔE/nm	ΔE/kcal mol^{-1}	CI vector	Contribution
0	0	1	---	---	22211110	0.7414
1	0	3	42625.7	0.7	22211110	0.7807
2	1	3	10841.3	2.6	22121110	0.9126
3	1	1	8507.7	3.4	22121110	0.9106
4	2	3	7259.0	3.9	22121110	0.9530
5	3	3	5744.8	5.0	22211110	0.8423
6	4	3	4062.1	7.0	21221110	0.8592
7	2	1	3918.3	7.3	21221110	0.8266
8	5	3	3642.1	7.9	21221110	0.8687
9	3	1	1474.8	19.4	22211101	0.7396
10	6	3	1431.5	20.0	22211101	0.7606
11	4	1	1426.6	20.0	21212110	0.4647
					12221110	0.4452
12	7	3	1404.4	20.4	21212110	0.4650
					12221110	0.4529
13	8	3	1321.4	21.6	12221110	0.4810
					21212110	0.4512
14	9	3	1298.6	22.0	22121101	0.9076
15	5	1	1283.7	22.3	22121101	0.8932
16	10	3	1248.0	22.9	22121101	0.9287
17	11	3	1205.1	23.7	22211101	0.8373
18	12	3	1189.6	24.0	22220110	0.8109
19	6	1	1189.5	24.0	22220110	0.8246
20	7	1	1075.3	26.6	21221101	0.7920

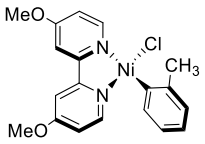

1A with Ni–C distance of 1.90 Å (near-equilibrium geometry) – CASSCF/NEVPT2 composition of the singlet ground state with CPCM(THF) (10e,9o Active Space) – 25 triplet roots, 15 singlet roots. Active Space Orbitals (in order for CI vector notation below): d(x^2-y^2)/C(sp^2), d(xy), d(yz), d(z^2), d(xz), d(x^2-y^2)/C(sp^2)*, π*(1), π*(2), π*(3).

CI vector	Transition	Contribution
222220000	Closed-shell singlet (CSS) d^8	0.5585
222210100	d(xz) → π*(1)	0.1562
122221000	d(x^2-y^2)/C(sp^2) → d(x^2-y^2)/C(sp^2)*	0.1275
221220100	d(yz) → π*(1)	0.0283
222210010	d(xz) → π*(2)	0.0211
022212100	2x[d(x^2-y^2)/C(sp^2)] + d(xz) → 2x[d(x^2-y^2)/C(sp^2)*] + π*(1)	0.0209
222022000	2x[d(z^2)] → 2x[d(x^2-y^2)/C(sp^2)*]	0.0114
222121000	d(z^2) → d(x^2-y^2)/C(sp^2)*	0.0112
221220001	d(yz) → π*(3)	0.0101
Sum of CSS		**56 %**
Sum of all MLCT		**22 %**
Sum of all d-d		**15 %**
Sum of mixed MLCT + d-d		**2 %**

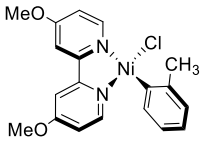

1A with Ni–C distance of 1.90 Å (near-equilibrium geometry) – CASSCF/QD-NEVPT2 composition of the singlet ground state with CPCM(THF) (10e,9o Active Space) – 25 triplet roots, 15 singlet roots. Active Space Orbitals (in order for CI vector notation below): d(x^2-y^2)/C(sp^2), d(xy), d(yz), d(z^2), d(xz), d(x^2-y^2)/C(sp^2)*, π*(1), π*(2), π*(3).

CI vector	Transition	Contribution
222220000	Closed-shell singlet (CSS) d^8	0.5978
122221000	d(x^2-y^2)/C(sp^2) → d(x^2-y^2)/C(sp^2)*	0.1372
222210100	d(xz) → π*(1)	0.1002
222210010	d(xz) → π*(2)	0.0302
221220100	d(yz) → π*(1)	0.0213
222121000	d(z^2) → d(x^2-y^2)/C(sp^2)*	0.0190
022212100	2x[d(x^2-y^2)/C(sp^2)] + d(xz) → 2x[d(x^2-y^2)/C(sp^2)*] + π*(1)	0.0137
222022000	2x[d(z^2)] → 2x[d(x^2-y^2)/C(sp^2)*]	0.0118
221220001	d(yz) → π*(3)	0.0117
Sum of CSS		**60 %**
Sum of all MLCT		**16 %**
Sum of all d-d		**17 %**
Sum of mixed MLCT + d-d		**1 %**

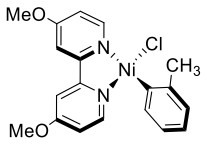

1A with Ni–C distance of 3.50 Å (dissociation limit) – CASSCF/NEVPT2 composition of the singlet ground state with CPCM(THF) (10e,8o Active Space) – 25 triplet roots, 15 singlet roots. Active Space Orbitals (in order for CI vector notation below): d(xy), d(yz), d(z²), d(xz), d(x²-y²)/C(sp²), d(x²-y²)/C(sp²)*, π*(1), π*(2).

CI vector	Transition	Contribution
22211110	d(xz) + d(x²-y²)/C(sp²) → d(x²-y²)/C(sp²)* + π*(1)	0.79242
22112110	d(z²) + d(xz) → d(x²-y²)/C(sp²)* + π*(1)	0.04955
11222110	d(xy) + d(yz) → d(x²-y²)/C(sp²)* + π*(1)	0.03582
22221100	d(x²-y²)/C(sp²) → d(x²-y²)/C(sp²)*	0.0304
22212010	d(xz) → π*(1)	0.0279
21221110	d(yz) + d(x²-y²)/C(sp²) → d(x²-y²)/C(sp²)* + π*(1)	0.02363
22210210	2x[d(x²-y²)/C(sp²)] + d(xz) → 2x[d(x²-y²)/C(sp²)*] + π*(1)	0.01248
21122110	d(yz) + d(z²) → d(x²-y²)/C(sp²)* + π*(1)	0.01224
Sum of CSS		**0 %**
Sum of all MLCT		**3 %**
Sum of all d-d		**3 %**
Sum of mixed MLCT + d-d		**93 %**

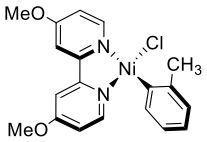

1A with Ni–C distance of 3.50 Å (dissociation limit) – CASSCF/QD-NEVPT2 composition of the singlet ground state with CPCM(THF) (10e,8o Active Space) – 25 triplet roots, 15 singlet roots. Active Space Orbitals (in order for CI vector notation below): d(xy), d(yz), d(z²), d(xz), d(x²-y²)/C(sp²), d(x²-y²)/C(sp²)*, π*(1), π*(2).

CI vector	Transition	Contribution
22211110	d(xz) + d(x²-y²)/C(sp²) → d(x²-y²)/C(sp²)* + π*(1)	0.7414
22112110	d(z²) + d(xz) → d(x²-y²)/C(sp²)* + π*(1)	0.0474
22211101	d(xz) + d(x²-y²)/C(sp²) → d(x²-y²)/C(sp²)* + π*(2)	0.0440
22221100	d(x²-y²)/C(sp²) → d(x²-y²)/C(sp²)*	0.0415
11222110	d(xy) + d(yz) → d(x²-y²)/C(sp²)* + π*(1)	0.0298
22212010	d(xz) → π*(1)	0.0278
21221110	d(yz) + d(x²-y²)/C(sp²) → d(x²-y²)/C(sp²)* + π*(1)	0.0221
22210210	2x[d(x²-y²)/C(sp²)] + d(xz) → 2x[d(x²-y²)/C(sp²)*] + π*(1)	0.0124
21122110	d(z^2) + d(yz) → d(x²-y²)/C(sp²)* + π*(1)	0.0124
Sum of CSS		**0 %**
Sum of all MLCT		**3 %**
Sum of all d-d		**4 %**
Sum of mixed MLCT + d-d		**91 %**

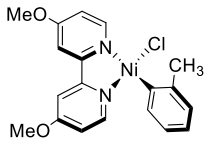

1A – CASSCF/NEVPT2 spin-orbit corrected absorption transitions for the CPCM(THF) phase spectrum (10e,9o Active Space) – 25 triplet roots, 15 singlet roots.

***E*/nm**	***E*/kcal mol^{-1}**	f_{osc}	***E*/nm**	***E*/kcal mol^{-1}**	f_{osc}
686.8	41.6	0.0003382	415.8	68.8	0.0001211
686.2	41.7	0.0000000	415.7	68.8	0.0002800
681.2	42.0	0.0086796	406.4	70.3	0.1124883
676.8	42.2	0.0006769	377.1	75.8	0.0000439
640.4	44.6	0.0089455	376.9	75.9	0.0000106
640.1	44.7	0.0004318	376.8	75.9	0.0041013
639.8	44.7	0.0000016	372.8	76.7	0.0127402
627.3	45.6	0.0012483	358.7	79.7	0.0086411
624.0	45.8	0.0000010	357.8	79.9	0.0002281
622.6	45.9	0.0001089	357.8	79.9	0.0000008
597.8	47.8	0.1072861	357.3	80.0	0.0050619
546.9	52.3	0.1027241	337.0	84.8	0.0516698
540.3	52.9	0.0000011	336.3	85.0	0.0027857
539.9	53.0	0.0000255	335.5	85.2	0.0000018
535.8	53.4	0.1342252	332.4	86.0	0.0000064
464.3	61.6	0.0121830	331.8	86.2	0.0000385
456.7	62.6	0.0029026	329.5	86.8	0.0000980
453.0	63.1	0.0039897	328.9	86.9	0.0000058
452.7	63.2	0.0013175	328.8	86.9	0.0002414
449.9	63.5	0.0023967	328.2	87.1	0.0002781
433.6	65.9	0.0000562	323.0	88.5	0.0000010
432.5	66.1	0.0001662	321.3	89.0	0.0000068
427.2	66.9	0.0001554	316.7	90.3	0.0000390
424.2	67.4	0.0112704	316.2	90.4	0.0000051
422.3	67.7	0.0000786	314.9	90.8	0.0000132
421.9	67.8	0.0001214	305.4	93.6	0.0000000
421.9	67.8	0.0006037	305.3	93.6	0.0000118
421.8	67.8	0.0012560	305.2	93.7	0.0001121

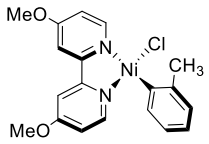

1A – CASSCF/QD-NEVPT2 spin-orbit corrected absorption transitions for the CPCM(THF) phase spectrum (10e,9o Active Space) – 25 triplet roots, 15 singlet roots.

***E*/nm**	***E*/kcal mol^{-1}**	f_{osc}	***E*/nm**	***E*/kcal mol^{-1}**	f_{osc}
681.5	42.0	0.0000139	419.3	68.2	0.0007890
681.2	42.0	0.0011798	418.0	68.4	0.0001416
676.3	42.3	0.0003461	400.8	71.3	0.1252700
674.6	42.4	0.0046394	374.1	76.4	0.0055795
666.6	42.9	0.0000015	374.0	76.4	0.0000359
663.1	43.1	0.0005436	374.0	76.5	0.0001227
662.3	43.2	0.0006081	369.7	77.3	0.0107469
617.1	46.3	0.0368074	356.8	80.1	0.0000034
615.4	46.5	0.0000740	356.8	80.1	0.0000878
614.1	46.6	0.0001545	356.0	80.3	0.0008873
594.0	48.1	0.0594332	354.6	80.6	0.0032993
539.6	53.0	0.2023447	337.8	84.7	0.0000227
534.2	53.5	0.0000651	337.7	84.7	0.0000062
533.8	53.6	0.0000589	337.4	84.7	0.0011136
530.8	53.9	0.0631327	331.7	86.2	0.0000101
473.3	60.4	0.0001518	330.4	86.5	0.0003428
460.7	62.1	0.0012913	329.9	86.7	0.0000081
458.3	62.4	0.0000015	326.6	87.5	0.0000077
457.9	62.4	0.0001221	319.5	89.5	0.0000301
453.6	63.0	0.0076981	317.6	90.0	0.0003420
452.0	63.2	0.0078709	315.9	90.5	0.0002084
444.8	64.3	0.0019030	314.6	90.9	0.0003474
438.6	65.2	0.0039537	314.4	90.9	0.0001153
421.7	67.8	0.0002489	314.0	91.1	0.0581782
420.3	68.0	0.0004779	312.7	91.4	0.0049695
420.2	68.0	0.0001098	309.7	92.3	0.0000072
420.1	68.1	0.0013274	308.0	92.8	0.0046242
419.8	68.1	0.0000462	306.6	93.3	0.0004543

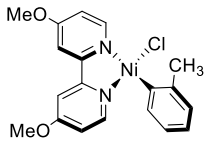

1A – TD-DFT (B3LYP) absorption transitions (singlets only) for the CPCM(THF) phase spectrum.

***E*/nm**	***E*/kcal mol^{-1}**	f_{osc}	***E*/nm**	***E*/kcal mol^{-1}**	f_{osc}
796.2	35.9	0.0000000	369.8	77.3	0.0000000
601.6	47.5	0.0000000	366.0	78.1	0.0000000
593.1	48.2	0.0000000	363.2	78.7	0.0334601
547.0	52.3	0.0004763	354.4	80.7	0.0000200
543.4	52.6	0.0000000	350.7	81.5	0.0000000
510.0	56.1	0.0000000	347.3	82.3	0.0000000
509.6	56.1	0.0045920	339.0	84.3	0.0109995
507.5	56.3	0.0023165	335.1	85.3	0.0000000
499.5	57.2	0.0003271	334.8	85.4	0.0000000
487.2	58.7	0.0238964	333.2	85.8	0.0000780
460.4	62.1	0.0000000	331.2	86.3	0.0000636
459.0	62.3	0.0000109	326.3	87.6	0.0000000
458.5	62.4	0.0000988	325.9	87.7	0.0000000
457.7	62.5	0.0001028	324.0	88.2	0.0000000
453.4	63.1	0.0000000	322.7	88.6	0.0205495
436.0	65.6	0.0481711	315.8	90.5	0.0230876
435.2	65.7	0.0001321	314.5	90.9	0.0000000
433.3	66.0	0.0000000	309.3	92.4	0.0000000
416.5	68.6	0.0000000	309.2	92.5	0.0234382
412.8	69.3	0.0004292	308.3	92.7	0.0000000
386.6	74.0	0.0000000	305.6	93.6	0.0014940
376.1	76.0	0.0011159	303.3	94.3	0.0000000

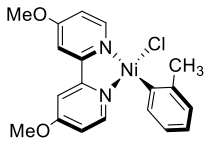

1A – TD-DFT (B3LYP) absorption transitions (singlets only) for the CPCM(Toluene) phase spectrum.

***E*/nm**	***E*/kcal mol^{-1}**	f_{osc}	***E*/nm**	***E*/kcal mol^{-1}**	f_{osc}
778.8	36.7	0.0000000	384.0	74.5	0.0000000
689.5	41.5	0.0000000	381.2	75.0	0.0000000
667.9	42.8	0.0005823	380.6	75.1	0.0036244
635.8	45.0	0.0000000	379.0	75.4	0.0000402
601.4	47.5	0.0000000	376.7	75.9	0.0000000
592.7	48.2	0.0000000	371.1	77.0	0.0098058
566.0	50.5	0.0010912	369.7	77.3	0.0000000
541.2	52.8	0.0000454	365.8	78.2	0.0000000
526.1	54.3	0.0000000	363.1	78.7	0.0000468
525.9	54.4	0.0125694	358.8	79.7	0.0097666
515.8	55.4	0.0000000	357.5	80.0	0.0000000
509.8	56.1	0.0001293	352.0	81.2	0.0213813
493.4	57.9	0.0000488	342.9	83.4	0.0036857
492.1	58.1	0.0110616	339.9	84.1	0.0000000
480.6	59.5	0.0438068	333.1	85.8	0.0000000
466.5	61.3	0.0000000	328.2	87.1	0.0000000
461.8	61.9	0.0003813	324.7	88.0	0.0000000
459.5	62.2	0.0067600	324.4	88.1	0.0001110
456.2	62.7	0.0009760	321.8	88.9	0.0000000
436.0	65.6	0.0000000	320.8	89.1	0.0200202
425.4	67.2	0.0008279	312.5	91.5	0.0000000
424.2	67.4	0.0000000	311.0	91.9	0.0000000
408.3	70.0	0.0000000	310.7	92.0	0.0000000
400.8	71.3	0.0391521	308.8	92.6	0.0322492
387.5	73.8	0.0000000	307.8	92.9	0.0000000
386.8	73.9	0.0000202	304.9	93.8	0.0000000

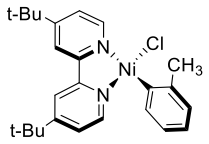

1B with Ni–C distance of 1.90 Å (near-equilibrium geometry) – CASSCF/NEVPT2 lowest transition energies with CPCM(THF) (10e,9o Active Space) – 25 triplet roots, 15 singlet roots. Active Space Orbitals (in order for CI vector notation below): d(x^2-y^2)/C(sp^2), d(xy), d(yz), d(z^2), d(xz), d(x^2-y^2)/C(sp^2)*, π*(1), π*(2), π*(3).

State	Root	Multiplicity	ΔE/nm	ΔE/kcal mol^{-1}	CI vector	Contribution
0	0	1	---	---	222220000	0.5263
					222210100	0.2000
					122221000	0.1125
1	0	3	1073.8	26.6	222121000	0.7657
					122122000	0.1649
2	1	3	926.7	30.9	222211000	0.5430
					221221000	0.2407
					122212000	0.1175
3	2	3	856.1	33.4	221221000	0.5192
					222211000	0.2513
4	3	3	699.9	40.8	222120100	0.8070
5	1	1	683.8	41.8	222120100	0.8050
6	4	3	649.4	44.0	222210100	0.8234
7	5	3	645.0	44.3	212221000	0.6920
					221212000	0.1407
					112222000	0.1057
8	2	1	611.3	46.8	222210100	0.3738
					221220100	0.3715
9	3	1	563.8	50.7	221220100	0.3777
					222210100	0.2185
					222220000	0.1004
10	6	3	559.1	51.1	221220100	0.7851
11	4	1	468.0	61.1	222121000	0.5333
					222210010	0.1498
12	5	1	460.9	62.0	222211000	0.7581
					122212000	0.1073
13	6	1	458.4	62.4	212220100	0.5696
					221221000	0.1206
					221211100	0.1058
14	7	1	445.9	64.1	212221000	0.6046
					222210010	0.1258
15	7	3	443.2	64.5	222120010	0.7986
16	8	1	441.8	64.7	222120010	0.7990
17	8	3	433.5	66.0	212220100	0.7368
18	9	1	427.9	66.8	221221000	0.6046
					212220100	0.1303
19	9	3	425.9	67.1	222210010	0.8159
20	10	1	420.2	68.0	222210010	0.4162
					222121000	0.1682

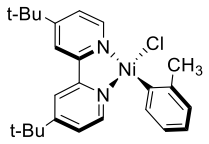

1B with Ni–C distance of 1.90 Å (near-equilibrium geometry) – CASSCF/QD-NEVPT2 lowest transition energies with CPCM(THF) (10e,9o Active Space) – 25 triplet roots, 15 singlet roots. Active Space Orbitals (in order for CI vector notation below): d(x^2-y^2)/C(sp^2), d(xy), d(yz), d(z^2), d(xz), d(x^2-y^2)/C(sp^2)*, π*(1), π*(2), π*(3).

State	Root	Multiplicity	ΔE/nm	ΔE/kcal mol^{-1}	CI vector	Contribution
0	0	1	---	---	222220000	0.5854
					122221000	0.1300
					222210100	0.1187
1	0	3	1043.4	27.4	222121000	0.7528
					122122000	0.1594
2	1	3	909.7	31.4	222211000	0.6100
					221221000	0.1675
					122212000	0.1319
3	2	3	835.7	34.2	221221000	0.5825
					222211000	0.1804
4	3	3	686.3	41.7	222120100	0.8000
5	1	1	670.5	42.6	222120100	0.7993
6	4	3	659.6	43.3	212221000	0.7139
7	5	3	637.4	44.9	222210100	0.8206
8	2	1	600.4	47.6	222210100	0.5392
					221220100	0.1857
9	3	1	548.8	52.1	221220100	0.5544
					222210100	0.1064
10	6	3	548.2	52.2	221220100	0.7675
11	4	1	463.2	61.7	222121000	0.3871
					222210010	0.3414
12	5	1	456.7	62.6	222211000	0.7259
13	6	1	451.1	63.4	212220100	0.6723
14	7	1	439.1	65.1	212221000	0.5952
15	7	3	437.8	65.3	222120010	0.7832
16	8	1	435.6	65.6	222120010	0.7792
17	8	3	427.1	66.9	212220100	0.7288
18	9	1	423.4	67.5	221221000	0.3894
					222121000	0.1515
					222210010	0.1413
19	9	3	420.6	68.0	222210010	0.8108
20	10	1	411.4	69.5	221221000	0.3519
					222121000	0.1524
					212221000	0.1012

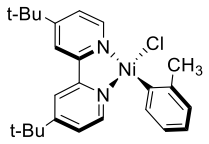

1B with Ni–C distance of 3.50 Å (dissociation limit) – CASSCF/NEVPT2 lowest transition energies with CPCM(THF) (10e,8o Active Space) – 25 triplet roots, 15 singlet roots. Active Space Orbitals (in order for CI vector notation below): d(xy), d(yz), d(z^2), d(xz), d(x^2-y^2)/C(sp^2), d(x^2-y^2)/C(sp^2)*, π*(1), π*(2).

State	Root	Multiplicity	ΔE/nm	ΔE/kcal mol^{-1}	CI vector	Contribution
0	0	1	---	---	22211110	0.7753
1	0	3	44365.5	0.6	22211110	0.8102
2	1	3	8375.6	3.4	22121110	0.9222
3	1	1	6595.7	4.3	22121110	0.9206
4	2	3	5824.3	4.9	22121110	0.9621
5	3	3	4895.1	5.8	22211110	0.8443
6	4	3	3542.5	8.1	21221110	0.8788
7	2	1	3398.0	8.4	21221110	0.8394
8	5	3	3191.8	9.0	21221110	0.8784
9	3	1	1396.4	20.5	21212110	0.4735
					12221110	0.4489
10	6	3	1377.1	20.8	21212110	0.4787
					12221110	0.4626
11	7	3	1263.4	22.6	12221110	0.4850
					21212110	0.4500
12	4	1	1236.5	23.1	22211101	0.7848
13	8	3	1205.6	23.7	22211101	0.8134
14	9	3	1183.1	24.2	22121101	0.9152
15	5	1	1181.4	24.2	22121101	0.8942
16	10	3	1162.5	24.6	22220110	0.8295
17	6	1	1159.7	24.7	22220110	0.8229
18	11	3	1151.5	24.8	22121101	0.9347
19	12	3	1093.9	26.1	22211101	0.8438
20	7	1	990.4	28.9	12212110	0.7903
					21122110	0.1171

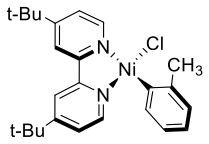

1B with Ni–C distance of 3.50 Å (dissociation limit) – CASSCF/QD-NEVPT2 lowest transition energies with CPCM(THF) (10e,8o Active Space) – 25 triplet roots, 15 singlet roots. Active Space Orbitals (in order for CI vector notation below): d(xy), d(yz), d(z^2), d(xz), d(x^2-y^2)/C(sp^2), d(x^2-y^2)/C(sp^2)*, π*(1), π*(2).

State	Root	Multiplicity	ΔE/nm	ΔE/kcal mol^{-1}	CI vector	Contribution
0	0	1	---	---	22211110	0.7381
1	0	3	40650.4	0.7	22211110	0.7773
2	1	3	7266.9	3.9	22121110	0.9208
3	1	1	5892.1	4.9	22121110	0.9199
4	2	3	5263.4	5.4	22121110	0.9624
5	3	3	4501.5	6.4	22211110	0.8443
6	4	3	3328.3	8.6	21221110	0.8798
7	2	1	3205.3	8.9	21221110	0.8317
8	5	3	3018.7	9.5	21221110	0.8744
9	3	1	1364.6	21.0	21212110	0.4795
					12221110	0.4422
10	6	3	1345.5	21.2	21212110	0.4877
					12221110	0.4573
11	7	3	1237.5	23.1	12221110	0.4797
					21212110	0.4539
12	4	1	1199.7	23.8	22211101	0.7526
13	8	3	1172.5	24.4	22211101	0.7641
14	9	3	1158.0	24.7	22121101	0.8987
15	5	1	1152.5	24.8	22121101	0.8501
16	10	3	1139.3	25.1	22220110	0.7711
17	6	1	1137.7	25.1	22220110	0.7868
18	11	3	1122.1	25.5	22121101	0.9029
19	12	3	1072.2	26.7	22211101	0.8448
20	7	1	999.6	28.6	12212110	0.4761
					21221101	0.3318

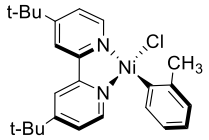

1B with Ni–C distance of 1.90 Å (near-equilibrium geometry) – CASSCF/NEVPT2 composition of the singlet ground state with CPCM(THF) (10e,9o Active Space) – 25 triplet roots, 15 singlet roots. Active Space Orbitals (in order for CI vector notation below): d(x^2-y^2)/C(sp^2), d(xy), d(yz), d(z^2), d(xz), d(x^2-y^2)/C(sp^2)*, π*(1), π*(2), π*(3).

CI vector	Transition	Contribution
222220000	Closed-shell singlet (CSS) d^8	0.5263
222210100	d(xz) → π*(1)	0.2000
122221000	d(x^2-y^2)/C(sp^2) → d(x^2-y^2)/C(sp^2)*	0.1125
221220100	d(xy) → π*(1)	0.0305
022212100	2x[d(x^2-y^2)/C(sp^2)] + d(xz) → 2x[d(x^2-y^2)/C(sp^2)*] + π*(1)	0.0269
222210010	d(xz) → π*(2)	0.0140
221220001	d(yz) → π*(3)	0.0115
122211100	d(x^2-y^2)/C(sp^2) + d(xz) → d(x^2-y^2)/C(sp^2)* + π*(1)	0.0102
Sum of CSS		**53 %**
Sum of all MLCT		**26 %**
Sum of all d-d		**11 %**
Sum of mixed MLCT + d-d		**4 %**

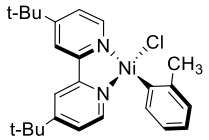

1B with Ni–C distance of 1.90 Å (near-equilibrium geometry) – CASSCF/QD-NEVPT2 composition of the singlet ground state with CPCM(THF) (10e,9o Active Space) – 25 triplet roots, 15 singlet roots. Active Space Orbitals (in order for CI vector notation below): d(x^2-y^2)/C(sp^2), d(xy), d(yz), d(z^2), d(xz), d(x^2-y^2)/C(sp^2)*, π*(1), π*(2), π*(3).

CI vector	Transition	Contribution
222220000	Closed-shell singlet (CSS) d^8	0.5854
122221000	d(x^2-y^2)/C(sp^2) → d(x^2-y^2)/C(sp^2)*	0.1300
222210100	d(xz) → π*(1)	0.1187
221220100	d(yz) → π*(1)	0.0223
222210010	d(xz) → π*(2)	0.0206
222121000	d(z^2) → d(x^2-y^2)/C(sp^2)*	0.0194
022212100	2x[d(x^2-y^2)/C(sp^2)] + d(xz) → 2x[d(x^2-y^2)/C(sp^2)*] + π*(1)	0.0165
221220001	d(yz) → π*(3)	0.0143
222022000	2x[d(z^2)] → 2x[d(x^2-y^2)/C(sp^2)*]	0.0107
Sum of CSS		**58 %**
Sum of all MLCT		**18 %**
Sum of all d-d		**16 %**
Sum of mixed MLCT + d-d		**2 %**

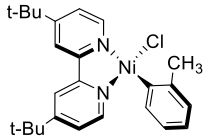

1B with Ni–C distance of 3.50 Å (dissociation limit) – CASSCF/NEVPT2 composition of the singlet ground state with CPCM(THF) (10e,8o Active Space) – 25 triplet roots, 15 singlet roots. Active Space Orbitals (in order for CI vector notation below): d(xy), d(yz), d(z^2), d(xz), d(x^2-y^2)/C(sp^2), d(x^2-y^2)/C(sp^2)*, π*(1), π*(2).

CI vector	Transition	Contribution
22211110	d(xz) + d(x^2-y^2)/C(sp^2) → d(x^2-y^2)/C(sp^2)* + π*(1)	0.7753
22112110	d(z^2) + d(xz) → d(x^2-y^2)/C(sp^2)* + π*(1)	0.0561
22221100	d(x^2-y^2)/C(sp^2) → d(x^2-y^2)/C(sp^2)*	0.0407
11222110	d(xy) + d(yz) → d(x^2-y^2)/C(sp^2)* + π*(1)	0.0342
21221110	d(yz) + d(x^2-y^2)/C(sp^2) → d(x^2-y^2)/C(sp^2)* + π*(1)	0.0300
22212010	d(xz) → π*(1)	0.0273
22210210	2x[d(x^2-y^2)/C(sp^2)] + d(xz) → 2x[d(x^2-y^2)/C(sp^2)*] + π*(1)	0.0121
Sum of CSS		**0 %**
Sum of all MLCT		**3 %**
Sum of all d-d		**4 %**
Sum of mixed MLCT + d-d		**91 %**

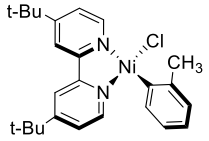

1B with Ni–C distance of 3.50 Å (dissociation limit) – CASSCF/QD-NEVPT2 composition of the singlet ground state with CPCM(THF) (10e,8o Active Space) – 25 triplet roots, 15 singlet roots. Active Space Orbitals (in order for CI vector notation below): d(xy), d(yz), d(z^2), d(xz), d(x^2-y^2)/C(sp^2), d(x^2-y^2)/C(sp^2)*, π*(1), π*(2).

CI vector	Transition	Contribution
22211110	d(xz) + d(x^2-y^2)/C(sp^2) → d(x^2-y^2)/C(sp^2)* + π*(1)	0.7381
22112110	d(z^2) + d(xz) → d(x^2-y^2)/C(sp^2)* + π*(1)	0.0545
22221100	d(x^2-y^2)/C(sp^2) → d(x^2-y^2)/C(sp^2)*	0.0495
21221110	d(yz) + d(x^2-y^2)/C(sp^2) → d(x^2-y^2)/C(sp^2)* + π*(1)	0.0335
11222110	d(xy) + d(yz) → d(x^2-y^2)/C(sp^2)* + π*(1)	0.0289
22212010	d(xz) → π*(1)	0.0278
22211101	d(xz) + d(x^2-y^2)/C(sp^2) → d(x^2-y^2)/C(sp^2)* + π*(2)	0.0270
22210210	2x[d(x^2-y^2)/C(sp^2)] + d(xz) → 2x[d(x^2-y^2)/C(sp^2)*] + π*(1)	0.0123
Sum of CSS		**0 %**
Sum of all MLCT		**3 %**
Sum of all d-d		**5 %**
Sum of mixed MLCT + d-d		**89 %**

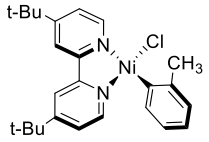

1B – CASSCF/NEVPT2 spin-orbit corrected absorption transitions for the CPCM(THF) phase spectrum (10e,9o Active Space) – 25 triplet roots, 15 singlet roots.

***E*/nm**	***E*/kcal mol^{-1}**	f_{osc}	***E*/nm**	***E*/kcal mol^{-1}**	f_{osc}
710.7	40.2	0.0001760	378.0	75.6	0.0000215
710.2	40.3	0.0000000	376.3	76.0	0.0030826
703.7	40.6	0.0057933	374.3	76.4	0.0167253
696.9	41.0	0.0012136	372.8	76.7	0.0143256
645.7	44.3	0.0015823	372.2	76.8	0.0000068
643.7	44.4	0.0000032	371.7	76.9	0.0107965
642.6	44.5	0.0000901	351.4	81.4	0.0886074
641.9	44.5	0.0121354	329.7	86.7	0.0000034
640.2	44.7	0.0000188	328.5	87.0	0.0000001
639.2	44.7	0.0001567	326.6	87.6	0.0000001
603.2	47.4	0.0821178	320.2	89.3	0.0012580
563.1	50.8	0.1484097	318.4	89.8	0.0000561
552.9	51.7	0.0000004	318.2	89.9	0.0000033
552.4	51.8	0.0000597	317.4	90.1	0.0000115
547.9	52.2	0.1227978	317.4	90.1	0.0000408
467.6	61.1	0.0294280	317.2	90.1	0.0001033
459.5	62.2	0.0000697	315.2	90.7	0.0000021
456.3	62.7	0.0001367	314.6	90.9	0.0000698
448.8	63.7	0.0114377	314.5	90.9	0.0000388
447.8	63.9	0.0000029	314.4	91.0	0.0001298
447.5	63.9	0.0039026	313.2	91.3	0.0000240
446.6	64.0	0.0006564	311.7	91.7	0.0000050
440.9	64.8	0.0005965	309.1	92.5	0.0000163
431.5	66.3	0.0000038	378.0	75.6	0.0000215
431.5	66.3	0.0006481	376.3	76.0	0.0030826
431.3	66.3	0.0003916	374.3	76.4	0.0167253
426.8	67.0	0.0061101	372.8	76.7	0.0143256
422.0	67.8	0.0006958	372.2	76.8	0.0000068
421.9	67.8	0.0001128	371.7	76.9	0.0107965
421.8	67.8	0.0013979	351.4	81.4	0.0886074
418.2	68.4	0.0947208	329.7	86.7	0.0000034
378.2	75.6	0.0019854	328.5	87.0	0.0000001
378.0	75.6	0.0000405	326.6	87.6	0.0000001

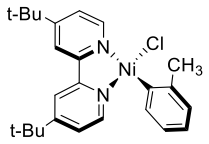

1B – CASSCF/QD-NEVPT2 spin-orbit corrected absorption transitions for the CPCM(THF) phase spectrum (10e,9o Active Space) – 25 triplet roots, 15 singlet roots.

***E*/nm**	***E*/kcal mol^{-1}**	f_{osc}	***E*/nm**	***E*/kcal mol^{-1}**	f_{osc}
696.1	41.1	0.0001416	416.5	68.6	0.0000408
696.0	41.1	0.0000002	416.3	68.7	0.0004648
691.0	41.4	0.0051942	410.1	69.7	0.0923703
682.8	41.9	0.0013330	373.7	76.5	0.0002387
656.1	43.6	0.0000216	373.5	76.6	0.0006092
655.2	43.6	0.0000138	373.4	76.6	0.0004617
652.4	43.8	0.0004268	372.7	76.7	0.0008966
631.7	45.3	0.0013541	372.1	76.8	0.0005703
630.2	45.4	0.0000641	371.9	76.9	0.0031336
628.3	45.5	0.0002382	371.5	77.0	0.0023907
596.2	48.0	0.0881912	367.4	77.8	0.0182278
547.5	52.2	0.1407730	349.5	81.8	0.0005362
542.3	52.7	0.0001741	349.5	81.8	0.0000559
541.8	52.8	0.0000716	349.2	81.9	0.0043313
538.2	53.1	0.1478686	343.6	83.2	0.0014779
464.1	61.6	0.0000794	326.4	87.6	0.0000252
455.0	62.8	0.0004961	325.7	87.8	0.0000043
448.9	63.7	0.0257590	322.6	88.6	0.0000053
442.2	64.7	0.0021120	320.5	89.2	0.0000192
442.0	64.7	0.0000154	320.2	89.3	0.0001464
440.6	64.9	0.0094372	320.1	89.3	0.0000017
440.1	65.0	0.0001729	316.0	90.5	0.0233363
434.3	65.8	0.0048184	315.9	90.5	0.0846200
425.3	67.2	0.0003825	314.5	90.9	0.0000103
425.2	67.2	0.0004524	310.5	92.1	0.0033691
425.0	67.3	0.0015977	309.4	92.4	0.0006259
421.6	67.8	0.0166611	307.2	93.1	0.0039749
416.7	68.6	0.0001628	305.0	93.7	0.0001600

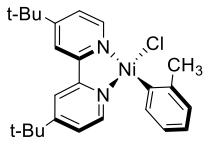

1B – TD-DFT (B3LYP) absorption transitions (singlets only) for the CPCM(THF) phase spectrum.

***E*/nm**	***E*/kcal mol^{-1}**	f_{osc}	***E*/nm**	***E*/kcal mol^{-1}**	f_{osc}
775.3	36.9	0.0000000	372.8	76.7	0.0000000
601.5	47.5	0.0000000	369.5	77.4	0.0000197
596.9	47.9	0.0000000	367.1	77.9	0.0225168
553.3	51.7	0.0000000	362.8	78.8	0.0000000
544.3	52.5	0.0010155	361.6	79.1	0.0000000
513.4	55.7	0.0000000	341.5	83.7	0.0212826
510.0	56.1	0.0016531	336.0	85.1	0.0000528
508.7	56.2	0.0066485	335.2	85.3	0.0004584
489.9	58.4	0.0000711	334.0	85.6	0.0280974
474.5	60.3	0.0231506	333.8	85.7	0.0000000
466.0	61.4	0.0000000	333.6	85.7	0.0000000
462.2	61.9	0.0005945	332.9	85.9	0.0000000
460.2	62.1	0.0000000	331.4	86.3	0.0061857
456.2	62.7	0.0001044	331.3	86.3	0.0000000
454.0	63.0	0.0001171	331.0	86.4	0.0000000
443.9	64.4	0.0000000	326.5	87.6	0.0090909
436.8	65.5	0.0003876	326.1	87.7	0.0002664
432.6	66.1	0.0640219	310.1	92.2	0.0000000
416.9	68.6	0.0000000	310.0	92.2	0.0000000
414.6	69.0	0.0002552	308.7	92.6	0.0000000
391.4	73.0	0.0000000	303.0	94.4	0.0000000
385.0	74.3	0.0003950	302.6	94.5	0.0033161
379.7	75.3	0.0000000	302.2	94.6	0.0000000

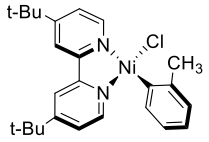

1B – TD-DFT (B3LYP) absorption transitions (singlets only) for the CPCM(Toluene) phase spectrum.

***E*/nm**	***E*/kcal mol^{-1}**	f_{osc}	***E*/nm**	***E*/kcal mol^{-1}**	f_{osc}
756.9	37.8	0.0000000	396.1	72.2	0.0004180
692.3	41.3	0.0000000	388.9	73.5	0.0000000
666.9	42.9	0.0006802	388.0	73.7	0.0033031
642.9	44.5	0.0000000	383.5	74.5	0.0000299
596.1	48.0	0.0000000	382.3	74.8	0.0000000
580.8	49.2	0.0000000	379.5	75.3	0.0000000
540.6	52.9	0.0003625	378.8	75.5	0.0000000
531.6	53.8	0.0164318	376.9	75.9	0.0000000
526.1	54.4	0.0000000	370.5	77.2	0.0136672
521.9	54.8	0.0000000	369.4	77.4	0.0000000
493.6	57.9	0.0018742	369.1	77.5	0.0000000
487.7	58.6	0.0000498	366.2	78.1	0.0035020
475.6	60.1	0.0023270	364.3	78.5	0.0214867
474.2	60.3	0.0068798	364.1	78.5	0.0000757
472.4	60.5	0.0583785	339.2	84.3	0.0000000
472.2	60.6	0.0008972	338.1	84.6	0.0010193
462.5	61.8	0.0000000	322.5	88.6	0.0000000
461.5	62.0	0.0002323	321.2	89.0	0.0000000
456.5	62.6	0.0079188	318.1	89.9	0.0000000
447.1	64.0	0.0000000	316.0	90.5	0.0000000
437.0	65.4	0.0002701	315.5	90.6	0.0144091
436.1	65.6	0.0000000	315.1	90.7	0.0000000
414.4	69.0	0.0000000	311.5	91.8	0.0000000
406.7	70.3	0.0262452	307.2	93.1	0.0000000
405.5	70.5	0.0000000	306.6	93.3	0.0145373
404.0	70.8	0.0000175	304.8	93.8	0.0983535

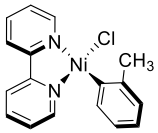

1C with Ni–C distance of 1.90 Å (near-equilibrium geometry) – CASSCF/NEVPT2 lowest transition energies with CPCM(THF) (10e,9o Active Space) – 25 triplet roots, 15 singlet roots. Active Space Orbitals (in order for CI vector notation below): d(xy), d(x^2-y^2)/C(sp^2), d(yz), d(z^2), d(xz), d(x^2-y^2)/C(sp^2)*, π*(1), π*(2), π*(3).

State	Root	Multiplicity	ΔE/nm	ΔE/kcal mol^{-1}	CI vector	Contribution
0	0	1	---	---	222220000	0.4707
					222210100	0.2626
1	0	3	1175.1	24.3	222121000	0.7308
					212122000	0.1607
2	1	3	988.1	28.9	222211000	0.4189
					221221000	0.3539
					212212000	0.1016
3	2	3	914.6	31.3	221221000	0.4120
					222211000	0.3465
4	3	3	779.6	36.7	222120100	0.7568
5	1	1	758.2	37.7	222120100	0.7661
6	4	3	711.7	40.2	222210100	0.7937
7	5	3	666.8	42.9	122221000	0.6534
					221212000	0.1308
					112222000	0.1011
8	2	1	658.1	43.4	221220100	0.5069
					222210100	0.2440
9	3	1	646.7	44.2	222210100	0.2604
					221220100	0.2513
					222220000	0.1508
10	6	3	612.0	46.7	221220100	0.7510
11	4	1	477.8	59.8	222121000	0.4509
					222210010	0.1810
					122221000	0.1014
12	5	1	476.9	59.9	122220100	0.6407
					221211100	0.1072
13	6	1	472.4	60.5	222211000	0.5308
					221221000	0.1881
14	7	3	459.1	62.3	122220100	0.7385
15	8	3	457.0	62.6	222120010	0.6761
16	7	1	454.9	62.9	222120010	0.6879
17	8	1	454.8	62.9	221221000	0.4761
					222211000	0.2273
18	9	1	449.0	63.7	122221000	0.4983
					222210010	0.1679
19	10	1	442.1	64.7	222121000	0.2385
					222210010	0.2331
					122221000	0.1009
20	9	3	435.9	65.6	222210010	0.7097

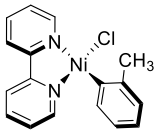

1C with Ni–C distance of 1.90 Å (near-equilibrium geometry) – CASSCF/QD-NEVPT2 lowest transition energies with CPCM(THF) (10e,9o Active Space) – 25 triplet roots, 15 singlet roots. Active Space Orbitals (in order for CI vector notation below): d(xy), d(x^2-y^2)/C(sp^2), d(yz), d(z^2), d(xz), d(x^2-y^2)/C(sp^2)*, π*(1), π*(2), π*(3).

State	Root	Multiplicity	ΔE/nm	ΔE/kcal mol^{-1}	CI vector	Contribution
0	0	1	---	---	222220000	0.5732
					222210100	0.1292
					212221000	0.1244
1	0	3	1082.0	26.4	222121000	0.7259
					212122000	0.1569
2	1	3	928.2	30.8	222211000	0.5359
					221221000	0.2306
					212212000	0.1258
3	2	3	856.4	33.4	221221000	0.5164
					222211000	0.2103
4	3	3	734.5	38.9	222120100	0.7195
5	1	1	716.5	39.9	222120100	0.7674
6	4	3	674.8	42.4	222210100	0.7887
7	5	3	647.1	44.2	122221000	0.6337
8	2	1	635.4	45.0	222210100	0.5553
					221220100	0.1250
9	3	1	587.1	48.7	221220100	0.6367
10	6	3	584.8	48.9	221220100	0.7263
11	4	1	463.5	61.7	222121000	0.3571
					222210010	0.2946
12	5	1	461.1	62.0	122220100	0.3566
					222211000	0.3112
13	6	1	456.2	62.7	222211000	0.3985
					122220100	0.3683
14	7	3	443.8	64.4	122220100	0.3996
					222120010	0.2648
15	8	3	442.0	64.7	122220100	0.3385
					222120010	0.3141
					222120001	0.1013
16	7	1	441.9	64.7	222120010	0.4054
					222120001	0.1446
					221221000	0.1178
17	8	1	438.6	65.2	221221000	0.2227
					222120010	0.1832
18	9	1	433.7	65.9	122221000	0.4209
19	10	1	426.3	67.1	221221000	0.2890
					122221000	0.2371
					222121000	0.1251
20	9	3	422.5	67.7	222210010	0.6393
					222210001	0.1518

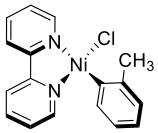

1C with Ni–C distance of 3.50 Å (dissociation limit) – CASSCF/NEVPT2 lowest transition energies with CPCM(THF) (10e,8o Active Space) – 25 triplet roots, 15 singlet roots. Active Space Orbitals (in order for CI vector notation below): d(xy), d(yz), d(z^2), d(xz), d(x^2-y^2)/C(sp^2), d(x^2-y^2)/C(sp^2)*, π*(1), π*(2).

State	Root	Multiplicity	ΔE/nm	ΔE/kcal mol^{-1}	CI vector	Contribution
0	0	1	---	---	22211110	0.7852
1	0	3	48887.7	0.6	22211110	0.8198
2	1	3	8698.6	3.3	22121110	0.9208
3	1	1	6772.2	4.2	22121110	0.9177
4	2	3	6026.1	4.7	22121110	0.9573
5	3	3	4848.7	5.9	22211110	0.8454
6	4	3	3525.2	8.1	21221110	0.8699
7	2	1	3360.4	8.5	21221110	0.8405
8	5	3	3171.6	9.0	21221110	0.8774
9	3	1	1399.9	20.4	21212110	0.4651
					12221110	0.4538
10	6	3	1381.1	20.7	21212110	0.4696
					12221110	0.4676
11	7	3	1266.6	22.6	12221110	0.4917
					21212110	0.4393
12	4	1	1160.7	24.6	22220110	0.8263
13	8	3	1152.9	24.8	22220110	0.7554
14	5	1	1124.4	25.4	22211101	0.7898
15	9	3	1105.4	25.9	22211101	0.7537
16	10	3	1095.1	26.1	22121101	0.9140
17	6	1	1094.1	26.1	22121101	0.8993
18	11	3	1069.5	26.7	22121101	0.9397
19	12	3	1010.2	28.3	22211101	0.8445
20	7	1	992.9	28.8	12212110	0.7939
					21122110	0.1241

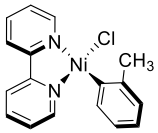

1C with Ni–C distance of 3.50 Å (dissociation limit) – CASSCF/QD-NEVPT2 lowest transition energies with CPCM(THF) (10e,8o Active Space) – 25 triplet roots, 15 singlet roots. Active Space Orbitals (in order for CI vector notation below): d(xy), d(yz), d(z^2), d(xz), d(x^2-y^2)/C(sp^2), d(x^2-y^2)/C(sp^2)*, π*(1), π*(2).

State	Root	Multiplicity	ΔE/nm	ΔE/kcal mol^{-1}	CI vector	Contribution
0	0	1	---	---	22211110	0.7633
1	0	3	45269.4	0.6	22211110	0.8022
2	1	3	8066.5	3.5	22121110	0.9182
3	1	1	6401.2	4.5	22121110	0.9148
4	2	3	5726.4	5.0	22121110	0.9548
5	3	3	4639.5	6.2	22211110	0.8428
6	4	3	3423.1	8.4	21221110	0.8678
7	2	1	3274.7	8.7	21221110	0.8317
8	5	3	3092.4	9.2	21221110	0.8711
9	3	1	1382.5	20.7	21212110	0.4679
					12221110	0.4544
10	6	3	1363.1	21.0	21212110	0.4750
					12221110	0.4695
11	7	3	1255.1	22.8	12221110	0.4870
					21212110	0.4431
12	8	3	1153.5	24.8	22220110	0.8088
13	4	1	1148.6	24.9	22220110	0.8171
14	5	1	1111.2	25.7	22211101	0.7195
15	9	3	1085.5	26.3	22211101	0.5496
					22121101	0.2802
16	10	3	1078.3	26.5	22121101	0.7152
					22211101	0.1758
17	6	1	1073.4	26.6	22121101	0.8547
18	11	3	1048.5	27.3	22121101	0.8725
19	12	3	997.6	28.7	22211101	0.8414
20	7	1	990.7	28.9	12212110	0.7368

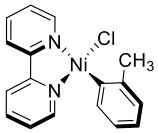

1C with Ni–C distance of 1.90 Å (near-equilibrium geometry) – CASSCF/NEVPT2 composition of the singlet ground state with CPCM(THF) (10e,9o Active Space) – 25 triplet roots, 15 singlet roots. Active Space Orbitals (in order for CI vector notation below): d(xy), d(x^2-y^2)/C(sp^2), d(yz), d(z^2), d(xz), d(x^2-y^2)/C(sp^2)*, π*(1), π*(2), π*(3).

CI vector	Transition	Contribution
222220000	Closed-shell singlet (CSS) d^8	0.4707
222210100	d(xz) → π*(1)	0.2626
212221000	d(x^2-y^2)/C(sp^2) → d(x^2-y^2)/C(sp^2)*	0.0947
202212100	2x[d(x^2-y^2)/C(sp^2)] + d(xz) → 2x[d(x^2-y^2)/C(sp^2)*] + π*(1)	0.0339
221220100	d(yz) → π*(1)	0.0287
222210010	d(xz) → π*(2)	0.0155
212211100	d(x^2-y^2)/C(sp^2) + d(xz) → d(x^2-y^2)/C(sp^2)* + π*(1)	0.0127
221220001	d(yz) → π*(3)	0.0117
Sum of CSS		**47 %**
Sum of all MLCT		**32 %**
Sum of all d-d		**9 %**
Sum of mixed MLCT + d-d		**5 %**

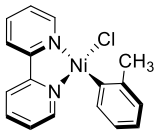

1C with Ni–C distance of 1.90 Å (near-equilibrium geometry) – CASSCF/QD-NEVPT2 composition of the singlet ground state with CPCM(THF) (10e,9o Active Space) – 25 triplet roots, 15 singlet roots. Active Space Orbitals (in order for CI vector notation below): d(xy), d(x^2-y^2)/C(sp^2), d(yz), d(z^2), d(xz), d(x^2-y^2)/C(sp^2)*, π*(1), π*(2), π*(3).

CI vector	Transition	Contribution
222220000	Closed-shell singlet (CSS) d^8	0.5732
222210100	d(xz) → π*(1)	0.1292
212221000	d(x^2-y^2)/C(sp^2) → d(x^2-y^2)/C(sp^2)*	0.1244
221220001	d(yz) → π*(3)	0.0277
222210010	d(xz) → π*(2)	0.0246
222121000	d(z^2) → d(x^2-y^2)/C(sp^2)*	0.0176
202212100	2x[d(x^2-y^2)/C(sp^2)] + d(xz) → 2x[d(x^2-y^2)/C(sp^2)*] + π*(1)	0.0175
221220100	d(yz) → π*(1)	0.0173
222022000	2x[d(z^2)] → 2x[d(x^2-y^2)/C(sp^2)*]	0.0102
Sum of CSS		**57 %**
Sum of all MLCT		**20 %**
Sum of all d-d		**15 %**
Sum of mixed MLCT + d-d		**2 %**

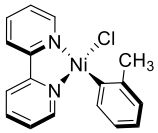

1C with Ni–C distance of 3.50 Å (dissociation limit) – CASSCF/NEVPT2 composition of the singlet ground state with CPCM(THF) (10e,8o Active Space) – 25 triplet roots, 15 singlet roots. Active Space Orbitals (in order for CI vector notation below): d(xy), d(yz), d(z^2), d(xz), d(x^2-y^2)/C(sp^2), d(x^2-y^2)/C(sp^2)*, π*(1), π*(2).

CI vector	Transition	Contribution
22211110	d(xz) + d(x^2-y^2)/C(sp^2) → d(x^2-y^2)/C(sp^2)* + π*(1)	0.7851
22112110	d(z^2) + d(xz) → d(x^2-y^2)/C(sp^2)* + π*(1)	0.0581
22221100	d(x^2-y^2)/C(sp^2) → d(x^2-y^2)/C(sp^2)*	0.0415
11222110	d(xy) + d(yz) → d(x^2-y^2)/C(sp^2)* + π*(1)	0.0333
22212010	d(xz) → π*(1)	0.0269
21221110	d(yz) + d(x^2-y^2)/C(sp^2) → d(x^2-y^2)/C(sp^2)* + π*(1)	0.0179
22210210	2x[d(x^2-y^2)/C(sp^2)] + d(xz) → 2x[d(x^2-y^2)/C(sp^2)*] + π*(1)	0.0122
Sum of CSS		**0 %**
Sum of all MLCT		**3 %**
Sum of all d-d		**4 %**
Sum of mixed MLCT + d-d		**91 %**

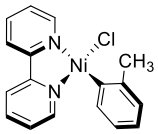

1C with Ni–C distance of 3.50 Å (dissociation limit) – CASSCF/QD-NEVPT2 composition of the singlet ground state with CPCM(THF) (10e,8o Active Space) – 25 triplet roots, 15 singlet roots. Active Space Orbitals (in order for CI vector notation below): d(xy), d(yz), d(z^2), d(xz), d(x^2-y^2)/C(sp^2), d(x^2-y^2)/C(sp^2)*, π*(1), π*(2).

CI vector	Transition	Contribution
22211110	d(xz) + d(x^2-y^2)/C(sp^2) → d(x^2-y^2)/C(sp^2)* + π*(1)	0.7633
22112110	d(z^2) + d(xz) → d(x^2-y^2)/C(sp^2)* + π*(1)	0.0575
22221100	d(x^2-y^2)/C(sp^2) → d(x^2-y^2)/C(sp^2)*	0.0480
11222110	d(xy) + d(yz) → d(x^2-y^2)/C(sp^2)* + π*(1)	0.0289
22212010	d(xz) → π*(1)	0.0280
21221110	d(yz) + d(x^2-y^2)/C(sp^2) → d(x^2-y^2)/C(sp^2)* + π*(1)	0.0213
22211101	d(xz) + d(x^2-y^2)/C(sp^2) → d(x^2-y^2)/C(sp^2)* + π*(2)	0.0130
22210210	2x[d(x^2-y^2)/C(sp^2)] + d(xz) → 2x[d(x^2-y^2)/C(sp^2)*] + π*(1)	0.0127
Sum of CSS		**0 %**
Sum of all MLCT		**3 %**
Sum of all d-d		**5 %**
Sum of mixed MLCT + d-d		**90 %**

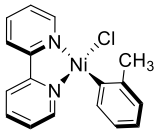

1C – CASSCF/NEVPT2 spin-orbit corrected absorption transitions for the CPCM(THF) phase spectrum (10e,9o Active Space) – 25 triplet roots, 15 singlet roots.

***E*/nm**	***E*/kcal mol^{-1}**	f_{osc}	***E*/nm**	***E*/kcal mol^{-1}**	f_{osc}
791.4	36.1	0.0001409	404.3	70.7	0.0000005
791.1	36.1	0.0000004	403.4	70.9	0.0001640
783.3	36.5	0.0057985	387.3	73.8	0.0009911
773.3	37.0	0.0003790	387.0	73.9	0.0000002
708.5	40.4	0.0034868	387.0	73.9	0.0000092
705.2	40.5	0.0000033	383.9	74.5	0.0052554
703.1	40.7	0.0000900	375.5	76.1	0.1628376
677.2	42.2	0.1027156	362.1	79.0	0.0135836
662.1	43.2	0.0000043	361.5	79.1	0.0000095
661.6	43.2	0.0000035	361.4	79.1	0.0000138
644.7	44.3	0.0082840	341.9	83.6	0.2021970
630.6	45.3	0.2062495	336.4	85.0	0.0001002
604.4	47.3	0.0200463	335.2	85.3	0.0000001
604.2	47.3	0.0006789	333.1	85.8	0.0000003
603.8	47.4	0.0000432	323.8	88.3	0.0000021
478.2	59.8	0.0391197	323.7	88.3	0.0004103
474.7	60.2	0.0002525	322.9	88.5	0.0005196
470.7	60.7	0.0001032	322.8	88.6	0.0000108
461.3	62.0	0.0000073	322.5	88.7	0.0000513
461.3	62.0	0.0000029	320.5	89.2	0.0000040
460.4	62.1	0.0064283	319.0	89.6	0.0000005
459.3	62.2	0.0024988	317.2	90.1	0.0000012
457.3	62.5	0.0001958	314.6	90.9	0.0001067
457.1	62.6	0.0000102	404.3	70.7	0.0000005
457.0	62.6	0.0007540	403.4	70.9	0.0001640
452.9	63.1	0.0016343	387.3	73.8	0.0009911
445.8	64.1	0.0050637	387.0	73.9	0.0000002
439.0	65.1	0.0574476	387.0	73.9	0.0000092
431.8	66.2	0.0000124	383.9	74.5	0.0052554
431.7	66.2	0.0000498	375.5	76.1	0.1628376
431.3	66.3	0.0005702	362.1	79.0	0.0135836
405.4	70.5	0.0200094	361.5	79.1	0.0000095
404.5	70.7	0.0020872	361.4	79.1	0.0000138

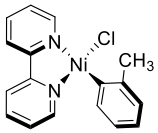

1C – CASSCF/QD-NEVPT2 spin-orbit corrected absorption transitions for the CPCM(THF) phase spectrum (10e,9o Active Space) – 25 triplet roots, 15 singlet roots.

***E*/nm**	***E*/kcal mol^{-1}**	f_{osc}	***E*/nm**	***E*/kcal mol^{-1}**	f_{osc}
744.4	38.4	0.0000042	418.8	68.3	0.0006234
743.6	38.4	0.0030625	418.6	68.3	0.0013536
739.7	38.7	0.0005384	417.9	68.4	0.0008402
729.9	39.2	0.0004037	391.8	73.0	0.0000033
670.2	42.7	0.0004854	391.7	73.0	0.0020846
668.8	42.8	0.0222618	391.2	73.1	0.0078593
668.2	42.8	0.0013591	390.6	73.2	0.0042777
648.4	44.1	0.0041488	377.9	75.7	0.0000206
641.6	44.6	0.0000051	377.4	75.8	0.0000392
640.5	44.6	0.0000443	377.4	75.8	0.0003230
625.3	45.7	0.0257412	373.6	76.5	0.0001854
581.1	49.2	0.2935383	366.1	78.1	0.0214988
577.8	49.5	0.0000432	365.9	78.1	0.0001393
577.5	49.5	0.0000524	365.8	78.2	0.0005547
576.8	49.6	0.0291096	361.1	79.2	0.1592524
465.1	61.5	0.0002482	338.7	84.4	0.0075171
459.2	62.3	0.0005166	338.5	84.5	0.0000290
454.5	62.9	0.0372295	338.5	84.5	0.0001680
446.9	64.0	0.0000942	330.6	86.5	0.2166402
446.9	64.0	0.0000686	328.0	87.2	0.0012190
446.2	64.1	0.0113825	327.3	87.3	0.0000947
443.6	64.5	0.0008598	324.2	88.2	0.0001391
441.3	64.8	0.0012906	317.7	90.0	0.0001597
440.9	64.9	0.0003869	315.9	90.5	0.0001654
440.7	64.9	0.0004738	312.0	91.7	0.0000574
436.0	65.6	0.0038788	310.7	92.0	0.0000537
431.2	66.3	0.0165864	308.6	92.7	0.0002910
424.8	67.3	0.0435680	306.4	93.3	0.0000902

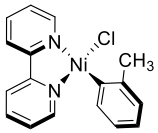

1C – TD-DFT (B3LYP) absorption transitions (singlets only) for the CPCM(THF) phase spectrum.

***E*/nm**	***E*/kcal mol^{-1}**	f_{osc}	***E*/nm**	***E*/kcal mol^{-1}**	f_{osc}
762.2	37.5	0.0000000	381.5	74.9	0.0000022
636.8	44.9	0.0000000	376.4	76.0	0.0000000
608.6	47.0	0.0008883	375.6	76.1	0.0080765
592.8	48.2	0.0000000	368.0	77.7	0.0014573
585.7	48.8	0.0000000	353.1	81.0	0.0000000
533.8	53.6	0.0000000	353.1	81.0	0.0000000
525.6	54.4	0.0016800	348.1	82.1	0.0199718
511.3	55.9	0.0084429	347.9	82.2	0.0000629
489.4	58.4	0.0000000	344.0	83.1	0.0000000
488.1	58.6	0.0005297	341.3	83.8	0.0119202
485.1	58.9	0.0000179	340.6	83.9	0.0240326
482.2	59.3	0.0000000	340.0	84.1	0.0002971
470.5	60.8	0.0153194	339.1	84.3	0.0000000
465.0	61.5	0.0000000	332.7	85.9	0.0000000
455.9	62.7	0.0007479	325.5	87.8	0.0000000
453.6	63.0	0.0001736	315.1	90.7	0.0000000
452.2	63.2	0.0003639	312.7	91.4	0.0061925
446.1	64.1	0.0571231	312.4	91.5	0.0000000
419.4	68.2	0.0000000	312.4	91.5	0.0253885
417.0	68.6	0.0002398	310.1	92.2	0.0000000
395.5	72.3	0.0000000	310.0	92.2	0.0000000
394.9	72.4	0.0004577	308.4	92.7	0.0001654
389.6	73.4	0.0000000	308.3	92.7	0.0000000
386.2	74.0	0.0000000	305.9	93.5	0.0000000
383.3	74.6	0.0000000	301.1	94.9	0.0037814

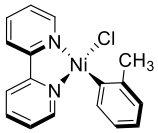

1C – TD-DFT (B3LYP) absorption transitions (singlets only) for the CPCM(Toluene) phase spectrum.

***E*/nm**	***E*/kcal mol^{-1}**	f_{osc}	***E*/nm**	***E*/kcal mol^{-1}**	f_{osc}
742.3	38.5	0.0000000	391.6	73.0	0.0000000
738.2	38.7	0.0000000	390.8	73.2	0.0000000
710.1	40.3	0.0006408	389.9	73.3	0.0000000
685.4	41.7	0.0000000	389.5	73.4	0.0000618
591.7	48.3	0.0000000	384.8	74.3	0.0000000
583.6	49.0	0.0000000	384.1	74.4	0.0000000
576.5	49.6	0.0004532	379.1	75.4	0.0140823
558.8	51.2	0.0174286	377.7	75.7	0.0007511
557.6	51.3	0.0000000	376.7	75.9	0.0023473
555.2	51.5	0.0000000	372.9	76.7	0.0071587
527.1	54.2	0.0000000	372.9	76.7	0.0270966
508.6	56.2	0.0003646	372.7	76.7	0.0000000
505.7	56.5	0.0004749	368.0	77.7	0.0000000
488.0	58.6	0.0514571	354.5	80.7	0.0000000
475.5	60.1	0.0058113	351.9	81.3	0.0000000
473.9	60.3	0.0037102	350.8	81.5	0.0007714
465.5	61.4	0.0000000	335.4	85.3	0.0000000
464.0	61.6	0.0002080	334.0	85.6	0.0000000
454.2	63.0	0.0006348	326.9	87.5	0.0000000
453.3	63.1	0.0037225	324.9	88.0	0.0175192
445.0	64.2	0.0003318	324.5	88.1	0.0669589
420.9	67.9	0.0000000	314.8	90.8	0.0000000
419.2	68.2	0.0095985	314.7	90.8	0.0000000
416.9	68.6	0.0000061	309.1	92.5	0.0000000
415.8	68.8	0.0000000	307.6	93.0	0.0034418
399.8	71.5	0.0000000	303.8	94.1	0.0001911
398.7	71.7	0.0031784	301.2	94.9	0.0016825

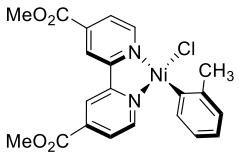

1D with Ni–C distance of 1.90 Å (near-equilibrium geometry) – CASSCF/NEVPT2 lowest transition energies with CPCM(THF) (10e,9o Active Space) – 25 triplet roots, 15 singlet roots. Active Space Orbitals (in order for CI vector notation below): d(yz), d(xy), d(xz), d(z^2), d(x^2-y^2)/C(sp^2), d(x^2-y^2)/C(sp^2)*, π*(1), π*(2), π*(3).

State	Root	Multiplicity	ΔE/nm	ΔE/kcal mol^{-1}	CI vector	Contribution
0	0	1	---	---	221220100	0.5068
					222220000	0.1320
1	0	3	17896.1	1.6	221221000	0.3990
					122221000	0.2368
2	1	3	2176.3	13.1	222120100	0.3912
					222210100	0.3333
3	1	1	2046.4	14.0	222120100	0.3938
					222210100	0.3329
4	2	3	1702.6	16.8	221220100	0.6996
5	3	3	1422.2	20.1	222211000	0.1994
					122211100	0.1795
					222121000	0.1419
					212221000	0.1156
					112221100	0.1152
6	2	1	1226.6	23.3	122220100	0.6133
					221220100	0.1311
7	4	3	1140.2	25.1	122220100	0.7452
8	3	1	988.6	28.9	221220010	0.5631
9	5	3	978.7	29.2	121221100	0.2572
					122221000	0.2237
					221221000	0.1715
					212211100	0.1162
10	4	1	811.4	35.2	222120010	0.4427
					222210010	0.2742
11	6	3	770.2	37.1	222120010	0.3884
					222210010	0.3333
12	7	3	741.1	38.6	212220100	0.6576
13	5	1	740.9	38.6	212220100	0.6467
14	6	1	708.8	40.3	221220001	0.3179
					122220001	0.1334
					122220010	0.1330
15	8	3	705.3	40.5	222120001	0.3824
					222210001	0.3249
16	9	3	704.0	40.6	221220010	0.7028
17	7	1	702.3	40.7	222120001	0.3895
					222210001	0.3317
18	8	1	688.4	41.5	122220010	0.5864
19	9	1	663.4	43.1	221220001	0.3637
					122220001	0.2663
20	10	3	588.4	48.6	122220010	0.7359

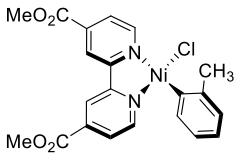

1D with Ni–C distance of 1.90 Å (near-equilibrium geometry) – CASSCF/QD-NEVPT2 lowest transition energies with CPCM(THF) (10e,9o Active Space) – 25 triplet roots, 15 singlet roots. Active Space Orbitals (in order for CI vector notation below): d(yz), d(xy), d(xz), d(z^2), d(x^2-y^2)/C(sp^2), d(x^2-y^2)/C(sp^2)*, π*(1), π*(2), π*(3).

State	Root	Multiplicity	ΔE/nm	ΔE/kcal mol^{-1}	CI vector	Contribution
0	0	1	---	---	222220000	0.2955
					221220100	0.1953
					122220001	0.1251
1	0	3	4017.8	7.1	221221000	0.5949
					221122000	0.1039
2	1	3	2689.2	10.6	222121000	0.4092
					222211000	0.2813
					222112000	0.1660
3	2	3	1777.3	16.1	122221000	0.6021
					122212000	0.1878
4	3	3	1290.6	22.2	222120100	0.3610
					222210100	0.3538
5	1	1	1244.7	23.0	222120100	0.3623
					222210100	0.3553
6	4	3	1102.7	25.9	221220100	0.6901
7	2	1	941.7	30.4	221220100	0.4474
					122220100	0.1736
8	5	3	839.6	34.1	122220100	0.7260
9	3	1	709.8	40.3	122220100	0.4316
					221220010	0.1771
10	4	1	620.5	46.1	222120010	0.3665
					222210010	0.3173
11	6	3	613.9	46.6	222120010	0.3628
					222210010	0.3124
12	5	1	596.0	48.0	212220100	0.6456
13	7	3	594.3	48.1	212220100	0.6600
14	8	3	572.1	50.0	221220010	0.6512
15	9	3	566.1	50.5	222120001	0.3619
					222210001	0.3090
16	6	1	563.8	50.7	222120001	0.3616
					222210001	0.3139
17	7	1	558.1	51.2	221220010	0.4121
					122220001	0.1354
18	8	1	534.5	53.5	221220001	0.5998
19	10	3	534.1	53.5	221220001	0.5744
20	11	3	514.0	55.6	212221000	0.2049
					211221100	0.1931
					112221100	0.1883

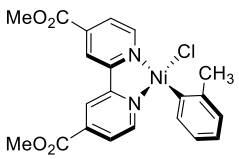

1D with Ni–C distance of 3.50 Å (dissociation limit) – CASSCF/NEVPT2 lowest transition energies with CPCM(THF) (10e,9o Active Space) – 25 triplet roots, 15 singlet roots. Active Space Orbitals (in order for CI vector notation below): d(xy), d(yz), d(xz), d(z^2), d(x^2-y^2)/C(sp^2), d(x^2-y^2)/C(sp^2)*, π*(1), π*(2), π*(3).

State	Root	Multiplicity	ΔE/nm	ΔE/kcal mol^{-1}	CI vector	Contribution
0	0	1	---	---	221211100	0.7473
1	0	3	44065.1	0.6	221211100	0.8013
2	1	3	8672.1	3.3	222111100	0.9271
3	1	1	6470.2	4.4	222111100	0.9211
4	2	3	5742.1	5.0	222111100	0.9905
5	3	3	4367.2	6.5	221211100	0.7253
					212211100	0.1102
6	4	3	3329.7	8.6	212211100	0.7282
					221211100	0.1229
7	2	1	3182.9	9.0	212211100	0.7860
8	5	3	3007.5	9.5	212211100	0.8422
9	3	1	1366.2	20.9	211221100	0.4715
					122211100	0.4399
10	6	3	1346.9	21.2	211221100	0.4771
					122211100	0.4645
11	7	3	1236.5	23.1	122211100	0.4819
					211221100	0.4407
12	8	3	1114.7	25.6	222201100	0.7572
13	4	1	1109.5	25.8	222201100	0.6855
					222111010	0.1505
14	5	1	1096.6	26.1	212211010	0.6073
					221211010	0.1368
15	9	3	1074.3	26.6	222111010	0.8720
16	10	3	1071.0	26.7	212211010	0.6467
					221211010	0.1513
17	6	1	1063.6	26.9	222111010	0.7696
					222201100	0.1336
18	11	3	1036.5	27.6	222111010	0.9712
19	7	1	1002.7	28.5	121221100	0.7046
20	12	3	1001.3	28.6	121221100	0.7056
					221121100	0.1021

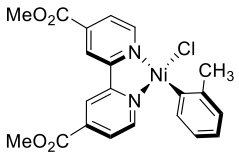

1D with Ni–C distance of 3.50 Å (dissociation limit) – CASSCF/QD-NEVPT2 lowest transition energies with CPCM(THF) (10e,9o Active Space) – 25 triplet roots, 15 singlet roots. Active Space Orbitals (in order for CI vector notation below): d(xy), d(yz), d(xz), d(z^2), d(x^2-y^2)/C(sp^2), d(x^2-y^2)/C(sp^2)*, π*(1), π*(2), π*(3).

State	Root	Multiplicity	ΔE/nm	ΔE/kcal mol^{-1}	CI vector	Contribution
0	0	1	---	---	221211100	0.6937
1	0	3	38910.5	0.7	221211100	0.7534
2	1	3	6456.6	4.4	222111100	0.9139
3	1	1	5127.9	5.6	222111100	0.9111
4	2	3	4661.4	6.1	222111100	0.9806
5	3	3	3702.3	7.7	221211100	0.6894
					212211100	0.1349
6	4	3	2891.9	9.9	212211100	0.7008
					221211100	0.1425
7	2	1	2856.9	10.0	212211100	0.7946
8	5	3	2683.3	10.7	212211100	0.8568
9	3	1	1280.1	22.3	211221100	0.4779
					122211100	0.4376
10	6	3	1262.3	22.6	211221100	0.4843
					122211100	0.4643
11	7	3	1166.1	24.5	122211100	0.4791
					211221100	0.4457
12	4	1	1081.5	26.4	222201100	0.7942
13	8	3	1076.7	26.6	222201100	0.7558
14	5	1	1030.6	27.7	212211010	0.4540
					221211010	0.1270
15	9	3	1007.2	28.4	222111010	0.8019
16	10	3	1004.0	28.5	212211010	0.4972
					221211010	0.1139
17	6	1	984.8	29.0	222111010	0.8237
18	11	3	982.1	29.1	222111010	0.9196
19	7	1	977.9	29.2	121221100	0.5530
20	12	3	971.7	29.4	121221100	0.6088
					221211010	0.1069

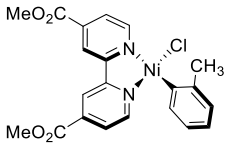

1D with Ni–C distance of 1.90 Å (near-equilibrium geometry) – CASSCF/NEVPT2 composition of the singlet ground state with CPCM(THF) (10e,9o Active Space) – 25 triplet roots, 15 singlet roots. Active Space Orbitals (in order for CI vector notation below): d(yz), d(xy), d(xz), d(z^2), d(x^2-y^2)/C(sp^2), d(x^2-y^2)/C(sp^2)*, π*(1), π*(2), π*(3).

CI vector	Transition	Contribution
221220100	d(xz) → π*(1)	0.5068
222220000	Closed-shell singlet (CSS) d^8	0.1320
122220100	d(yz) → π*(1)	0.0906
222120100	d(z^2) → π*(1)	0.0571
221112100	d(x^2-y^2)/C(sp^2) + d(xz) + d(z^2) → 2x[d(x^2-y^2)/C(sp^2)*] + π*(1)	0.0333
221202100	2x[d(x^2-y^2)/C(sp^2)] + d(xz) → 2x[d(x^2-y^2)/C(sp^2)*] + π*(1)	0.0295
221121100	d(xz) + d(z^2) → d(x^2-y^2)/C(sp^2)* + π*(1)	0.0250
221211100	d(x^2-y^2)/C(sp^2) + d(xz) → d(x^2-y^2)/C(sp^2)* + π*(1)	0.0141
222211000	d(x^2-y^2)/C(sp^2) → d(x^2-y^2)/C(sp^2)*	0.0131
221022100	d(xz) + 2x[d(z^2)] → 2x[d(x^2-y^2)/C(sp^2)*] + π*(1)	0.0124
Sum of CSS		**51 %**
Sum of all MLCT		**65 %**
Sum of all d-d		**1 %**
Sum of mixed MLCT + d-d		**11 %**

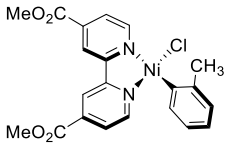

1D with Ni–C distance of 1.90 Å (near-equilibrium geometry) – CASSCF/QD-NEVPT2 composition of the singlet ground state with CPCM(THF) (10e,9o Active Space) – 25 triplet roots, 15 singlet roots. Active Space Orbitals (in order for CI vector notation below): d(yz), d(xy), d(xz), d(z^2), d(x^2-y^2)/C(sp^2), d(x^2-y^2)/C(sp^2)*, π*(1), π*(2), π*(3).

CI vector	Transition	Contribution
222220000	Closed-shell singlet (CSS) d^8	0.2955
221220100	d(xz) → π*(1)	0.1953
122220001	d(yz) → π*(3)	0.1251
122220100	d(yz) → π*(1)	0.0941
222211000	d(x^2-y^2)/C(sp^2) → d(x^2-y^2)/C(sp^2)*	0.0595
221220010	d(xz) → π*(2)	0.0297
222121000	d(z^2) → d(x^2-y^2)/C(sp^2)*	0.0225
222120100	d(z^2) → π*(1)	0.0224
122202001	2x[d(x^2-y^2)/C(sp^2)] + d(yz) → 2x[d(x^2-y^2)/C(sp^2)*] + π*(3)	0.0139
221112100	d(x^2-y^2)/C(sp^2) + d(xz) + d(z^2) → 2x[d(x^2-y^2)/C(sp^2)*] + π*(1)	0.0137
221202100	2x[d(x^2-y^2)/C(sp^2)] + d(xz) → 2x[d(x^2-y^2)/C(sp^2)*] + π*(1)	0.0122
122211001	d(yz) + d(x^2-y^2)/C(sp^2) → d(x^2-y^2)/C(sp^2)* + π*(3)	0.0100
Sum of CSS		**30 %**
Sum of all MLCT		**47 %**
Sum of all d-d		**8 %**
Sum of mixed MLCT + d-d		**5 %**

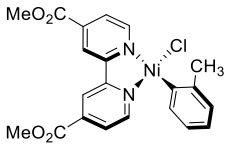

1D with Ni–C distance of 3.50 Å (dissociation limit) – CASSCF/NEVPT2 composition of the singlet ground state with CPCM(THF) (10e,9o Active Space) – 25 triplet roots, 15 singlet roots. Active Space Orbitals (in order for CI vector notation below): d(xy), d(yz), d(xz), d(z²), d(x²-y²)/C(sp²), d(x²-y²)/C(sp²)*, π*(1), π*(2), π*(3).

CI vector	Transition	Contribution
221211100	d(xz) + d(x²-y²)/C(sp²) → d(x²-y²)/C(sp²)* + π*(1)	0.7473
222211000	d(x²-y²)/C(sp²) → d(x²-y²)/C(sp²)*	0.0447
212121100	d(yz) + d(z²) → d(x²-y²)/C(sp²)* + π*(1)	0.0422
221220100	d(xz) → π*(1)	0.0404
212211100	d(yz) + d(x²-y²)/C(sp²) → d(x²-y²)/C(sp²)* + π*(1)	0.0353
112221100	d(xy) + d(yz) → d(x²-y²)/C(sp²)* + π*(1)	0.0289
221202100	2x[d(x²-y²)/C(sp²)] + d(xz) → 2x[d(x²-y²)/C(sp²)*] + π*(1)	0.0222
221121100	d(xz) + d(z²) → d(x²-y²)/C(sp²)* + π*(1)	0.0163
Sum of CSS		**0 %**
Sum of all MLCT		**4 %**
Sum of all d-d		**4 %**
Sum of mixed MLCT + d-d		**89 %**

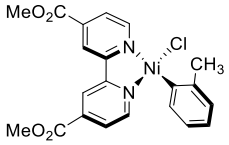

1D with Ni–C distance of 3.50 Å (dissociation limit) – CASSCF/QD-NEVPT2 composition of the singlet ground state with CPCM(THF) (10e,9o Active Space) – 25 triplet roots, 15 singlet roots. Active Space Orbitals (in order for CI vector notation below): d(xy), d(yz), d(xz), d(z²), d(x²-y²)/C(sp²), d(x²-y²)/C(sp²)*, π*(1), π*(2), π*(3).

CI vector	Transition	Contribution
221211100	d(xz) + d(x²-y²)/C(sp²) → d(x²-y²)/C(sp²)* + π*(1)	0.6937
222211000	d(x²-y²)/C(sp²) → d(x²-y²)/C(sp²)*	0.0621
221220100	d(xz) → π*(1)	0.0400
212121100	d(yz) + d(z²) → d(x²-y²)/C(sp²)* + π*(1)	0.0383
212211010	d(yz) + d(x²-y²)/C(sp²) → d(x²-y²)/C(sp²)* + π*(2)	0.0314
221211001	d(xz) + d(x²-y²)/C(sp²) → d(x²-y²)/C(sp²)* + π*(3)	0.0266
112221100	d(xy) + d(yz) → d(x²-y²)/C(sp²)* + π*(1)	0.0229
221202100	2x[d(x²-y²)/C(sp²)] + d(xz) → 2x[d(x²-y²)/C(sp²)*] + π*(1)	0.0218
212211100	d(yz) + d(x²-y²)/C(sp²) → d(x²-y²)/C(sp²)* + π*(1)	0.0154
212211001	d(yz) + d(x²-y²)/C(sp²) → d(x²-y²)/C(sp²)* + π*(3)	0.0136
221121100	d(xz) + d(z²) → d(x²-y²)/C(sp²)* + π*(1)	0.0103
Sum of CSS		**0 %**
Sum of all MLCT		**4 %**
Sum of all d-d		**6 %**
Sum of mixed MLCT + d-d		**87 %**

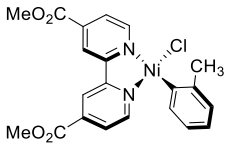

1D – CASSCF/NEVPT2 spin-orbit corrected absorption transitions for the CPCM(THF) phase spectrum (10e,9o Active Space) – 25 triplet roots, 15 singlet roots.

***E*/nm**	***E*/kcal mol^{-1}**	f_{osc}	***E*/nm**	***E*/kcal mol^{-1}**	f_{osc}
779.3	36.7	0.0034686	444.6	64.3	0.0000021
776.8	36.8	0.0000009	429.4	66.6	0.0003160
762.0	37.5	0.0026391	429.0	66.6	0.0000025
733.1	39.0	0.0002951	428.9	66.7	0.0005347
732.8	39.0	0.0001765	426.3	67.1	0.0002466
732.7	39.0	0.0000699	425.9	67.1	0.0006335
732.6	39.0	0.0000716	423.5	67.5	0.0001846
724.1	39.5	0.0078199	422.0	67.7	0.0005327
709.7	40.3	0.0209191	421.5	67.8	0.0000816
707.9	40.4	0.0346133	418.0	68.4	0.0012669
703.7	40.6	0.0000962	412.8	69.3	0.0000186
700.9	40.8	0.0000301	410.4	69.7	0.0006448
694.4	41.2	0.0014733	408.6	70.0	0.0000156
691.7	41.3	0.0000215	399.4	71.6	0.0000207
680.3	42.0	0.0216781	398.0	71.8	0.0003211
661.2	43.2	0.0817267	396.4	72.1	0.0000096
649.6	44.0	0.0801269	380.9	75.1	0.0006906
580.5	49.3	0.0007728	380.7	75.1	0.0003543
579.9	49.3	0.0002952	380.2	75.2	0.0012778
579.5	49.3	0.0000062	370.4	77.2	0.0002712
551.9	51.8	0.0000122	368.4	77.6	0.0006926
551.9	51.8	0.0000543	357.3	80.0	0.0000411
541.5	52.8	0.0006074	356.7	80.1	0.0000425
534.1	53.5	0.0005288	356.4	80.2	0.0000445
531.6	53.8	0.0000467	324.7	88.1	0.0000296
531.5	53.8	0.0000135	324.4	88.1	0.0000002
518.8	55.1	0.0003635	322.7	88.6	0.0000162
516.3	55.4	0.0000097	316.5	90.3	0.0000036
516.0	55.4	0.0000720	309.0	92.5	0.0001581
457.8	62.5	0.0000029	308.1	92.8	0.0000007
457.2	62.5	0.0002359	307.5	93.0	0.0000018
455.7	62.7	0.0002385	305.5	93.6	0.0008940

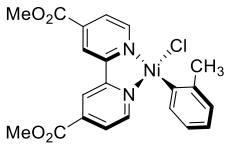

1D – CASSCF/QD-NEVPT2 spin-orbit corrected absorption transitions for the CPCM(THF) phase spectrum (10e,9o Active Space) – 25 triplet roots, 15 singlet roots.

***E*/nm**	***E*/kcal mol^{-1}**	f_{osc}	***E*/nm**	***E*/kcal mol^{-1}**	f_{osc}
706.5	40.5	0.0000567	485.2	58.9	0.0015741
625.8	45.7	0.0165492	457.2	62.5	0.0006183
620.2	46.1	0.0010650	457.1	62.5	0.0000589
619.9	46.1	0.0000398	457.1	62.6	0.0041246
615.0	46.5	0.0002970	397.4	71.9	0.0007074
593.3	48.2	0.1226378	394.0	72.6	0.0008267
590.5	48.4	0.0000965	393.9	72.6	0.0000051
590.4	48.4	0.0000090	393.9	72.6	0.0000063
590.2	48.4	0.0000096	348.9	82.0	0.0000589
572.9	49.9	0.0017640	348.6	82.0	0.0000295
571.6	50.0	0.0000158	346.2	82.6	0.0000130
571.5	50.0	0.0003246	340.4	84.0	0.0000142
569.8	50.2	0.0992976	337.6	84.7	0.0000091
566.7	50.5	0.0107312	337.4	84.7	0.0000217
565.6	50.5	0.0070692	334.0	85.6	0.0012096
565.4	50.6	0.0010411	333.8	85.6	0.0002021
551.5	51.8	0.0048365	333.4	85.8	0.0002679
527.7	54.2	0.0110551	332.1	86.1	0.0000177
527.6	54.2	0.0023156	331.1	86.4	0.0000434
527.2	54.2	0.0201183	325.0	88.0	0.0000149
525.1	54.5	0.0043555	324.2	88.2	0.0000494
511.4	55.9	0.0000723	323.9	88.3	0.0000260
510.7	56.0	0.0004219	314.9	90.8	0.0011092
509.8	56.1	0.0034986	313.4	91.2	0.0000026
491.2	58.2	0.2083714	311.8	91.7	0.0000378
485.3	58.9	0.0015191	304.4	93.9	0.0002759
485.2	58.9	0.0020957	303.6	94.2	0.0000455

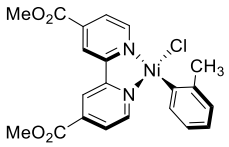

1D – TD-DFT (B3LYP) absorption transitions (singlets only) for the CPCM(THF) phase spectrum.

***E*/nm**	***E*/kcal mol^{-1}**	f_{osc}	***E*/nm**	***E*/kcal mol^{-1}**	f_{osc}
799.6	35.8	0.0000000	420.2	68.0	0.0000000
762.6	37.5	0.0005842	414.8	68.9	0.0039215
735.6	38.9	0.0000000	413.9	69.1	0.0000000
729.4	39.2	0.0000000	412.0	69.4	0.0000801
667.1	42.9	0.0000000	404.3	70.7	0.0000000
656.3	43.6	0.0012606	402.6	71.0	0.0000000
596.3	47.9	0.0231600	394.8	72.4	0.0000304
583.3	49.0	0.0000000	391.9	72.9	0.0891486
578.5	49.4	0.0000000	391.1	73.1	0.0098014
557.6	51.3	0.0000000	388.0	73.7	0.0000000
554.7	51.5	0.0000000	385.8	74.1	0.0000000
549.1	52.1	0.0016902	375.5	76.1	0.0004797
519.7	55.0	0.0000000	361.7	79.1	0.0000000
503.1	56.8	0.0000000	352.6	81.1	0.0000000
502.2	56.9	0.0006492	348.3	82.1	0.0286645
493.4	57.9	0.0000384	348.0	82.2	0.0000000
485.6	58.9	0.0005823	337.0	84.8	0.0000000
474.5	60.3	0.0462504	334.7	85.4	0.0000000
473.8	60.3	0.0001103	330.4	86.5	0.0000000
472.7	60.5	0.0024552	329.4	86.8	0.0000000
454.9	62.9	0.0274735	328.5	87.0	0.0193181
454.0	63.0	0.0000000	326.4	87.6	0.0000000
453.5	63.0	0.0000295	324.3	88.2	0.0000000
448.8	63.7	0.0000000	318.4	89.8	0.0000000
448.2	63.8	0.0002354	311.1	91.9	0.3176534
448.0	63.8	0.0005233	311.0	91.9	0.0000000
446.7	64.0	0.0658083	310.0	92.2	0.0000000
440.6	64.9	0.0000844	306.1	93.4	0.0000397
433.0	66.0	0.0000000	303.4	94.2	0.0066809
425.5	67.2	0.0000000			

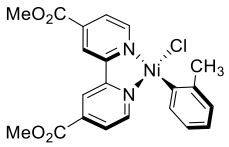

1D – TD-DFT (B3LYP) absorption transitions (singlets only) for the CPCM(Toluene) phase spectrum.

***E*/nm**	***E*/kcal mol^{-1}**	f_{osc}	***E*/nm**	***E*/kcal mol^{-1}**	f_{osc}
791.2	36.1	0.0000000	432.6	66.1	0.0000635
770.3	37.1	0.0042634	427.5	66.9	0.0001879
767.8	37.2	0.0000000	426.6	67.0	0.0000000
736.1	38.8	0.0000000	426.6	67.0	0.0000000
701.5	40.8	0.0000000	423.9	67.5	0.0000726
676.4	42.3	0.0220306	420.1	68.1	0.0820356
665.6	43.0	0.0000000	411.2	69.5	0.0000000
640.5	44.6	0.0000000	392.7	72.8	0.0000000
627.2	45.6	0.0000213	390.5	73.2	0.0259368
617.0	46.3	0.0047542	384.2	74.4	0.0129249
581.3	49.2	0.0000000	383.2	74.6	0.0000000
578.5	49.4	0.0000000	381.5	74.9	0.0000000
575.0	49.7	0.0000000	380.8	75.1	0.0000000
572.9	49.9	0.0001907	339.0	84.3	0.0000000
547.2	52.3	0.0000338	336.6	85.0	0.0000000
542.0	52.7	0.0000000	332.1	86.1	0.0035968
541.4	52.8	0.0536190	330.7	86.4	0.0000532
511.8	55.9	0.0001293	324.6	88.1	0.0000000
507.5	56.3	0.0000000	324.1	88.2	0.0000000
500.6	57.1	0.0000000	323.7	88.3	0.0000000
499.6	57.2	0.0000000	319.5	89.5	0.0000000
498.4	57.4	0.0000244	319.1	89.6	0.0001933
487.2	58.7	0.0732367	315.9	90.5	0.0000544
480.6	59.5	0.0034132	314.9	90.8	0.0001303
472.3	60.5	0.0042310	311.7	91.7	0.0005891
471.9	60.6	0.0029585	311.7	91.7	0.0000000
471.2	60.7	0.0000000	311.3	91.8	0.3140109
466.1	61.3	0.0000153	310.8	92.0	0.0115011
464.8	61.5	0.0095820	309.4	92.4	0.0000000
460.9	62.0	0.0000000	308.1	92.8	0.0000000
447.5	63.9	0.0008162	306.3	93.4	0.0020859
447.1	63.9	0.0054379	304.7	93.8	0.0000000
435.3	65.7	0.0000000			

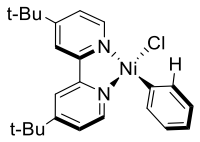

2B with Ni–C distance of 1.90 Å (near-equilibrium geometry) – CASSCF/NEVPT2 lowest transition energies with CPCM(THF) (10e,9o Active Space) – 25 triplet roots, 15 singlet roots. Active Space Orbitals (in order for CI vector notation below): $d(x^2\text{-}y^2)/C(sp^2)$, d(xy), d(yz), $d(z^2)$, d(xz), $d(x^2\text{-}y^2)/C(sp^2)^*$, π*(1), π*(2), π*(3).

State	Root	Multiplicity	ΔE/nm	ΔE/kcal mol^{-1}	CI vector	Contribution
0	0	1	---	---	222220000	0.5456
					222210100	0.1816
					122221000	0.1180
1	0	3	1038.1	27.5	222121000	0.7778
					122122000	0.1624
2	1	3	901.0	31.7	222211000	0.5782
					221221000	0.2126
					122212000	0.1228
3	2	3	829.3	34.5	221221000	0.5557
					222211000	0.2208
4	3	3	703.0	40.7	222120100	0.8153
5	1	1	686.6	41.6	222120100	0.8134
6	4	3	652.2	43.8	222210100	0.7582
7	5	3	628.7	45.5	212221000	0.6416
					221212000	0.1353
8	2	1	613.0	46.6	222210100	0.4067
					221220100	0.3413
9	6	3	560.3	51.0	221220100	0.7955
10	3	1	550.8	51.9	221220100	0.4150
					222210100	0.2080
11	4	1	460.3	62.1	212220100	0.5162
					221221000	0.1613
					221211100	0.1035
12	5	1	458.4	62.4	222121000	0.3888
					222120010	0.2962
13	6	1	451.8	63.3	222120010	0.5104
					222121000	0.2251
14	7	1	450.3	63.5	222211000	0.6982
15	8	1	442.4	64.6	212221000	0.6543
16	7	3	431.6	66.2	212220100	0.7396
17	8	3	425.9	67.1	222210010	0.8183
18	9	1	420.6	68.0	221221000	0.5735
					212220100	0.2093
19	9	3	413.6	69.1	222120010	0.6587
					211222000	0.1430
20	10	1	410.3	69.7	222210010	0.6243

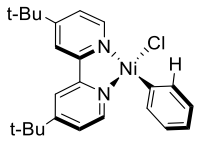

2B with Ni–C distance of 1.90 Å (near-equilibrium geometry) – CASSCF/QD-NEVPT2 lowest transition energies with CPCM(THF) (10e,9o Active Space) – 25 triplet roots, 15 singlet roots. Active Space Orbitals (in order for CI vector notation below): d(x^2-y^2)/C(sp^2), d(xy), d(yz), d(z^2), d(xz), d(x^2-y^2)/C(sp^2)*, π*(1), π*(2), π*(3).

State	Root	Multiplicity	ΔE/nm	ΔE/kcal mol^{-1}	CI vector	Contribution
0	0	1	---	---	222220000	0.5840
					122221000	0.1275
					222210100	0.1249
1	0	3	1025.9	27.9	222121000	0.7678
					122122000	0.1569
2	1	3	897.6	31.9	222211000	0.6015
					221221000	0.1813
					122212000	0.1264
3	2	3	821.2	34.8	221221000	0.5802
					222211000	0.1940
4	3	3	697.4	41.0	222120100	0.8085
5	1	1	681.1	42.0	222120100	0.8079
6	4	3	678.0	42.2	222210100	0.5725
					212221000	0.2309
7	5	3	628.9	45.5	212221000	0.5196
					222210100	0.2486
8	2	1	607.6	47.1	222210100	0.4974
					221220100	0.2488
9	6	3	553.8	51.6	221220100	0.7754
10	3	1	547.2	52.2	221220100	0.5007
					222210100	0.1516
11	4	1	475.1	60.2	222120010	0.7948
12	5	1	461.2	62.0	212220100	0.6845
					221211100	0.1008
13	7	3	455.8	62.7	222120010	0.7963
14	6	1	448.5	63.8	222211000	0.6837
15	7	1	446.9	64.0	222210010	0.3695
					222121000	0.1841
					212221000	0.1360
16	8	1	433.2	66.0	212221000	0.5154
					222121000	0.1800
17	8	3	429.1	66.6	212220100	0.7416
18	9	3	422.9	67.6	222210010	0.8139
19	9	1	413.1	69.2	221221000	0.7477
20	10	1	400.5	71.4	222121000	0.3498
					222210010	0.2407

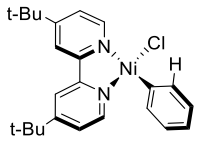

2B with Ni–C distance of 3.50 Å (dissociation limit) – CASSCF/NEVPT2 lowest transition energies with CPCM(THF) (10e,8o Active Space) – 25 triplet roots, 15 singlet roots. Active Space Orbitals (in order for CI vector notation below): d(xy), d(yz), d(z^2), d(xz), d(x^2-y^2)/C(sp^2), d(x^2-y^2)/C(sp^2)*, π*(1), π*(2).

State	Root	Multiplicity	ΔE/nm	ΔE/kcal mol^{-1}	CI vector	Contribution
0	0	1	---	---	22211110	0.7772
1	0	3	69140.1	0.4	22211110	0.7940
2	1	3	9978.8	2.9	22121110	0.8712
3	1	1	6981.8	4.1	22121110	0.9000
4	2	3	6451.0	4.4	22121110	0.9172
5	3	3	5163.0	5.5	22211110	0.8138
6	4	3	3842.7	7.4	21221110	0.8415
7	2	1	3540.6	8.1	21221110	0.8332
8	5	3	3358.9	8.5	21221110	0.8584
9	3	1	1436.7	19.9	21212110	0.4815
					12221110	0.4360
10	6	3	1423.4	20.1	21212110	0.4808
					12221110	0.4410
11	7	3	1310.9	21.8	12221110	0.4561
					21212110	0.4463
12	4	1	1229.4	23.3	22211101	0.7843
13	8	3	1218.1	23.5	22211101	0.8060
14	9	3	1195.0	23.9	22121101	0.8874
15	5	1	1188.3	24.1	22121101	0.8603
16	10	3	1167.5	24.5	22121101	0.8885
17	6	1	1155.8	24.7	22220110	0.7980
18	11	3	1138.5	25.1	22220110	0.8318
19	12	3	1099.3	26.0	22211101	0.8464
20	13	3	1023.5	27.9	12212110	0.7826
					21122110	0.1030

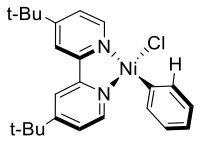

2B with Ni–C distance of 3.50 Å (dissociation limit) – CASSCF/QD-NEVPT2 lowest transition energies with CPCM(THF) (10e,8o Active Space) – 25 triplet roots, 15 singlet roots. Active Space Orbitals (in order for CI vector notation below): d(xy), d(yz), d(z^2), d(xz), d(x^2-y^2)/C(sp^2), d(x^2-y^2)/C(sp^2)*, π*(1), π*(2).

State	Root	Multiplicity	ΔE/nm	ΔE/kcal mol^{-1}	CI vector	Contribution
0	0	1	---	---	22211110	0.7413
1	0	3	66445.2	0.4	22211110	0.7695
2	1	3	8477.4	3.4	22121110	0.8735
3	1	1	6262.1	4.6	22121110	0.8969
4	2	3	5834.6	4.9	22121110	0.9129
5	3	3	4760.8	6.0	22211110	0.8247
6	4	3	3616.0	7.9	21221110	0.8550
7	2	1	3349.9	8.5	21221110	0.8256
8	5	3	3187.5	9.0	21221110	0.8522
9	3	1	1405.7	20.3	21212110	0.4868
					12221110	0.4303
10	6	3	1392.7	20.5	21212110	0.4869
					12221110	0.4345
11	7	3	1285.0	22.3	12221110	0.4548
					21212110	0.4535
12	4	1	1201.6	23.8	22211101	0.7249
13	8	3	1190.2	24.0	22211101	0.7475
14	9	3	1170.2	24.4	22121101	0.8462
15	5	1	1158.2	24.7	22121101	0.8168
16	10	3	1139.5	25.1	22121101	0.8717
17	6	1	1131.4	25.3	22220110	0.7379
18	11	3	1116.7	25.6	22220110	0.8015
19	12	3	1079.4	26.5	22211101	0.8423
20	7	1	1026.4	27.9	12212110	0.5926
					21221101	0.1969

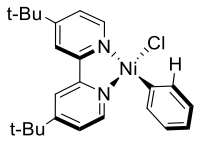

2B with Ni–C distance of 1.90 Å (near-equilibrium geometry) – CASSCF/NEVPT2 composition of the singlet ground state with CPCM(THF) (10e,9o Active Space) – 25 triplet roots, 15 singlet roots. Active Space Orbitals (in order for CI vector notation below): $d(x^2\text{-}y^2)/C(sp^2)$, d(xy), d(yz), $d(z^2)$, d(xz), $d(x^2\text{-}y^2)/C(sp^2)^*$, π*(1), π*(2), π*(3).

CI vector	Transition	Contribution
222220000	Closed-shell singlet (CSS) d^8	0.5456
222210100	d(xz) → π*(1)	0.1816
122221000	$d(x^2\text{-}y^2)/C(sp^2)$ → $d(x^2\text{-}y^2)/C(sp^2)^*$	0.1180
221220100	d(yz) → π*(1)	0.0291
022212100	$2x[d(x^2\text{-}y^2)/C(sp^2)]$ + d(xz) → $2x[d(x^2\text{-}y^2)/C(sp^2)^*]$ + π*(1)	0.0242
222210010	d(xz) → π*(2)	0.0140
221220001	d(yz) → π*(3)	0.0123
222022000	$2x[d(z^2)]$ → $2x[d(x^2\text{-}y^2)/C(sp^2)^*]$	0.0106
Sum of CSS		**55 %**
Sum of all MLCT		**24 %**
Sum of all d-d		**13 %**
Sum of mixed MLCT + d-d		**2 %**

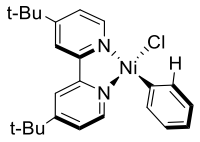

2B with Ni–C distance of 1.90 Å (near-equilibrium geometry) – CASSCF/QD-NEVPT2 composition of the singlet ground state with CPCM(THF) (10e,9o Active Space) – 25 triplet roots, 15 singlet roots. Active Space Orbitals (in order for CI vector notation below): $d(x^2\text{-}y^2)/C(sp^2)$, d(xy), d(yz), $d(z^2)$, d(xz), $d(x^2\text{-}y^2)/C(sp^2)^*$, π*(1), π*(2), π*(3).

CI vector	Transition	Contribution
222220000	Closed-shell singlet (CSS) d^8	0.5840
122221000	$d(x^2\text{-}y^2)/C(sp^2)$ → $d(x^2\text{-}y^2)/C(sp^2)^*$	0.1275
222210100	d(xz) → π*(1)	0.1249
221220100	d(yz) → π*(1)	0.0242
222210010	d(xz) → π*(2)	0.0220
022212100	$2x[d(x^2\text{-}y^2)/C(sp^2)]$ + d(xz) → $2x[d(x^2\text{-}y^2)/C(sp^2)^*]$ + π*(1)	0.0170
222121000	$d(z^2)$ → $d(x^2\text{-}y^2)/C(sp^2)^*$	0.0165
221220001	d(yz) → π*(3)	0.0141
222022000	$2x[d(z^2)]$ → $2x[d(x^2\text{-}y^2)/C(sp^2)^*]$	0.0110
Sum of CSS		**58 %**
Sum of all MLCT		**19 %**
Sum of all d-d		**16 %**
Sum of mixed MLCT + d-d		**2 %**

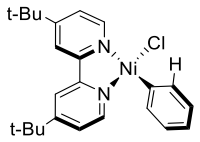

2B with Ni–C distance of 3.50 Å (dissociation limit) – CASSCF/NEVPT2 composition of the singlet ground state with CPCM(THF) (10e,8o Active Space) – 25 triplet roots, 15 singlet roots. Active Space Orbitals (in order for CI vector notation below): d(xy), d(yz), d(z²), d(xz), d(x²-y²)/C(sp²), d(x²-y²)/C(sp²)*, π*(1), π*(2).

CI vector	Transition	Contribution
22211110	d(xz) + d(x²-y²)/C(sp²) → d(x²-y²)/C(sp²)* + π*(1)	0.7772
22112110	d(z²) + d(xz) → d(x²-y²)/C(sp²)* + π*(1)	0.0471
22221100	d(x²-y²)/C(sp²) → d(x²-y²)/C(sp²)*	0.0410
21221110	d(yz) + d(x²-y²)/C(sp²) → d(x²-y²)/C(sp²)* + π*(1)	0.0407
11222110	d(xy) + d(yz) → d(x²-y²)/C(sp²)* + π*(1)	0.0386
22212010	d(xz) → π*(1)	0.0189
Sum of CSS		**0 %**
Sum of all MLCT		**2 %**
Sum of all d-d		**4 %**
Sum of mixed MLCT + d-d		**90 %**

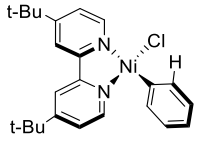

2B with Ni–C distance of 3.50 Å (dissociation limit) – CASSCF/QD-NEVPT2 composition of the singlet ground state with CPCM(THF) (10e,8o Active Space) – 25 triplet roots, 15 singlet roots. Active Space Orbitals (in order for CI vector notation below): d(xy), d(yz), d(z²), d(xz), d(x²-y²)/C(sp²), d(x²-y²)/C(sp²)*, π*(1), π*(2).

CI vector	Transition	Contribution
22211110	d(xz) + d(x²-y²)/C(sp²) → d(x²-y²)/C(sp²)* + π*(1)	0.74133
22221100	d(x²-y²)/C(sp²) → d(x²-y²)/C(sp²)*	0.04960
22112110	d(z²) + d(xz) → d(x²-y²)/C(sp²)* + π*(1)	0.04593
21221110	d(yz) + d(x²-y²)/C(sp²) → d(x²-y²)/C(sp²)* + π*(1)	0.04405
11222110	d(xy) + d(yz) → d(x²-y²)/C(sp²)* + π*(1)	0.03338
22211101	d(xz) + d(x²-y²)/C(sp²) → d(x²-y²)/C(sp²)* + π*(2)	0.02664
22212010	d(xz) → π*(1)	0.01909
Sum of CSS		**0 %**
Sum of all MLCT		**2 %**
Sum of all d-d		**5 %**
Sum of mixed MLCT + d-d		**89 %**

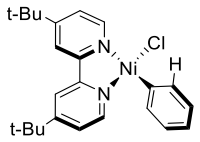

2B – CASSCF/NEVPT2 spin-orbit corrected absorption transitions for the CPCM(THF) phase spectrum (10e,9o Active Space) – 25 triplet roots, 15 singlet roots.

***E*/nm**	***E*/kcal mol^{-1}**	f_{osc}	***E*/nm**	***E*/kcal mol^{-1}**	f_{osc}
799.5	35.8	0.0000553	410.1	69.7	0.0002082
713.6	40.1	0.0001600	409.4	69.8	0.0000677
713.2	40.1	0.0000000	405.8	70.5	0.0756448
706.8	40.5	0.0054254	378.0	75.6	0.0112399
699.6	40.9	0.0008986	377.9	75.7	0.0047785
647.9	44.1	0.0050859	377.4	75.8	0.0001328
645.4	44.3	0.0000003	377.1	75.8	0.0041179
643.6	44.4	0.0001685	375.7	76.1	0.0019773
626.4	45.6	0.0159925	375.1	76.2	0.0218253
625.4	45.7	0.0000193	372.7	76.7	0.0000044
625.1	45.7	0.0000001	372.6	76.7	0.0004174
605.1	47.3	0.0735360	355.1	80.5	0.0787551
557.7	51.3	0.0369130	333.0	85.9	0.0000210
554.0	51.6	0.0000008	332.8	85.9	0.0000045
553.6	51.7	0.0000444	330.7	86.4	0.0000115
541.9	52.8	0.2333280	326.3	87.6	0.0001015
459.5	62.2	0.0053875	326.2	87.7	0.0000833
458.4	62.4	0.0001951	325.9	87.7	0.0000372
452.8	63.1	0.0076765	324.2	88.2	0.0000000
449.1	63.7	0.0001221	322.6	88.6	0.0000167
441.7	64.7	0.0044719	318.3	89.8	0.0001216
430.1	66.5	0.0000058	316.7	90.3	0.0000426
430.1	66.5	0.0000326	316.6	90.3	0.0000005
429.7	66.5	0.0000012	316.6	90.3	0.0000321
429.6	66.5	0.0006666	316.6	90.3	0.0001643
429.4	66.6	0.0002837	313.0	91.4	0.0000035
423.2	67.6	0.0000395	308.4	92.7	0.0000013
421.1	67.9	0.0040174	307.6	93.0	0.0000026
419.2	68.2	0.0441516			

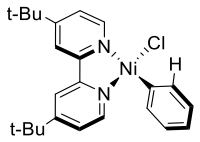

2B – CASSCF/QD-NEVPT2 spin-orbit corrected absorption transitions for the CPCM(THF) phase spectrum (10e,9o Active Space) – 25 triplet roots, 15 singlet roots.

***E*/nm**	***E*/kcal mol^{-1}**	f_{osc}	***E*/nm**	***E*/kcal mol^{-1}**	f_{osc}
794.3	36.0	0.0000385	420.1	68.1	0.0003888
712.1	40.2	0.0001757	411.9	69.4	0.0006827
712.1	40.2	0.0000045	400.0	71.5	0.1292814
702.1	40.7	0.0033452	378.4	75.6	0.0020776
700.9	40.8	0.0024356	378.4	75.6	0.0000884
666.1	42.9	0.0000562	378.3	75.6	0.0034397
665.9	42.9	0.0021472	375.9	76.1	0.0014447
661.6	43.2	0.0003926	375.4	76.2	0.0011323
624.9	45.8	0.0000488	375.2	76.2	0.0048228
624.6	45.8	0.0069733	375.0	76.2	0.0009868
624.2	45.8	0.0000515	372.0	76.9	0.0116913
602.1	47.5	0.0835467	353.3	80.9	0.0048063
551.1	51.9	0.0572286	353.3	80.9	0.0012139
548.2	52.2	0.0000305	353.2	80.9	0.0001900
547.7	52.2	0.0000486	348.3	82.1	0.0900471
539.4	53.0	0.2175792	323.2	88.5	0.0001679
476.9	60.0	0.0001619	322.7	88.6	0.0000071
460.5	62.1	0.0005656	319.4	89.5	0.0000010
458.8	62.3	0.0064505	317.1	90.2	0.0000393
458.6	62.3	0.0008539	316.8	90.2	0.0001101
458.5	62.4	0.0005151	316.7	90.3	0.0001944
447.0	64.0	0.0035433	315.1	90.7	0.0001556
442.2	64.7	0.0048121	311.5	91.8	0.0000973
431.9	66.2	0.0000294	309.7	92.3	0.0004006
427.1	66.9	0.0000128	306.7	93.2	0.0000328
427.1	67.0	0.0017963	303.0	94.4	0.0000351
426.8	67.0	0.0000862	301.9	94.7	0.0000044
421.1	67.9	0.0000096	300.2	95.2	0.0001988
420.6	68.0	0.0000103			

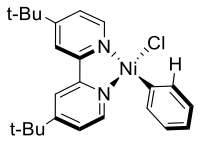

2B – TD-DFT (B3LYP) absorption transitions (singlets only) for the CPCM(THF) phase spectrum.

***E*/nm**	***E*/kcal mol^{-1}**	f_{osc}	***E*/nm**	***E*/kcal mol^{-1}**	f_{osc}
764.9	37.4	0.0000000	371.4	77.0	0.0000000
600.9	47.6	0.0000000	370.3	77.2	0.0003848
589.4	48.5	0.0000000	370.2	77.2	0.0000108
550.7	51.9	0.0000000	366.6	78.0	0.0136999
535.1	53.4	0.0007501	366.4	78.0	0.0000000
502.7	56.9	0.0072053	360.5	79.3	0.0000000
490.1	58.3	0.0000000	340.1	84.1	0.0014672
490.0	58.3	0.0001204	336.2	85.1	0.0209975
487.2	58.7	0.0011137	334.9	85.4	0.0000000
473.3	60.4	0.0245223	334.8	85.4	0.0000610
460.3	62.1	0.0000000	334.6	85.4	0.0000000
451.0	63.4	0.0000212	331.0	86.4	0.0001762
450.8	63.4	0.0001539	330.4	86.5	0.0128130
443.0	64.5	0.0000000	328.9	86.9	0.0000000
436.1	65.6	0.0001472	328.5	87.0	0.0000000
432.8	66.1	0.0000000	316.7	90.3	0.0520096
430.5	66.4	0.0628299	309.2	92.5	0.0000000
416.7	68.6	0.0000000	308.4	92.7	0.0000000
414.4	69.0	0.0002393	304.4	93.9	0.0000000
389.5	73.4	0.0000000	302.8	94.4	0.0000000
386.6	74.0	0.0092081	302.1	94.6	0.0007255
379.4	75.4	0.0000000			

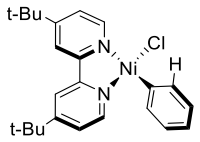

2B – TD-DFT (B3LYP) absorption transitions (singlets only) for the CPCM(Toluene) phase spectrum.

***E*/nm**	***E*/kcal mol^{-1}**	f_{osc}	***E*/nm**	***E*/kcal mol^{-1}**	f_{osc}
747.5	38.3	0.0000000	404.9	70.6	0.0231058
695.9	41.1	0.0000000	385.2	74.2	0.0000000
670.3	42.7	0.0006102	383.5	74.5	0.0000704
643.6	44.4	0.0000000	382.3	74.8	0.0000000
588.9	48.6	0.0000000	381.9	74.9	0.0000000
570.8	50.1	0.0000000	378.4	75.6	0.0015694
544.1	52.6	0.0004860	371.6	76.9	0.0000000
529.1	54.0	0.0176466	370.8	77.1	0.0092365
528.7	54.1	0.0000000	367.3	77.8	0.0000000
515.9	55.4	0.0000000	365.0	78.3	0.0249818
496.1	57.6	0.0000000	363.7	78.6	0.0000000
494.2	57.9	0.0006866	358.7	79.7	0.0001205
484.2	59.0	0.0000218	351.3	81.4	0.0005934
474.1	60.3	0.0089933	350.4	81.6	0.0509278
472.7	60.5	0.0027699	342.2	83.6	0.0000000
471.2	60.7	0.0582278	338.1	84.6	0.0000000
466.3	61.3	0.0000000	337.0	84.8	0.0009801
463.3	61.7	0.0002079	333.0	85.9	0.0000000
450.5	63.5	0.0076628	332.9	85.9	0.0000000
449.8	63.6	0.0008759	325.4	87.9	0.0000000
429.3	66.6	0.0000000	322.7	88.6	0.0035716
419.8	68.1	0.0002479	315.7	90.6	0.0000000
415.8	68.8	0.0000000	307.7	92.9	0.0000000
407.8	70.1	0.0000000	306.3	93.3	0.0710369
406.4	70.4	0.0000111	304.8	93.8	0.0000000

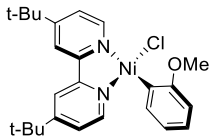

3B with Ni–C distance of 1.90 Å (near-equilibrium geometry) – CASSCF/NEVPT2 lowest transition energies with CPCM(THF) (10e,9o Active Space) – 25 triplet roots, 15 singlet roots. Active Space Orbitals (in order for CI vector notation below): d(x^2-y^2)/C(sp^2), d(xy), d(yz), d(z^2), d(xz), d(x^2-y^2)/C(sp^2)*, π*(1), π*(2), π*(3).

State	Root	Multiplicity	ΔE/nm	ΔE/kcal mol^{-1}	CI vector	Contribution
0	0	1	---	---	222220000	0.5786
					222210100	0.1373
					122221000	0.1302
1	0	3	1085.8	26.3	222121000	0.7866
					122122000	0.1613
2	1	3	932.7	30.7	222211000	0.5926
					221221000	0.1933
					122212000	0.1246
3	2	3	853.9	33.5	221221000	0.5720
					222211000	0.2039
4	3	3	680.4	42.0	222120100	0.8311
5	1	1	666.2	42.9	222120100	0.8278
6	4	3	641.0	44.6	212221000	0.6996
					221212000	0.1548
					112222000	0.1061
7	5	3	627.3	45.6	222210100	0.8298
8	2	1	595.2	48.0	222210100	0.4886
					221220100	0.2613
9	6	3	546.7	52.3	221220100	0.8022
10	3	1	527.9	54.2	221220100	0.4983
					222210100	0.1705
11	4	1	469.0	61.0	222121000	0.6396
12	5	1	468.4	61.0	212220100	0.3220
					221221000	0.2667
					222211000	0.1612
13	6	1	449.9	63.5	222211000	0.5975
					221221000	0.1960
14	7	1	447.1	63.9	212221000	0.7119
15	7	3	433.9	65.9	222120010	0.8234
16	8	1	432.3	66.1	222120010	0.8171
17	8	3	415.4	68.8	222210010	0.8223
18	9	1	414.1	69.0	212220100	0.3980
					221221000	0.3421
19	9	3	409.0	69.9	212220100	0.6609
20	10	1	399.6	71.6	222210010	0.7394

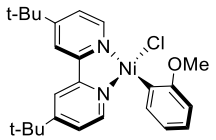

3B with Ni–C distance of 1.90 Å (near-equilibrium geometry) – CASSCF/QD-NEVPT2 lowest transition energies with CPCM(THF) (10e,9o Active Space) – 25 triplet roots, 15 singlet roots. Active Space Orbitals (in order for CI vector notation below): d(x^2-y^2)/C(sp^2), d(xy), d(yz), d(z^2), d(xz), d(x^2-y^2)/C(sp^2)*, π*(1), π*(2), π*(3).

State	Root	Multiplicity	ΔE/nm	ΔE/kcal mol^{-1}	CI vector	Contribution
0	0	1	---	---	222220000	0.5939
					122221000	0.1286
					222210100	0.1051
1	0	3	1078.3	26.5	222121000	0.7575
					122122000	0.1515
2	1	3	932.4	30.7	222211000	0.6055
					221221000	0.1573
					122212000	0.1249
3	2	3	847.1	33.8	221221000	0.5922
					222211000	0.1796
4	3	3	677.6	42.2	212221000	0.5341
					222120100	0.2426
5	4	3	674.8	42.4	222120100	0.5827
					212221000	0.2271
6	1	1	661.6	43.2	222120100	0.8239
7	5	3	622.7	45.9	222210100	0.8183
8	2	1	592.2	48.3	222210100	0.5286
					221220100	0.2271
9	6	3	541.3	52.8	221220100	0.7968
10	3	1	527.8	54.2	221220100	0.5247
					222210100	0.1483
11	4	1	474.0	60.3	212220100	0.5626
					221211100	0.1015
12	5	1	468.5	61.0	222121000	0.5290
					212221000	0.1799
13	6	1	450.4	63.5	222211000	0.6457
14	7	1	445.3	64.2	212221000	0.5940
					222121000	0.1154
15	7	3	434.4	65.8	212220100	0.7219
16	8	3	431.2	66.3	222120010	0.8016
17	8	1	429.4	66.6	222120010	0.7935
18	9	3	412.6	69.3	222210010	0.8196
19	9	1	404.3	70.7	221221000	0.5796
					212220100	0.1243
20	10	1	393.4	72.7	222210010	0.5087

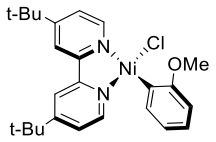

3B with Ni–C distance of 3.50 Å (dissociation limit) – CASSCF/NEVPT2 lowest transition energies with CPCM(THF) (10e,8o Active Space) – 25 triplet roots, 15 singlet roots. Active Space Orbitals (in order for CI vector notation below): d(xy), d(yz), d(z^2), d(xz), d(x^2-y^2)/C(sp^2), d(x^2-y^2)/C(sp^2)*, π*(1), π*(2).

State	Root	Multiplicity	ΔE/nm	ΔE/kcal mol^{-1}	CI vector	Contribution
0	0	1	---	---	22211110	0.6940
					22121110	0.1643
1	0	3	711917.0	0.0	22211110	0.7287
					22121110	0.1322
2	1	3	14938.8	1.9	22121110	0.9699
3	1	1	10484.0	2.7	22121110	0.8135
					22211110	0.1364
4	2	3	9875.0	2.9	22121110	0.8518
					22211110	0.1089
5	3	3	6497.9	4.4	22211110	0.9061
6	4	3	3953.1	7.2	21221110	0.8544
7	2	1	3891.3	7.3	21221110	0.8093
8	5	3	3829.5	7.5	21221110	0.8170
9	3	1	2710.0	10.6	22220110	0.8816
10	6	3	2692.1	10.6	22220110	0.8931
11	7	3	1373.0	20.8	22121101	0.9474
12	4	1	1266.1	22.6	22211101	0.8448
13	5	1	1259.1	22.7	22121101	0.9606
14	8	3	1250.4	22.9	22121101	0.9558
15	9	3	1244.5	23.0	22211101	0.7974
16	6	1	1240.0	23.1	12221110	0.5807
					21212110	0.3353
17	10	3	1236.9	23.1	12221110	0.5839
					21212110	0.3351
18	11	3	1198.9	23.8	12221110	0.6090
					21212110	0.3197
19	12	3	1127.6	25.4	22211101	0.8087
20	13	3	1013.9	28.2	21221101	0.8444

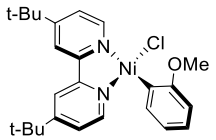

3B with Ni–C distance of 3.50 Å (dissociation limit) – CASSCF/QD-NEVPT2 lowest transition energies with CPCM(THF) (10e,8o Active Space) – 25 triplet roots, 15 singlet roots. Active Space Orbitals (in order for CI vector notation below): d(xy), d(yz), d(z^2), d(xz), d(x^2-y^2)/C(sp^2), d(x^2-y^2)/C(sp^2)*, π*(1), π*(2).

State	Root	Multiplicity	ΔE/nm	ΔE/kcal mol^{-1}	CI vector	Contribution
0	0	1	---	---	22211110	0.6759
1	0	3	16954.9	1.7	22211110	0.7599
2	1	3	7157.7	4.0	22121110	0.8827
3	1	1	5804.8	4.9	22121110	0.8794
4	2	3	4524.5	6.3	22121110	0.9784
5	3	3	4345.6	6.6	22211110	0.7949
6	4	3	3252.7	8.8	21221110	0.8209
7	2	1	3166.1	9.0	21221110	0.7710
8	5	3	2764.0	10.3	21221110	0.8667
9	3	1	1289.1	22.2	21212110	0.4410
					12221110	0.4144
10	6	3	1253.7	22.8	21212110	0.4640
					12221110	0.4522
11	7	3	1208.7	23.7	22220110	0.6853
12	4	1	1191.6	24.0	22211101	0.5548
					22220110	0.1447
13	5	1	1179.8	24.2	22220110	0.6356
					22211101	0.1454
14	8	3	1165.3	24.5	12221110	0.4108
					21212110	0.3831
					22220110	0.1134
15	9	3	1147.2	24.9	22121101	0.8612
16	6	1	1139.3	25.1	22121101	0.8488
17	10	3	1128.9	25.3	22211101	0.7524
18	11	3	1077.5	26.5	22121101	0.9425
19	12	3	1038.0	27.5	22211101	0.8061
20	7	1	962.8	29.7	21221101	0.7467

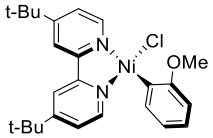

3B with Ni–C distance of 1.90 Å (near-equilibrium geometry) – CASSCF/NEVPT2 composition of the singlet ground state with CPCM(THF) (10e,9o Active Space) – 25 triplet roots, 15 singlet roots. Active Space Orbitals (in order for CI vector notation below): $d(x^2\text{-}y^2)/C(sp^2)$, d(xy), d(yz), $d(z^2)$, d(xz), $d(x^2\text{-}y^2)/C(sp^2)^*$, $\pi^*(1)$, $\pi^*(2)$, $\pi^*(3)$.

CI vector	Transition	Contribution
222220000	Closed-shell singlet (CSS) d^8	0.5786
222210100	$d(xz) \rightarrow \pi^*(1)$	0.1373
122221000	$d(x^2\text{-}y^2)/C(sp^2) \rightarrow d(x^2\text{-}y^2)/C(sp^2)^*$	0.1302
221220100	$d(yz) \rightarrow \pi^*(1)$	0.0290
022212100	$2x[d(x^2\text{-}y^2)/C(sp^2)] + d(xz) \rightarrow 2x[d(x^2\text{-}y^2)/C(sp^2)^*] + \pi^*(1)$	0.0185
222210010	$d(xz) \rightarrow \pi^*(2)$	0.0135
222022000	$2x[d(z^2)] \rightarrow 2x[d(x^2\text{-}y^2)/C(sp^2)^*]$	0.0125
221220001	$d(yz) \rightarrow \pi^*(3)$	0.0114
Sum of CSS		**58 %**
Sum of all MLCT		**19 %**
Sum of all d-d		**14 %**
Sum of mixed MLCT + d-d		**2 %**

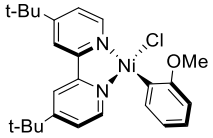

3B with Ni–C distance of 1.90 Å (near-equilibrium geometry) – CASSCF/QD-NEVPT2 composition of the singlet ground state with CPCM(THF) (10e,9o Active Space) – 25 triplet roots, 15 singlet roots. Active Space Orbitals (in order for CI vector notation below): $d(x^2\text{-}y^2)/C(sp^2)$, d(xy), d(yz), $d(z^2)$, d(xz), $d(x^2\text{-}y^2)/C(sp^2)^*$, $\pi^*(1)$, $\pi^*(2)$, $\pi^*(3)$.

CI vector	Transition	Contribution
222220000	Closed-shell singlet (CSS) d^8	0.5939
122221000	$d(x^2\text{-}y^2)/C(sp^2) \rightarrow d(x^2\text{-}y^2)/C(sp^2)^*$	0.1286
222210100	$d(xz) \rightarrow \pi^*(1)$	0.1051
221220100	$d(yz) \rightarrow \pi^*(1)$	0.0262
222210010	$d(xz) \rightarrow \pi^*(2)$	0.0212
222120001	$d(z^2) \rightarrow \pi^*(3)$	0.0188
022212100	$2x[d(x^2\text{-}y^2)/C(sp^2)] + d(xz) \rightarrow 2x[d(x^2\text{-}y^2)/C(sp^2)^*] + \pi^*(1)$	0.0143
222121000	$d(z^2) \rightarrow d(x^2\text{-}y^2)/C(sp^2)^*$	0.0134
221220001	$d(yz) \rightarrow \pi^*(3)$	0.0117
222022000	$2x[d(z^2)] \rightarrow 2x[d(x^2\text{-}y^2)/C(sp^2)^*]$	0.0116
Sum of CSS		**59 %**
Sum of all MLCT		**18 %**
Sum of all d-d		**15 %**
Sum of mixed MLCT + d-d		**1 %**

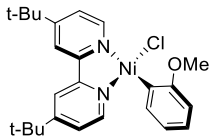

3B with Ni–C distance of 3.50 Å (dissociation limit) – CASSCF/NEVPT2 composition of the singlet ground state with CPCM(THF) (10e,8o Active Space) – 25 triplet roots, 15 singlet roots. Active Space Orbitals (in order for CI vector notation below): d(xy), d(yz), d(z²), d(xz), d(x²-y²)/C(sp²), d(x²-y²)/C(sp²)*, π*(1), π*(2).

CI vector	Transition	Contribution
22211110	d(xz) + d(x²-y²)/C(sp²) → d(x²-y²)/C(sp²)* + π*(1)	0.6940
22121110	d(x²-y²)/C(sp²) + d(z²) → d(x²-y²)/C(sp²)* + π*(1)	0.1643
21221110	d(yz) + d(x²-y²)/C(sp²) → d(x²-y²)/C(sp²)* + π*(1)	0.0344
22112110	d(z²) + d(xz) → d(x²-y²)/C(sp²)* + π*(1)	0.0339
22221100	d(x²-y²)/C(sp²) → d(x²-y²)/C(sp²)*	0.0329
11222110	d(xy) + d(yz) → d(x²-y²)/C(sp²)* + π*(1)	0.0174
Sum of CSS		**0 %**
Sum of all MLCT		**0 %**
Sum of all d-d		**3 %**
Sum of mixed MLCT + d-d		**94 %**

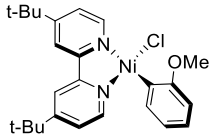

3B with Ni–C distance of 3.50 Å (dissociation limit) – CASSCF/QD-NEVPT2 composition of the singlet ground state with CPCM(THF) (10e,8o Active Space) – 25 triplet roots, 15 singlet roots. Active Space Orbitals (in order for CI vector notation below): d(xy), d(yz), d(z²), d(xz), d(x²-y²)/C(sp²), d(x²-y²)/C(sp²)*, π*(1), π*(2).

CI vector	Transition	Contribution
22211110	d(xz) + d(x²-y²)/C(sp²) → d(x²-y²)/C(sp²)* + π*(1)	0.6759
22212010	d(xz) → π*(1)	0.0606
22112110	d(z²) + d(xz) → d(x²-y²)/C(sp²)* + π*(1)	0.0556
22221100	d(x²-y²)/C(sp²) → d(x²-y²)/C(sp²)*	0.0488
21221110	d(yz) + d(x²-y²)/C(sp²) → d(x²-y²)/C(sp²)* + π*(1)	0.0413
22211101	d(xz) + d(x²-y²)/C(sp²) → d(x²-y²)/C(sp²)* + π*(2)	0.0289
22210210	2x[d(x²-y²)/C(sp²) + d(xz)] → 2x[d(x²-y²)/C(sp²)*] + π*(1)	0.0269
11222110	d(xy) + d(yz) → d(x²-y²)/C(sp²)* + π*(1)	0.0233
Sum of CSS		**0 %**
Sum of all MLCT		**6 %**
Sum of all d-d		**5 %**
Sum of mixed MLCT + d-d		**85 %**

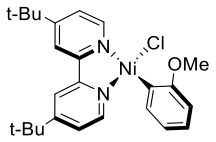

3B – CASSCF/NEVPT2 spin-orbit corrected absorption transitions for the CPCM(THF) phase spectrum (10e,9o Active Space) – 25 triplet roots, 15 singlet roots.

***E*/nm**	***E*/kcal mol^{-1}**	f_{osc}	***E*/nm**	***E*/kcal mol^{-1}**	f_{osc}
689.6	41.5	0.0002633	407.4	70.2	0.0003498
689.3	41.5	0.0000012	407.2	70.2	0.0002181
684.4	41.8	0.0046114	407.1	70.2	0.0000046
677.2	42.2	0.0026877	398.6	71.7	0.1196569
637.6	44.8	0.0000961	371.0	77.1	0.0000001
637.2	44.9	0.0026217	371.0	77.1	0.0000664
637.1	44.9	0.0025379	370.6	77.1	0.0050557
623.1	45.9	0.0017026	369.5	77.4	0.0050975
621.7	46.0	0.0000008	353.0	81.0	0.0069280
620.1	46.1	0.0002654	351.5	81.3	0.0001092
588.7	48.6	0.0863704	351.5	81.3	0.0000012
542.0	52.7	0.0062593	344.7	83.0	0.0590034
540.5	52.9	0.0000011	338.8	84.4	0.0000827
540.0	52.9	0.0000938	338.3	84.5	0.0000094
521.9	54.8	0.2340130	333.8	85.7	0.0002150
467.5	61.2	0.0039504	333.1	85.8	0.0000279
466.4	61.3	0.0000905	330.7	86.5	0.0019654
449.3	63.6	0.0003048	328.5	87.0	0.0600651
446.0	64.1	0.0003265	326.1	87.7	0.0000844
438.0	65.3	0.0000003	322.4	88.7	0.0004089
438.0	65.3	0.0000064	320.3	89.3	0.0001004
436.6	65.5	0.0021742	317.7	90.0	0.0000359
435.7	65.6	0.0073985	312.6	91.5	0.0006191
413.5	69.1	0.0000342	312.1	91.6	0.0000106
412.0	69.4	0.0000452	312.1	91.6	0.0000087
412.0	69.4	0.0000294	312.0	91.6	0.0002604
411.6	69.5	0.0002800			

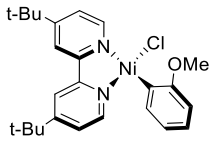

3B – CASSCF/QD-NEVPT2 spin-orbit corrected absorption transitions for the CPCM(THF) phase spectrum (10e,9o Active Space) – 25 triplet roots, 15 singlet roots.

***E*/nm**	***E*/kcal mol^{-1}**	f_{osc}	***E*/nm**	***E*/kcal mol^{-1}**	f_{osc}
684.8	41.8	0.0000756	409.1	69.9	0.0002117
684.7	41.8	0.0000609	403.1	70.9	0.0001532
681.0	42.0	0.0060365	392.8	72.8	0.1232790
674.2	42.4	0.0009035	368.9	77.5	0.0000156
672.0	42.5	0.0001606	368.9	77.5	0.0000702
669.7	42.7	0.0011916	368.7	77.6	0.0079337
668.0	42.8	0.0000276	366.8	78.0	0.0019092
618.4	46.2	0.0013148	350.2	81.7	0.0000599
617.2	46.3	0.0000051	350.2	81.7	0.0001282
615.7	46.4	0.0004056	349.5	81.8	0.0042934
587.1	48.7	0.0923034	341.0	83.8	0.0417531
537.0	53.2	0.0117632	334.5	85.5	0.0003180
535.4	53.4	0.0000026	333.6	85.7	0.0001221
534.8	53.5	0.0001810	331.5	86.2	0.0001862
521.9	54.8	0.2241353	329.7	86.7	0.0000114
471.2	60.7	0.0000953	329.7	86.7	0.0002678
467.1	61.2	0.0038936	328.6	87.0	0.0178893
449.1	63.7	0.0004997	322.8	88.6	0.0001349
444.9	64.3	0.0004266	320.6	89.2	0.0000358
435.2	65.7	0.0000020	319.6	89.5	0.0008111
435.1	65.7	0.0000274	317.9	89.9	0.0006066
433.4	66.0	0.0016452	314.1	91.0	0.0000128
432.4	66.1	0.0008911	312.9	91.4	0.0018466
432.2	66.2	0.0000064	312.3	91.6	0.0001073
432.1	66.2	0.0000865	311.3	91.8	0.0000976
431.1	66.3	0.0058660	310.7	92.0	0.0133577
409.7	69.8	0.0001399	309.5	92.4	0.0563392
409.2	69.9	0.0003481	309.3	92.4	0.0000230

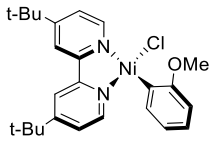

3B – TD-DFT (B3LYP) absorption transitions (singlets only) for the CPCM(THF) phase spectrum.

***E*/nm**	***E*/kcal mol^{-1}**	f_{osc}	***E*/nm**	***E*/kcal mol^{-1}**	f_{osc}
615.8	46.4	0.0000000	410.3	69.7	0.0002329
522.1	54.8	0.0044852	421.1	67.9	0.0000000
508.5	56.2	0.0003901	428.6	66.7	0.0003379
594.1	48.1	0.0000000	385.3	74.2	0.0000000
541.5	52.8	0.0005359	362.9	78.8	0.0219428
545.1	52.5	0.0000000	367.8	77.7	0.0000000
469.1	60.9	0.0000079	366.9	77.9	0.0000956
462.5	61.8	0.0002722	318.5	89.8	0.0000000
595.9	48.0	0.0000000	323.7	88.3	0.0000000
548.2	52.2	0.0002849	334.1	85.6	0.0186734
478.2	59.8	0.0268718	316.2	90.4	0.0000000
456.5	62.6	0.0000000	315.6	90.6	0.0000000
427.8	66.8	0.0628958	361.1	79.2	0.0000000
378.8	75.5	0.0000000	389.4	73.4	0.0020826
439.4	65.1	0.0000000	327.4	87.3	0.0090556
434.2	65.9	0.0002349	332.0	86.1	0.0171221
370.1	77.3	0.0000000	325.6	87.8	0.0000000
459.3	62.2	0.0000000	310.5	92.1	0.0000000
457.8	62.5	0.0007110	300.0	95.3	0.0000000
412.5	69.3	0.0000000	324.3	88.2	0.0001193

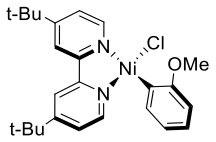

3B – TD-DFT (B3LYP) absorption transitions (singlets only) for the CPCM(Toluene) phase spectrum.

***E*/nm**	***E*/kcal mol^{-1}**	f_{osc}	***E*/nm**	***E*/kcal mol^{-1}**	f_{osc}
799.2	35.8	0.0000000	403.0	70.9	0.0000796
714.4	40.0	0.0000000	382.6	74.7	0.0000000
688.0	41.6	0.0000000	382.1	74.8	0.0000000
655.6	43.6	0.0007345	376.5	75.9	0.0000000
637.6	44.8	0.0000000	376.4	76.0	0.0045989
615.9	46.4	0.0000000	374.0	76.5	0.0000000
548.5	52.1	0.0011810	362.8	78.8	0.0000000
537.7	53.2	0.0091244	362.1	79.0	0.0114354
525.5	54.4	0.0000000	361.6	79.1	0.0266339
521.2	54.9	0.0008560	358.9	79.7	0.0000143
514.2	55.6	0.0008955	356.9	80.1	0.0005318
511.0	56.0	0.0000000	344.6	83.0	0.0000000
506.8	56.4	0.0007487	344.0	83.1	0.0087796
505.8	56.5	0.0000000	341.7	83.7	0.0000000
490.1	58.3	0.0002850	340.2	84.0	0.0006497
473.2	60.4	0.0035455	334.8	85.4	0.0088549
473.0	60.4	0.0126856	334.2	85.5	0.0000000
468.6	61.0	0.0575560	331.8	86.2	0.0000000
463.1	61.7	0.0079904	327.9	87.2	0.0000000
461.5	62.0	0.0000000	322.0	88.8	0.0385638
459.0	62.3	0.0000000	317.7	90.0	0.0000000
458.7	62.3	0.0002141	314.1	91.0	0.0000000
438.3	65.2	0.0037579	309.0	92.5	0.0731414
422.2	67.7	0.0000000	308.3	92.7	0.0000000
416.9	68.6	0.0000000	305.4	93.6	0.0000000
404.9	70.6	0.0247324	301.0	95.0	0.0000000
404.5	70.7	0.0000000			

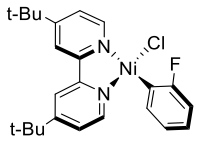

4B with Ni–C distance of 1.90 Å (near-equilibrium geometry) – CASSCF/NEVPT2 lowest transition energies with CPCM(THF) (10e,9o Active Space) – 25 triplet roots, 15 singlet roots. Active Space Orbitals (in order for CI vector notation below): d(x^2-y^2)/C(sp^2), d(yz), d(xz), d(xy), d(z^2), d(x^2-y^2)/C(sp^2)*, π*(1), π*(2), π*(3).

State	Root	Multiplicity	ΔE/nm	ΔE/kcal mol^{-1}	CI vector	Contribution
0	0	1	---	---	222220000	0.6681
					122221000	0.1705
1	0	3	1116.3	25.6	222211000	0.8372
					122212000	0.1524
2	1	3	961.9	29.7	221221000	0.5481
					222121000	0.2298
3	2	3	871.1	32.8	212221000	0.7256
					112222000	0.1259
4	3	3	769.5	37.2	222210100	0.8667
5	1	1	755.5	37.8	222210100	0.8678
6	4	3	708.3	40.4	221220100	0.4861
					212220100	0.2263
7	5	3	637.8	44.8	222121000	0.4359
					221221000	0.2210
8	6	3	615.0	46.5	212220100	0.5650
					222120100	0.1793
9	2	1	543.6	52.6	222211000	0.5503
					221220100	0.1870
10	3	1	530.1	53.9	212220100	0.5131
					222121000	0.1264
11	4	1	524.9	54.5	221220100	0.2776
					222211000	0.2340
12	5	1	483.6	59.1	222121000	0.3170
					212220100	0.2065
					221221000	0.1468
13	6	1	467.7	61.1	221221000	0.5198
					222121000	0.2854
14	7	3	467.4	61.2	222210010	0.8651
15	7	1	465.6	61.4	222210010	0.8646
16	8	3	458.2	62.4	222120100	0.4778
					221220100	0.2440
17	9	3	446.5	64.0	221220010	0.4939
					212220010	0.2037
					222120010	0.1396
18	8	1	445.7	64.1	222120100	0.4689
					221220100	0.2374
19	9	1	442.5	64.6	212221000	0.7404
20	10	1	426.4	67.1	221220010	0.4860
					212220010	0.1751
					222120010	0.1430

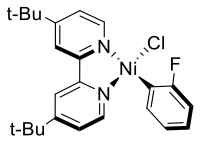

4B with Ni–C distance of 1.90 Å (near-equilibrium geometry) – CASSCF/QD-NEVPT2 lowest transition energies with CPCM(THF) (10e,9o Active Space) – 25 triplet roots, 15 singlet roots. Active Space Orbitals (in order for CI vector notation below): d(x^2-y^2)/C(sp^2), d(yz), d(xz), d(xy), d(z^2), d(x^2-y^2)/C(sp^2)*, π*(1), π*(2), π*(3).

State	Root	Multiplicity	ΔE/nm	ΔE/kcal mol^{-1}	CI vector	Contribution
0	0	1	---	---	222220000	0.5990
					122221000	0.1326
					212220100	0.1122
1	0	3	1049.6	27.2	222211000	0.8218
					122212000	0.1450
2	1	3	936.2	30.5	221221000	0.5441
					222121000	0.2579
3	2	3	839.8	34.0	212221000	0.7691
					112222000	0.1306
4	3	3	738.6	38.7	222210100	0.8651
5	1	1	720.9	39.7	222210100	0.8614
6	2	1	691.6	41.3	221220100	0.4837
					222120100	0.2840
7	4	3	677.6	42.2	221220100	0.4143
					212220100	0.1652
					222120100	0.1307
8	5	3	665.3	43.0	222121000	0.4108
					221221000	0.2059
9	6	3	591.2	48.4	212220100	0.5540
					222120100	0.1768
10	3	1	568.4	50.3	212220100	0.6203
11	4	1	489.7	58.4	222120100	0.2450
					221221000	0.1940
					222121000	0.1489
12	7	3	452.9	63.1	222210010	0.8342
13	5	1	450.7	63.4	222210010	0.8471
14	8	3	443.6	64.5	222120100	0.4643
					221220100	0.2504
15	6	1	437.8	65.3	222211000	0.5877
					221220010	0.1239
16	9	3	432.5	66.1	221220010	0.4654
					212220010	0.2300
					222120010	0.1337
17	7	1	432.4	66.1	212221000	0.5217
					221221000	0.2366
18	8	1	414.0	69.1	222121000	0.4230
					221221000	0.2357
19	9	1	398.5	71.7	221220010	0.2665
					222211000	0.1836
20	10	3	397.3	72.0	222210001	0.8399

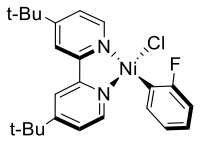

4B with Ni–C distance of 3.50 Å (dissociation limit) – CASSCF/NEVPT2 lowest transition energies with CPCM(THF) (10e,8o Active Space) – 25 triplet roots, 15 singlet roots. Active Space Orbitals (in order for CI vector notation below): d(xy), d(yz), d(z^2), d(xz), d(x^2-y^2)/C(sp^2), d(x^2-y^2)/C(sp^2)*, π*(1), π*(2).

State	Root	Multiplicity	ΔE/nm	ΔE/kcal mol^{-1}	CI vector	Contribution
0	0	1	---	---	22211110	0.7747
1	0	3	45427.0	0.6	22211110	0.8100
2	1	3	8534.1	3.4	22121110	0.9350
3	1	1	6562.5	4.4	22121110	0.9384
4	2	3	5835.5	4.9	22121110	0.9764
5	3	3	4915.1	5.8	22211110	0.8444
6	4	3	3587.1	8.0	21221110	0.8786
7	2	1	3428.9	8.3	21221110	0.8374
8	5	3	3204.4	8.9	21221110	0.8774
9	3	1	1356.0	21.1	21212110	0.4732
					12221110	0.4583
10	6	3	1339.8	21.3	21212110	0.4773
					12221110	0.4716
11	4	1	1237.7	23.1	22211101	0.7763
12	7	3	1231.9	23.2	12221110	0.4933
					21212110	0.4487
13	5	1	1228.9	23.3	22220110	0.8295
14	8	3	1226.5	23.3	22220110	0.8381
15	9	3	1218.3	23.5	22211101	0.8106
16	10	3	1186.1	24.1	22121101	0.9313
17	6	1	1174.7	24.3	22121101	0.9035
18	11	3	1154.9	24.8	22121101	0.9439
19	12	3	1100.3	26.0	22211101	0.8329
20	13	3	991.7	28.8	21221101	0.8682

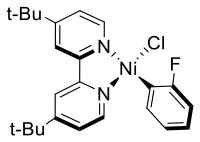

4B with Ni–C distance of 3.50 Å (dissociation limit) – CASSCF/QD-NEVPT2 lowest transition energies with CPCM(THF) (10e,8o Active Space) – 25 triplet roots, 15 singlet roots. Active Space Orbitals (in order for CI vector notation below): d(xy), d(yz), d(z^2), d(xz), d(x^2-y^2)/C(sp^2), d(x^2-y^2)/C(sp^2)*, π*(1), π*(2).

State	Root	Multiplicity	ΔE/nm	ΔE/kcal mol^{-1}	CI vector	Contribution
0	0	1	---	---	22211110	0.73235
1	0	3	41152.3	0.7	22211110	0.77291
2	1	3	7275.9	3.9	22121110	0.93354
3	1	1	5794.1	4.9	22121110	0.93771
4	2	3	5218.9	5.5	22121110	0.97586
5	3	3	4476.3	6.4	22211110	0.83912
6	4	3	3344.9	8.5	21221110	0.87400
7	2	1	3213.2	8.9	21221110	0.82626
8	5	3	3013.8	9.5	21221110	0.86940
9	3	1	1322.9	21.6	21212110	0.47358
					12221110	0.44733
10	6	3	1306.9	21.9	21212110	0.48204
					12221110	0.46299
11	7	3	1208.0	23.7	12221110	0.32174
					21212110	0.29576
					22220110	0.28837
12	4	1	1205.8	23.7	22220110	0.52330
					22211101	0.28057
13	8	3	1193.3	24.0	22220110	0.54411
					12221110	0.17092
					21212110	0.15958
14	5	1	1190.5	24.0	22211101	0.46334
					22220110	0.29535
15	9	3	1178.8	24.3	22211101	0.77145
16	10	3	1158.0	24.7	22121101	0.91283
17	6	1	1140.1	25.1	22121101	0.89932
18	11	3	1122.5	25.5	22121101	0.95424
19	12	3	1076.2	26.6	22211101	0.83819
20	7	1	975.1	29.3	21221101	0.67726
					12212110	0.16841

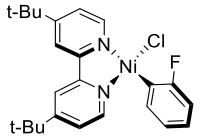

4B with Ni–C distance of 1.90 Å (near-equilibrium geometry) – CASSCF/NEVPT2 composition of the singlet ground state with CPCM(THF) (10e,9o Active Space) – 25 triplet roots, 15 singlet roots. Active Space Orbitals (in order for CI vector notation below): d(x^2-y^2)/C(sp^2), d(yz), d(xz), d(xy), d(z^2), d(x^2-y^2)/C(sp^2)*, π*(1), π*(2), π*(3).

CI vector	Transition	Contribution
222220000	Closed-shell singlet (CSS) d^8	0.6681
122221000	d(x^2-y^2)/C(sp^2) → d(x^2-y^2)/C(sp^2)*	0.1705
212220100	d(yz) → π*(1)	0.0498
222202000	2x[d(z^2)] → 2x[d(x^2-y^2)/C(sp^2)*]	0.0201
221220100	d(xz) → π*(1)	0.0197
202222000	2x[d(yz)] → 2x[d(x^2-y^2)/C(sp^2)*]	0.0105
Sum of CSS		**67 %**
Sum of all MLCT		**7 %**
Sum of all d-d		**20 %**
Sum of mixed MLCT + d-d		**0 %**

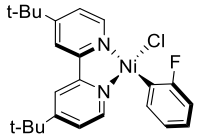

4B with Ni–C distance of 1.90 Å (near-equilibrium geometry) – CASSCF/QD-NEVPT2 composition of the singlet ground state with CPCM(THF) (10e,9o Active Space) – 25 triplet roots, 15 singlet roots. Active Space Orbitals (in order for CI vector notation below): d(x^2-y^2)/C(sp^2), d(yz), d(xz), d(xy), d(z^2), d(x^2-y^2)/C(sp^2)*, π*(1), π*(2), π*(3).

CI vector	Transition	Contribution
222220000	Closed-shell singlet (CSS) d^8	0.5990
122221000	d(x^2-y^2)/C(sp^2) → d(x^2-y^2)/C(sp^2)*	0.1326
212220100	d(yz) → π*(1)	0.1122
221220100	d(xz) → π*(1)	0.0425
012222100	2x[d(x^2-y^2)/C(sp^2)] + d(yz) → 2x[d(x^2-y^2)/C(sp^2)*] + π*(1)	0.0122
222202000	2x[d(z^2)] → 2x[d(x^2-y^2)/C(sp^2)*]	0.0119
221220010	d(xz) → π*(2)	0.0115
212220010	d(yz) → π*(2)	0.0106
Sum of CSS		**60 %**
Sum of all MLCT		**18 %**
Sum of all d-d		**14 %**
Sum of mixed MLCT + d-d		**1 %**

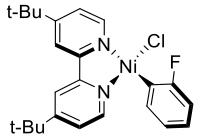

4B with Ni–C distance of 3.50 Å (dissociation limit) – CASSCF/NEVPT2 composition of the singlet ground state with CPCM(THF) (10e,8o Active Space) – 25 triplet roots, 15 singlet roots. Active Space Orbitals (in order for CI vector notation below): d(xy), d(yz), d(z²), d(xz), d(x²-y²)/C(sp²), d(x²-y²)/C(sp²)*, π*(1), π*(2).

CI vector	Transition	Contribution
22211110	d(xz) + d(x²-y²)/C(sp²) → d(x²-y²)/C(sp²)* + π*(1)	0.7747
22112110	d(z²) + d(xz) → d(x²-y²)/C(sp²)* + π*(1)	0.0553
22221100	d(x²-y²)/C(sp²) → d(x²-y²)/C(sp²)*	0.0414
21221110	d(yz) + d(x²-y²)/C(sp²) → d(x²-y²)/C(sp²)* + π*(1)	0.0342
11222110	d(xy) + d(yz) → d(x²-y²)/C(sp²)* + π*(1)	0.0308
22212010	d(xz) → π*(1)	0.0264
22210210	2x[d(x²-y²)/C(sp²)] + d(xz) → 2x[d(x²-y²)/C(sp²)*] + π*(1)	0.0125
Sum of CSS		**0 %**
Sum of all MLCT		**3 %**
Sum of all d-d		**4 %**
Sum of mixed MLCT + d-d		**91 %**

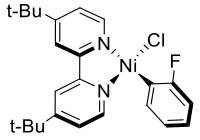

4B with Ni–C distance of 3.50 Å (dissociation limit) – CASSCF/QD-NEVPT2 composition of the singlet ground state with CPCM(THF) (10e,8o Active Space) – 25 triplet roots, 15 singlet roots. Active Space Orbitals (in order for CI vector notation below): d(xy), d(yz), d(z²), d(xz), d(x²-y²)/C(sp²), d(x²-y²)/C(sp²)*, π*(1), π*(2).

CI vector	Transition	Contribution
22211110	d(xz) + d(x²-y²)/C(sp²) → d(x²-y²)/C(sp²)* + π*(1)	0.73235
22112110	d(z²) + d(xz) → d(x²-y²)/C(sp²)* + π*(1)	0.05285
22221100	d(x²-y²)/C(sp²) → d(x²-y²)/C(sp²)*	0.05101
21221110	d(yz) + d(x²-y²)/C(sp²) → d(x²-y²)/C(sp²)* + π*(1)	0.03885
22211101	d(xz) + d(x²-y²)/C(sp²) → d(x²-y²)/C(sp²)* + π*(2)	0.03020
22212010	d(xz) → π*(1)	0.02676
11222110	d(xy) + d(yz) → d(x²-y²)/C(sp²)* + π*(1)	0.02594
22210210	2x[d(x²-y²)/C(sp²)] + d(xz) → 2x[d(x²-y²)/C(sp²)*] + π*(1)	0.01264
Sum of CSS		**0 %**
Sum of all MLCT		**3 %**
Sum of all d-d		**5 %**
Sum of mixed MLCT + d-d		**89 %**

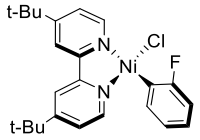

4B – CASSCF/NEVPT2 spin-orbit corrected absorption transitions for the CPCM(THF) phase spectrum (10e,9o Active Space) – 25 triplet roots, 15 singlet roots.

***E*/nm**	***E*/kcal mol^{-1}**	f_{osc}	***E*/nm**	***E*/kcal mol^{-1}**	f_{osc}
781.8	36.6	0.0000000	441.9	64.7	0.0002555
780.7	36.6	0.0000793	425.7	67.2	0.0657171
772.3	37.0	0.0006429	401.1	71.3	0.0016833
770.2	37.1	0.0007335	398.7	71.7	0.0000159
700.7	40.8	0.0000006	398.5	71.7	0.0000012
699.5	40.9	0.0001296	397.9	71.9	0.0055517
696.6	41.0	0.0004054	396.3	72.2	0.0011486
634.3	45.1	0.0000001	382.5	74.7	0.0000013
633.9	45.1	0.0000001	381.9	74.9	0.0000086
633.5	45.1	0.0009612	379.5	75.3	0.0001564
612.2	46.7	0.0029874	360.7	79.3	0.0000137
605.8	47.2	0.0000003	360.6	79.3	0.0000000
605.6	47.2	0.0000459	355.3	80.5	0.0000998
540.4	52.9	0.0262353	348.6	82.0	0.0000001
527.1	54.2	0.0615065	346.8	82.4	0.0000001
521.6	54.8	0.0360768	345.9	82.7	0.0000442
481.9	59.3	0.0780234	345.4	82.8	0.0000044
472.2	60.5	0.0000001	344.7	82.9	0.0000280
472.2	60.6	0.0000259	343.2	83.3	0.0000001
470.7	60.7	0.0002642	337.7	84.7	0.0000692
470.0	60.8	0.0059274	336.6	84.9	0.0000054
466.8	61.3	0.0002590	333.1	85.8	0.0000030
455.9	62.7	0.0000003	331.0	86.4	0.0000003
455.5	62.8	0.0003353	330.8	86.4	0.0000002
455.1	62.8	0.0055889	330.8	86.4	0.0000021
443.9	64.4	0.0000450	330.8	86.4	0.0001542
442.7	64.6	0.0000133	328.6	87.0	0.0000003
442.6	64.6	0.0000485	325.8	87.8	0.0000044
442.5	64.6	0.0000521			

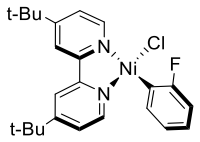

4B – CASSCF/QD-NEVPT2 spin-orbit corrected absorption transitions for the CPCM(THF) phase spectrum (10e,9o Active Space) – 25 triplet roots, 15 singlet roots.

***E*/nm**	***E*/kcal mol^{-1}**	f_{osc}	***E*/nm**	***E*/kcal mol^{-1}**	f_{osc}
752.5	38.0	0.0023096	399.5	71.6	0.0001764
749.2	38.2	0.0000005	398.9	71.7	0.0001139
745.6	38.3	0.0008461	397.1	72.0	0.0002370
734.0	39.0	0.0009831	395.5	72.3	0.0777954
691.6	41.3	0.0151809	389.0	73.5	0.0007604
671.3	42.6	0.0000190	388.5	73.6	0.0008365
670.4	42.6	0.0001256	388.4	73.6	0.0000254
661.5	43.2	0.0000193	386.6	74.0	0.0006103
660.9	43.3	0.0011625	382.7	74.7	0.0012577
660.5	43.3	0.0000658	369.4	77.4	0.0000116
658.8	43.4	0.0047940	368.8	77.5	0.0005857
586.6	48.7	0.0006598	367.5	77.8	0.0000781
583.0	49.0	0.0000091	346.0	82.6	0.0000053
582.5	49.1	0.0000703	344.7	82.9	0.0000048
561.6	50.9	0.0002441	344.4	83.0	0.0003245
487.2	58.7	0.0003048	340.0	84.1	0.0004053
457.3	62.5	0.0000356	339.1	84.3	0.0000187
457.3	62.5	0.0007316	336.3	85.0	0.0000319
455.5	62.8	0.0329965	330.2	86.6	0.0000122
455.3	62.8	0.0041465	328.5	87.0	0.0000641
441.7	64.7	0.0013810	324.0	88.3	0.0001573
441.6	64.7	0.0000308	323.2	88.4	0.0000046
441.5	64.8	0.0000041	322.6	88.6	0.0000073
435.8	65.6	0.0846472	322.2	88.7	0.0000710
431.6	66.2	0.0714012	322.0	88.8	0.0000057
429.0	66.6	0.0032299	319.9	89.4	0.0004750
428.9	66.7	0.0077691	317.1	90.2	0.0007867
428.8	66.7	0.0015794	312.7	91.4	0.0002954
412.3	69.3	0.0001265	312.4	91.5	0.0000005
400.2	71.5	0.0011359	311.2	91.9	0.0000011

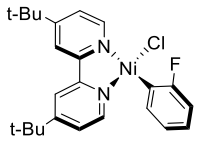

4B – TD-DFT (B3LYP) absorption transitions (singlets only) for the CPCM(THF) phase spectrum.

***E*/nm**	***E*/kcal mol^{-1}**	f_{osc}	***E*/nm**	***E*/kcal mol^{-1}**	f_{osc}
617.7	46.3	0.0000000	365.1	78.3	0.0009386
556.9	51.3	0.0000000	355.2	80.5	0.0000000
521.7	54.8	0.0034084	353.0	81.0	0.0000000
517.5	55.2	0.0000000	352.5	81.1	0.0000308
507.5	56.3	0.0001425	351.4	81.4	0.0206623
499.6	57.2	0.0004345	343.2	83.3	0.0000000
482.3	59.3	0.0009345	334.9	85.4	0.0026885
480.8	59.5	0.0000000	333.1	85.8	0.0135067
471.0	60.7	0.0003180	323.8	88.3	0.0010484
465.6	61.4	0.0001467	316.4	90.4	0.0364402
465.6	61.4	0.0281084	315.3	90.7	0.0322596
439.7	65.0	0.0009878	313.8	91.1	0.0000000
439.1	65.1	0.0000000	313.6	91.2	0.0000000
433.4	66.0	0.0000000	311.5	91.8	0.0000000
431.6	66.3	0.0000000	310.2	92.2	0.0000000
426.4	67.1	0.0002184	309.2	92.5	0.0000000
411.8	69.4	0.0608424	305.8	93.5	0.0000000
394.9	72.4	0.0000000	302.9	94.4	0.0235678
393.0	72.8	0.0002359	302.5	94.5	0.0000000
378.0	75.6	0.0000000	301.3	94.9	0.0182939
373.1	76.6	0.0000000			

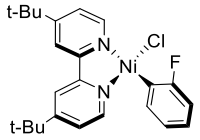

4B – TD-DFT (B3LYP) absorption transitions (singlets only) for the CPCM(Toluene) phase spectrum.

***E*/nm**	***E*/kcal mol^{-1}**	f_{osc}	***E*/nm**	***E*/kcal mol^{-1}**	f_{osc}
640.2	44.7	0.0000000	375.0	76.2	0.0000566
618.0	46.3	0.0000000	368.1	77.7	0.0017947
603.4	47.4	0.0000000	364.3	78.5	0.0000000
564.1	50.7	0.0000000	363.3	78.7	0.0000000
562.4	50.8	0.0004359	362.9	78.8	0.0000000
551.6	51.8	0.0010006	355.6	80.4	0.0081281
528.4	54.1	0.0069019	353.4	80.9	0.0202531
514.5	55.6	0.0001273	353.1	81.0	0.0242333
513.1	55.7	0.0000000	351.8	81.3	0.0007075
511.0	56.0	0.0004670	347.9	82.2	0.0000000
498.9	57.3	0.0255201	342.6	83.5	0.0000000
495.7	57.7	0.0000000	337.5	84.7	0.0000000
485.5	58.9	0.0000000	332.2	86.1	0.0000000
483.7	59.1	0.0086188	329.6	86.7	0.0000000
467.9	61.1	0.0006026	329.4	86.8	0.0016969
464.0	61.6	0.0002605	323.7	88.3	0.0234331
454.1	63.0	0.0473800	321.6	88.9	0.0000000
438.3	65.2	0.0002123	319.8	89.4	0.0092522
437.9	65.3	0.0000000	312.9	91.4	0.0000000
415.5	68.8	0.0000000	312.9	91.4	0.0271423
413.8	69.1	0.0006227	312.4	91.5	0.0000000
411.3	69.5	0.0000000	308.9	92.5	0.0000000
393.7	72.6	0.0238081	308.3	92.7	0.0000000
386.7	73.9	0.0000000	304.1	94.0	0.0000000
386.0	74.1	0.0000345	300.5	95.2	0.0020476
380.9	75.1	0.0000000			

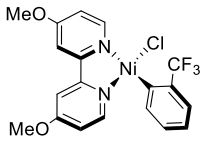

5A with Ni–C distance of 1.90 Å (near-equilibrium geometry) – CASSCF/NEVPT2 lowest transition energies with CPCM(THF) (10e,9o Active Space) – 25 triplet roots, 15 singlet roots. Active Space Orbitals (in order for CI vector notation below): d(x^2-y^2)/C(sp^2), d(yz), d(z^2), d(xz), d(xy), d(x^2-y^2)/C(sp^2)*, π*(1), π*(2), π*(3).

State	Root	Multiplicity	ΔE/nm	ΔE/kcal mol^{-1}	CI vector	Contribution
0	0	1	---	---	222220000	0.6682
					122221000	0.2011
1	0	3	1228.2	23.3	221221000	0.7954
					121222000	0.1612
2	1	3	1055.9	27.1	222121000	0.7883
					122122000	0.1607
3	2	3	957.0	29.9	212221000	0.7769
					112222000	0.1404
4	3	3	716.8	39.9	221220100	0.8315
5	4	3	666.4	42.9	222120100	0.6694
					212220100	0.1659
6	5	3	662.2	43.2	222211000	0.6519
					212122000	0.2006
					122212000	0.1128
7	1	1	642.4	44.5	221220100	0.6701
8	6	3	579.5	49.3	212220100	0.6601
					222120100	0.1636
9	2	1	560.5	51.0	222120100	0.5853
					222211000	0.1177
10	3	1	549.6	52.0	212220100	0.7173
11	4	1	527.1	54.2	221221000	0.6045
					221220100	0.1073
12	5	1	481.0	59.4	222121000	0.7524
					122122000	0.1080
13	6	1	470.8	60.7	222211000	0.7042
14	7	1	465.1	61.5	212221000	0.7369
					112222000	0.1042
15	7	3	463.9	61.6	221220010	0.8274
16	8	1	460.7	62.1	221220010	0.8242
17	8	3	445.8	64.1	222120010	0.6866
					212220010	0.1424
18	9	3	437.9	65.3	222210100	0.7303
					212121100	0.1030
19	9	1	430.6	66.4	222210100	0.7204
20	10	1	419.0	68.2	222120010	0.6617
					212220010	0.1178

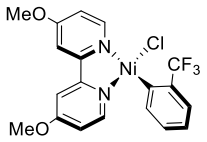

5A with Ni–C distance of 1.90 Å (near-equilibrium geometry) – CASSCF/QD-NEVPT2 lowest transition energies with CPCM(THF) (10e,9o Active Space) – 25 triplet roots, 15 singlet roots. Active Space Orbitals (in order for CI vector notation below): d(x^2-y^2)/C(sp^2), d(yz), d(z^2), d(xz), d(xy), d(x^2-y^2)/C(sp^2)*, π*(1), π*(2), π*(3).

State	Root	Multiplicity	ΔE/nm	ΔE/kcal mol^{-1}	CI vector	Contribution
0	0	1	---	---	222220000	0.6088
					122221000	0.1616
1	0	3	1137.7	25.1	221221000	0.7961
					121222000	0.1564
2	1	3	1017.4	28.1	222121000	0.7788
					122122000	0.1445
3	2	3	912.2	31.3	212221000	0.7822
					112222000	0.1419
4	1	1	737.5	38.8	221220100	0.7863
5	3	3	690.6	41.4	222211000	0.7536
					122212000	0.1133
6	4	3	682.4	41.9	221220100	0.8148
7	2	1	644.0	44.4	222120100	0.7066
8	5	3	634.9	45.0	222120100	0.6819
					212220100	0.1452
9	6	3	557.4	51.3	212220100	0.6744
					222120100	0.1415
10	3	1	540.1	52.9	212220100	0.6746
11	4	1	480.8	59.5	222121000	0.4849
					222210100	0.2378
12	5	1	452.1	63.2	221221000	0.4354
					221220010	0.2746
13	7	3	445.7	64.2	221220010	0.8223
14	6	1	439.8	65.0	212221000	0.3448
					221220010	0.3238
15	7	1	436.2	65.5	212221000	0.2095
					221220010	0.2061
					221221000	0.1913
16	8	3	428.7	66.7	222120010	0.6617
					212220010	0.1629
17	9	3	425.2	67.2	222210100	0.7198
					212121100	0.1002
18	8	1	423.1	67.6	222211000	0.6536
					222120010	0.1232
19	9	1	399.5	71.6	222210100	0.3810
					212221000	0.1395
					222121000	0.1024
20	10	1	391.0	73.1	222120010	0.4466
					222211000	0.1092

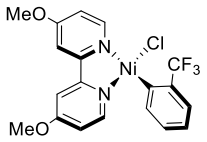

5A with Ni–C distance of 3.50 Å (dissociation limit) – CASSCF/NEVPT2 lowest transition energies with CPCM(THF) (10e,8o Active Space) – 25 triplet roots, 15 singlet roots. Active Space Orbitals (in order for CI vector notation below): d(xy), d(yz), d(z^2), d(xz), d(x^2-y^2)/C(sp^2), d(x^2-y^2)/C(sp^2)*, π*(1), π*(2).

State	Root	Multiplicity	ΔE/nm	ΔE/kcal mol^{-1}	CI vector	Contribution
0	0	1	---	---	22211110	0.7871
1	0	3	55769.1	0.5	22211110	0.8239
2	1	3	15550.6	1.8	22121110	0.9392
3	1	1	10973.8	2.6	22121110	0.9314
4	2	3	9247.7	3.1	22121110	0.9721
5	3	3	6819.8	4.2	22211110	0.8468
6	4	3	4583.8	6.2	21221110	0.8782
7	2	1	4365.6	6.5	21221110	0.8470
8	5	3	4054.0	7.1	21221110	0.8823
9	3	1	1548.4	18.5	22211101	0.6819
					22121101	0.1414
10	6	3	1506.5	19.0	22211101	0.7205
					22121101	0.1331
11	4	1	1448.5	19.7	21212110	0.4783
					12221110	0.4608
12	7	3	1429.9	20.0	21212110	0.4818
					12221110	0.4728
13	8	3	1343.3	21.3	12221110	0.4855
					21212110	0.4615
14	9	3	1336.4	21.4	22121101	0.9217
15	5	1	1332.2	21.5	22121101	0.7904
					22211101	0.1225
16	10	3	1299.0	22.0	22121101	0.8502
					22211101	0.1027
17	6	1	1265.6	22.6	22220110	0.8247
18	11	3	1262.6	22.6	22220110	0.8301
19	12	3	1236.8	23.1	22211101	0.8279
20	13	3	1094.4	26.1	21221101	0.8594

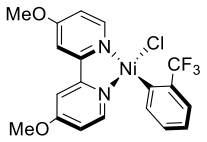

5A with Ni–C distance of 3.50 Å (dissociation limit) – CASSCF/QD-NEVPT2 lowest transition energies with CPCM(THF) (10e,8o Active Space) – 25 triplet roots, 15 singlet roots. Active Space Orbitals (in order for CI vector notation below): d(xy), d(yz), d(z^2), d(xz), d(x^2-y^2)/C(sp^2), d(x^2-y^2)/C(sp^2)*, π*(1), π*(2).

State	Root	Multiplicity	ΔE/nm	ΔE/kcal mol^{-1}	CI vector	Contribution
0	0	1	---	---	22211110	0.7397
1	0	3	48638.1	0.6	22211110	0.7761
2	1	3	11059.5	2.6	22121110	0.9380
3	1	1	8488.2	3.4	22121110	0.9403
4	2	3	7441.6	3.8	22121110	0.9749
5	3	3	5812.6	4.9	22211110	0.8428
6	4	3	4088.6	7.0	21221110	0.8775
7	2	1	3929.7	7.3	21221110	0.8400
8	5	3	3672.4	7.8	21221110	0.8784
9	3	1	1467.7	19.5	22211101	0.7295
10	6	3	1432.9	20.0	22211101	0.7543
11	4	1	1398.2	20.4	21212110	0.4707
					12221110	0.4406
12	7	3	1380.1	20.7	21212110	0.4736
					12221110	0.4505
13	8	3	1300.0	22.0	12221110	0.4725
					21212110	0.4556
14	9	3	1288.9	22.2	22121101	0.9282
15	5	1	1271.3	22.5	22121101	0.8944
16	10	3	1245.7	23.0	22121101	0.8392
					22220110	0.1025
17	6	1	1224.2	23.4	22220110	0.7998
18	11	3	1219.5	23.4	22220110	0.7179
					22121101	0.1240
19	12	3	1199.0	23.8	22211101	0.8424
20	7	1	1065.4	26.8	21221101	0.8314

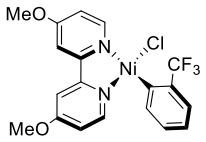

5A with Ni–C distance of 1.90 Å (near-equilibrium geometry) – CASSCF/NEVPT2 composition of the singlet ground state with CPCM(THF) (10e,9o Active Space) – 25 triplet roots, 15 singlet roots. Active Space Orbitals (in order for CI vector notation below): $d(x^2\text{-}y^2)/C(sp^2)$, $d(yz)$, $d(z^2)$, $d(xz)$, $d(xy)$, $d(x^2\text{-}y^2)/C(sp^2)^*$, $\pi^*(1)$, $\pi^*(2)$, $\pi^*(3)$.

CI vector	Transition	Contribution
222220000	Closed-shell singlet (CSS) d^8	0.6682
122221000	$d(x^2\text{-}y^2)/C(sp^2) \rightarrow d(x^2\text{-}y^2)/C(sp^2)^*$	0.2011
212220100	$d(yz) \rightarrow \pi^*(1)$	0.0288
220222000	$2x[d(z^2)] \rightarrow 2x[d(x^2\text{-}y^2)/C(sp^2)^*]$	0.0213
222120100	$d(xz) \rightarrow \pi^*(1)$	0.0174
222022000	$2x[d(xz)] \rightarrow 2x[d(x^2\text{-}y^2)/C(sp^2)^*]$	0.0148
202222000	$2x[d(yz)] \rightarrow 2x[d(x^2\text{-}y^2)/C(sp^2)^*]$	0.0131
Sum of CSS		**67 %**
Sum of all MLCT		**5 %**
Sum of all d-d		**25 %**
Sum of mixed MLCT + d-d		**0 %**

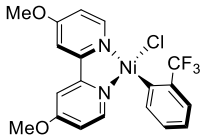

5A with Ni–C distance of 1.90 Å (near-equilibrium geometry) – CASSCF/QD-NEVPT2 composition of the singlet ground state with CPCM(THF) (10e,9o Active Space) – 25 triplet roots, 15 singlet roots. Active Space Orbitals (in order for CI vector notation below): $d(x^2\text{-}y^2)/C(sp^2)$, $d(yz)$, $d(z^2)$, $d(xz)$, $d(xy)$, $d(x^2\text{-}y^2)/C(sp^2)^*$, $\pi^*(1)$, $\pi^*(2)$, $\pi^*(3)$.

CI vector	Transition	Contribution
222220000	Closed-shell singlet (CSS) d^8	0.6088
122221000	$d(x^2\text{-}y^2)/C(sp^2) \rightarrow d(x^2\text{-}y^2)/C(sp^2)^*$	0.1616
212220100	$d(yz) \rightarrow \pi^*(1)$	0.0725
222120100	$d(xz) \rightarrow \pi^*(1)$	0.0486
222120010	$d(xz) \rightarrow \pi^*(2)$	0.0205
220222000	$2x[d(z^2)] \rightarrow 2x[d(x^2\text{-}y^2)/C(sp^2)^*]$	0.0139
212220010	$d(yz) \rightarrow \pi^*(2)$	0.0116
Sum of CSS		**61 %**
Sum of all MLCT		**15 %**
Sum of all d-d		**18 %**
Sum of mixed MLCT + d-d		**0 %**

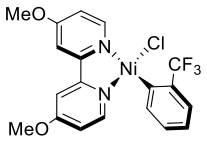

5A with Ni–C distance of 3.50 Å (dissociation limit) – CASSCF/NEVPT2 composition of the singlet ground state with CPCM(THF) (10e,8o Active Space) – 25 triplet roots, 15 singlet roots. Active Space Orbitals (in order for CI vector notation below): d(xy), d(yz), d(z²), d(xz), d(x²-y²)/C(sp²), d(x²-y²)/C(sp²)*, π*(1), π*(2).

CI vector	Transition	Contribution
22211110	d(xz) + d(x²-y²)/C(sp²) → d(x²-y²)/C(sp²)* + π*(1)	0.7871
22112110	d(z²) + d(xz) → d(x²-y²)/C(sp²)* + π*(1)	0.0498
11222110	d(xy) + d(yz) → d(x²-y²)/C(sp²)* + π*(1)	0.0341
22221100	d(x²-y²)/C(sp²) → d(x²-y²)/C(sp²)*	0.0303
21221110	d(yz) + d(x²-y²)/C(sp²) → d(x²-y²)/C(sp²)* + π*(1)	0.0275
22212010	d(xz) → π*(1)	0.0245
21122110	d(yz) + d(z²) → d(x²-y²)/C(sp²)* + π*(1)	0.0126
22210210	2x[d(x²-y²)/C(sp²)] + d(xz) → 2x[d(x²-y²)/C(sp²)*] + π*(1)	0.0112
Sum of CSS		**0 %**
Sum of all MLCT		**2 %**
Sum of all d-d		**3 %**
Sum of mixed MLCT + d-d		**92 %**

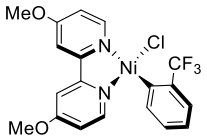

5A with Ni–C distance of 3.50 Å (dissociation limit) – CASSCF/QD-NEVPT2 composition of the singlet ground state with CPCM(THF) (10e,8o Active Space) – 25 triplet roots, 15 singlet roots. Active Space Orbitals (in order for CI vector notation below): d(xy), d(yz), d(z²), d(xz), d(x²-y²)/C(sp²), d(x²-y²)/C(sp²)*, π*(1), π*(2).

CI vector	Transition	Contribution
22211110	d(xz) + d(x²-y²)/C(sp²) → d(x²-y²)/C(sp²)* + π*(1)	0.7397
22112110	d(z²) + d(xz) → d(x²-y²)/C(sp²)* + π*(1)	0.0478
22211101	d(xz) + d(x²-y²)/C(sp²) → d(x²-y²)/C(sp²)* + π*(2)	0.0456
22221100	d(x²-y²)/C(sp²) → d(x²-y²)/C(sp²)*	0.0421
21221110	d(yz) + d(x²-y²)/C(sp²) → d(x²-y²)/C(sp²)* + π*(1)	0.0289
11222110	d(xy) + d(yz) → d(x²-y²)/C(sp²)* + π*(1)	0.0286
22212010	d(xz) → π*(1)	0.0245
21122110	d(yz) + d(z²) → d(x²-y²)/C(sp²)* + π*(1)	0.0127
22210210	2x[d(x²-y²)/C(sp²)] + d(xz) → 2x[d(x²-y²)/C(sp²)*] + π*(1)	0.0112
Sum of CSS		**0 %**
Sum of all MLCT		**2 %**
Sum of all d-d		**4 %**
Sum of mixed MLCT + d-d		**91 %**

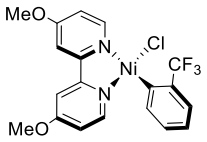

5A – CASSCF/NEVPT2 spin-orbit corrected absorption transitions for the CPCM(THF) phase spectrum (10e,9o Active Space) – 25 triplet roots, 15 singlet roots.

***E*/nm**	***E*/kcal mol^{-1}**	f_{osc}	***E*/nm**	***E*/kcal mol^{-1}**	f_{osc}
727.7	39.3	0.0000000	440.2	65.0	0.0000333
727.4	39.3	0.0001255	435.8	65.6	0.0000020
720.4	39.7	0.0013855	435.6	65.6	0.0004637
677.9	42.2	0.0002915	435.5	65.7	0.0003644
659.1	43.4	0.0000026	428.9	66.7	0.0004910
658.2	43.4	0.0004405	419.0	68.2	0.0555604
658.0	43.5	0.0009273	396.1	72.2	0.0000324
657.9	43.5	0.0000334	396.0	72.2	0.0000003
656.1	43.6	0.0000623	395.0	72.4	0.0069851
636.2	44.9	0.0013500	367.5	77.8	0.0027465
582.4	49.1	0.0222252	360.1	79.4	0.0000033
571.5	50.0	0.0000002	358.4	79.8	0.0000018
571.0	50.1	0.0000891	356.5	80.2	0.0000001
550.7	51.9	0.0462952	350.6	81.5	0.0002295
544.2	52.5	0.0689565	349.2	81.9	0.0000013
523.8	54.6	0.0073317	345.1	82.9	0.0001047
480.1	59.6	0.0001107	342.2	83.6	0.0000055
469.0	61.0	0.0028735	339.4	84.2	0.0000004
468.9	61.0	0.0005841	336.5	85.0	0.0000003
468.6	61.0	0.0005584	326.0	87.7	0.0000007
466.3	61.3	0.0004236	325.9	87.7	0.0001545
466.0	61.4	0.0033030	325.9	87.7	0.0000060
464.2	61.6	0.0013212	301.3	94.9	0.0000008
441.1	64.8	0.0000228	301.3	94.9	0.0000089
441.0	64.8	0.0001296	301.2	94.9	0.0000001

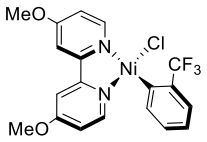

5A – CASSCF/QD-NEVPT2 spin-orbit corrected absorption transitions for the CPCM(THF) phase spectrum (10e,9o Active Space) – 25 triplet roots, 15 singlet roots.

***E*/nm**	***E*/kcal mol^{-1}**	f_{osc}	***E*/nm**	***E*/kcal mol^{-1}**	f_{osc}
743.7	38.4	0.0043592	424.3	67.4	0.0291560
694.4	41.2	0.0000313	423.3	67.5	0.0005625
692.6	41.3	0.0000037	423.2	67.6	0.0001703
691.4	41.4	0.0001142	423.2	67.6	0.0002439
685.9	41.7	0.0000230	419.6	68.1	0.0011378
685.5	41.7	0.0000006	398.1	71.8	0.0009310
682.6	41.9	0.0000228	392.8	72.8	0.0469430
643.0	44.5	0.0000536	383.7	74.5	0.0132725
631.3	45.3	0.0000974	383.0	74.7	0.0023325
628.7	45.5	0.0000029	382.9	74.7	0.0000539
620.7	46.1	0.0001633	379.5	75.3	0.0115176
552.7	51.7	0.0002165	350.9	81.5	0.0000928
550.9	51.9	0.0000391	349.8	81.7	0.0000396
550.1	52.0	0.0000016	346.9	82.4	0.0000086
534.0	53.5	0.0019465	341.5	83.7	0.0000195
478.7	59.7	0.0012088	339.5	84.2	0.0001433
454.2	63.0	0.0003541	334.5	85.5	0.0000033
450.4	63.5	0.0005539	333.3	85.8	0.0000828
450.3	63.5	0.0000046	331.0	86.4	0.0000956
447.0	64.0	0.0172130	327.5	87.3	0.0001993
441.9	64.7	0.1192444	319.4	89.5	0.0000182
435.7	65.6	0.0115876	319.4	89.5	0.0000047
426.8	67.0	0.0005033	319.4	89.5	0.0002590
424.6	67.3	0.0000250			

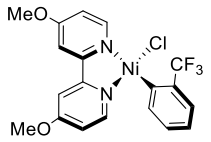

5A – TD-DFT (B3LYP) absorption transitions (singlets only) for the CPCM(THF) phase spectrum.

***E*/nm**	***E*/kcal mol^{-1}**	f_{osc}	***E*/nm**	***E*/kcal mol^{-1}**	f_{osc}
617.6	46.3	0.0000000	372.1	76.8	0.0018163
538.9	53.1	0.0000000	364.7	78.4	0.0000000
526.8	54.3	0.0026130	362.6	78.9	0.0000000
524.3	54.5	0.0008767	352.9	81.0	0.0000000
514.6	55.6	0.0001662	345.8	82.7	0.0294493
503.8	56.8	0.0000000	332.5	86.0	0.0002838
473.8	60.3	0.0001474	323.7	88.3	0.0000000
467.1	61.2	0.0280085	322.6	88.6	0.0000000
463.2	61.7	0.0001371	321.6	88.9	0.0000000
426.7	67.0	0.0000000	319.5	89.5	0.0088811
414.8	68.9	0.0037821	316.1	90.5	0.0128510
411.3	69.5	0.0451656	315.6	90.6	0.0000000
411.1	69.5	0.0004231	313.7	91.1	0.0000000
408.6	70.0	0.0000000	308.8	92.6	0.0000000
399.7	71.5	0.0000000	308.2	92.8	0.0164028
384.7	74.3	0.0000000	305.8	93.5	0.0000000
384.6	74.3	0.0005443	302.3	94.6	0.0000000

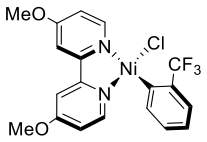

5A – TD-DFT (B3LYP) absorption transitions (singlets only) for the CPCM(Toluene) phase spectrum.

***E*/nm**	***E*/kcal mol^{-1}**	f_{osc}	***E*/nm**	***E*/kcal mol^{-1}**	f_{osc}
618.8	46.2	0.0000000	358.7	79.7	0.0003967
613.4	46.6	0.0000000	356.0	80.3	0.0000000
581.4	49.2	0.0000000	355.9	80.3	0.0054505
574.1	49.8	0.0009198	355.8	80.4	0.0000000
530.0	53.9	0.0041366	350.5	81.6	0.0050564
517.0	55.3	0.0006762	345.9	82.7	0.0049042
513.4	55.7	0.0258027	343.8	83.2	0.0000000
492.9	58.0	0.0000000	336.8	84.9	0.0134649
482.1	59.3	0.0000000	334.2	85.6	0.0000000
470.6	60.8	0.0003034	328.6	87.0	0.0000000
470.4	60.8	0.0000000	325.7	87.8	0.0000000
469.7	60.9	0.0046153	322.7	88.6	0.0053990
465.6	61.4	0.0000544	312.5	91.5	0.0000000
465.5	61.4	0.0053189	312.3	91.6	0.0008353
459.3	62.3	0.0323322	312.2	91.6	0.0000000
425.6	67.2	0.0006041	311.9	91.7	0.0244716
416.3	68.7	0.0000000	311.7	91.7	0.0000000
387.5	73.8	0.0009981	310.9	92.0	0.0000000
381.7	74.9	0.0358144	306.6	93.3	0.0000000
381.4	75.0	0.0000000	302.9	94.4	0.0000000
381.3	75.0	0.0000000	302.4	94.5	0.0245231
366.9	77.9	0.0000000	301.3	94.9	0.0000000
361.4	79.1	0.0000000			

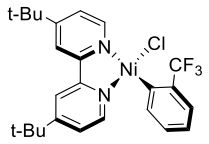

5B with Ni–C distance of 1.90 Å (near-equilibrium geometry) – CASSCF/NEVPT2 lowest transition energies with CPCM(THF) (10e,9o Active Space) – 25 triplet roots, 15 singlet roots. Active Space Orbitals (in order for CI vector notation below): d(x^2-y^2)/C(sp^2), d(xy), d(yz), d(z^2), d(xz), d(x^2-y^2)/C(sp^2)*, π*(1), π*(2), π*(3).

State	Root	Multiplicity	ΔE/nm	ΔE/kcal mol^{-1}	CI vector	Contribution
0	0	1	---	---	222220000	0.6130
					122221000	0.1533
1	0	3	988.5	28.9	222211000	0.5353
					222121000	0.2726
2	1	3	856.5	33.4	222121000	0.3752
					222211000	0.2249
					221221000	0.1842
3	2	3	783.5	36.5	221221000	0.5651
					222121000	0.1533
4	3	3	680.1	42.0	222210100	0.5656
					222120100	0.2926
5	1	1	666.7	42.9	222210100	0.5630
					222120100	0.2924
6	4	3	625.6	45.7	222120100	0.5494
					222210100	0.2925
7	5	3	591.6	48.3	212221000	0.6849
					112222000	0.1082
8	2	1	590.0	48.5	222120100	0.2946
					221220100	0.2824
9	6	3	550.3	52.0	221220100	0.7918
10	3	1	513.7	55.7	221220100	0.4651
					222120100	0.1740
11	4	1	451.7	63.3	221221000	0.3554
					222121000	0.1758
12	5	1	448.3	63.8	222211000	0.4873
					222121000	0.2427
13	7	3	429.8	66.5	222210010	0.5656
					222120010	0.2870
14	6	1	427.9	66.8	222210010	0.5638
					222120010	0.2853
15	7	1	424.2	67.4	222121000	0.3404
					221221000	0.2770
16	8	1	422.7	67.6	212221000	0.7112
17	8	3	417.0	68.6	212220100	0.7424
18	9	3	411.1	69.6	222120010	0.5442
					222210010	0.2872
19	9	1	400.6	71.4	212220100	0.6219
					221221000	0.1064
20	10	1	393.5	72.7	222120010	0.5021
					222210010	0.2672

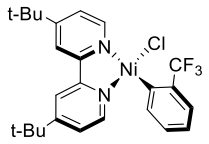

5B with Ni–C distance of 1.90 Å (near-equilibrium geometry) – CASSCF/QD-NEVPT2 lowest transition energies with CPCM(THF) (10e,9o Active Space) – 25 triplet roots, 15 singlet roots. Active Space Orbitals (in order for CI vector notation below): d(x^2-y^2)/C(sp^2), d(xy), d(yz), d(z^2), d(xz), d(x^2-y^2)/C(sp^2)*, π*(1), π*(2), π*(3).

State	Root	Multiplicity	ΔE/nm	ΔE/kcal mol^{-1}	CI vector	Contribution
0	0	1	---	---	222220000	0.5893
					122221000	0.1375
1	0	3	989.2	28.9	222211000	0.5366
					222121000	0.2580
2	1	3	867.8	32.9	222121000	0.3381
					221221000	0.2468
3	2	3	785.1	36.4	221221000	0.4995
					222121000	0.1908
4	3	3	676.4	42.3	222210100	0.5559
					222120100	0.2891
5	1	1	664.1	43.1	222210100	0.5732
					222120100	0.2831
6	4	3	631.0	45.3	212221000	0.5541
					222120100	0.1386
7	5	3	618.7	46.2	222120100	0.4023
					222210100	0.2302
8	2	1	592.2	48.3	221220100	0.3597
					222120100	0.2658
9	6	3	548.0	52.2	221220100	0.7743
10	3	1	517.0	55.3	221220100	0.4027
					222120100	0.1871
11	4	1	475.5	60.1	212220100	0.4754
					221221000	0.1327
12	5	1	449.8	63.6	222211000	0.4273
					222121000	0.1955
13	7	3	428.7	66.7	222210010	0.5529
					222120010	0.2789
14	6	1	426.5	67.0	222210010	0.3865
					222120010	0.2413
15	7	1	424.3	67.4	222121000	0.3795
					221221000	0.1696
16	8	1	419.5	68.2	212221000	0.4735
					222121000	0.1324
17	8	3	416.9	68.6	212220100	0.7423
18	9	3	409.5	69.8	222120010	0.5466
					222210010	0.2802
19	9	1	389.1	73.5	222120010	0.2976
					222210010	0.1885
20	10	1	381.1	75.0	221221000	0.3693
					212220100	0.2237

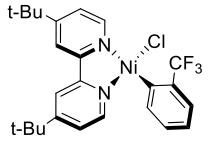

5B with Ni–C distance of 3.50 Å (dissociation limit) – CASSCF/NEVPT2 lowest transition energies with CPCM(THF) (10e,8o Active Space) – 25 triplet roots, 15 singlet roots. Active Space Orbitals (in order for CI vector notation below): d(xy), d(yz), d(z^2), d(xz), d(x^2-y^2)/C(sp^2), d(x^2-y^2)/C(sp^2)*, π*(1), π*(2).

State	Root	Multiplicity	ΔE/nm	ΔE/kcal mol^{-1}	CI vector	Contribution
0	0	1	---	---	22211110	0.7774
1	0	3	46023.6	0.6	22211110	0.8118
2	1	3	8458.0	3.4	22121110	0.9398
3	1	1	6592.9	4.3	22121110	0.9371
4	2	3	5878.4	4.9	22121110	0.9779
5	3	3	4913.0	5.8	22211110	0.8483
6	4	3	3533.7	8.1	21221110	0.8840
7	2	1	3394.7	8.4	21221110	0.8426
8	5	3	3200.6	8.9	21221110	0.8812
9	3	1	1365.4	20.9	21212110	0.4756
					12221110	0.4544
10	6	3	1349.8	21.2	21212110	0.4805
					12221110	0.4677
11	4	1	1241.0	23.0	22211101	0.7911
12	7	3	1237.2	23.1	12221110	0.4922
					21212110	0.4535
13	8	3	1212.2	23.6	22211101	0.8210
14	9	3	1198.5	23.9	22220110	0.8361
15	5	1	1198.2	23.9	22220110	0.8348
16	10	3	1182.5	24.2	22121101	0.9343
17	6	1	1180.1	24.2	22121101	0.9209
18	11	3	1152.5	24.8	22121101	0.9635
19	12	3	1094.1	26.1	22211101	0.8417
20	13	3	986.2	29.0	21221101	0.8738

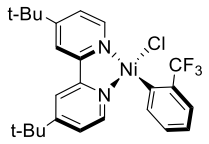

5B with Ni–C distance of 3.50 Å (dissociation limit) – CASSCF/QD-NEVPT2 lowest transition energies with CPCM(THF) (10e,8o Active Space) – 25 triplet roots, 15 singlet roots. Active Space Orbitals (in order for CI vector notation below): d(xy), d(yz), d(z^2), d(xz), d(x^2-y^2)/C(sp^2), d(x^2-y^2)/C(sp^2)*, π*(1), π*(2).

State	Root	Multiplicity	ΔE/nm	ΔE/kcal mol^{-1}	CI vector	Contribution
0	0	1	---	---	22211110	0.7386
1	0	3	41963.9	0.7	22211110	0.7774
2	1	3	7274.8	3.9	22121110	0.9385
3	1	1	5852.7	4.9	22121110	0.9370
4	2	3	5279.0	5.4	22121110	0.9787
5	3	3	4495.8	6.4	22211110	0.8436
6	4	3	3310.2	8.6	21221110	0.8795
7	2	1	3193.2	9.0	21221110	0.8325
8	5	3	3018.1	9.5	21221110	0.8752
9	3	1	1333.6	21.4	21212110	0.4786
					12221110	0.4453
10	6	3	1317.9	21.7	21212110	0.4879
					12221110	0.4611
11	7	3	1211.8	23.6	12221110	0.4650
					21212110	0.4348
12	4	1	1199.9	23.8	22211101	0.7540
13	8	3	1176.0	24.3	22211101	0.5754
					22220110	0.1859
14	5	1	1172.0	24.4	22220110	0.8046
15	9	3	1169.2	24.5	22220110	0.5908
					22211101	0.2056
16	10	3	1156.1	24.7	22121101	0.9139
17	6	1	1149.9	24.9	22121101	0.8873
18	11	3	1123.7	25.4	22121101	0.9555
19	12	3	1071.5	26.7	22211101	0.8453
20	7	1	982.7	29.1	21221101	0.5914
					12212110	0.2454

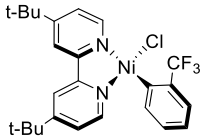

5B with Ni–C distance of 1.90 Å (near-equilibrium geometry) – CASSCF/NEVPT2 composition of the singlet ground state with CPCM(THF) (10e,9o Active Space) – 25 triplet roots, 15 singlet roots. Active Space Orbitals (in order for CI vector notation below): $d(x^2\text{-}y^2)/C(sp^2)$, d(xy), d(yz), $d(z^2)$, d(xz), $d(x^2\text{-}y^2)/C(sp^2)^*$, π*(1), π*(2), π*(3).

CI vector	Transition	Contribution
222220000	Closed-shell singlet (CSS) d^8	0.6130
122221000	$d(x^2\text{-}y^2)/C(sp^2) \rightarrow d(x^2\text{-}y^2)/C(sp^2)^*$	0.1533
222120100	$d(z^2) \rightarrow \pi^*(1)$	0.0717
222210100	$d(xz) \rightarrow \pi^*(1)$	0.0387
221220100	$d(yz) \rightarrow \pi^*(1)$	0.0188
221220001	$d(yz) \rightarrow \pi^*(3)$	0.0132
222202000	$2x[d(xz)] \rightarrow 2x[d(x^2\text{-}y^2)/C(sp^2)^*]$	0.0129
222022000	$2x[d(z^2)] \rightarrow 2x[d(x^2\text{-}y^2)/C(sp^2)^*]$	0.0113
222120010	$d(z^2) \rightarrow \pi^*(2)$	0.0103
Sum of CSS		**61 %**
Sum of all MLCT		**15 %**
Sum of all d-d		**18 %**
Sum of mixed MLCT + d-d		**0 %**

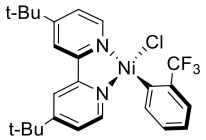

5B with Ni–C distance of 1.90 Å (near-equilibrium geometry) – CASSCF/QD-NEVPT2 composition of the singlet ground state with CPCM(THF) (10e,9o Active Space) – 25 triplet roots, 15 singlet roots. Active Space Orbitals (in order for CI vector notation below): $d(x^2\text{-}y^2)/C(sp^2)$, d(xy), d(yz), $d(z^2)$, d(xz), $d(x^2\text{-}y^2)/C(sp^2)^*$, π*(1), π*(2), π*(3).

CI vector	Transition	Contribution
222220000	Closed-shell singlet (CSS) d^8	0.58926
122221000	$d(x^2\text{-}y^2)/C(sp^2) \rightarrow d(x^2\text{-}y^2)/C(sp^2)^*$	0.13746
222120100	$d(z^2) \rightarrow \pi^*(1)$	0.08390
222210100	$d(xz) \rightarrow \pi^*(1)$	0.04183
221220100	$d(yz) \rightarrow \pi^*(1)$	0.02295
222120010	$d(z^2) \rightarrow \pi^*(2)$	0.02061
221220001	$d(yz) \rightarrow \pi^*(3)$	0.01262
222202000	$2x[d(xz)] \rightarrow 2x[d(x^2\text{-}y^2)/C(sp^2)^*]$	0.01109
Sum of CSS		**59 %**
Sum of all MLCT		**18 %**
Sum of all d-d		**15 %**
Sum of mixed MLCT + d-d		**0 %**

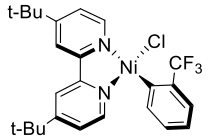

5B with Ni–C distance of 3.50 Å (dissociation limit) – CASSCF/NEVPT2 composition of the singlet ground state with CPCM(THF) (10e,8o Active Space) – 25 triplet roots, 15 singlet roots. Active Space Orbitals (in order for CI vector notation below): d(xy), d(yz), d(z^2), d(xz), d(x^2-y^2)/C(sp^2), d(x^2-y^2)/C(sp^2)*, π*(1), π*(2).

CI vector	Transition	Contribution
22211110	d(xz) + d(x^2-y^2)/C(sp^2) → d(x^2-y^2)/C(sp^2)* + π*(1)	0.7774
22112110	d(z^2) + d(xz) → d(x^2-y^2)/C(sp^2)* + π*(1)	0.0569
22221100	d(x^2-y^2)/C(sp^2) → d(x^2-y^2)/C(sp^2)*	0.0410
11222110	d(xy) + d(yz) → d(x^2-y^2)/C(sp^2)* + π*(1)	0.0310
21221110	d(yz) + d(x^2-y^2)/C(sp^2) → d(x^2-y^2)/C(sp^2)* + π*(1)	0.0298
22212010	d(xz) → π*(1)	0.0265
22210210	2x[d(x^2-y^2)/C(sp^2)] + d(xz) → 2x[d(x^2-y^2)/C(sp^2)*] + π*(1)	0.0120
Sum of CSS		**0 %**
Sum of all MLCT		**3 %**
Sum of all d-d		**4 %**
Sum of mixed MLCT + d-d		**91 %**

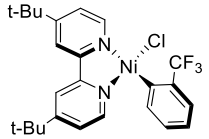

5B with Ni–C distance of 3.50 Å (dissociation limit) – CASSCF/QD-NEVPT2 composition of the singlet ground state with CPCM(THF) (10e,8o Active Space) – 25 triplet roots, 15 singlet roots. Active Space Orbitals (in order for CI vector notation below): d(xy), d(yz), d(z^2), d(xz), d(x^2-y^2)/C(sp^2), d(x^2-y^2)/C(sp^2)*, π*(1), π*(2).

CI vector	Transition	Contribution
22211110	d(xz) + d(x^2-y^2)/C(sp^2) → d(x^2-y^2)/C(sp^2)* + π*(1)	0.7386
22112110	d(z^2) + d(xz) → d(x^2-y^2)/C(sp^2)* + π*(1)	0.0546
22221100	d(x^2-y^2)/C(sp^2) → d(x^2-y^2)/C(sp^2)*	0.0502
21221110	d(yz) + d(x^2-y^2)/C(sp^2) → d(x^2-y^2)/C(sp^2)* + π*(1)	0.0340
22211101	d(xz) + d(x^2-y^2)/C(sp^2) → d(x^2-y^2)/C(sp^2)* + π*(2)	0.0282
22212010	d(xz) → π*(1)	0.0270
11222110	d(xy) + d(yz) → d(x^2-y^2)/C(sp^2)* + π*(1)	0.0261
22210210	2x[d(x^2-y^2)/C(sp^2)] + d(xz) → 2x[d(x^2-y^2)/C(sp^2)*] + π*(1)	0.0122
Sum of CSS		**0 %**
Sum of all MLCT		**3 %**
Sum of all d-d		**5 %**
Sum of mixed MLCT + d-d		**89 %**

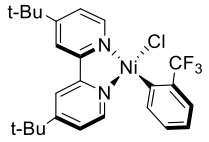

5B – CASSCF/NEVPT2 spin-orbit corrected absorption transitions for the CPCM(THF) phase spectrum (10e,9o Active Space) – 25 triplet roots, 15 singlet roots.

***E*/nm**	***E*/kcal mol^{-1}**	f_{osc}	***E*/nm**	***E*/kcal mol^{-1}**	f_{osc}
775.3	36.9	0.0000035	407.4	70.2	0.0000892
773.4	37.0	0.0000058	399.5	71.6	0.0018597
758.8	37.7	0.0000320	392.4	72.9	0.1140947
689.3	41.5	0.0002312	381.4	75.0	0.0059127
689.1	41.5	0.0000027	381.0	75.0	0.0000009
684.3	41.8	0.0034615	380.3	75.2	0.0000480
677.7	42.2	0.0007548	379.9	75.3	0.0004501
620.8	46.1	0.0014952	367.3	77.8	0.0013154
620.4	46.1	0.0000474	363.4	78.7	0.0000009
619.3	46.2	0.0001672	363.3	78.7	0.0000107
592.2	48.3	0.0394283	362.9	78.8	0.0063497
588.8	48.6	0.0000042	354.4	80.7	0.0566202
588.4	48.6	0.0000584	351.3	81.4	0.0000155
581.6	49.2	0.0304658	351.2	81.4	0.0000160
544.2	52.5	0.0009812	349.2	81.9	0.0002629
543.5	52.6	0.0000377	333.8	85.7	0.0031656
543.2	52.6	0.0001405	333.6	85.7	0.0000029
509.2	56.2	0.2122996	333.6	85.7	0.0004599
450.3	63.5	0.0002267	315.9	90.5	0.0000020
446.9	64.0	0.0018854	314.6	90.9	0.0000000
433.8	65.9	0.0000005	313.4	91.2	0.0000007
433.7	65.9	0.0000021	309.3	92.4	0.0000839
432.1	66.2	0.0006937	308.5	92.7	0.0000159
431.7	66.2	0.0066270	307.7	92.9	0.0003997
423.6	67.5	0.0009687	307.7	92.9	0.0000187
421.9	67.8	0.0006371	307.6	92.9	0.0001200
415.1	68.9	0.0007007	307.6	92.9	0.0001895
415.0	68.9	0.0004855	305.0	93.7	0.0000080
414.7	68.9	0.0001347	302.7	94.4	0.0000249
407.9	70.1	0.0000059	300.4	95.2	0.0000012
407.7	70.1	0.0000003			

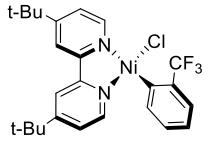

5B – CASSCF/QD-NEVPT2 spin-orbit corrected absorption transitions for the CPCM(THF) phase spectrum (10e,9o Active Space) – 25 triplet roots, 15 singlet roots.

***E*/nm**	***E*/kcal mol^{-1}**	f_{osc}	***E*/nm**	***E*/kcal mol^{-1}**	f_{osc}
777.6	36.8	0.0000778	406.7	70.3	0.0000488
776.9	36.8	0.0000167	406.0	70.4	0.0006701
763.5	37.4	0.0000307	389.7	73.4	0.0006836
685.4	41.7	0.0003172	380.5	75.1	0.1222785
685.1	41.7	0.0000073	378.0	75.6	0.0006220
680.7	42.0	0.0035585	377.5	75.7	0.0002213
674.2	42.4	0.0006906	377.3	75.8	0.0016576
626.8	45.6	0.0000131	376.6	75.9	0.0004395
626.2	45.7	0.0000234	373.7	76.5	0.0000126
624.8	45.8	0.0013510	373.6	76.5	0.0013881
615.4	46.5	0.0020069	372.5	76.8	0.0053733
614.6	46.5	0.0000535	364.7	78.4	0.0006193
613.5	46.6	0.0002180	353.7	80.8	0.0000692
586.3	48.8	0.0684383	353.6	80.9	0.0002588
542.6	52.7	0.0018515	351.7	81.3	0.0004618
541.3	52.8	0.0000294	346.1	82.6	0.0557373
540.9	52.9	0.0000813	332.5	86.0	0.0000116
512.5	55.8	0.2095695	332.4	86.0	0.0002597
472.8	60.5	0.0002479	331.9	86.2	0.0095683
449.1	63.7	0.0016598	317.0	90.2	0.0000170
432.6	66.1	0.0000006	316.3	90.4	0.0000687
432.5	66.1	0.0000263	313.8	91.1	0.0000830
430.7	66.4	0.0006058	309.1	92.5	0.0000073
429.4	66.6	0.0001960	308.7	92.6	0.0002560
423.1	67.6	0.0002920	308.3	92.7	0.0005793
418.7	68.3	0.0021084	306.5	93.3	0.0001046
415.2	68.9	0.0000006	305.3	93.6	0.0002346
415.1	68.9	0.0013927	305.2	93.7	0.0000807
414.9	68.9	0.0000855	301.6	94.8	0.0003092
407.0	70.3	0.0002981	300.7	95.1	0.0001700

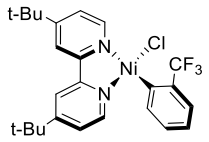

5B – TD-DFT (B3LYP) absorption transitions (singlets only) for the CPCM(THF) phase spectrum.

***E*/nm**	***E*/kcal mol^{-1}**	f_{osc}	***E*/nm**	***E*/kcal mol^{-1}**	f_{osc}
740.5	38.6	0.0000000	363.6	78.6	0.0091097
560.6	51.0	0.0000000	349.3	81.9	0.0001469
555.3	51.5	0.0000000	348.0	82.2	0.0208281
520.5	54.9	0.0000000	345.8	82.7	0.0000000
496.1	57.6	0.0043794	340.4	84.0	0.0000000
492.5	58.1	0.0010825	337.4	84.7	0.0000000
485.0	59.0	0.0016025	322.5	88.7	0.0047156
451.3	63.3	0.0236140	319.5	89.5	0.0000000
442.5	64.6	0.0000000	318.7	89.7	0.0281766
440.7	64.9	0.0002167	317.9	89.9	0.0049837
432.8	66.1	0.0001295	317.4	90.1	0.0000000
422.7	67.6	0.0000000	314.3	91.0	0.0394408
419.3	68.2	0.0515983	308.9	92.6	0.0000000
416.0	68.7	0.0029390	307.9	92.9	0.0000000
414.1	69.0	0.0000000	307.8	92.9	0.0000000
413.2	69.2	0.0126997	307.3	93.0	0.0013021
387.8	73.7	0.0003870	307.2	93.1	0.0102675
383.8	74.5	0.0000000	303.8	94.1	0.0000000
380.0	75.2	0.0000000	303.1	94.3	0.0000000
371.4	77.0	0.0000000			

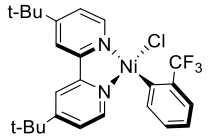

5B – TD-DFT (B3LYP) absorption transitions (singlets only) for the CPCM(Toluene) phase spectrum.

***E*/nm**	***E*/kcal mol^{-1}**	f_{osc}	***E*/nm**	***E*/kcal mol^{-1}**	f_{osc}
726.1	39.4	0.0000000	363.1	78.7	0.0000000
623.8	45.8	0.0000000	362.4	78.9	0.0000990
592.8	48.2	0.0000000	354.5	80.6	0.0000000
592.2	48.3	0.0008706	353.3	80.9	0.0003420
560.6	51.0	0.0000000	352.9	81.0	0.0000000
507.7	56.3	0.0130239	346.0	82.6	0.0301789
499.0	57.3	0.0000000	344.7	82.9	0.0000000
486.5	58.8	0.0000000	343.5	83.2	0.0047315
481.0	59.4	0.0278899	331.0	86.4	0.0075129
477.1	59.9	0.0000000	328.8	87.0	0.0010329
473.8	60.3	0.0000542	323.4	88.4	0.0203753
467.4	61.2	0.0134871	322.2	88.7	0.0000000
442.0	64.7	0.0257018	321.7	88.9	0.0000000
440.7	64.9	0.0069457	318.8	89.7	0.0000000
438.3	65.2	0.0000293	316.9	90.2	0.0000000
432.0	66.2	0.0064669	312.2	91.6	0.0000000
425.5	67.2	0.0005553	311.3	91.9	0.0193375
422.7	67.6	0.0000000	309.8	92.3	0.0000000
421.5	67.8	0.0015698	307.5	93.0	0.0000000
419.2	68.2	0.0000000	306.3	93.3	0.0000000
414.4	69.0	0.0000000	304.5	93.9	0.0876530
383.9	74.5	0.0234636	302.2	94.6	0.0031766
379.9	75.3	0.0000000	300.3	95.2	0.0000000
377.2	75.8	0.0001594	300.0	95.3	0.1308097
373.4	76.6	0.0000000			

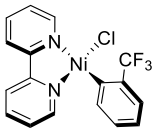

5C with Ni–C distance of 1.90 Å (near-equilibrium geometry) – CASSCF/NEVPT2 lowest transition energies with CPCM(THF) (10e,9o Active Space) – 25 triplet roots, 15 singlet roots. Active Space Orbitals (in order for CI vector notation below): d(x^2-y^2)/C(sp^2), d(xy), d(xz), d(z^2), d(yz), d(x^2-y^2)/C(sp^2)*, π*(1), π*(2), π*(3).

State	Root	Multiplicity	ΔE/nm	ΔE/kcal mol^{-1}	CI vector	Contribution
0	0	1	---	---	222220000	0.5954
					122221000	0.1449
1	0	3	984.1	29.1	221221000	0.5231
					222121000	0.1681
2	1	3	856.4	33.4	222121000	0.5088
					221221000	0.2458
3	2	3	779.2	36.7	222211000	0.6343
					222121000	0.1158
4	3	3	708.5	40.4	221220100	0.5655
					222120100	0.1768
5	1	1	693.7	41.2	221220100	0.5702
					222120100	0.1683
6	4	3	650.2	44.0	222210100	0.3204
					221220100	0.2802
7	2	1	611.3	46.8	222120100	0.5807
					221220100	0.1927
8	5	3	592.6	48.2	212221000	0.7045
					112222000	0.1096
9	6	3	567.3	50.4	222120100	0.4191
					222210100	0.4046
10	3	1	530.7	53.9	222210100	0.5772
11	4	1	459.5	62.2	222121000	0.4598
					212220100	0.2402
12	5	1	448.8	63.7	221221000	0.4763
					222211000	0.1348
13	7	3	427.8	66.8	221220010	0.5626
					222120010	0.1745
14	6	1	426.5	67.0	222211000	0.6397
					221221000	0.1620
15	7	1	425.8	67.2	221220010	0.5623
					222120010	0.1757
16	8	1	424.3	67.4	212221000	0.7656
17	8	3	419.1	68.2	212220100	0.7253
18	9	3	408.7	70.0	222210010	0.2990
					221220010	0.2798
					222120010	0.2608
19	9	1	407.1	70.2	212220100	0.5167
					222121000	0.2072
20	10	1	393.4	72.7	222120010	0.2928
					221220010	0.2660

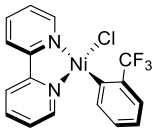

5C with Ni–C distance of 1.90 Å (near-equilibrium geometry) – CASSCF/QD-NEVPT2 lowest transition energies with CPCM(THF) (10e,9o Active Space) – 25 triplet roots, 15 singlet roots. Active Space Orbitals (in order for CI vector notation below): d(x^2-y^2)/C(sp^2), d(xy), d(xz), d(z^2), d(yz), d(x^2-y^2)/C(sp^2)*, π*(1), π*(2), π*(3).

State	Root	Multiplicity	ΔE/nm	ΔE/kcal mol^{-1}	CI vector	Contribution
0	0	1	---	---	222220000	0.5758
					122221000	0.1265
1	0	3	970.2	29.5	221221000	0.5109
					222121000	0.1655
2	1	3	856.7	33.4	222121000	0.5286
					221221000	0.2274
3	2	3	770.4	37.1	222211000	0.6433
					122212000	0.1145
4	3	3	696.2	41.1	221220100	0.5345
					222120100	0.1839
5	1	1	682.6	41.9	221220100	0.5684
					222120100	0.1662
6	4	3	641.7	44.6	221220100	0.2656
					222120100	0.2568
7	5	3	619.2	46.2	212221000	0.6759
8	2	1	607.3	47.1	222120100	0.6033
					221220100	0.1904
9	6	3	559.0	51.2	222210100	0.4057
					222120100	0.3934
10	3	1	531.4	53.8	222210100	0.5523
11	4	1	481.7	59.4	212220100	0.6250
					222121000	0.1072
12	5	1	448.1	63.8	221221000	0.4282
					222121000	0.1171
13	7	3	433.0	66.0	212220100	0.7584
14	8	3	425.6	67.2	221220010	0.5031
					222120010	0.1632
15	6	1	424.9	67.3	222211000	0.3459
					221220010	0.1307
16	7	1	422.0	67.8	221220010	0.3763
					222211000	0.2062
17	8	1	420.5	68.0	212221000	0.5511
					222120010	0.1387
18	9	3	405.4	70.5	222210010	0.2950
					221220010	0.2925
					222120010	0.2353
19	9	1	389.8	73.4	222120010	0.1923
					221220010	0.1770
20	10	3	387.8	73.7	221220001	0.5007
					222120001	0.1586

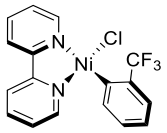

5C with Ni–C distance of 3.50 Å (dissociation limit) – CASSCF/NEVPT2 lowest transition energies with CPCM(THF) (10e,8o Active Space) – 25 triplet roots, 15 singlet roots. Active Space Orbitals (in order for CI vector notation below): d(xy), d(x^2-y^2)/C(sp^2), d(yz), d(z^2), d(xz), d(x^2-y^2)/C(sp^2)*, π*(1), π*(2).

State	Root	Multiplicity	ΔE/nm	ΔE/kcal mol^{-1}	CI vector	Contribution
0	0	1	---	---	22211110	0.8430
1	0	3	433933.0	0.1	22211110	0.7178
2	1	3	22467.1	1.3	22121110	0.7274
3	1	1	8013.3	3.6	22121110	0.9019
4	2	3	7762.1	3.7	22121110	0.8874
5	3	3	5916.6	4.8	22211110	0.8099
6	4	3	4294.4	6.7	21221110	0.7569
7	5	3	3567.4	8.0	21221110	0.8551
8	2	1	3540.3	8.1	21221110	0.8559
9	6	3	1591.3	18.0	21212110	0.4451
					12221110	0.4050
10	3	1	1546.0	18.5	21212110	0.4928
					12221110	0.4423
11	7	3	1432.3	20.0	21212110	0.4592
					12221110	0.4503
12	8	3	1154.3	24.8	12212110	0.7728
13	4	1	1132.7	25.2	12212110	0.8380
14	9	3	1127.2	25.4	22211101	0.8163
15	5	1	1122.1	25.5	22211101	0.8120
16	10	3	1111.0	25.7	22121101	0.8788
17	6	1	1106.9	25.8	22220110	0.7119
18	7	1	1105.1	25.9	22121101	0.8794
19	11	3	1083.9	26.4	22121101	0.8959
20	12	3	1059.3	27.0	22220110	0.8218

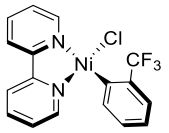

5C with Ni–C distance of 3.50 Å (dissociation limit) – CASSCF/QD-NEVPT2 lowest transition energies with CPCM(THF) (10e,8o Active Space) – 25 triplet roots, 15 singlet roots. Active Space Orbitals (in order for CI vector notation below): d(xy), d(x^2-y^2)/C(sp^2), d(yz), d(z^2), d(xz), d(x^2-y^2)/C(sp^2)*, π*(1), π*(2).

State	Root	Multiplicity	ΔE/nm	ΔE/kcal mol^{-1}	CI vector	Contribution
1	0	1	---	---	22211110	0.7077
2	0	3	1.4	20911.8	22211110	0.7827
3	1	3	3.8	7623.7	22121110	0.8933
4	1	1	4.7	6047.8	22121110	0.8955
5	2	3	5.8	4902.2	22121110	0.9739
6	3	3	6.4	4450.2	22211110	0.8018
7	4	3	8.7	3298.5	21221110	0.8341
8	2	1	9.0	3169.8	21221110	0.7906
9	5	3	10.2	2809.9	21221110	0.8723
10	3	1	21.9	1305.5	21212110	0.4541
					12221110	0.4319
11	6	3	22.5	1273.3	21212110	0.4717
					12221110	0.4631
12	7	3	23.7	1207.2	22220110	0.5383
					12221110	0.1650
					21212110	0.1506
13	4	1	24.1	1188.4	22220110	0.7941
14	8	3	24.3	1177.3	12221110	0.3182
					21212110	0.2977
					22220110	0.2786
15	5	1	26.0	1100.8	22211101	0.6807
16	9	3	26.7	1072.2	22121101	0.7818
17	6	1	26.9	1061.1	22121101	0.8146
18	10	3	27.0	1059.1	22211101	0.6835
					22121101	0.1395
19	11	3	28.2	1012.7	22121101	0.9312
20	12	3	28.9	988.9	22211101	0.8022

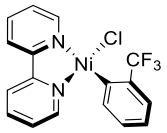

5C with Ni–C distance of 1.90 Å (near-equilibrium geometry) – CASSCF/NEVPT2 composition of the singlet ground state with CPCM(THF) (10e,9o Active Space) – 25 triplet roots, 15 singlet roots. Active Space Orbitals (in order for CI vector notation below): $d(x^2\text{-}y^2)/C(sp^2)$, d(xy), d(xz), $d(z^2)$, d(yz), $d(x^2\text{-}y^2)/C(sp^2)^*$, $\pi^*(1)$, $\pi^*(2)$, $\pi^*(3)$.

CI vector	Transition	Contribution
222220000	Closed-shell singlet (CSS) d^8	0.5954
122221000	$d(x^2\text{-}y^2)/C(sp^2) \rightarrow d(x^2\text{-}y^2)/C(sp^2)^*$	0.1449
222210100	$d(yz) \rightarrow \pi^*(1)$	0.1178
221220100	$d(xz) \rightarrow \pi^*(1)$	0.0347
022212100	$2x[d(x^2\text{-}y^2)/C(sp^2)] + d(yz) \rightarrow 2x[d(x^2\text{-}y^2)/C(sp^2)^*] + \pi^*(1)$	0.0132
220222000	$2x[d(xz)] \rightarrow 2x[d(x^2\text{-}y^2)/C(sp^2)^*]$	0.0122
222120001	$d(z^2) \rightarrow \pi^*(3)$	0.0117
Sum of CSS		**60 %**
Sum of all MLCT		**16 %**
Sum of all d-d		**16 %**
Sum of mixed MLCT + d-d		**1 %**

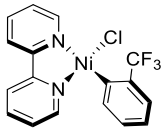

5C with Ni–C distance of 1.90 Å (near-equilibrium geometry) – CASSCF/QD-NEVPT2 composition of the singlet ground state with CPCM(THF) (10e,9o Active Space) – 25 triplet roots, 15 singlet roots. Active Space Orbitals (in order for CI vector notation below): $d(x^2\text{-}y^2)/C(sp^2)$, d(xy), d(xz), $d(z^2)$, d(yz), $d(x^2\text{-}y^2)/C(sp^2)^*$, $\pi^*(1)$, $\pi^*(2)$, $\pi^*(3)$.

CI vector	Transition	Contribution
222220000	Closed-shell singlet (CSS) d^8	0.5758
122221000	$d(x^2\text{-}y^2)/C(sp^2) \rightarrow d(x^2\text{-}y^2)/C(sp^2)^*$	0.1265
222210100	$d(yz) \rightarrow \pi^*(1)$	0.1218
221220100	$d(xz) \rightarrow \pi^*(1)$	0.0340
222120001	$d(z^2) \rightarrow \pi^*(3)$	0.0267
222210010	$d(yz) \rightarrow \pi^*(2)$	0.0148
022212100	$2x[d(x^2\text{-}y^2)/C(sp^2)] + d(yz) \rightarrow 2x[d(x^2\text{-}y^2)/C(sp^2)^*] + \pi^*(1)$	0.0135
Sum of CSS		**58 %**
Sum of all MLCT		**20 %**
Sum of all d-d		**13 %**
Sum of mixed MLCT + d-d		**1 %**

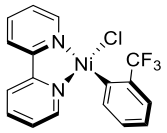

5C with Ni–C distance of 3.50 Å (dissociation limit) – CASSCF/NEVPT2 composition of the singlet ground state with CPCM(THF) (10e,8o Active Space) – 25 triplet roots, 15 singlet roots. Active Space Orbitals (in order for CI vector notation below): d(xy), d(x^2-y^2)/C(sp^2), d(yz), d(z^2), d(xz), d(x^2-y^2)/C(sp^2)*, π*(1), π*(2).

CI vector	Transition	Contribution
22211110	d(z^2) + d(xz) → d(x^2-y^2)/C(sp^2)* + π*(1)	0.8430
11222110	d(xy) + d(x^2-y^2)/C(sp^2) → d(x^2-y^2)/C(sp^2)* + π*(1)	0.0497
22221100	d(xz) → d(x^2-y^2)/C(sp^2)*	0.0411
22112110	d(yz) + d(z^2) → d(x^2-y^2)/C(sp^2)* + π*(1)	0.0284
21122110	d(x^2-y^2)/C(sp^2) + d(yz) → d(x^2-y^2)/C(sp^2)* + π*(1)	0.0143
Sum of CSS		**0 %**
Sum of all MLCT		**0 %**
Sum of all d-d		**4 %**
Sum of mixed MLCT + d-d		**94 %**

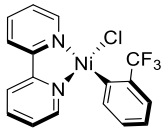

5C with Ni–C distance of 3.50 Å (dissociation limit) – CASSCF/QD-NEVPT2 composition of the singlet ground state with CPCM(THF) (10e,8o Active Space) – 25 triplet roots, 15 singlet roots. Active Space Orbitals (in order for CI vector notation below): d(xy), d(x^2-y^2)/C(sp^2), d(yz), d(z^2), d(xz), d(x^2-y^2)/C(sp^2)*, π*(1), π*(2).

CI vector	Transition	Contribution
22211110	d(z^2) + d(xz) → d(x^2-y^2)/C(sp^2)* + π*(1)	0.7077
22112110	d(yz) + d(z^2) → d(x^2-y^2)/C(sp^2)* + π*(1)	0.0599
22212010	d(z^2) → π*(1)	0.0533
22221100	d(xz) → d(x^2-y^2)/C(sp^2)*	0.0488
21221110	d(x^2-y^2)/C(sp^2) + d(xz) → d(x^2-y^2)/C(sp^2)* + π*(1)	0.0364
11222110	d(xy) + d(x^2-y^2)/C(sp^2) → d(x^2-y^2)/C(sp^2)* + π*(1)	0.0243
22210210	d(yz) + 2x[d(xz)] → 2x[d(x^2-y^2)/C(sp^2)*] + π*(1)	0.0241
22211101	d(z^2) + d(xz) → d(x^2-y^2)/C(sp^2)* + π*(2)	0.0145
Sum of CSS		**0 %**
Sum of all MLCT		**5 %**
Sum of all d-d		**5 %**
Sum of mixed MLCT + d-d		**87 %**

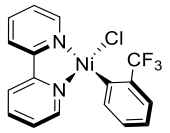

5C – CASSCF/NEVPT2 spin-orbit corrected absorption transitions for the CPCM(THF) phase spectrum (10e,9o Active Space) – 25 triplet roots, 15 singlet roots.

***E*/nm**	***E*/kcal mol^{-1}**	f_{osc}	***E*/nm**	***E*/kcal mol^{-1}**	f_{osc}
771.2	37.1	0.0000025	405.1	70.6	0.0000553
769.6	37.2	0.0000090	392.3	72.9	0.0942350
755.5	37.8	0.0000619	386.4	74.0	0.0003623
718.6	39.8	0.0002211	364.8	78.4	0.0024644
718.3	39.8	0.0000018	364.2	78.5	0.0000104
712.7	40.1	0.0032726	364.0	78.6	0.0047577
705.8	40.5	0.0005742	363.7	78.6	0.0003078
645.1	44.3	0.0014162	363.5	78.7	0.0005484
644.4	44.4	0.0000045	363.3	78.7	0.0056258
643.1	44.5	0.0001086	362.2	78.9	0.0947149
608.2	47.0	0.0656460	361.4	79.1	0.0001273
589.9	48.5	0.0000191	346.2	82.6	0.0000019
589.4	48.5	0.0000078	346.1	82.6	0.0000110
587.6	48.7	0.0008252	341.0	83.8	0.0362738
561.0	51.0	0.0013321	339.4	84.2	0.0001071
560.2	51.0	0.0000112	335.0	85.3	0.0000078
559.8	51.1	0.0000419	334.5	85.5	0.0048052
525.4	54.4	0.2370075	327.3	87.4	0.1734043
458.0	62.4	0.0001610	317.6	90.0	0.0000446
447.4	63.9	0.0019124	317.0	90.2	0.0032582
431.7	66.2	0.0000203	315.0	90.8	0.0002640
431.7	66.2	0.0000020	314.3	91.0	0.0000315
429.9	66.5	0.0051154	311.5	91.8	0.0073473
429.9	66.5	0.0008695	311.3	91.8	0.0004756
426.8	67.0	0.0005686	309.7	92.3	0.0000095
423.7	67.5	0.0006059	307.3	93.0	0.0003671
417.3	68.5	0.0008650	307.2	93.1	0.0000249
416.6	68.6	0.0001637	307.2	93.1	0.0000262
416.6	68.6	0.0000785	306.8	93.2	0.0006461
406.2	70.4	0.0002483	305.3	93.7	0.0002974
405.5	70.5	0.0001825	302.4	94.5	0.0001211
405.3	70.6	0.0000480	301.1	95.0	0.0000152

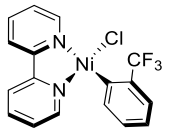

5C – CASSCF/QD-NEVPT2 spin-orbit corrected absorption transitions for the CPCM(THF) phase spectrum (10e,9o Active Space) – 25 triplet roots, 15 singlet roots.

***E*/nm**	***E*/kcal mol^{-1}**	f_{osc}	***E*/nm**	***E*/kcal mol^{-1}**	f_{osc}
763.4	37.5	0.0000045	402.7	71.0	0.0000200
763.0	37.5	0.0000080	402.2	71.1	0.0001142
750.5	38.1	0.0000678	390.8	73.2	0.0017081
705.9	40.5	0.0002985	389.7	73.4	0.0000092
705.5	40.5	0.0000002	389.6	73.4	0.0010704
700.8	40.8	0.0036045	387.6	73.8	0.0018656
693.6	41.2	0.0007913	382.2	74.8	0.0959134
636.7	44.9	0.0022416	380.0	75.2	0.0106898
636.2	44.9	0.0000008	369.0	77.5	0.0000029
635.2	45.0	0.0000994	368.9	77.5	0.0000196
616.1	46.4	0.0000188	368.5	77.6	0.0013688
615.7	46.4	0.0006190	361.9	79.0	0.0006556
614.5	46.5	0.0007662	359.4	79.6	0.0000410
601.2	47.6	0.0646565	359.2	79.6	0.0088950
553.8	51.6	0.0040293	358.9	79.7	0.0009258
552.4	51.8	0.0000021	349.8	81.7	0.0882684
551.8	51.8	0.0000678	335.1	85.3	0.0000039
526.4	54.3	0.2325002	334.9	85.4	0.0089677
478.9	59.7	0.0001625	334.9	85.4	0.0009882
447.2	63.9	0.0019357	318.2	89.9	0.2236957
431.2	66.3	0.0001980	314.5	90.9	0.0004537
431.2	66.3	0.0003570	313.8	91.1	0.0006551
431.2	66.3	0.0005773	311.3	91.8	0.0000737
429.1	66.6	0.0000083	306.3	93.3	0.0000052
429.1	66.6	0.0001184	305.9	93.5	0.0000708
427.6	66.9	0.0009475	305.7	93.5	0.0000159
426.9	67.0	0.0003153	304.5	93.9	0.0009223
422.6	67.7	0.0004073	302.6	94.5	0.0000601
418.6	68.3	0.0002422	300.2	95.2	0.0022000
402.7	71.0	0.0000927			

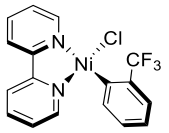

5C – TD-DFT (B3LYP) absorption transitions (singlets only) for the CPCM(THF) phase spectrum.

***E*/nm**	***E*/kcal mol^{-1}**	f_{osc}	***E*/nm**	***E*/kcal mol^{-1}**	f_{osc}
730.2	39.2	0.0000000	360.9	79.2	0.0000000
580.2	49.3	0.0000000	358.7	79.7	0.0000060
561.8	50.9	0.0000000	357.1	80.1	0.0070012
546.3	52.3	0.0000000	352.5	81.1	0.0000000
518.0	55.2	0.0023225	348.9	81.9	0.0000000
499.2	57.3	0.0053683	336.5	85.0	0.0000000
474.3	60.3	0.0000890	334.1	85.6	0.0065927
453.8	63.0	0.0000000	325.1	87.9	0.0265813
448.4	63.8	0.0170550	321.5	88.9	0.0000000
445.4	64.2	0.0000000	319.6	89.5	0.0205561
438.1	65.3	0.0008455	319.2	89.6	0.0091146
436.4	65.5	0.0304925	317.5	90.1	0.0119539
436.1	65.6	0.0010648	315.2	90.7	0.0000000
430.6	66.4	0.0062312	312.5	91.5	0.0000000
428.1	66.8	0.0193447	312.0	91.6	0.0000000
410.5	69.7	0.0000000	311.9	91.7	0.0000000
401.8	71.2	0.0000000	310.3	92.1	0.0336837
395.2	72.3	0.0035365	309.2	92.5	0.0000000
389.0	73.5	0.0002908	303.7	94.2	0.0000000
387.5	73.8	0.0000000	302.3	94.6	0.0141345
372.8	76.7	0.0000000	300.1	95.3	0.0037223

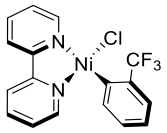

5C – TD-DFT (B3LYP) absorption transitions (singlets only) for the CPCM(Toluene) phase spectrum.

***E*/nm**	***E*/kcal mol^{-1}**	f_{osc}	***E*/nm**	***E*/kcal mol^{-1}**	f_{osc}
714.7	40.0	0.0000000	383.4	74.6	0.0000000
657.3	43.5	0.0000000	381.7	74.9	0.0000000
632.0	45.2	0.0007808	367.1	77.9	0.0000000
631.0	45.3	0.0000000	357.4	80.0	0.0274102
561.7	50.9	0.0000000	352.2	81.2	0.0000000
537.7	53.2	0.0000000	351.4	81.4	0.0000000
525.4	54.4	0.0154291	346.8	82.4	0.0017050
520.0	55.0	0.0085450	345.5	82.7	0.0012754
508.3	56.2	0.0000000	345.4	82.8	0.0000000
502.5	56.9	0.0000000	345.3	82.8	0.0000000
473.8	60.4	0.0000291	345.1	82.9	0.0054869
465.5	61.4	0.0093342	344.9	82.9	0.0071996
460.7	62.1	0.0074491	335.4	85.2	0.0190400
451.0	63.4	0.0011631	333.9	85.6	0.0000000
446.1	64.1	0.0000000	331.2	86.3	0.0008952
445.6	64.2	0.0378068	330.3	86.6	0.0253975
438.5	65.2	0.0008962	329.7	86.7	0.0000000
432.6	66.1	0.0029823	319.0	89.6	0.0000000
428.2	66.8	0.0003323	316.7	90.3	0.0000000
426.4	67.1	0.0000000	309.5	92.4	0.0000000
424.2	67.4	0.0000000	308.8	92.6	0.0000000
398.2	71.8	0.0077311	307.3	93.0	0.0000000
389.7	73.4	0.0000838	304.9	93.8	0.0037630
386.1	74.1	0.0000000	302.6	94.5	0.0798152
383.6	74.5	0.0012814	302.4	94.6	0.0060800

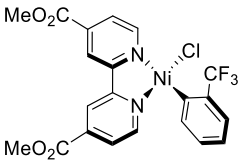

5D with Ni–C distance of 1.90 Å (near-equilibrium geometry) – CASSCF/NEVPT2 lowest transition energies with CPCM(THF) (10e,9o Active Space) – 25 triplet roots, 15 singlet roots. Active Space Orbitals (in order for CI vector notation below): d(xy), d(x^2-y^2)/C(sp^2), d(yz), d(xz), d(z^2), d(x^2-y^2)/C(sp^2)*, π*(1), π*(2), π*(3).

State	Root	Multiplicity	ΔE/nm	ΔE/kcal mol^{-1}	CI vector	Contribution
0	0	1	---	---	222220000	0.4852
					222120100	0.2865
1	0	3	983.4	29.1	222211000	0.7552
					212212000	0.1022
2	1	3	846.3	33.8	222210100	0.7611
3	2	3	846.1	33.8	221221000	0.4009
					222121000	0.3605
4	1	1	828.0	34.5	222210100	0.8191
5	3	3	775.0	36.9	222121000	0.4015
					221221000	0.3434
6	4	3	763.1	37.5	222120100	0.7477
7	2	1	697.6	41.0	221220100	0.6280
					222120100	0.1395
8	5	3	648.2	44.1	221220100	0.7298
9	3	1	631.3	45.3	222120100	0.3667
					221220100	0.1552
					222220000	0.1511
10	6	3	595.6	48.0	122221000	0.4831
					212221000	0.2074
					221122000	0.1218
11	7	3	490.8	58.3	222210010	0.8110
12	4	1	490.2	58.3	122220100	0.4638
					212220100	0.1889
					221121100	0.1012
13	5	1	489.9	58.4	222210010	0.8063
14	8	3	475.7	60.1	122220100	0.5435
					212220100	0.2219
15	9	3	463.7	61.7	222120010	0.7497
16	6	1	458.7	62.3	222211000	0.4023
					222120010	0.2317
					122221000	0.1210
17	10	3	458.6	62.3	222210001	0.8081
18	7	1	457.7	62.5	222210001	0.7743
19	8	1	438.4	65.2	222121000	0.5914
20	11	3	431.8	66.2	222120001	0.7548

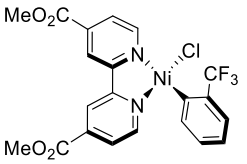

5D with Ni–C distance of 1.90 Å (near-equilibrium geometry) – CASSCF/QD-NEVPT2 lowest transition energies with CPCM(THF) (10e,9o Active Space) – 25 triplet roots, 15 singlet roots. Active Space Orbitals (in order for CI vector notation below): d(xy), d(x^2-y^2)/C(sp^2), d(yz), d(xz), d(z^2), d(x^2-y^2)/C(sp^2)*, π*(1), π*(2), π*(3).

State	Root	Multiplicity	ΔE/nm	ΔE/kcal mol^{-1}	CI vector	Contribution
0	0	1	---	---	222220000	0.5474
					222120100	0.1874
1	0	3	976.9	29.3	222211000	0.5815
					222210100	0.2126
2	1	3	852.4	33.5	221221000	0.3000
					222210100	0.2727
					222121000	0.1554
3	2	3	838.3	34.1	222121000	0.2481
					222120100	0.2362
					222210100	0.2024
4	1	1	807.4	35.4	222210100	0.8154
5	3	3	760.1	37.6	221221000	0.3310
					222120100	0.2764
					222210100	0.1329
6	4	3	709.7	40.3	222121000	0.3679
					222120100	0.2309
					221220100	0.1136
7	2	1	689.8	41.4	221220100	0.4020
					222120100	0.3202
8	5	3	637.3	44.9	221220100	0.6499
9	3	1	613.5	46.6	221220100	0.3764
					222120100	0.2350
10	6	3	596.8	47.9	122221000	0.4801
					212221000	0.2023
11	4	1	484.6	59.0	122220100	0.5112
					212220100	0.2029
12	7	3	482.1	59.3	222210010	0.8016
13	5	1	481.3	59.4	222210010	0.7047
14	6	1	474.5	60.3	222120010	0.5251
15	8	3	467.9	61.1	122220100	0.5386
					212220100	0.2152
16	9	3	455.8	62.7	222120010	0.7465
17	7	1	452.5	63.2	222210001	0.7621
18	10	3	451.0	63.4	222210001	0.8027
19	8	1	433.2	66.0	222120001	0.3915
					222121000	0.2096
20	11	3	424.4	67.4	222120001	0.7536

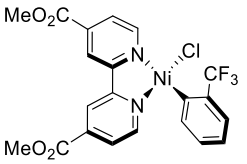

5D with Ni–C distance of 3.50 Å (dissociation limit) – CASSCF/NEVPT2 lowest transition energies with CPCM(THF) (10e,8o Active Space) – 25 triplet roots, 15 singlet roots. Active Space Orbitals (in order for CI vector notation below): d(xy), d(yz), d(xz), d(z^2), d(x^2-y^2)/C(sp^2), d(x^2-y^2)/C(sp^2)*, π*(1), π*(2).

State	Root	Multiplicity	ΔE/nm	ΔE/kcal mol^{-1}	CI vector	Contribution
0	0	3	---	---	22211110	0.7621
1	0	1	144645.0	0.2	22211110	0.8389
2	1	3	23693.9	1.2	22121110	0.6080
					21221110	0.1898
3	1	1	8845.5	3.2	22121110	0.6997
					21221110	0.2182
4	2	3	8675.4	3.3	22121110	0.7141
					21221110	0.1922
5	3	3	5781.4	4.9	22211110	0.8421
6	4	3	4231.4	6.8	21221110	0.6016
					22121110	0.1771
7	5	3	3628.0	7.9	21221110	0.6604
					22121110	0.1760
8	2	1	3577.8	8.0	21221110	0.6547
					22121110	0.1885
9	6	3	1562.1	18.3	12221110	0.4151
					21212110	0.3615
					22112110	0.1032
10	3	1	1516.7	18.9	12221110	0.4489
					21212110	0.3929
					22112110	0.1122
11	7	3	1409.8	20.3	12221110	0.4589
					21212110	0.3610
					22112110	0.1057
12	8	3	1206.5	23.7	22121101	0.6931
					21221101	0.2127
13	4	1	1198.6	23.9	22121101	0.6882
					21221101	0.2179
14	9	3	1180.3	24.2	22121101	0.7223
					21221101	0.1867
15	10	3	1128.3	25.3	12212110	0.8523
16	5	1	1123.9	25.4	22220110	0.7236
17	6	1	1108.6	25.8	12212110	0.9091
18	11	3	1078.2	26.5	22220110	0.7051
19	7	1	1071.6	26.7	22211101	0.4251
					21221101	0.3329
					22121101	0.1168
20	12	3	1069.0	26.7	22211101	0.5558
					21221101	0.2265

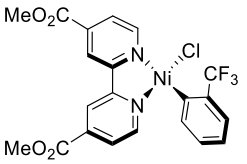

5D with Ni–C distance of 3.50 Å (dissociation limit) – CASSCF/QD-NEVPT2 lowest transition energies with CPCM(THF) (10e,8o Active Space) – 25 triplet roots, 15 singlet roots. Active Space Orbitals (in order for CI vector notation below): d(xy), d(yz), d(xz), d(z^2), d(x^2-y^2)/C(sp^2), d(x^2-y^2)/C(sp^2)*, π*(1), π*(2).

State	Root	Multiplicity	ΔE/nm	ΔE/kcal mol^{-1}	CI vector	Contribution
0	0	3	---	---	22121110	0.6856
1	0	1	---	0.0	22121110	0.6873
2	1	3	17796.8	1.6	22211110	0.7623
					12221110	0.1589
3	2	3	10695.2	2.7	22211110	0.7181
					12221110	0.1469
4	1	1	10486.6	2.7	22211110	0.7183
					12221110	0.1470
5	3	3	4896.9	5.8	22121110	0.7002
					21221110	0.1404
6	4	3	3499.6	8.2	21221110	0.6906
					22121110	0.1453
7	5	3	3401.6	8.4	21221110	0.7252
8	2	1	3397.1	8.4	21221110	0.7257
9	6	3	1523.2	18.8	21122110	0.4624
					12221110	0.4050
10	3	1	1522.2	18.8	21122110	0.4629
					12221110	0.4058
11	7	3	1371.9	20.8	21122110	0.4434
					12221110	0.4199
12	8	3	1241.1	23.0	22211101	0.7597
					12221101	0.1564
13	9	3	1230.7	23.2	22211101	0.7592
					12221101	0.1538
14	4	1	1227.8	23.3	22211101	0.7591
					12221101	0.1534
15	5	1	1151.9	24.8	12122110	0.5827
					22121101	0.1314
16	10	3	1149.8	24.9	12122110	0.5849
					22121101	0.1424
17	11	3	1068.5	26.8	22121101	0.5647
					12122110	0.1030
18	6	1	1068.3	26.8	22121101	0.5689
19	12	3	1050.7	27.2	22121101	0.7059
					21221101	0.1284
20	7	1	1021.0	28.0	22220110	0.5580
					22121101	0.1287
					21221101	0.1006

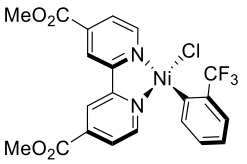

5D with Ni–C distance of 1.90 Å (near-equilibrium geometry) – CASSCF/NEVPT2 composition of the singlet ground state with CPCM(THF) (10e,9o Active Space) – 25 triplet roots, 15 singlet roots. Active Space Orbitals (in order for CI vector notation below): d(xy), d(x^2-y^2)/C(sp^2), d(yz), d(xz), d(z^2), d(x^2-y^2)/C(sp^2)*, π*(1), π*(2), π*(3).

CI vector	Transition	Contribution
222220000	Closed-shell singlet (CSS) d^8	0.4852
222120100	d(xz) → π*(1)	0.2865
212221000	d(x^2-y^2)/C(sp^2) → d(x^2-y^2)/C(sp^2)*	0.0658
122221000	d(xy) → d(x^2-y^2)/C(sp^2)*	0.0266
202122100	2x[d(x^2-y^2)/C(sp^2)] + d(xz) → 2x[d(x^2-y^2)/C(sp^2)*] + π*(1)	0.0180
112122100	d(x^2-y^2)/C(sp^2) + d(xy) + d(xz) → 2x[d(x^2-y^2)/C(sp^2)*] + π*(1)	0.0136
221220010	d(yz) → π*(2)	0.0106
221220100	d(yz)→ π*(1)	0.0106
Sum of CSS		**49 %**
Sum of all MLCT		**31 %**
Sum of all d-d		**9 %**
Sum of mixed MLCT + d-d		**3 %**

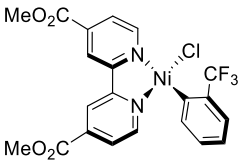

5D with Ni–C distance of 1.90 Å (near-equilibrium geometry) – CASSCF/QD-NEVPT2 composition of the singlet ground state with CPCM(THF) (10e,9o Active Space) – 25 triplet roots, 15 singlet roots. Active Space Orbitals (in order for CI vector notation below): d(xy), d(x^2-y^2)/C(sp^2), d(yz), d(xz), d(z^2), d(x^2-y^2)/C(sp^2)*, π*(1), π*(2), π*(3).

CI vector	Transition	Contribution
222220000	Closed-shell singlet (CSS) d^8	0.5474
222120100	d(xz) → π*(1)	0.1874
212221000	d(x^2-y^2)/C(sp^2) → d(x^2-y^2)/C(sp^2)*	0.0772
122221000	d(xy) → d(x^2-y^2)/C(sp^2)*	0.0316
221220010	d(yz) → π*(2)	0.0207
221220001	d(yz) → π*(3)	0.0190
222120010	d(xz)→ π*(2)	0.0124
202122100	2x[d(x^2-y^2)/C(sp^2)] + d(xz) → 2x[d(x^2-y^2)/C(sp^2)*] + π*(1)	0.0123
Sum of CSS		**55 %**
Sum of all MLCT		**24 %**
Sum of all d-d		**11 %**
Sum of mixed MLCT + d-d		**1 %**

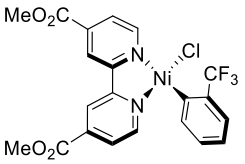

5D with Ni–C distance of 3.50 Å (dissociation limit) – CASSCF/NEVPT2 composition of the singlet ground state with CPCM(THF) (10e,8o Active Space) – 25 triplet roots, 15 singlet roots. Active Space Orbitals (in order for CI vector notation below): d(xy), d(yz), d(xz), d(z^2), d(x^2-y^2)/C(sp^2), d(x^2-y^2)/C(sp^2)*, π*(1), π*(2).

CI vector	Transition	Contribution
22211110	d(x^2-y^2)/C(sp^2) + d(z^2) → d(x^2-y^2)/C(sp^2)* + π*(1)	0.8389
22221100	d(x^2-y^2)/C(sp^2) → d(x^2-y^2)/C(sp^2)*	0.0436
11222110	d(xy) + d(yz) → d(x^2-y^2)/C(sp^2)* + π*(1)	0.0393
22121110	d(xz) + d(x^2-y^2)/C(sp^2) → d(x^2-y^2)/C(sp^2)* + π*(1)	0.0261
21122110	d(yz) + d(xz) → d(x^2-y^2)/C(sp^2)* + π*(1)	0.0259
12122110	d(xy) + d(xz) → d(x^2-y^2)/C(sp^2)* + π*(1)	0.0115
Sum of CSS		**0 %**
Sum of all MLCT		**0 %**
Sum of all d-d		**4 %**
Sum of mixed MLCT + d-d		**94 %**

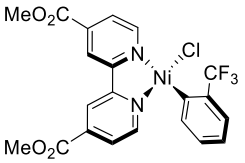

5D with Ni–C distance of 3.50 Å (dissociation limit) – CASSCF/QD-NEVPT2 composition of the singlet ground state with CPCM(THF) (10e,8o Active Space) – 25 triplet roots, 15 singlet roots. Active Space Orbitals (in order for CI vector notation below): d(xy), d(yz), d(xz), d(z^2), d(x^2-y^2)/C(sp^2), d(x^2-y^2)/C(sp^2)*, π*(1), π*(2).

CI vector	Transition	Contribution
22121110	d(xz) + d(x^2-y^2)/C(sp^2) → d(x^2-y^2)/C(sp^2)* + π*(1)	0.68730
22211110	d(x^2-y^2)/C(sp^2) + d(z^2) → d(x^2-y^2)/C(sp^2)* + π*(1)	0.07561
21221110	d(yz) + d(x^2-y^2)/C(sp^2) → d(x^2-y^2)/C(sp^2)* + π*(1)	0.06710
22221100	d(x^2-y^2)/C(sp^2) → d(x^2-y^2)/C(sp^2)*	0.04856
11222110	d(xy) + d(yz) → d(x^2-y^2)/C(sp^2)* + π*(1)	0.03911
21221101	d(yz) + d(x^2-y^2)/C(sp^2) → d(x^2-y^2)/C(sp^2)* + π*(2)	0.01809
12122110	d(xy) + d(xz) → d(x^2-y^2)/C(sp^2)* + π*(1)	0.01636
22112110	d(xz) + d(z^2) → d(x^2-y^2)/C(sp^2)* + π*(1)	0.01541
12221110	d(xy) + d(x^2-y^2)/C(sp^2) → d(x^2-y^2)/C(sp^2)* + π*(1)	0.01174
Sum of CSS		**0 %**
Sum of all MLCT		**0%**
Sum of all d-d		**5 %**
Sum of mixed MLCT + d-d		**93 %**

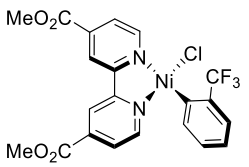

5D – CASSCF/NEVPT2 spin-orbit corrected absorption transitions for the CPCM(THF) phase spectrum (10e,9o Active Space) – 25 triplet roots, 15 singlet roots.

***E*/nm**	***E*/kcal mol^{-1}**	f_{osc}	***E*/nm**	***E*/kcal mol^{-1}**	f_{osc}
768.8	37.2	0.0002621	460.1	62.1	0.0001112
766.3	37.3	0.0003275	459.8	62.2	0.0001265
756.5	37.8	0.0006884	455.5	62.8	0.0651811
755.0	37.9	0.0015997	437.2	65.4	0.0412818
753.7	37.9	0.0002683	430.8	66.4	0.1601436
750.4	38.1	0.0009108	429.9	66.5	0.0005208
689.2	41.5	0.0584753	428.9	66.7	0.0088018
642.9	44.5	0.0336157	428.3	66.8	0.0051300
639.3	44.7	0.0000029	427.1	66.9	0.0060153
639.2	44.7	0.0000743	426.3	67.1	0.0180058
629.8	45.4	0.1950159	414.0	69.1	0.0003513
592.7	48.2	0.0000052	413.7	69.1	0.0000000
592.3	48.3	0.0000018	412.5	69.3	0.0095940
585.4	48.8	0.0349406	412.1	69.4	0.0414799
495.5	57.7	0.0000006	403.7	70.8	0.0767962
495.5	57.7	0.0028604	393.1	72.7	0.0000011
494.8	57.8	0.0006131	393.0	72.8	0.0002871
493.3	58.0	0.0181431	392.9	72.8	0.0008391
487.7	58.6	0.0008271	379.4	75.4	0.2089767
473.6	60.4	0.0000207	334.4	85.5	0.0000001
473.4	60.4	0.0000095	334.3	85.5	0.0003608
473.4	60.4	0.0004618	334.3	85.5	0.0004196
462.5	61.8	0.0033080	306.5	93.3	0.0000049
462.5	61.8	0.0044412	305.5	93.6	0.0000004
462.1	61.9	0.0034408	303.8	94.1	0.0000011
461.4	62.0	0.0015125	300.7	95.1	0.0000223
460.3	62.1	0.0231218			

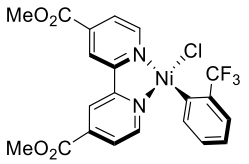

5D – CASSCF/QD-NEVPT2 spin-orbit corrected absorption transitions for the CPCM(THF) phase spectrum (10e,9o Active Space) – 25 triplet roots, 15 singlet roots.

***E*/nm**	***E*/kcal mol^{-1}**	f_{osc}	***E*/nm**	***E*/kcal mol^{-1}**	f_{osc}
758.6	37.7	0.0030556	452.2	63.2	0.0001246
754.0	37.9	0.0008331	451.8	63.3	0.0001250
746.9	38.3	0.0003013	450.6	63.5	0.0208336
707.4	40.4	0.0019030	430.2	66.5	0.0012843
704.5	40.6	0.0080976	423.0	67.6	0.0268139
701.7	40.7	0.0002133	421.9	67.8	0.0029053
685.2	41.7	0.0307524	421.5	67.8	0.0035269
630.4	45.4	0.0267623	420.7	68.0	0.0160554
628.5	45.5	0.0003751	415.5	68.8	0.1136537
628.1	45.5	0.0038891	409.2	69.9	0.0271454
608.8	47.0	0.2415429	407.5	70.2	0.0044751
593.9	48.1	0.0007335	407.5	70.2	0.0002885
592.6	48.2	0.0001039	405.8	70.5	0.0087835
590.1	48.5	0.0200192	401.9	71.1	0.0764542
489.9	58.4	0.0268488	393.7	72.6	0.0345167
486.6	58.8	0.0000154	385.9	74.1	0.0008208
486.1	58.8	0.0007498	385.9	74.1	0.0000373
485.5	58.9	0.0086927	385.8	74.1	0.0000942
482.0	59.3	0.0004380	368.5	77.6	0.2180530
469.2	60.9	0.0471928	330.5	86.5	0.0002236
465.8	61.4	0.0002292	330.4	86.5	0.0000148
465.7	61.4	0.0003089	330.4	86.5	0.0002164
465.6	61.4	0.0008977	308.7	92.6	0.0001099
456.3	62.7	0.0597101	308.3	92.8	0.0000443
454.8	62.9	0.0000150	305.3	93.6	0.0000624
454.7	62.9	0.0000819	300.2	95.2	0.0000058
454.1	63.0	0.0069101			

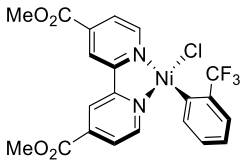

5D – TD-DFT (B3LYP) absorption transitions (singlets only) for the CPCM(THF) phase spectrum.

***E*/nm**	***E*/kcal mol^{-1}**	f_{osc}	***E*/nm**	***E*/kcal mol^{-1}**	f_{osc}
776.6	36.8	0.0000000	389.9	73.3	0.0000000
703.6	40.6	0.0000000	378.6	75.5	0.0000000
690.8	41.4	0.0000000	376.9	75.9	0.0000000
674.9	42.4	0.0007586	375.7	76.1	0.0287201
669.3	42.7	0.0000000	371.1	77.0	0.0000000
564.9	50.6	0.0000000	367.5	77.8	0.0075658
559.5	51.1	0.0234375	362.2	78.9	0.0398702
547.8	52.2	0.0000000	360.4	79.3	0.0206610
533.1	53.6	0.0000000	356.9	80.1	0.0000000
521.1	54.9	0.0000000	355.5	80.4	0.0221700
519.9	55.0	0.0043885	350.2	81.6	0.0000000
472.0	60.6	0.0000000	343.3	83.3	0.0445044
468.8	61.0	0.0003831	343.2	83.3	0.0000000
466.5	61.3	0.0002023	341.1	83.8	0.0260263
466.0	61.4	0.0016708	340.3	84.0	0.0000000
460.7	62.1	0.0471579	336.1	85.1	0.0000000
457.4	62.5	0.0073902	334.9	85.4	0.0000000
454.1	63.0	0.0000000	333.5	85.7	0.0000000
452.2	63.2	0.0001540	332.1	86.1	0.0154172
427.7	66.8	0.0074542	331.1	86.4	0.0000000
425.1	67.3	0.0092833	327.6	87.3	0.1124738
424.9	67.3	0.0041785	319.6	89.5	0.0000000
423.2	67.6	0.0638089	319.4	89.5	0.1815339
418.1	68.4	0.0002807	318.0	89.9	0.0000000
413.4	69.2	0.0000000	314.0	91.1	0.0001908
410.9	69.6	0.0000000	312.7	91.4	0.0000827
408.5	70.0	0.0000000	312.6	91.5	0.0000000
392.9	72.8	0.0000000	302.3	94.6	0.0000000
390.3	73.3	0.0011420			

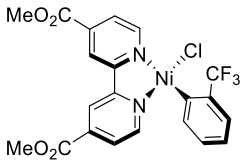

5D – TD-DFT (B3LYP) absorption transitions (singlets only) for the CPCM(Toluene) phase spectrum.

***E*/nm**	***E*/kcal mol^{-1}**	f_{osc}	***E*/nm**	***E*/kcal mol^{-1}**	f_{osc}
781.7	36.6	0.0000000	412.7	69.3	0.0137589
768.1	37.2	0.0000000	411.8	69.4	0.0000000
763.8	37.4	0.0000000	407.8	70.1	0.0000000
757.5	37.7	0.0006640	406.7	70.3	0.0000000
676.0	42.3	0.0000000	386.8	73.9	0.0011484
634.1	45.1	0.0028257	383.7	74.5	0.0356216
626.8	45.6	0.0271883	383.5	74.6	0.0000000
621.0	46.0	0.0000000	382.7	74.7	0.0335421
585.9	48.8	0.0000000	377.9	75.7	0.0000000
574.4	49.8	0.0000000	377.1	75.8	0.0366655
547.2	52.3	0.0000000	375.0	76.2	0.0000000
523.5	54.6	0.0001008	368.0	77.7	0.0291842
522.3	54.7	0.0014984	358.0	79.9	0.0000000
511.4	55.9	0.0000000	353.0	81.0	0.0000000
505.4	56.6	0.0000000	352.8	81.0	0.0000000
479.7	59.6	0.0000000	346.1	82.6	0.0263784
476.4	60.0	0.0441221	345.7	82.7	0.0000000
465.3	61.4	0.0061578	336.6	84.9	0.0000000
464.3	61.6	0.0120738	333.3	85.8	0.0000000
464.0	61.6	0.0690113	331.5	86.2	0.0000000
458.9	62.3	0.0017587	331.3	86.3	0.0000000
454.7	62.9	0.0039244	329.0	86.9	0.0008015
454.1	63.0	0.0010237	313.4	91.2	0.0000000
449.8	63.6	0.0000000	312.5	91.5	0.2994258
449.4	63.6	0.0000000	310.5	92.1	0.0000000
444.4	64.3	0.0000000	309.2	92.5	0.0002027
438.1	65.3	0.0034260	306.4	93.3	0.0004112
425.8	67.1	0.0000000	305.3	93.7	0.0224672
425.3	67.2	0.0001655	304.9	93.8	0.0056620
425.3	67.2	0.0006827	304.3	94.0	0.0019081
423.0	67.6	0.0001306	300.2	95.2	0.0000000

S3. References.

(1) Marshall, W. J.; Grushin, V. V. Activation of Chlorobenzene with Ni(0) N,N-Chelates — A Remarkably Profound Effect of a Minuscule Change in Ligand Structure. *Can. J. Chem.* **2005**, *83* (6–7), 640–645. https://doi.org/10.1139/v05-022.

(2) Ting, S. I.; Garakyaraghi, S.; Taliaferro, C. M.; Shields, B. J.; Scholes, G. D.; Castellano, F. N.; Doyle, A. G. 3d-d Excited States of Ni(II) Complexes Relevant to Photoredox Catalysis: Spectroscopic Identification and Mechanistic Implications. *J. Am. Chem. Soc.* **2020**, *142* (12), 5800–5810. https://doi.org/10.1021/jacs.0c00781.

(3) Shields, J. D.; Gray, E. E.; Doyle, A. G. A Modular, Air-Stable Nickel Precatalyst. *Org. Lett.* **2015**, *17* (9), 2166–2169. https://doi.org/10.1021/acs.orglett.5b00766.

(4) Janeta, M.; Heidlas, J. X.; Daugulis, O.; Brookhart, M. 2,4,6-Triphenylpyridinium: A Bulky, Highly Electron-Withdrawing Substituent That Enhances Properties of Nickel(II) Ethylene Polymerization Catalysts. *Angew. Chem. Int. Ed.* **2021**, *60* (9), 4566–4569. https://doi.org/10.1002/anie.202013854.

(5) Shields, B. J.; Kudisch, B.; Scholes, G. D.; Doyle, A. G. Long-Lived Charge-Transfer States of Nickel(II) Aryl Halide Complexes Facilitate Bimolecular Photoinduced Electron Transfer. *J. Am. Chem. Soc.* **2018**, *140* (8), 3035–3039. https://doi.org/10.1021/jacs.7b13281.

(6) Hansch, Corwin.; Leo, A.; Taft, R. W. A Survey of Hammett Substituent Constants and Resonance and Field Parameters. *Chem. Rev.* **1991**, *91* (2), 165–195. https://doi.org/10.1021/cr00002a004.

(7) Yang, L.; Lu, H.-H.; Lai, C.-H.; Li, G.; Zhang, W.; Cao, R.; Liu, F.; Wang, C.; Xiao, J.; Xue, D. Light-Promoted Nickel Catalysis: Etherification of Aryl Electrophiles with Alcohols Catalyzed by a NiII-Aryl Complex. *Angew. Chem. Int. Ed.* **2020**, *59* (31), 12714–12719. https://doi.org/10.1002/anie.202003359.

(8) Shin, J.; Lee, J.; Suh, J.-M.; Park, K. Ligand-Field Transition-Induced C–S Bond Formation from Nickelacycles. *Chem. Sci.* **2021**, *12* (48), 15908–15915. https://doi.org/10.1039/D1SC05113J.

(9) Till, N. A.; Oh, S.; MacMillan, D. W. C.; Bird, M. J. The Application of Pulse Radiolysis to the Study of Ni(I) Intermediates in Ni-Catalyzed Cross-Coupling Reactions. *J. Am. Chem. Soc.* **2021**, *143* (25), 9332–9337. https://doi.org/10.1021/jacs.1c04652.

(10) Clifford, S.; Maeder, M. Model-Based Analysis for Kinetic and Equilibrium Investigations. *Crit. Rev. Anal. Chem.* **2006**, *36*, 199–209. https://doi.org/10.1080/10408340600969619.

(11) Gampp, H.; Maeder, M.; Meyer, C. J.; Zuberbühler, A. D. Calculation of Equilibrium Constants from Multiwavelength Spectroscopic Data--II: SPECFIT: Two User-Friendly Programs in Basic and Standard FORTRAN 77. *Talanta* **1985**, *32* (4), 257–264. https://doi.org/10.1016/0039-9140(85)80077-1.

(12) Mohadjer Beromi, M.; Brudvig, G. W.; Hazari, N.; Lant, H. M. C.; Mercado, B. Q. Synthesis and Reactivity of Paramagnetic Nickel Polypyridyl Complexes Relevant to C(Sp2)–C(Sp3)Coupling Reactions. *Angew. Chem. Int. Ed.* **2019**, *58* (18), 6094–6098. https://doi.org/10.1002/anie.201901866.

(13) Engel, T.; Reid, P. *Physical Chemistry*, 2nd ed.; Pearson Prentice Hall, 2010.

(14) Stadler, E.; Eibel, A.; Fast, D.; Freißmuth, H.; Holly, C.; Wiech, M.; Moszner, N.; Gescheidt, G. A Versatile Method for the Determination of Photochemical Quantum

Yields via Online UV-Vis Spectroscopy. *Photochem. Photobiol. Sci.* **2018**, *17* (5), 660–669. https://doi.org/10.1039/C7PP00401J.
(15) Neese, F. Software Update: The ORCA Program System, Version 4.0. *WIREs Comput. Mol. Sci.* **2018**, *8* (1), e1327. https://doi.org/10.1002/wcms.1327.
(16) Neese, F. The ORCA Program System. *WIREs Comput. Mol. Sci.* **2012**, *2* (1), 73–78. https://doi.org/10.1002/wcms.81.
(17) Perdew, J. P. Density-Functional Approximation for the Correlation Energy of the Inhomogeneous Electron Gas. *Phys. Rev. B* **1986**, *33* (12), 8822–8824. https://doi.org/10.1103/PhysRevB.33.8822.
(18) Becke, A. D. Density-Functional Exchange-Energy Approximation with Correct Asymptotic Behavior. *Phys. Rev. A* **1988**, *38* (6), 3098–3100. https://doi.org/10.1103/PhysRevA.38.3098.
(19) Weigend, F.; Ahlrichs, R. Balanced Basis Sets of Split Valence, Triple Zeta Valence and Quadruple Zeta Valence Quality for H to Rn: Design and Assessment of Accuracy. *Phys. Chem. Chem. Phys.* **2005**, *7* (18), 3297–3305. https://doi.org/10.1039/B508541A.
(20) Grimme, S.; Antony, J.; Ehrlich, S.; Krieg, H. A Consistent and Accurate Ab Initio Parametrization of Density Functional Dispersion Correction (DFT-D) for the 94 Elements H-Pu. *J. Chem. Phys.* **2010**, *132* (15), 154104. https://doi.org/10.1063/1.3382344.
(21) Grimme, S.; Ehrlich, S.; Goerigk, L. Effect of the Damping Function in Dispersion Corrected Density Functional Theory. *J. Comput. Chem.* **2011**, *32* (7), 1456–1465. https://doi.org/10.1002/jcc.21759.
(22) Barone, V.; Cossi, M. Quantum Calculation of Molecular Energies and Energy Gradients in Solution by a Conductor Solvent Model. *J. Phys. Chem. A* **1998**, *102* (11), 1995–2001. https://doi.org/10.1021/jp9716997.
(23) Klamt, A.; Schüürmann, G. COSMO: A New Approach to Dielectric Screening in Solvents with Explicit Expressions for the Screening Energy and Its Gradient. *J. Chem. Soc. Perkin Trans. 2* **1993**, No. 5, 799–805. https://doi.org/10.1039/P29930000799.
(24) Eichkorn, K.; Treutler, O.; Öhm, H.; Häser, M.; Ahlrichs, R. Auxiliary Basis Sets to Approximate Coulomb Potentials. *Chem. Phys. Lett.* **1995**, *240* (4), 283–290. https://doi.org/10.1016/0009-2614(95)00621-A.
(25) Löwdin, P. On the Non-Orthogonality Problem Connected with the Use of Atomic Wave Functions in the Theory of Molecules and Crystals. *J. Chem. Phys.* **1950**, *18* (3), 365–375. https://doi.org/10.1063/1.1747632.
(26) Becke, A. D. Density-functional Thermochemistry. III. The Role of Exact Exchange. *J. Chem. Phys.* **1993**, *98* (7), 5648–5652. https://doi.org/10.1063/1.464913.
(27) Lee, C.; Yang, W.; Parr, R. G. Development of the Colle-Salvetti Correlation-Energy Formula into a Functional of the Electron Density. *Phys. Rev. B* **1988**, *37* (2), 785–789. https://doi.org/10.1103/PhysRevB.37.785.
(28) Neese, F.; Wennmohs, F.; Hansen, A.; Becker, U. Efficient, Approximate and Parallel Hartree–Fock and Hybrid DFT Calculations. A 'Chain-of-Spheres' Algorithm for the Hartree–Fock Exchange. *Chem. Phys.* **2009**, *356* (1), 98–109. https://doi.org/10.1016/j.chemphys.2008.10.036.
(29) Roos, B. O.; Taylor, P. R.; Sigbahn, P. E. M. A Complete Active Space SCF Method (CASSCF) Using a Density Matrix Formulated Super-CI Approach. *Chem. Phys.* **1980**, *48* (2), 157–173. https://doi.org/10.1016/0301-0104(80)80045-0.

(30) Siegbahn, P. E. M.; Almlöf, J.; Heiberg, A.; Roos, B. O. The Complete Active Space SCF (CASSCF) Method in a Newton–Raphson Formulation with Application to the HNO Molecule. *J. Chem. Phys.* **1981**, *74* (4), 2384–2396. https://doi.org/10.1063/1.441359.
(31) Angeli, C.; Cimiraglia, R.; Evangelisti, S.; Leininger, T.; Malrieu, J.-P. Introduction of N-Electron Valence States for Multireference Perturbation Theory. *J. Chem. Phys.* **2001**, *114* (23), 10252–10264. https://doi.org/10.1063/1.1361246.
(32) Angeli, C.; Cimiraglia, R.; Malrieu, J.-P. N-Electron Valence State Perturbation Theory: A Fast Implementation of the Strongly Contracted Variant. *Chem. Phys. Lett.* **2001**, *350* (3), 297–305. https://doi.org/10.1016/S0009-2614(01)01303-3.
(33) Angeli, C.; Cimiraglia, R.; Malrieu, J.-P. N-Electron Valence State Perturbation Theory: A Spinless Formulation and an Efficient Implementation of the Strongly Contracted and of the Partially Contracted Variants. *J. Chem. Phys.* **2002**, *117* (20), 9138–9153. https://doi.org/10.1063/1.1515317.
(34) Angeli, C.; Borini, S.; Cestari, M.; Cimiraglia, R. A Quasidegenerate Formulation of the Second Order N-Electron Valence State Perturbation Theory Approach. *J. Chem. Phys.* **2004**, *121* (9), 4043–4049. https://doi.org/10.1063/1.1778711.
(35) Lang, L.; Sivalingam, K.; Neese, F. The Combination of Multipartitioning of the Hamiltonian with Canonical Van Vleck Perturbation Theory Leads to a Hermitian Variant of Quasidegenerate N-Electron Valence Perturbation Theory. *J. Chem. Phys.* **2020**, *152* (1), 014109. https://doi.org/10.1063/1.5133746.
(36) Grimme, S. Improved Second-Order Møller–Plesset Perturbation Theory by Separate Scaling of Parallel- and Antiparallel-Spin Pair Correlation Energies. *J. Chem. Phys.* **2003**, *118* (20), 9095–9102. https://doi.org/10.1063/1.1569242.
(37) Riplinger, C.; Neese, F. An Efficient and near Linear Scaling Pair Natural Orbital Based Local Coupled Cluster Method. *J. Chem. Phys.* **2013**, *138* (3), 034106. https://doi.org/10.1063/1.4773581.
(38) Riplinger, C.; Sandhoefer, B.; Hansen, A.; Neese, F. Natural Triple Excitations in Local Coupled Cluster Calculations with Pair Natural Orbitals. *J. Chem. Phys.* **2013**, *139* (13), 134101. https://doi.org/10.1063/1.4821834.
(39) Weigend, F.; Ahlrichs, R. Balanced Basis Sets of Split Valence, Triple Zeta Valence and Quadruple Zeta Valence Quality for H to Rn: Design and Assessment of Accuracy. *Phys. Chem. Chem. Phys.* **2005**, *7* (18), 3297–3305. https://doi.org/10.1039/B508541A.

S4. NMR Spectra.

Proton nuclear magnetic resonance (^{1}H NMR) and fluorine nuclear magnetic resonance (^{19}F NMR) spectra were recorded on a 400 MHz Varian Spectrometer with broadband auto-tune OneProbe. All ^{13}C NMR spectra were collected on a Bruker AV-III HD 400 MHz spectrometer. ^{13}C NMR spectra were ^{1}H decoupled. Chemical shifts are reported in parts per million (δ in ppm, s: singlet, d: doublet, t: triplet, m: multiplet) and are referenced to residual solvent signal (CD_2Cl_2 = δ 5.32 ppm, CD_3CN = δ 1.94 ppm). Fluorine NMR were externally referenced to neat fluorobenzene (δ = -113.15 ppm).

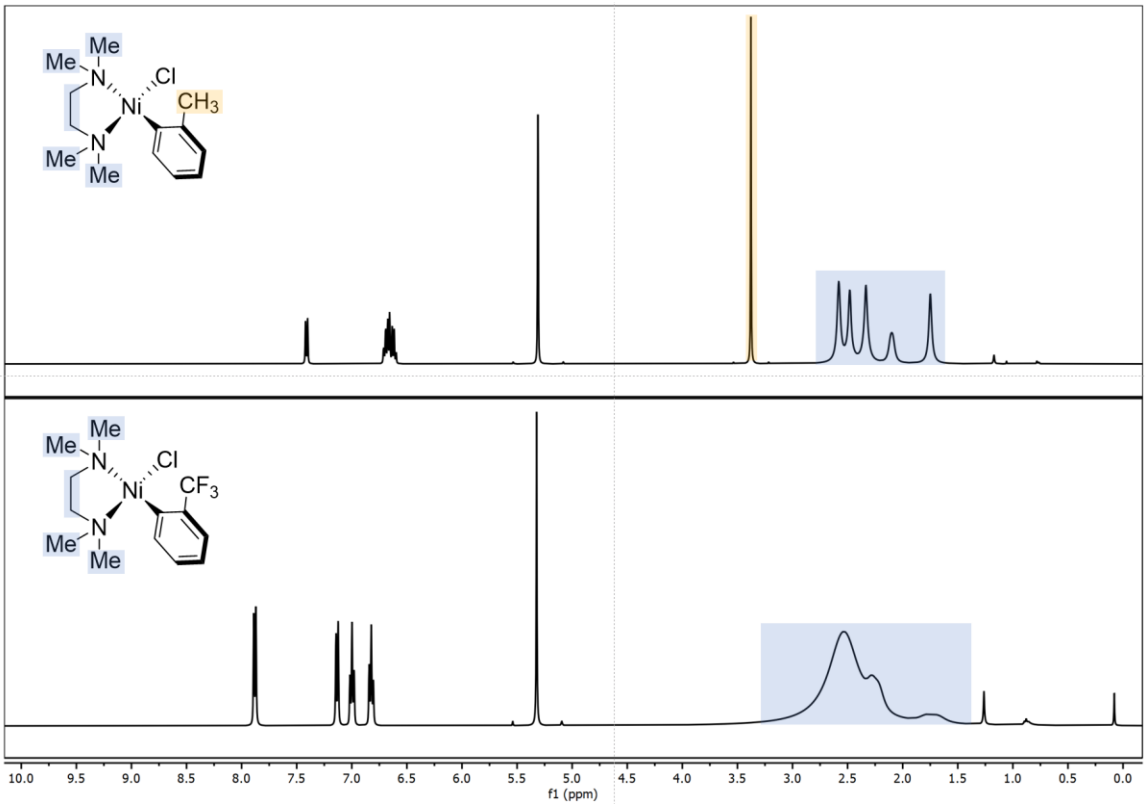

Figure S71. Comparison between the ^{1}H NMR (400 MHz, CD_2Cl_2) spectra of the Ni(TMEDA) complexes. More detailed spectra are given below.

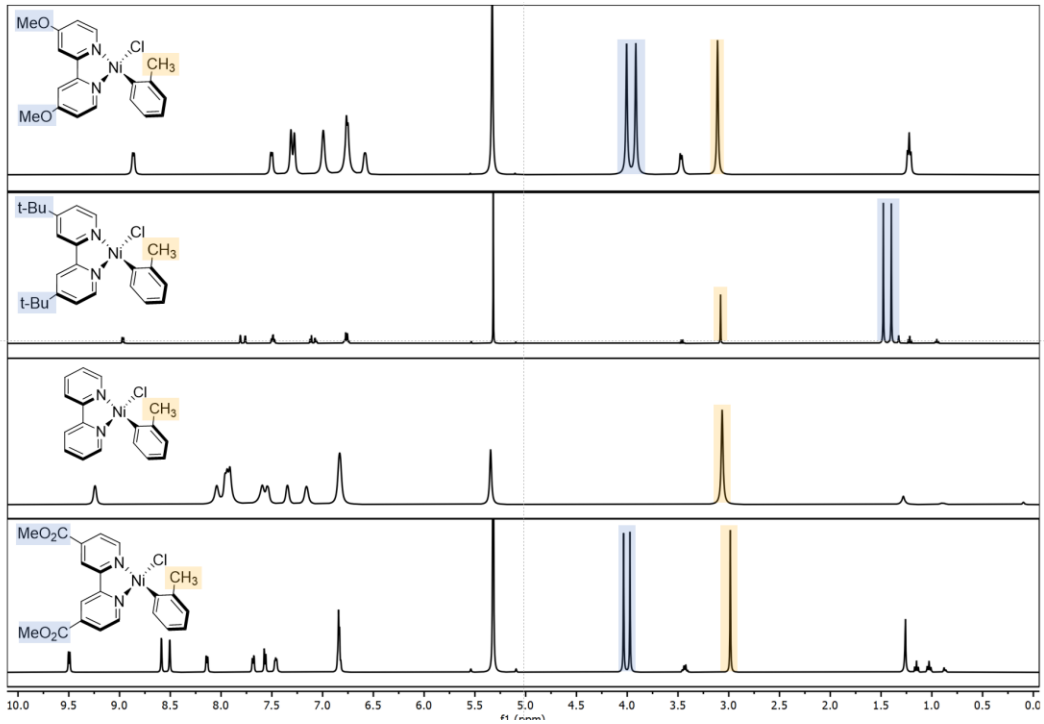

Figure S72. Comparison between the ^{1}H NMR (400 MHz, CD_2Cl_2) spectra of **1A**–**1D**. More detailed spectra are given below.

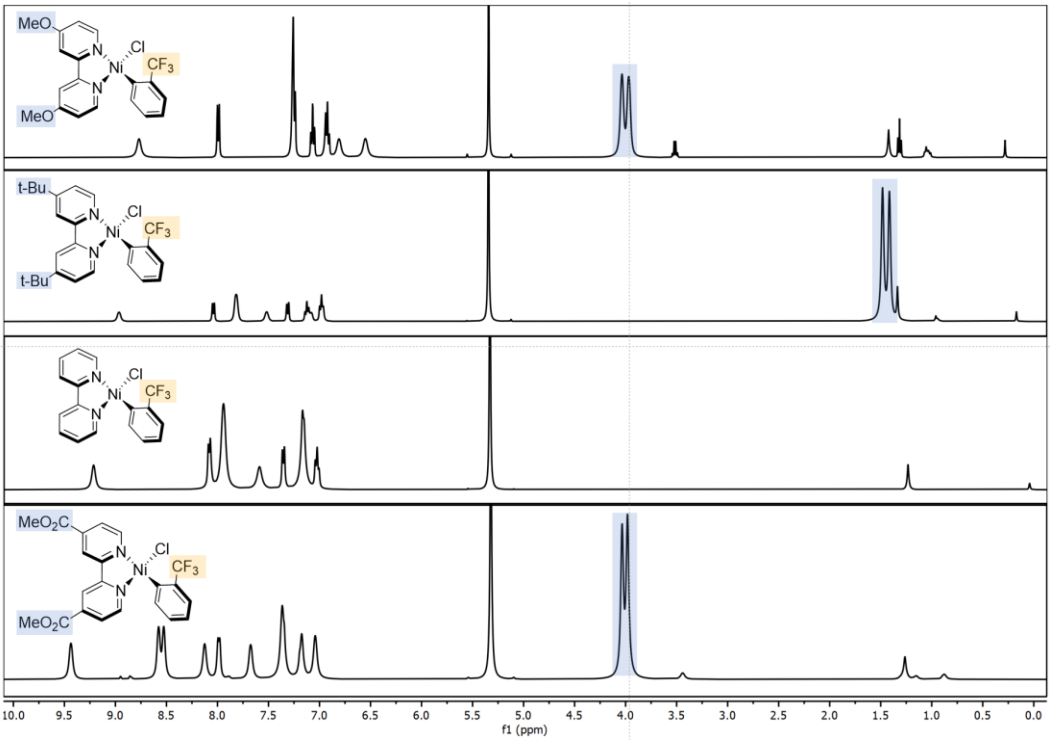

Figure S73. Comparison between the ^{1}H NMR (400 MHz, CD_2Cl_2) spectra of **5A**–**5D**. More detailed spectra are given below.

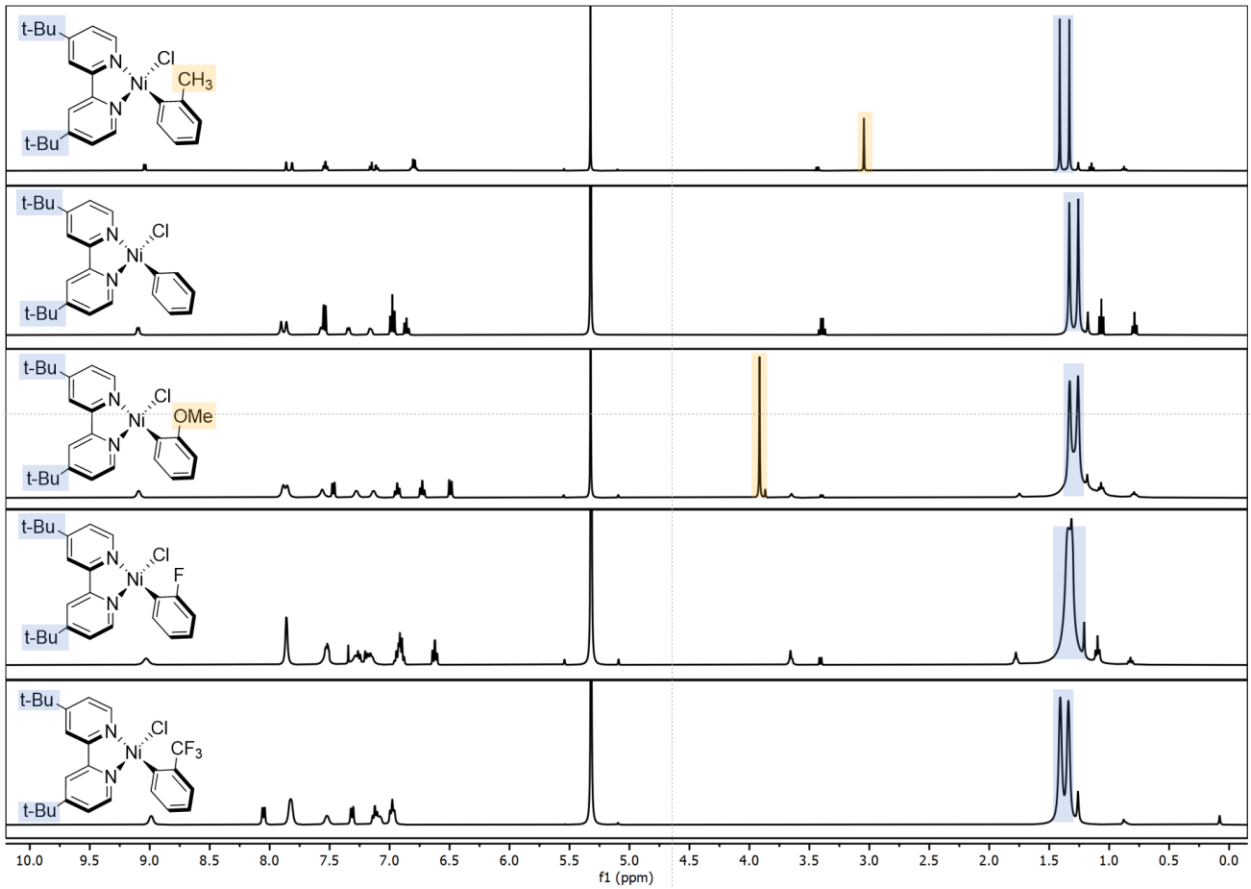

Figure S74. Comparison between the ^{1}H NMR (400 MHz, CD_2Cl_2) spectra of **1B**–**5B**. More detailed spectra are given below.

^{1}H NMR (400 MHz, CD_2Cl_2): Ni(TMEDA)(CH_3Ph)Cl

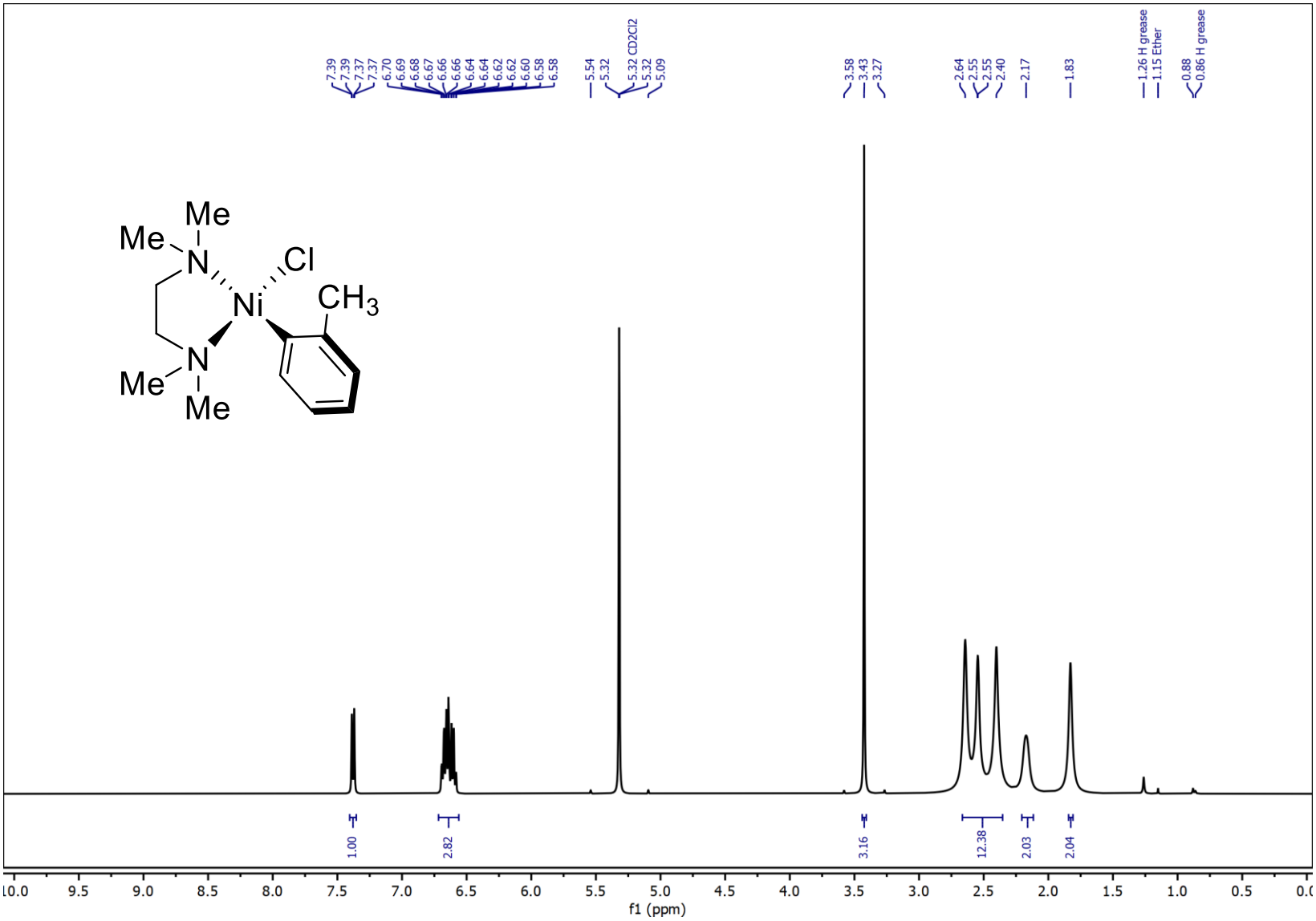

^{13}C NMR (100 MHz, CD_2Cl_2): Ni(TMEDA)(CH_3Ph)Cl

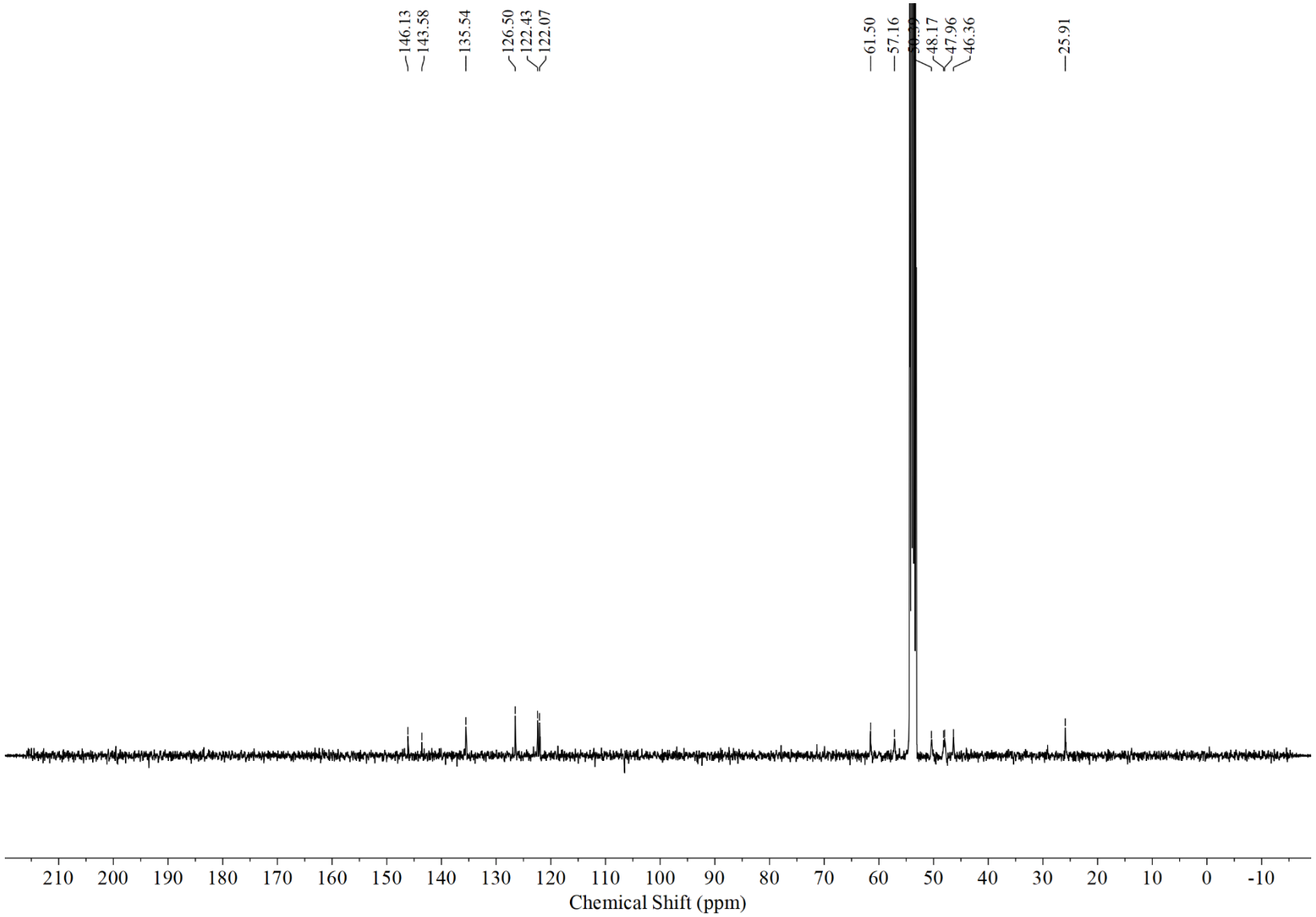

^{1}H NMR (400 MHz, CD_2Cl_2): Ni(TMEDA)(CF_3Ph)Cl

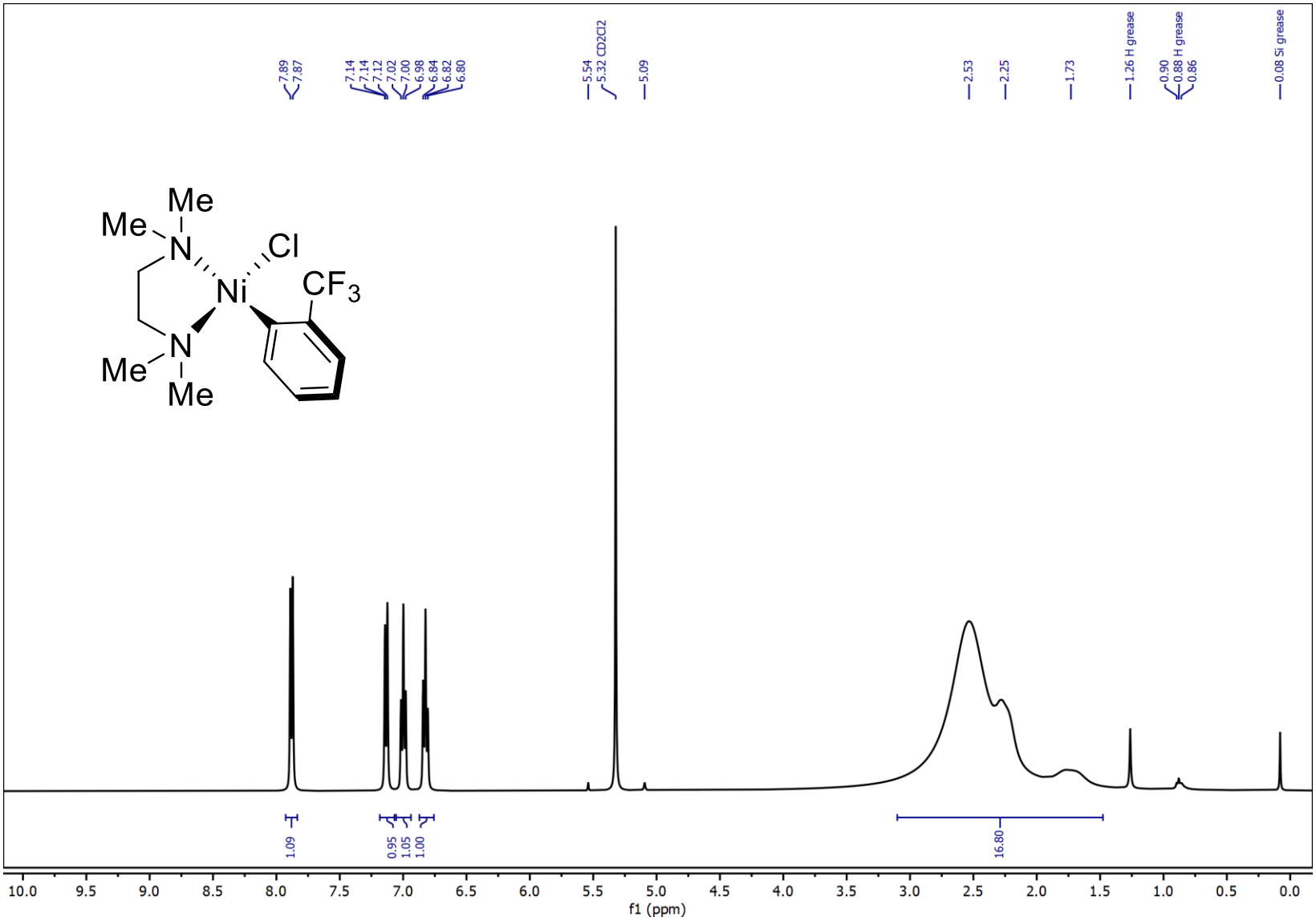

^{13}C NMR (100 MHz, CD_2Cl_2): Ni(TMEDA)(CF_3Ph)Cl

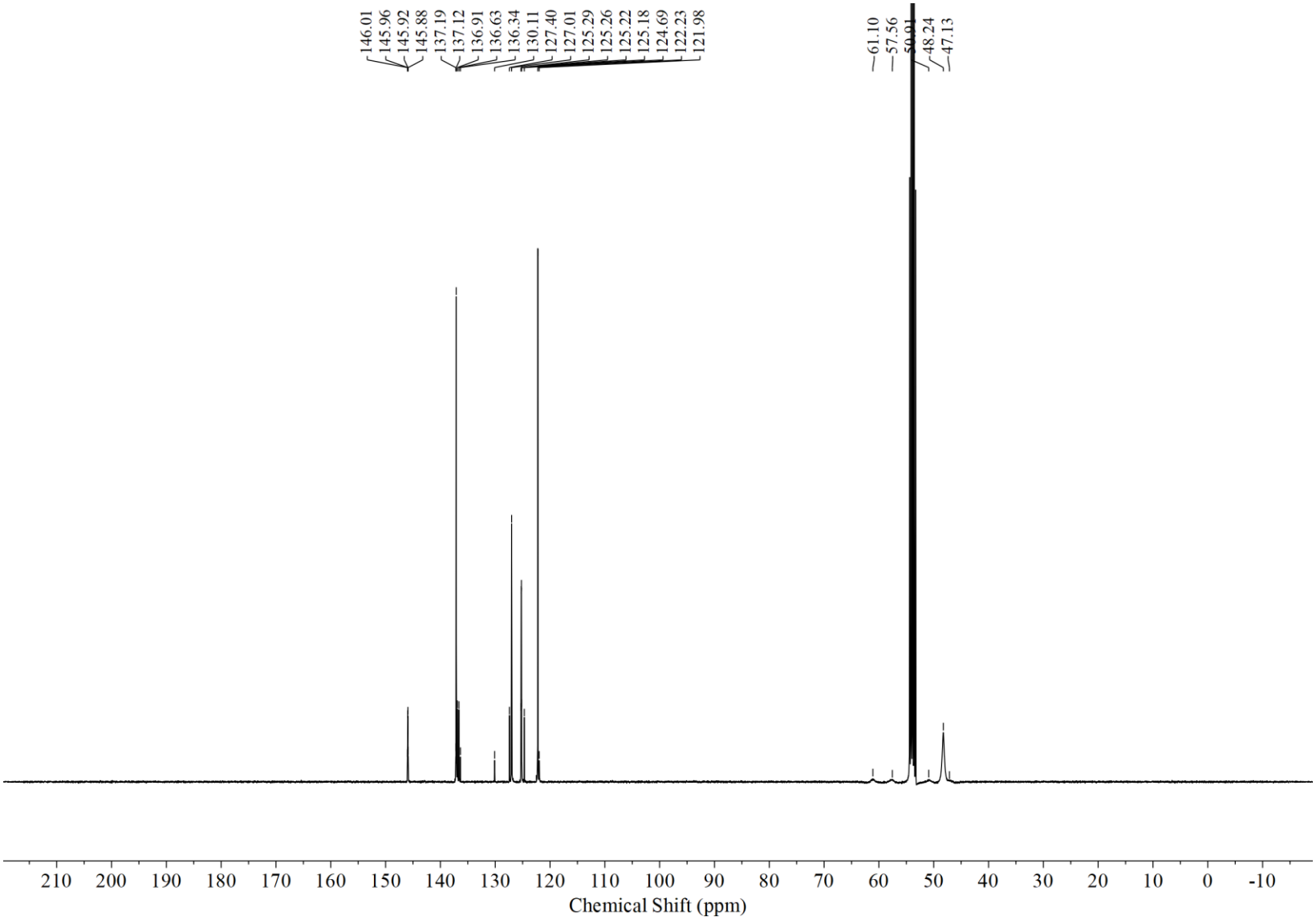

^{1}H NMR (400 MHz, CD_2Cl_2): Ni(^{MeO}bpy)(CH_3Ph)Cl, 1A

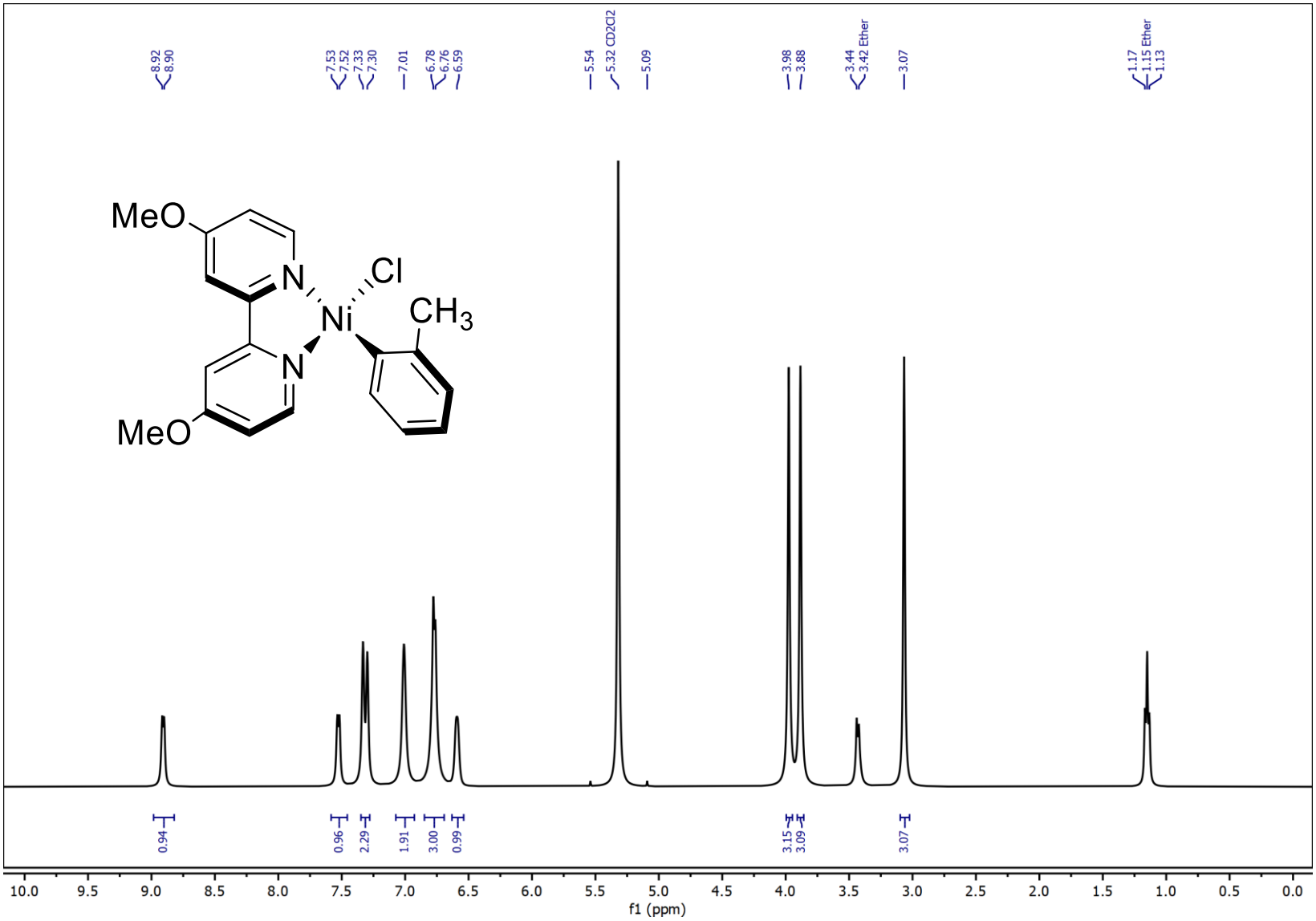

^{13}C NMR (100 MHz, CD_2Cl_2): Ni(^{MeO}bpy)(CH_3Ph)Cl, 1A

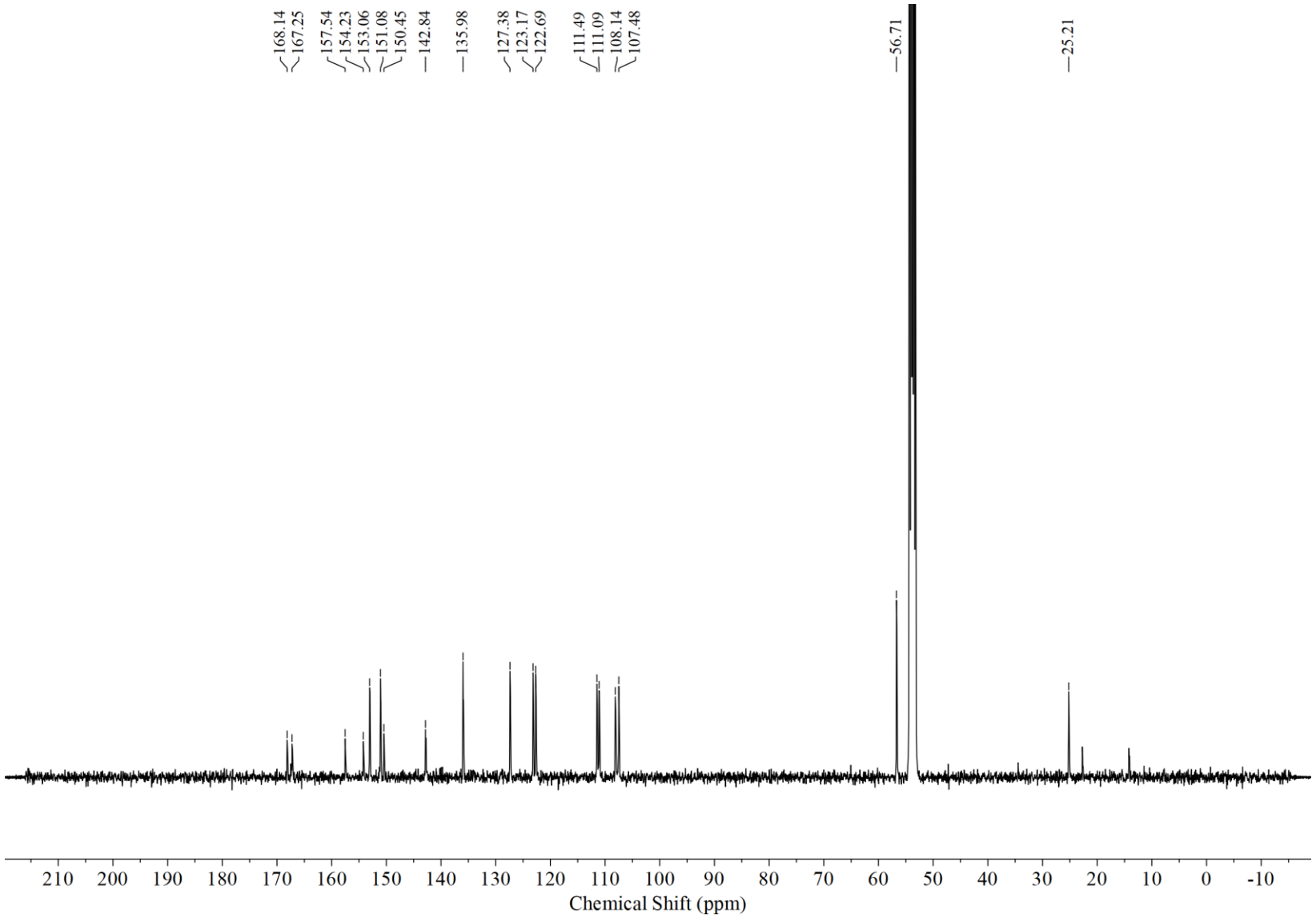

^{1}H NMR (400 MHz, CD_2Cl_2): Ni($^{t\text{-Bu}}$bpy)(CH_3Ph)Cl, 1B

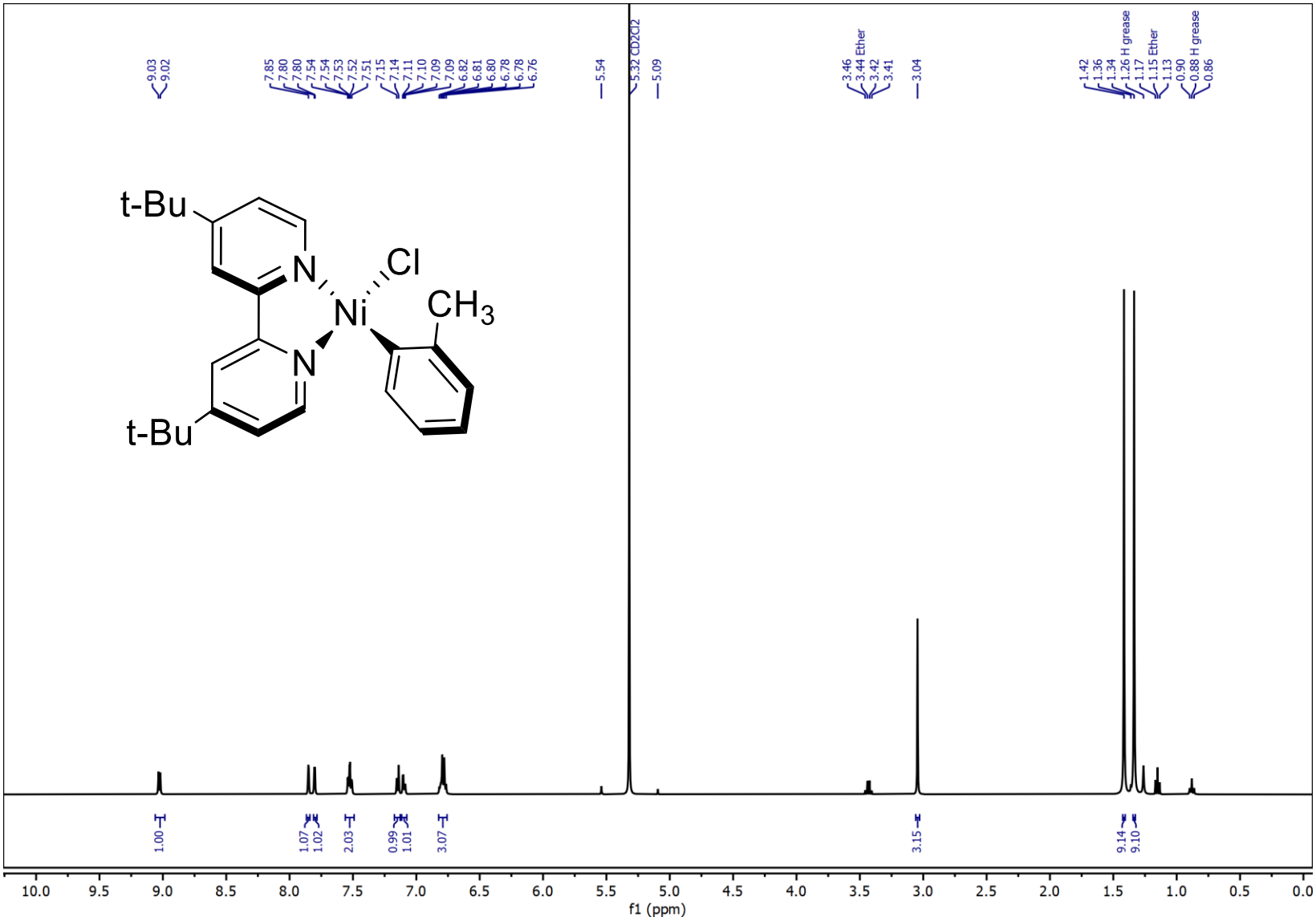

^{13}C NMR (100 MHz, CD_2Cl_2): Ni($^{t\text{-}Bu}$bpy)(CH_3Ph)Cl, 1B

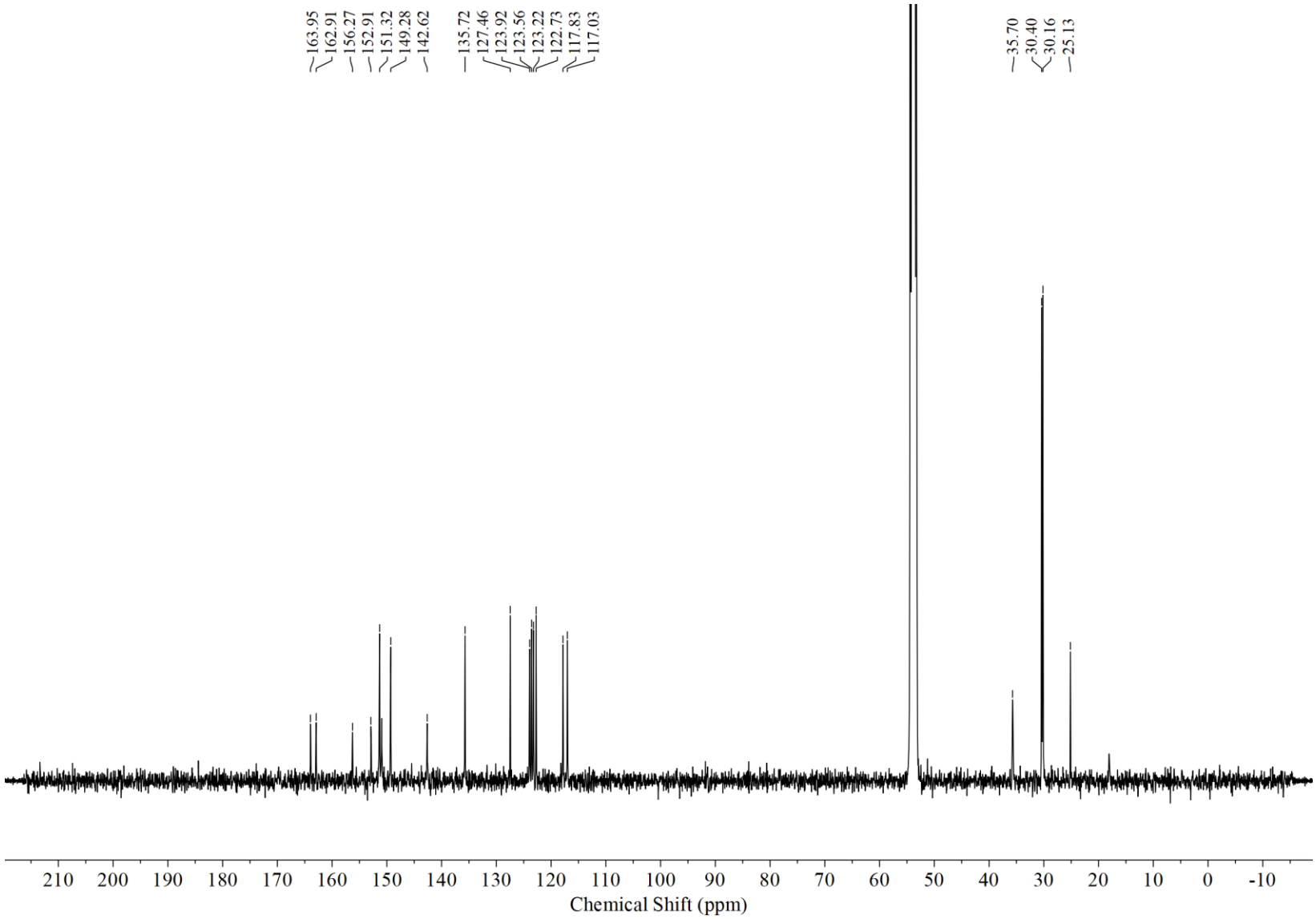

^{1}H NMR (400 MHz, CD_2Cl_2): Ni(^{H}bpy)(CH_3Ph)Cl, 1C

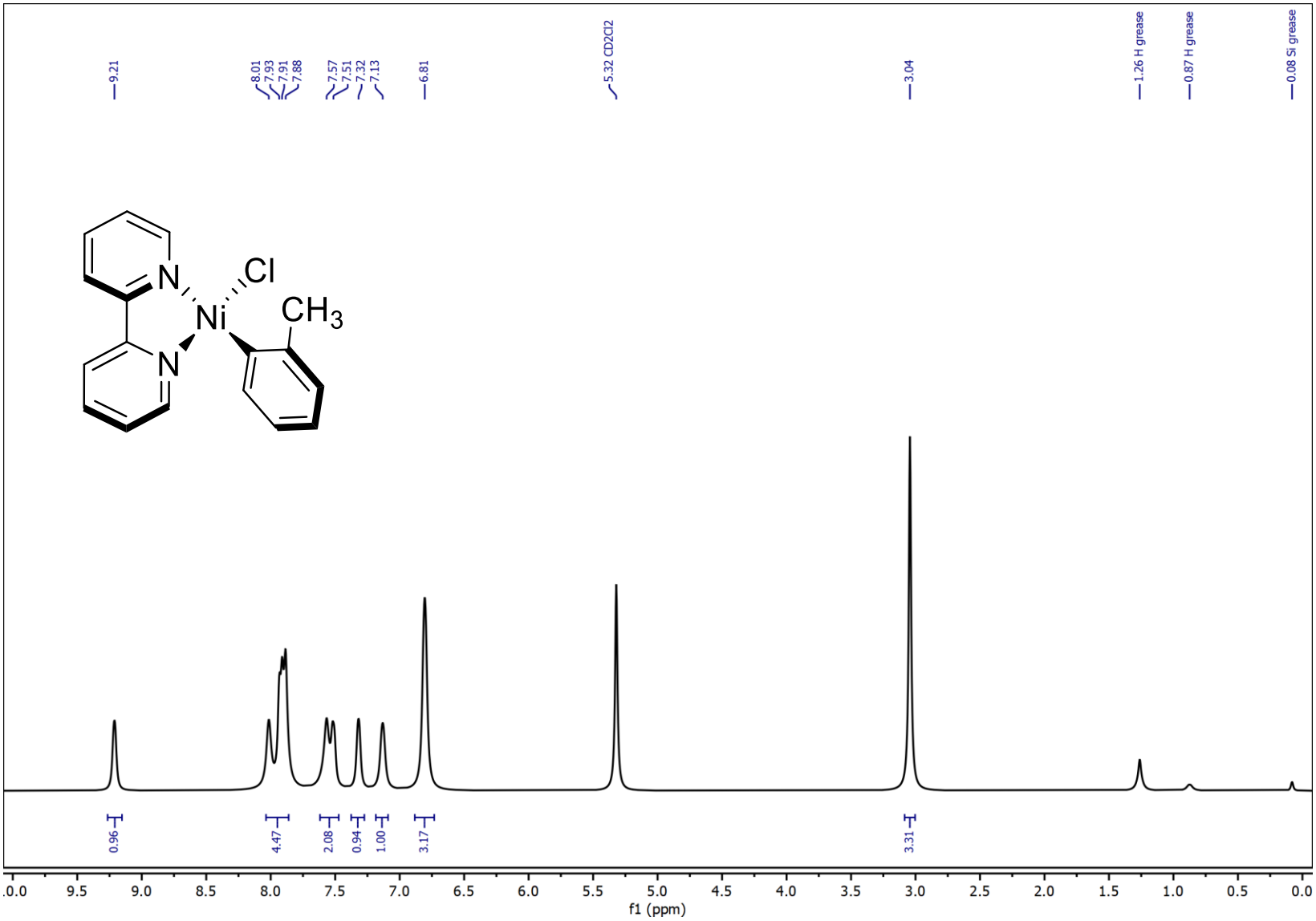

^{13}C NMR (100 MHz, CD_2Cl_2): Ni(^{H}bpy)(CH_3Ph)Cl, 1C

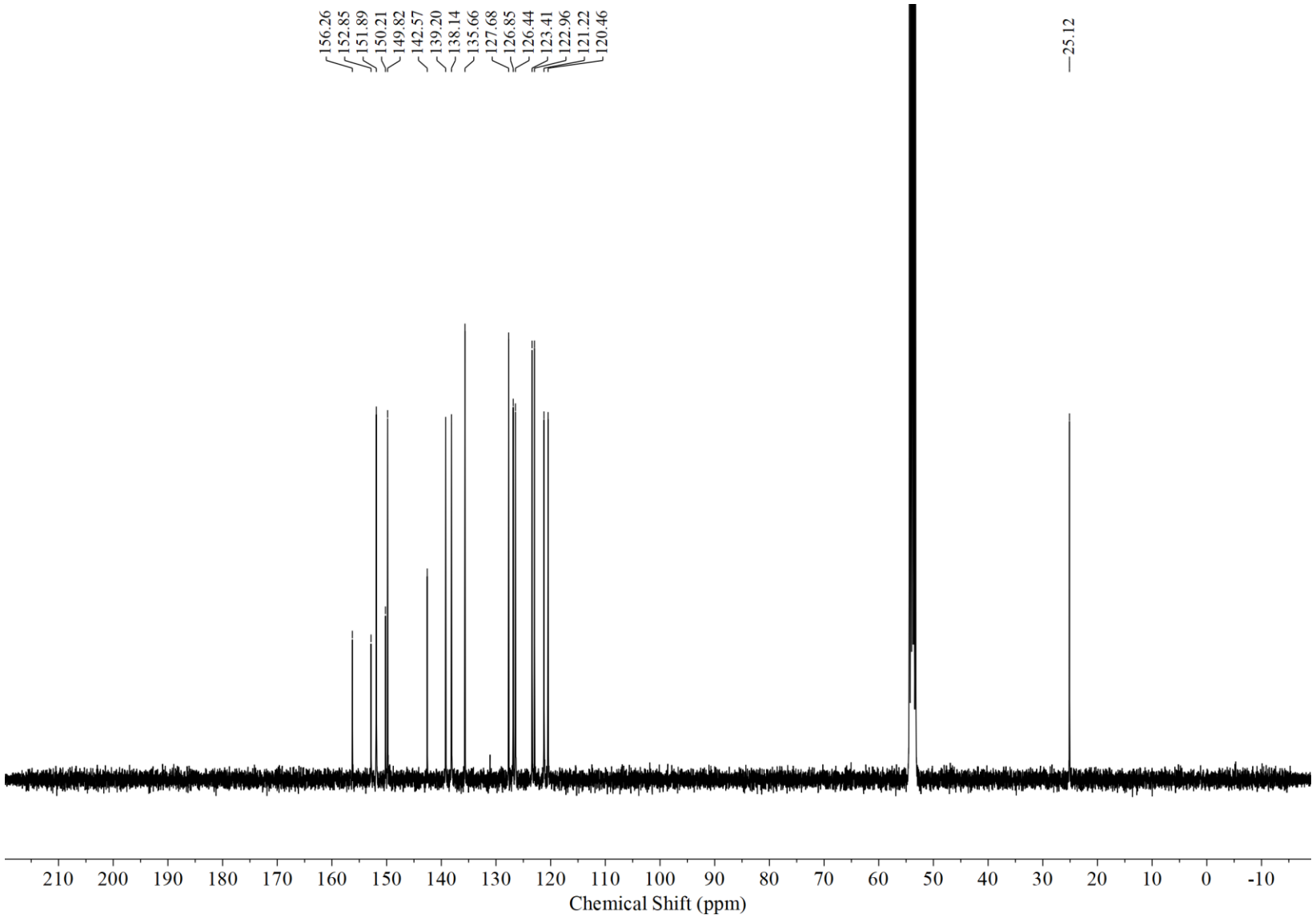

^{1}H NMR (400 MHz, CD_2Cl_2): Ni(^{MeOOC}bpy)(CH_3Ph)Cl, 1D

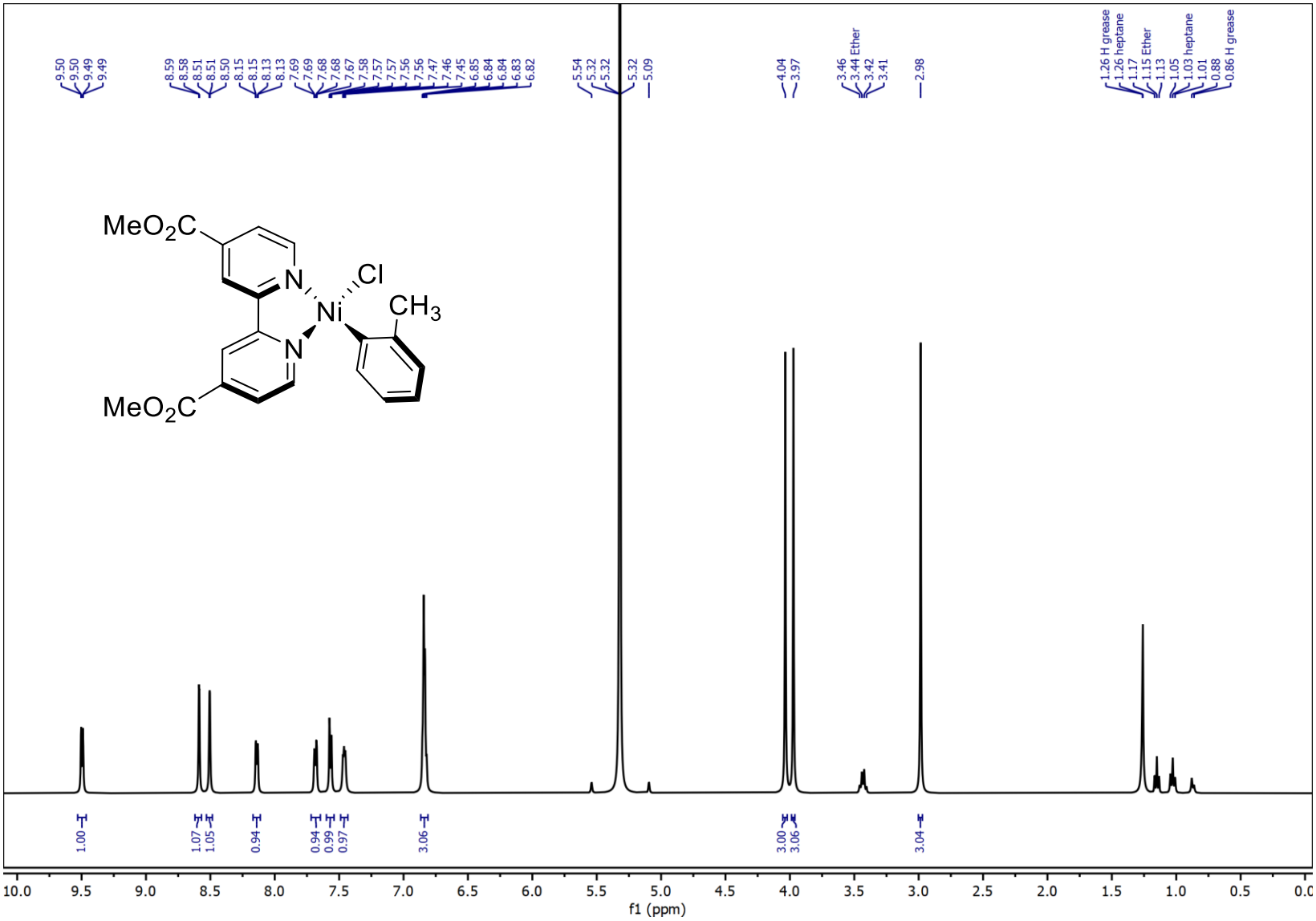

^{13}C NMR (100 MHz, CD_2Cl_2): Ni(^{MeOOC}bpy)(CH_3Ph)Cl, 1D

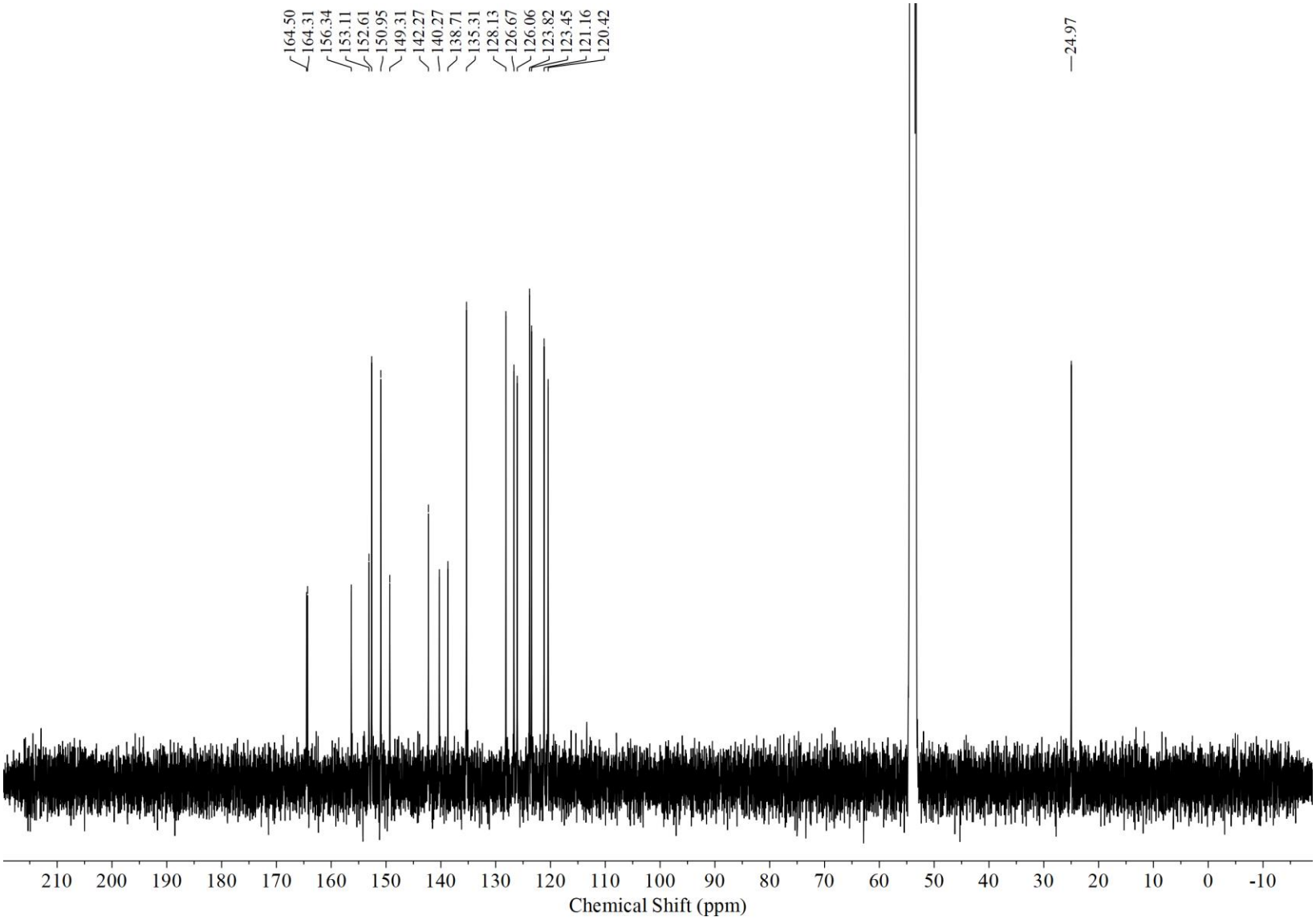

^{1}H NMR (400 MHz, CD_2Cl_2): Ni($^{t\text{-Bu}}$bpy)(Ph)Cl, 2B

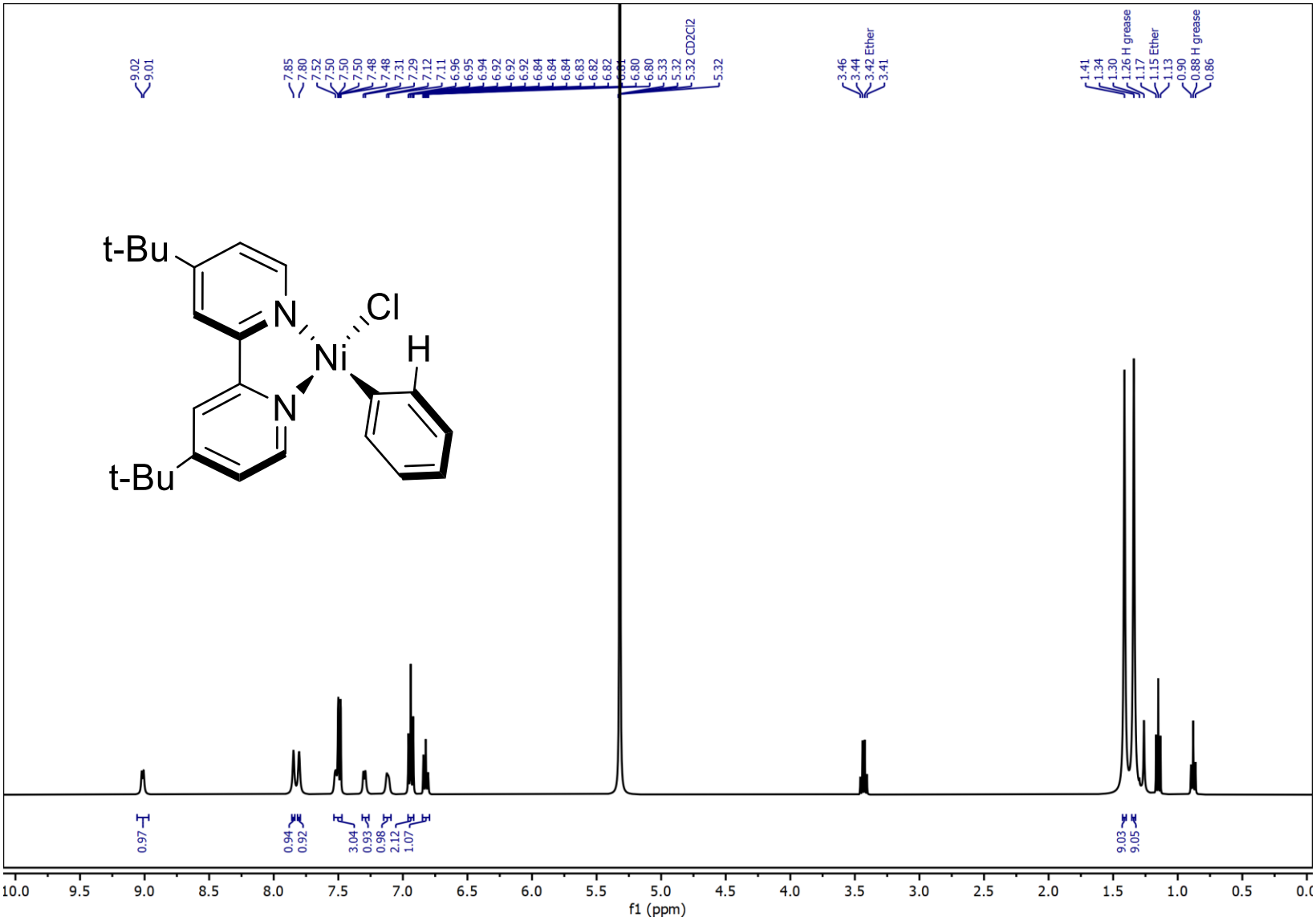

^{13}C NMR (100 MHz, CD_2Cl_2): Ni($^{t\text{-}Bu}$bpy)(Ph)Cl, 2B

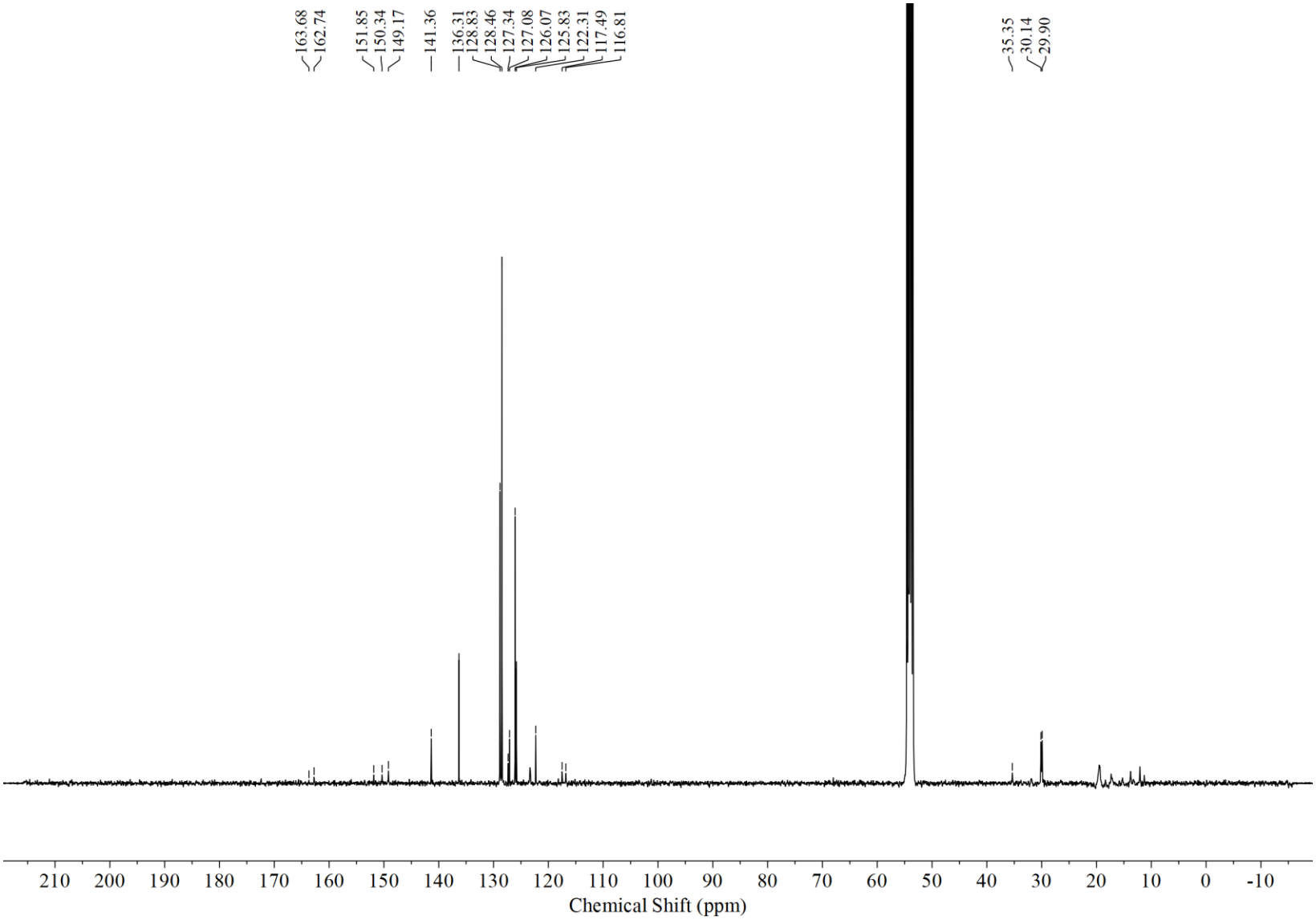

^{1}H NMR (400 MHz, CD_2Cl_2): Ni($^{t\text{-Bu}}$bpy)(CH_3OPh)Cl, 3B

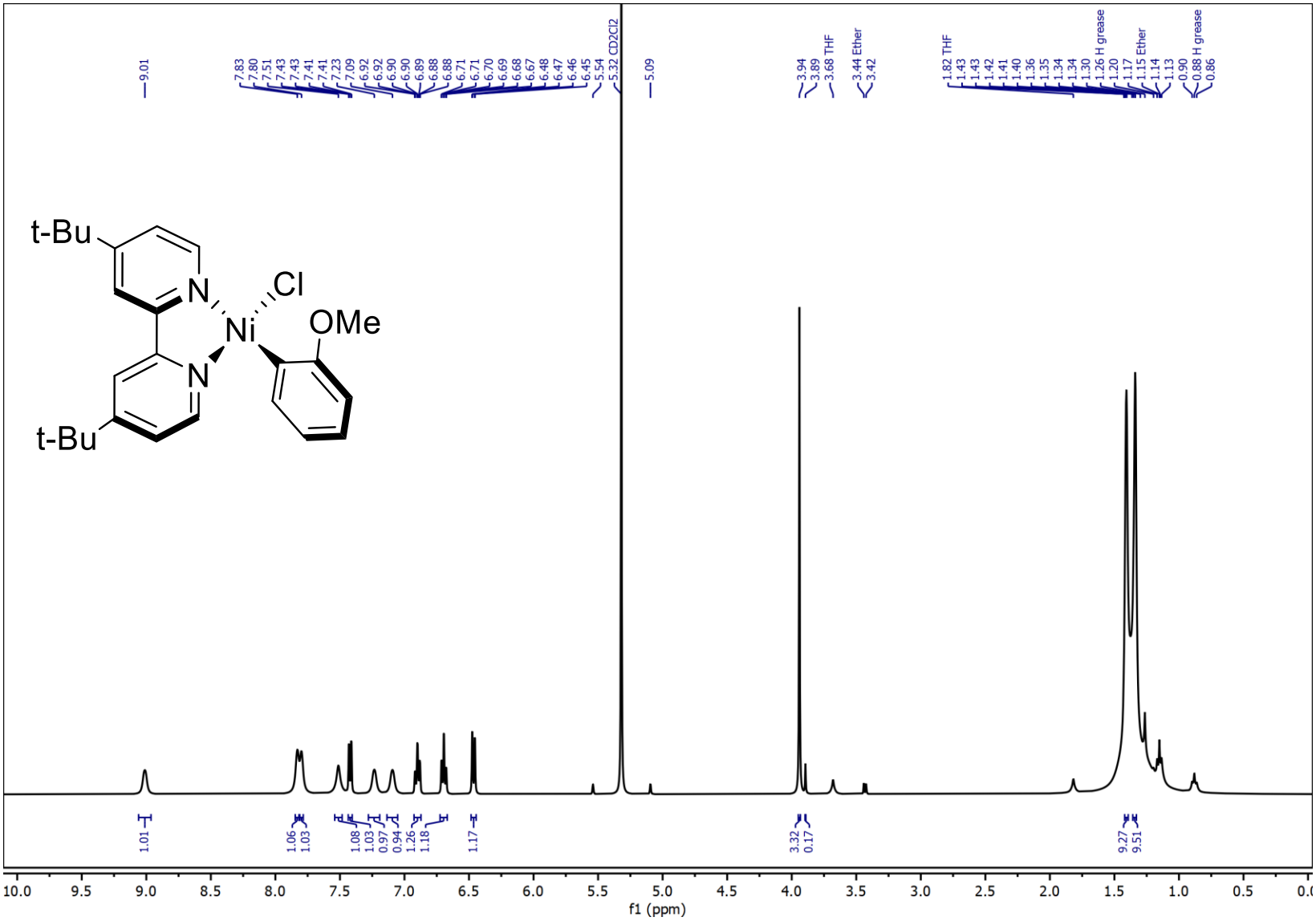

^{13}C NMR (100 MHz, CD_2Cl_2): Ni($^{t\text{-}Bu}$bpy)(CH_3OPh)Cl, 3B

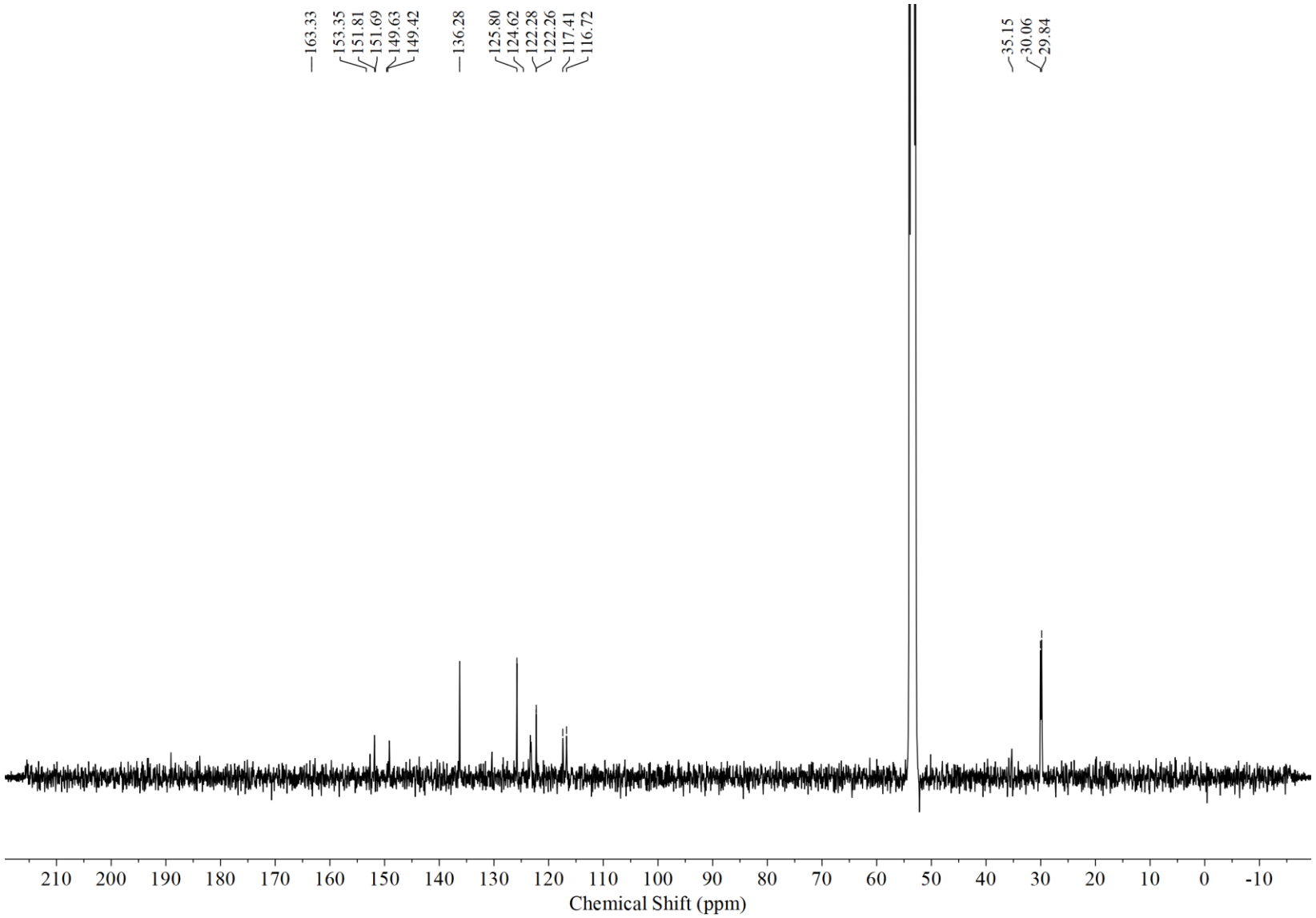

^{1}H NMR (400 MHz, CD_2Cl_2): Ni($^{t\text{-}Bu}$bpy)(F-Ph)Cl, 4B

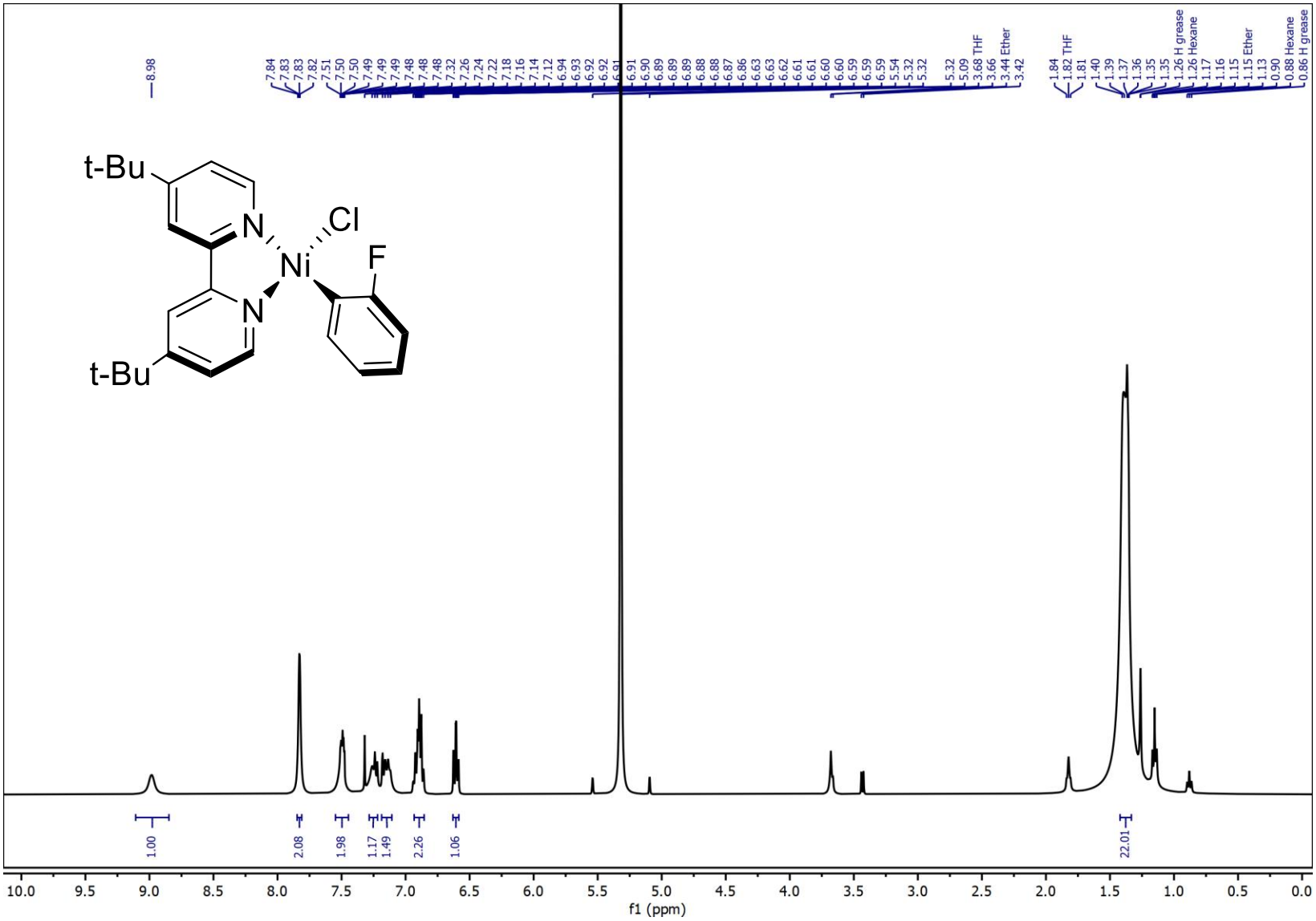

^{13}C NMR (100 MHz, CD_2Cl_2): Ni($^{t\text{-}Bu}$bpy)(F-Ph)Cl, 4B

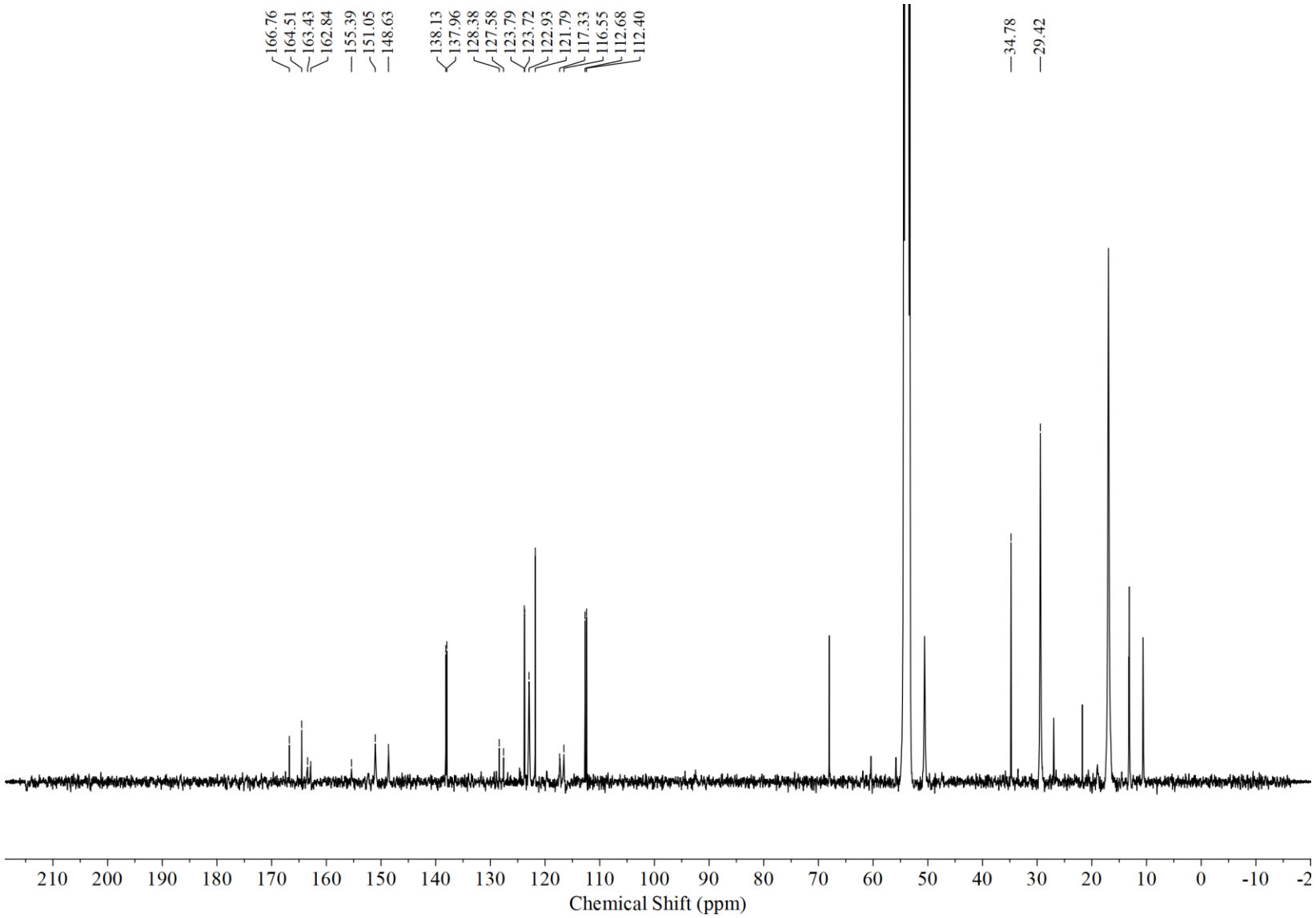

^{1}H NMR (400 MHz, CD_2Cl_2): Ni(^{MeO}bpy)(CF_3Ph)Cl, 5A

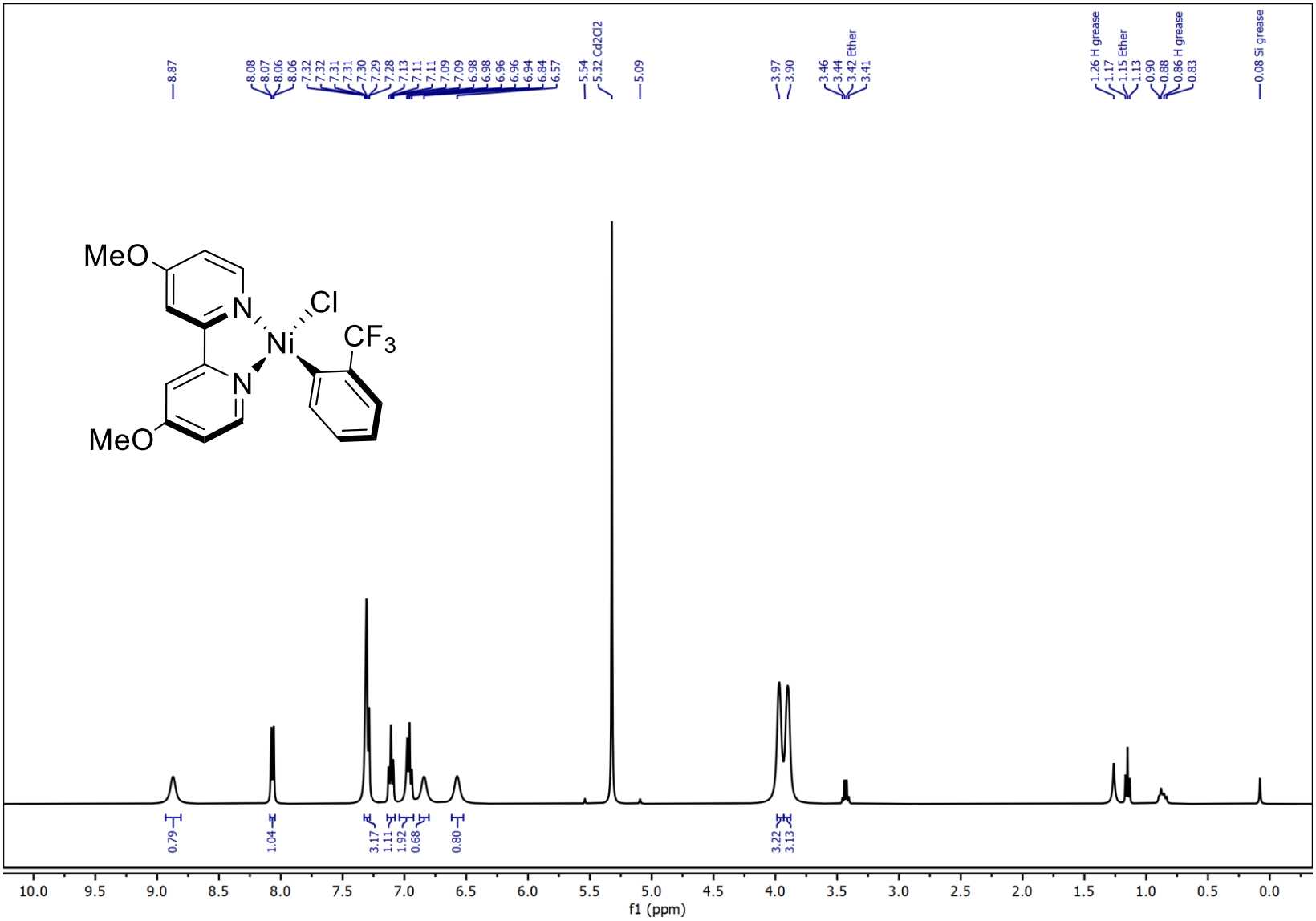

^{13}C NMR (100 MHz, CD_2Cl_2): Ni(^{MeO}bpy)(CF_3Ph)Cl, 5A

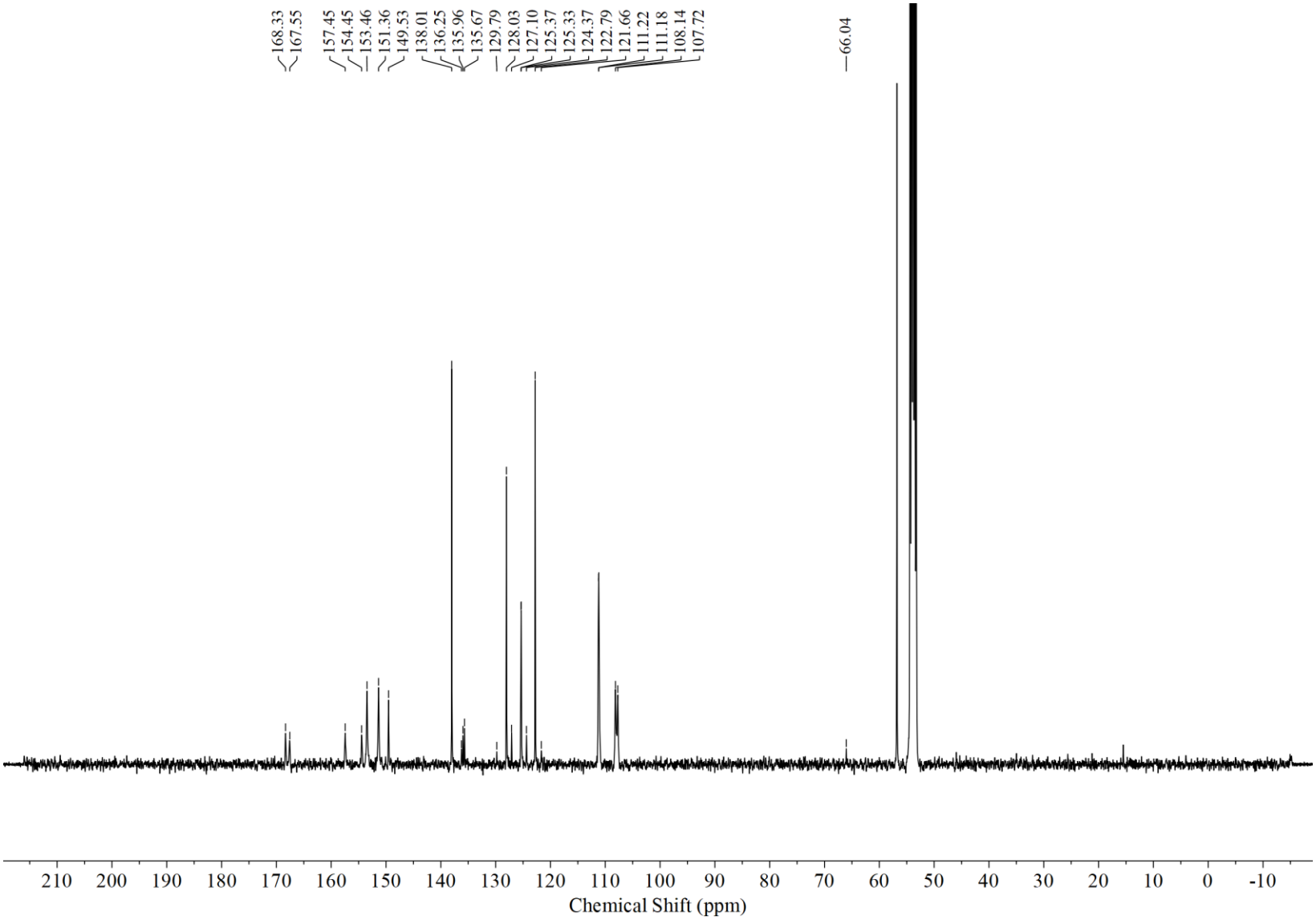

^{1}H NMR (400 MHz, CD_2Cl_2): Ni($^{t\text{-Bu}}$bpy)(CF_3Ph)Cl, 5B

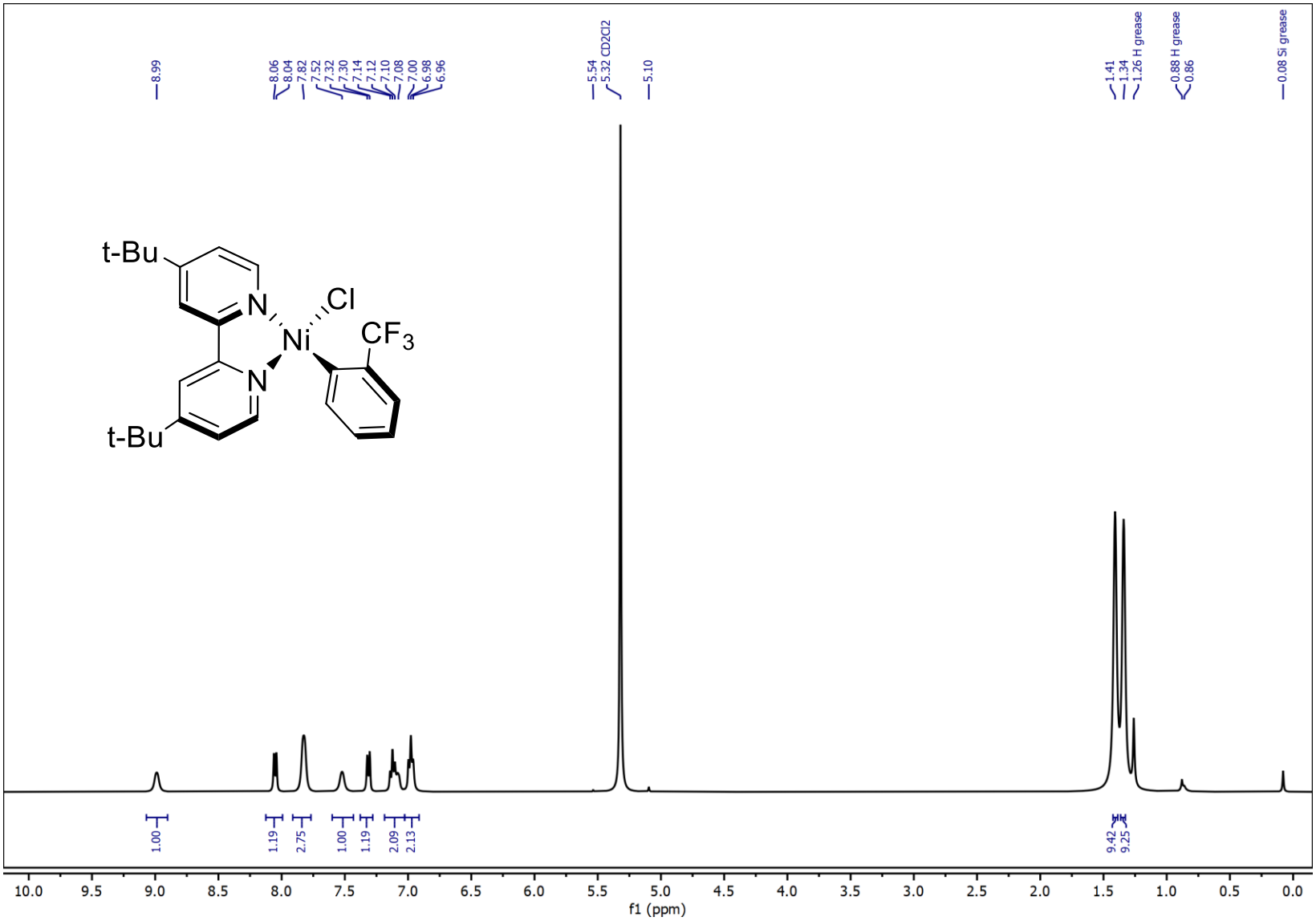

^{13}C NMR (100 MHz, CD_2Cl_2): Ni($^{t\text{-}Bu}$bpy)(CF_3Ph)Cl, 5B

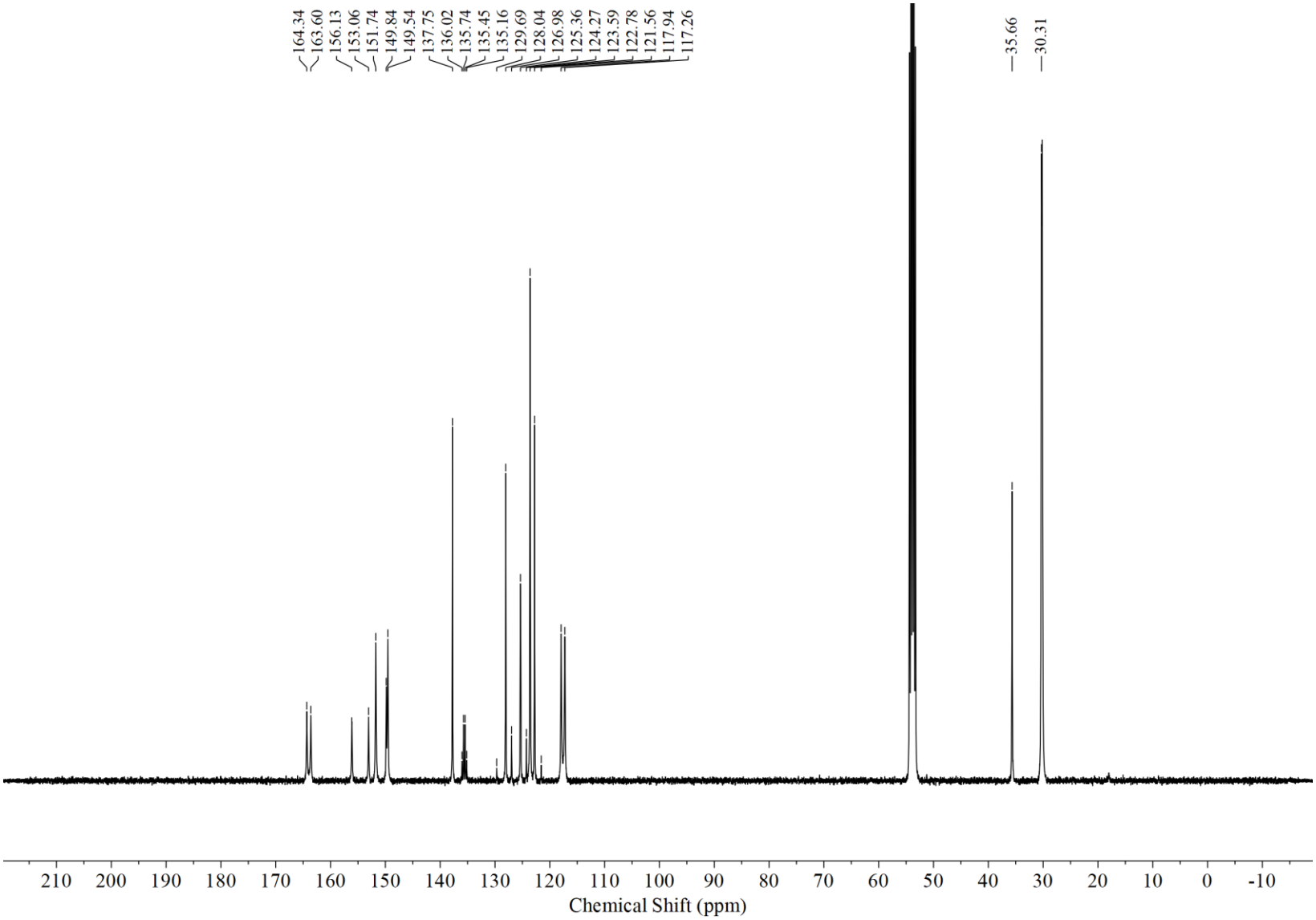

^{1}H NMR (400 MHz, CD_2Cl_2): Ni(^{H}bpy)(CF_3Ph)Cl, 5C

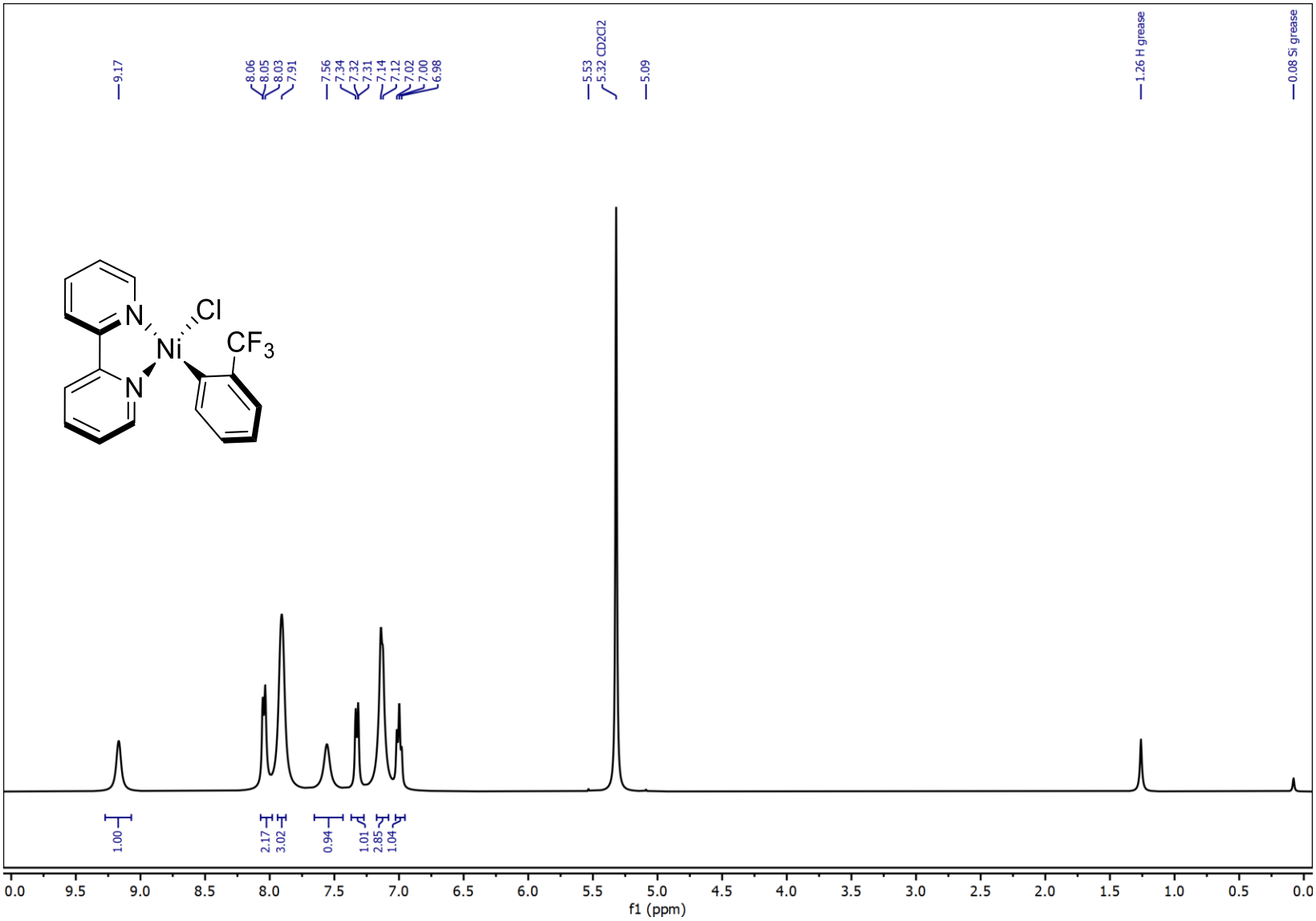

^{13}C NMR (100 MHz, CD_2Cl_2): Ni(^{H}bpy)(CF_3Ph)Cl, 5C

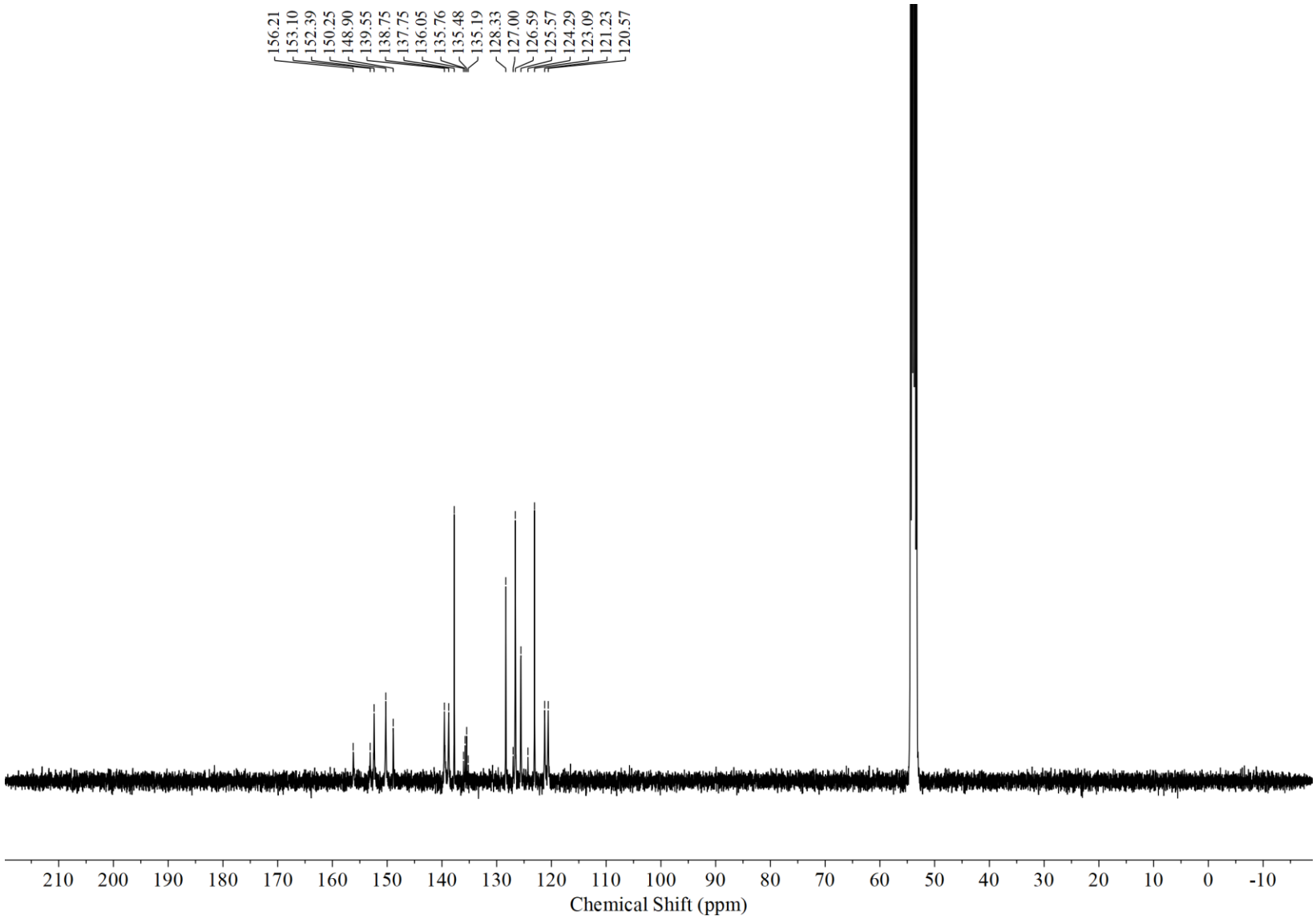

^{1}H NMR (400 MHz, CD_2Cl_2): Ni(^{MeOOC}bpy)(CF_3Ph)Cl, 5D

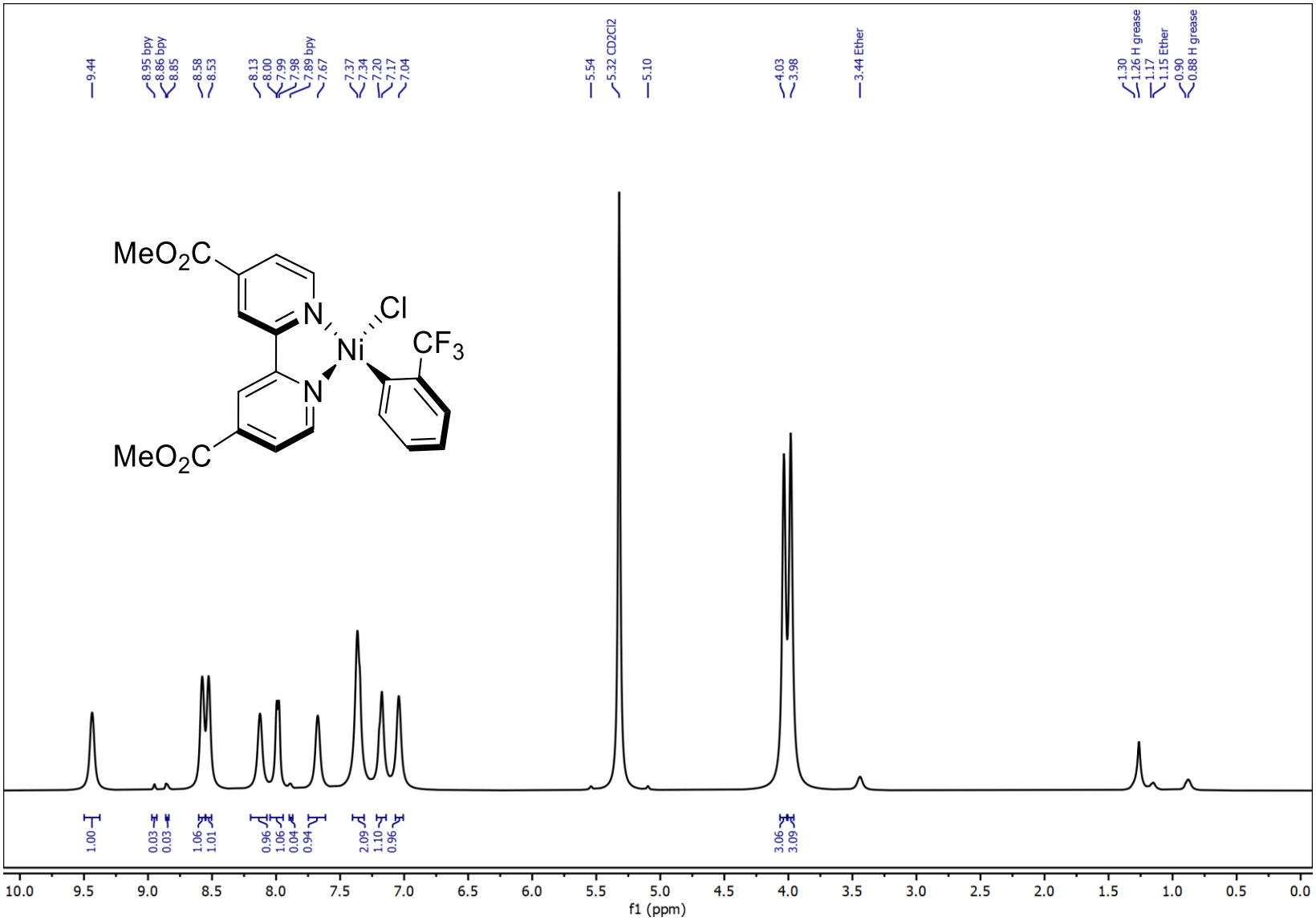

^{13}C NMR (100 MHz, CD_2Cl_2): Ni(^{MeOOC}bpy)(CF_3Ph)Cl, 5D

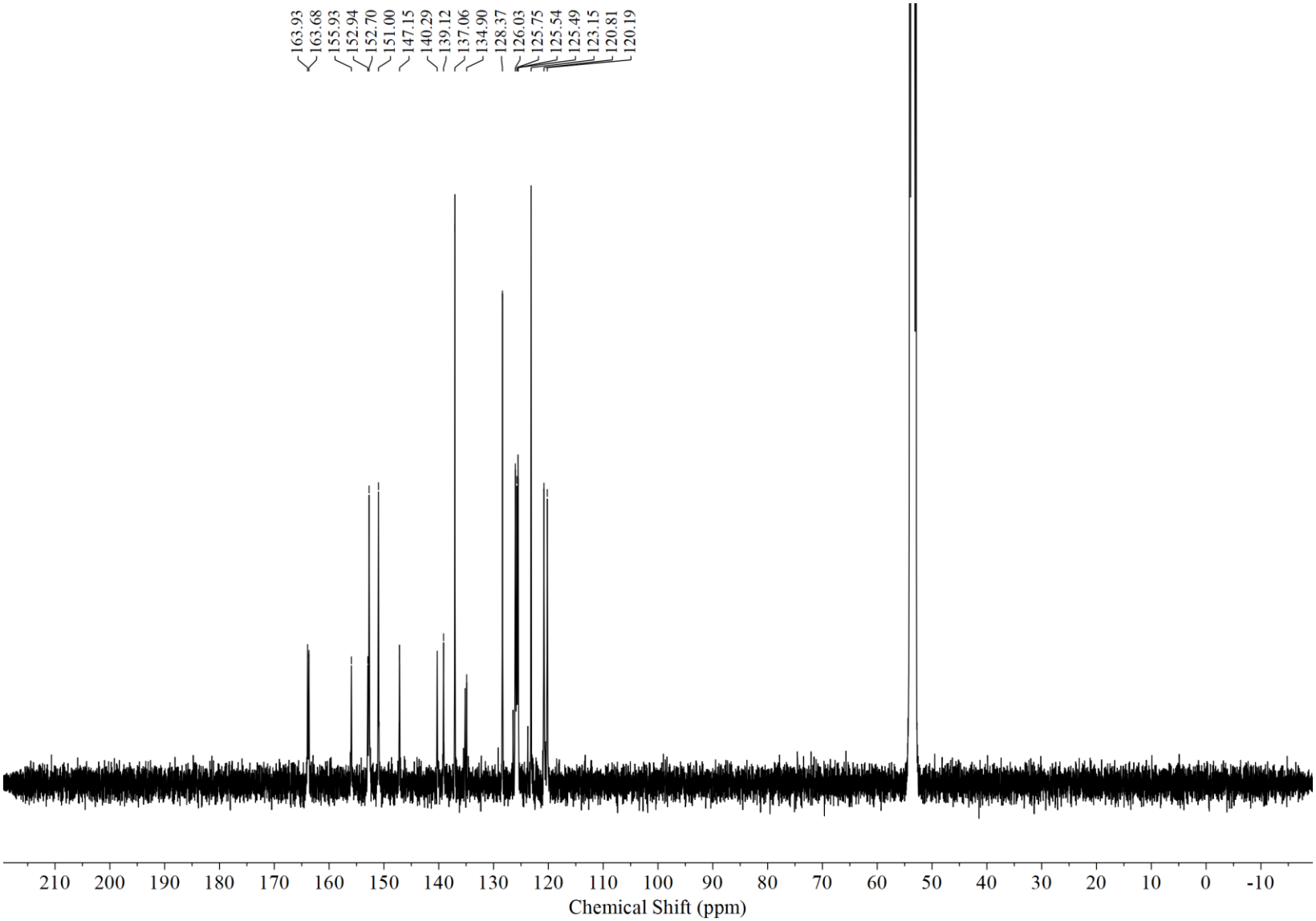

^{1}H NMR (400 MHz, CD_2Cl_2): Ni($^{t\text{-Bu}}$bpy)(CH_3Ph)Br, 1B–Br

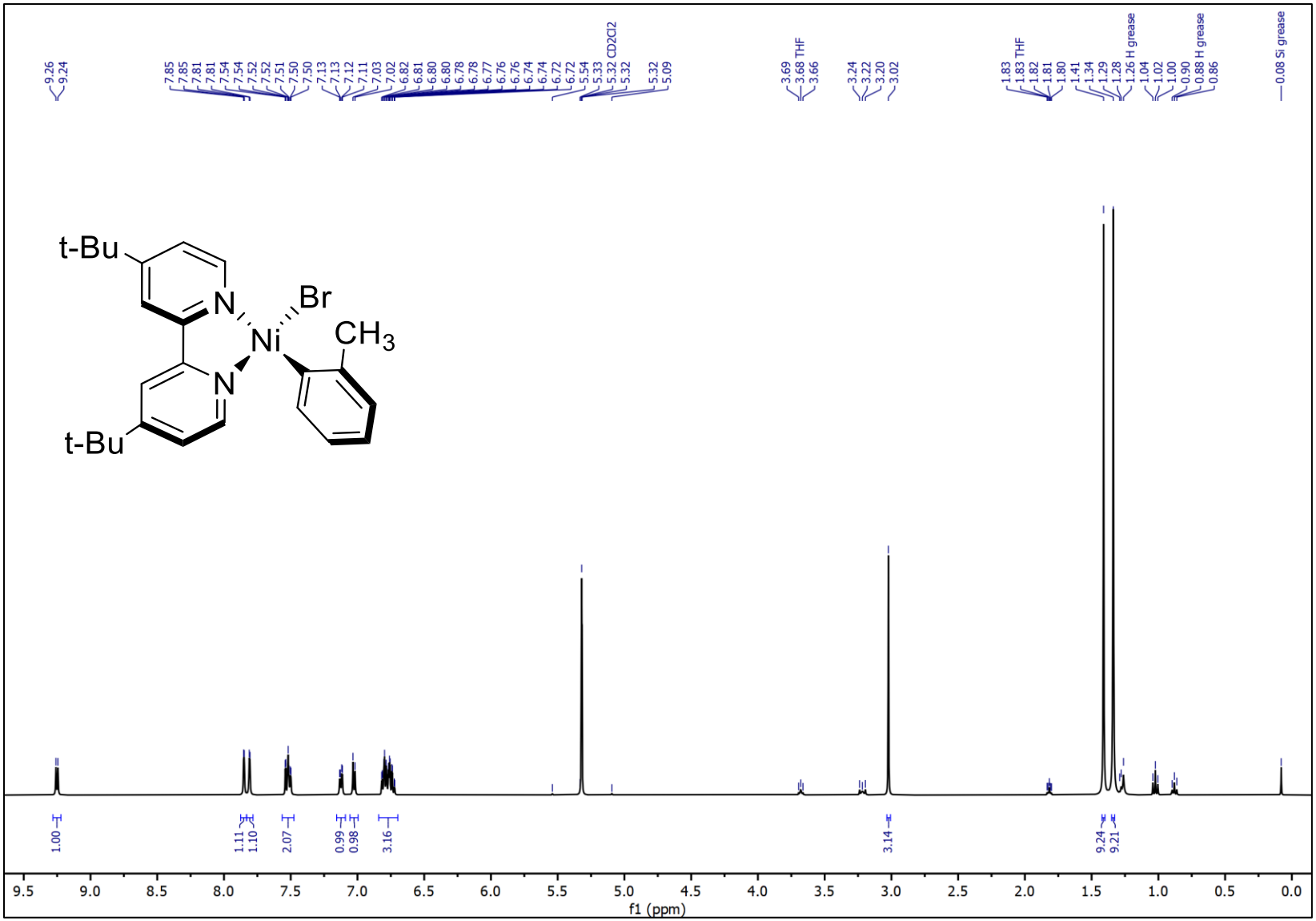

^{13}C NMR (100 MHz, CD_2Cl_2): Ni($^{t\text{-}Bu}$bpy)(CH_3Ph)Br, 1B–Br

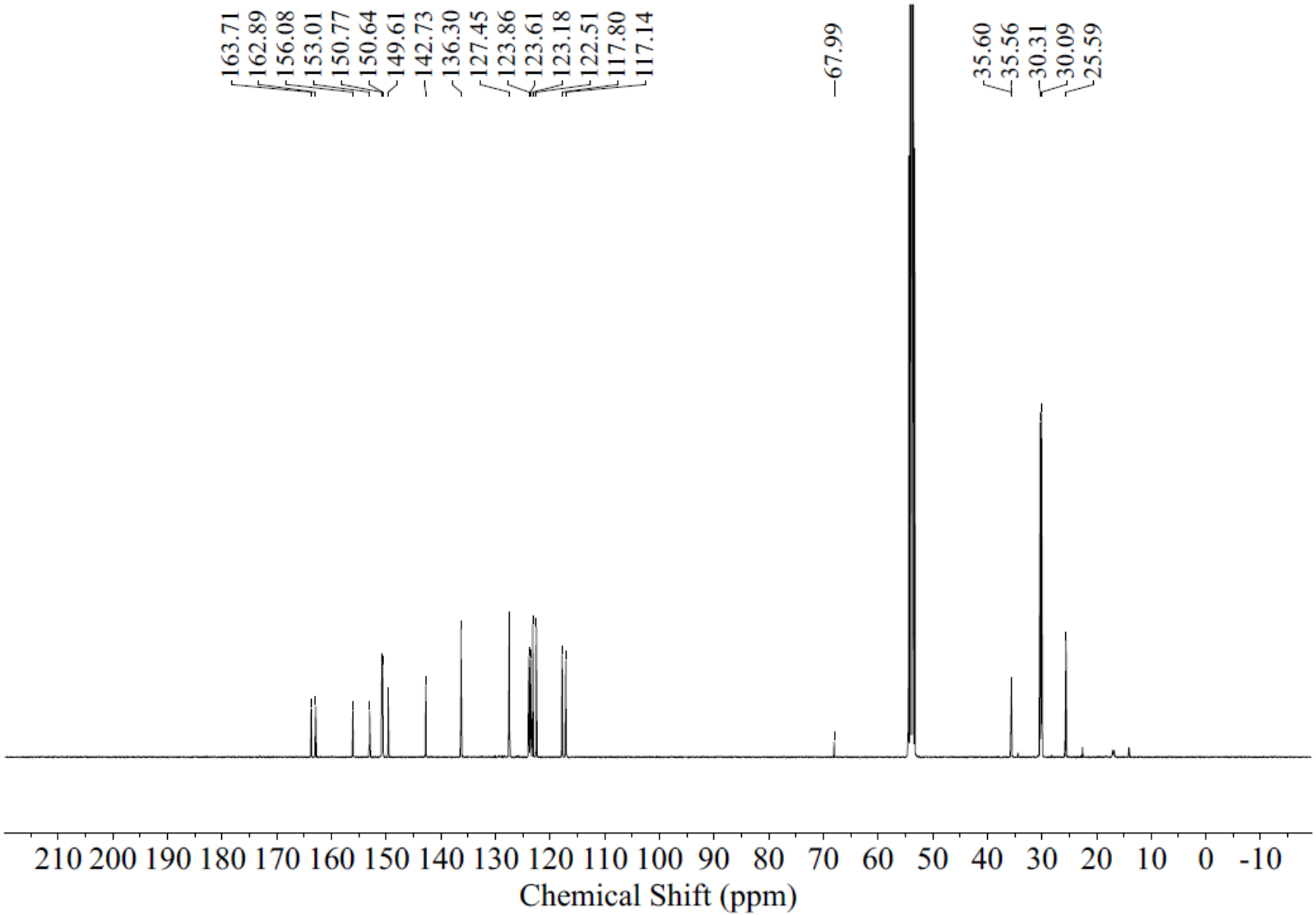

^{19}F NMR (400 MHz, CD_2Cl_2): Ni(TMEDA)(CF_3Ph)Cl

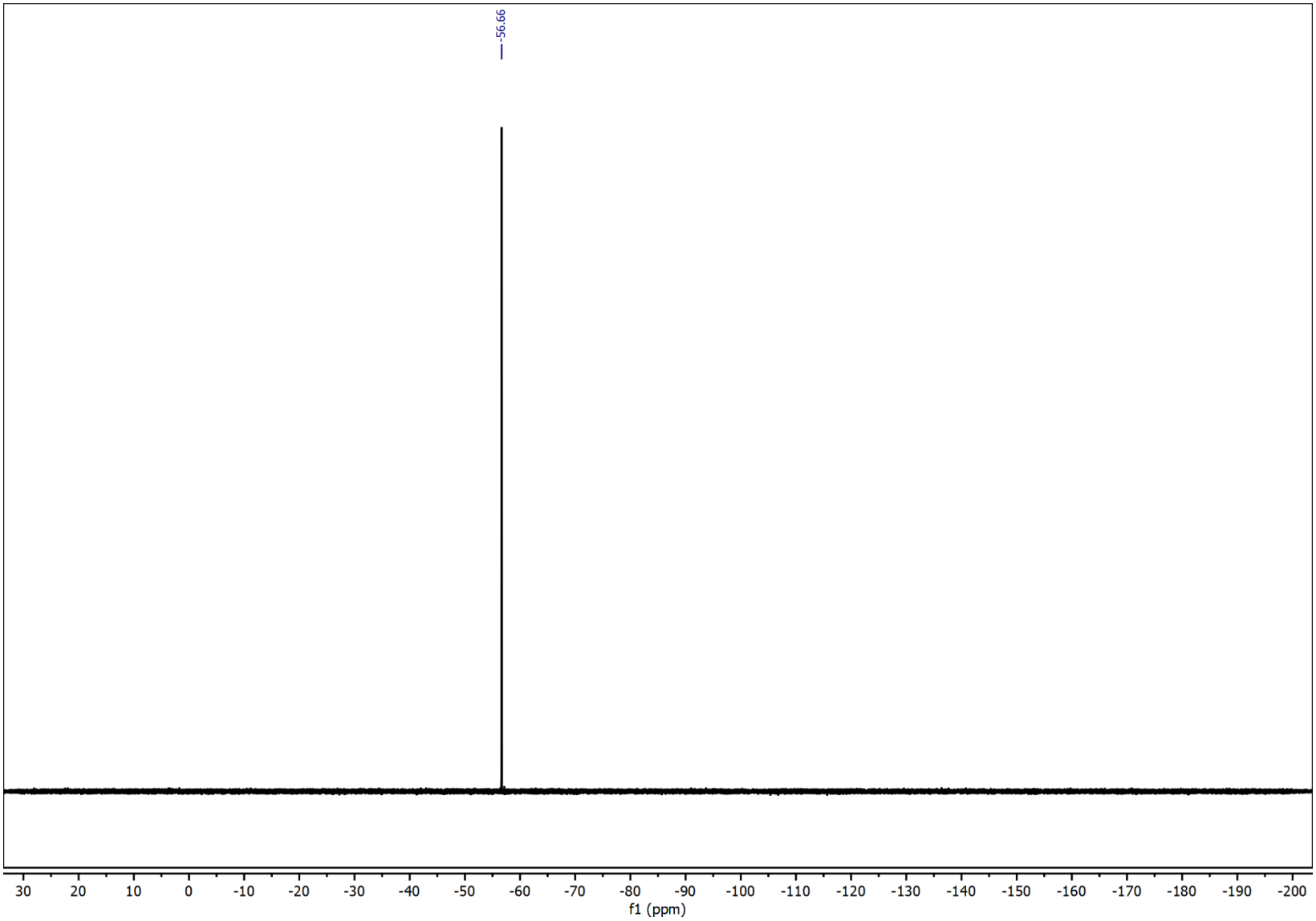

^{19}F NMR (400 MHz, CD_2Cl_2): Ni(^{MeO}bpy)(CF_3Ph)Cl, 5A

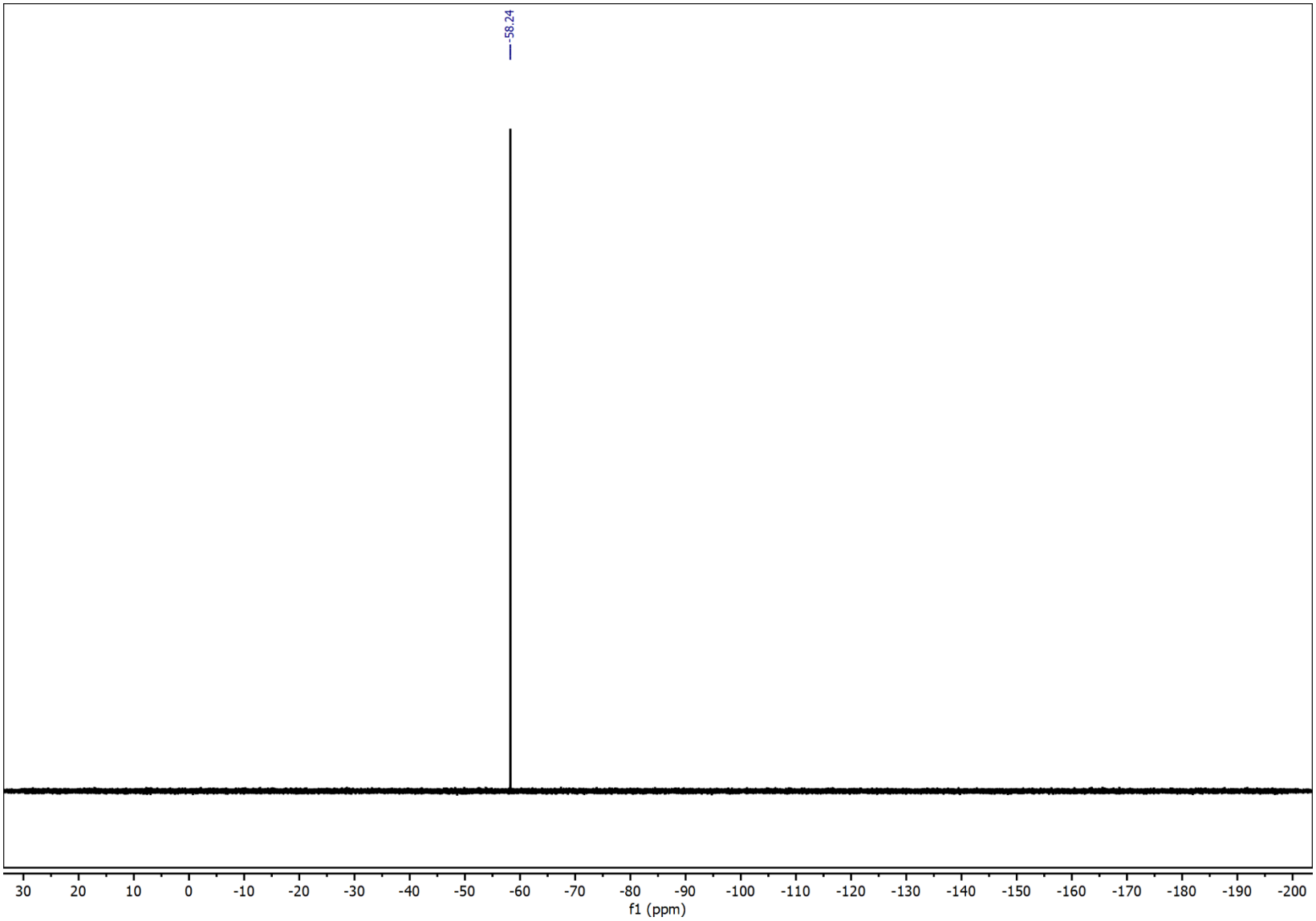

^{19}F NMR (400 MHz, CD_2Cl_2): Ni($^{t\text{-}Bu}$bpy)(CF_3Ph)Cl, 5B

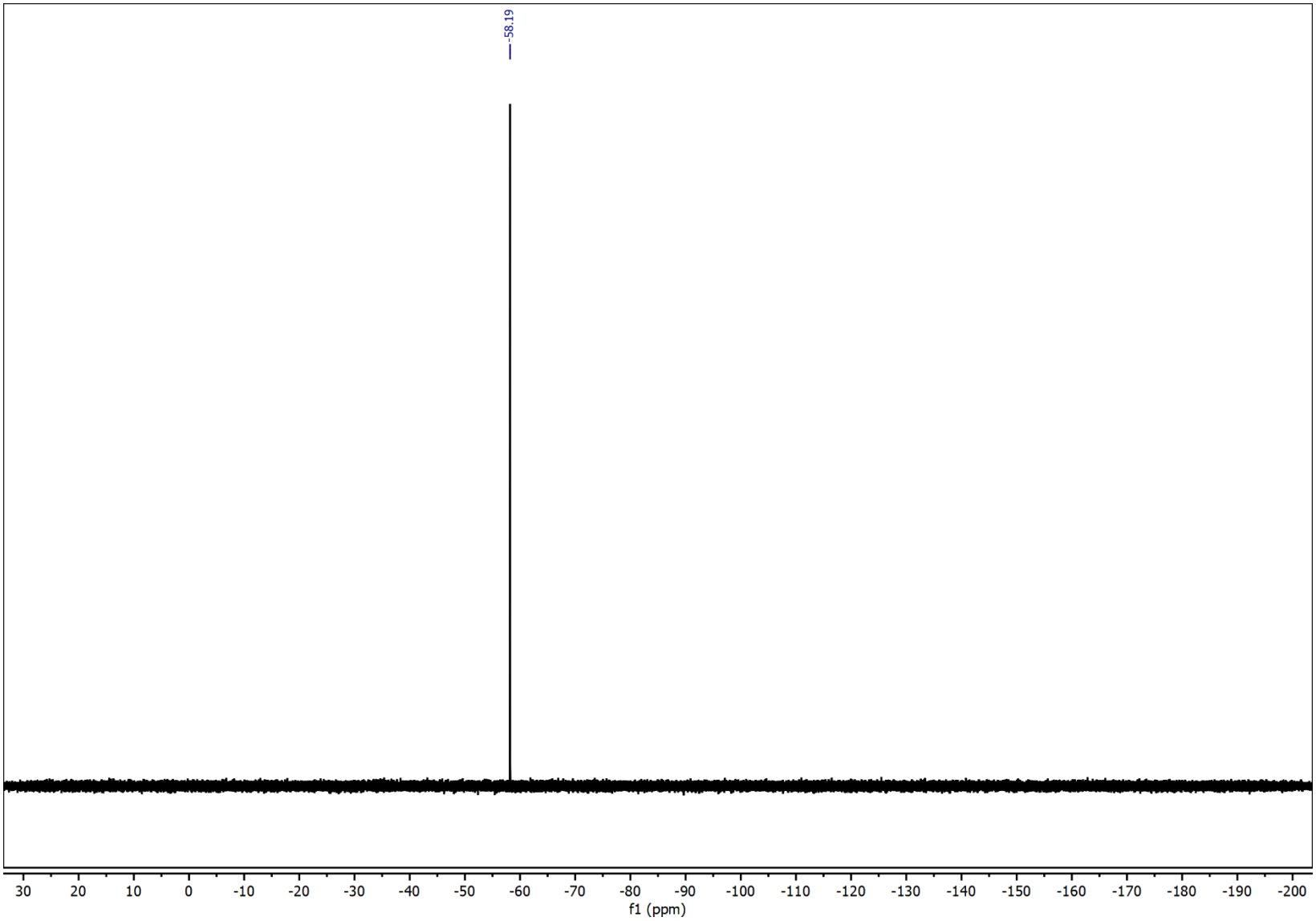

^{19}F NMR (400 MHz, CD_2Cl_2): Ni(^{H}bpy)(CF_3Ph)Cl, 5C

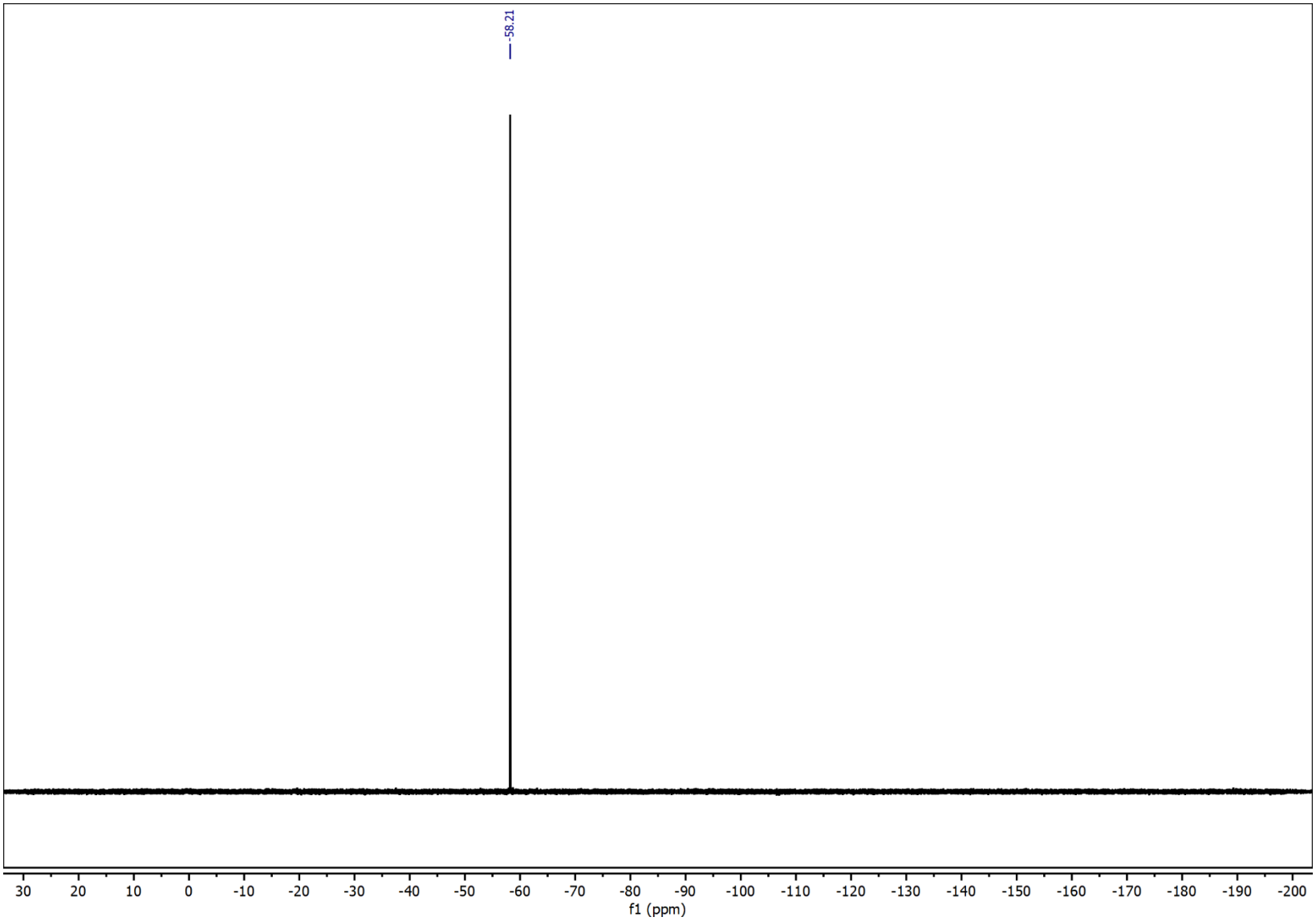

^{19}F NMR (400 MHz, CD_2Cl_2): Ni(^{MeOOC}bpy)(CF_3Ph)Cl, 5D

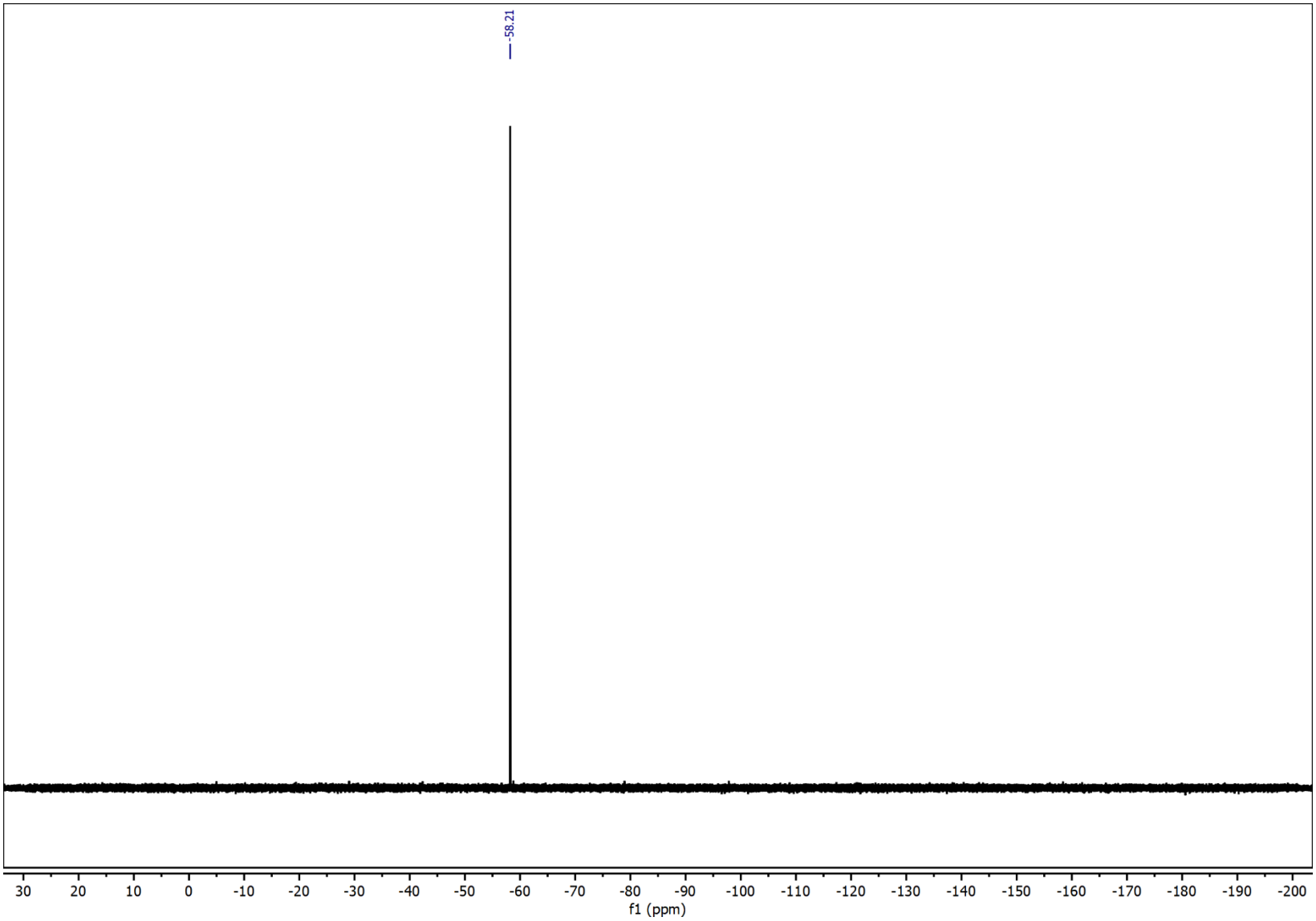

^{19}F NMR (400 MHz, CD_2Cl_2): Ni($^{t\text{-}Bu}$bpy)(F-Ph)Cl, 4B